UNIVERSITAT DE VALÈNCIA
FACULTAD DE FÍSICA

TESIS DOCTORAL:

THE BSM HUNTING GUIDE AFTER RUN I

Programa de Doctorado en Física

Cristian Bosch Serrano
Departamento de Física Teórica
Directora: Dr. Gabriela Barenboim
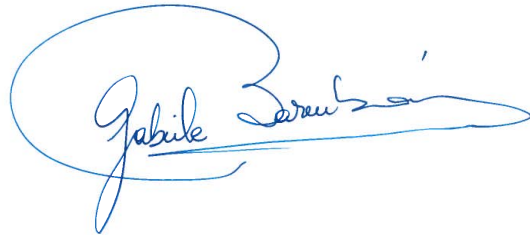
Enero 2017

Gabriela Barenboim, Profesora del Departamento de Física Teórica de la Universitat de València,

Certifica:

Que la presente memoria "The BSM hunting guide after Run I" ha sido realizada bajo su dirección en la Universitat de València por *Cristian Bosch Serrano* y constituye su Tesis para optar al grado de Doctor en Ciencias Físicas.

Y para que así conste, en cumplimiento de la legislación vigente, presenta en la Universitat de València la referida Tesis Doctoral y firma el presente certificado en:

València, a 27 de febrero de 2017.

Gabriela Barenboim

Contents

1

Resumen

1.1 Fenomenología MSSM

La presente tesis doctoral cuenta con un amplio núcleo de análisis fenomenológico de Modelos Mínimos Estándar Supersimétricos (MSSM, siglas en inglés) y dos artículos que si bien no guardan relación directa, tienen en común con las publicaciones anteriores ser un estudio de modelos Más Allá del Modelo Estándar (BSM), ambos con su apartado de fenomenología en diferentes experimentos. La idea es mostrar qué temas resultan de interés inmediato en la física de altas energías y cuáles son los mecanismos mediante los cuales son estudiados de forma teórica aunque manteniendo una estrecha relación con los diferentes experimentos que actualmente sirven de fuente directa e indirecta para dar testimonio de nueva física.

En física de partículas, cuando nos referimos a fenomenología implicamos el estudio teórico que aporta predicciones (normalmente límites) sobre los resultados experimentales respecto a los parámetros de la teoría. En el caso que nos concierne, contamos con tres publicaciones (más una comunicación oral que es un resumen de la primera) dedicadas a delimitar el espacio de parámetros favorable a la aparición directa o la influencia indirecta de partículas pertenecientes a MSSM en experimentos de aceleradores de partículas, un artículo que estudia la posibilidad de encontrar no-Gausianidad en el Fondo de Radiación Cósmico (CMB) por la sonda Planck para un modelo de inflación con dos campos y una publicación donde se modeliza una posible dinámica de condensación de neutrinos estériles, cuya verificación podría producirse por la huella que dejan en el espectro de ondas gravitacionales.

Centrémonos en lo referente al MSSM. El descubrimiento del bosón de Higgs en 2012 completó el puzzle de las partículas que componen el Modelo Estándar (SM), tras ser predicho como origen de la masa de los bosones intermediarios de la interacción débil. Inmediatamente comenzó la competición entre modelos BSM para ver cuál sería el primero cuyas partículas aparecerían en el gran colisionador de hadrones (LHC). En nuestro caso, el MSSM es un tratamiento simple de modelos supersimétricos con un número bajo de parámetros. El interés en elegir supersimetría por encima de otros modelos radica en sus posibilidades:

- El problema de la jerarquía. De no haber ninguna nueva física más allá del SM, no supone un verdadero problema. Introducir nueva física supone regularizar la integral con una nueva escala, escala que provoca que la teoría de perturbaciones
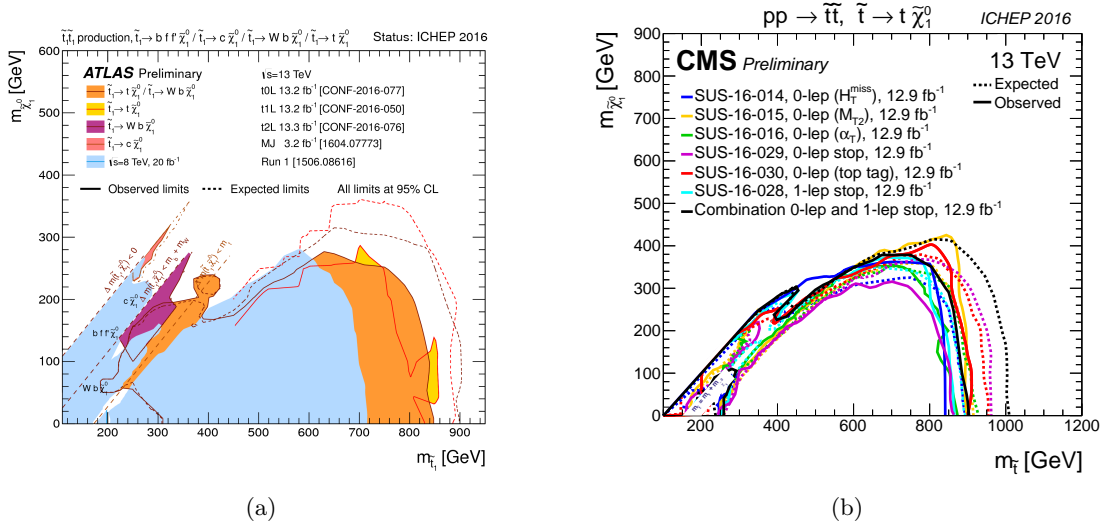
Figure 1.1: Límites presentados en ICHEP 2016 para las masas de $\tilde{t}$ y $\widetilde{\chi}_1^0$ at ATLAS (a) y CMS (b).

conduzca a resultados infinitos. No obstante, la supersimetría ofrece una posible solución en caso de encontrarla. Si la supersimetría se rompiera a la escala electrodébil, los supercompañeros (bosones correspondientes a los fermiones del SM y viceversa) lograrían que las correcciones generadas por perturbaciones (un ejemplo son las perturbaciones a la masa del Higgs) sean canceladas por las introducidas a causa de estas nuevas partículas, de signo contrario. Esto evitaría el ajuste fino que es actualmente necesario para lograr la jerarquía entre escala de Planck y escala electrodébil, tomando la escala de Planck como el cutoff de la nueva teoría SUSY efectiva válida a energías de posiblemente decenas de TeV.

- La partícula supersimétrica más ligera es candidata a formar la materia oscura. A día de hoy, el origen de la materia oscura es una de las preguntas más importantes sin resolver a la que se enfrenta la física. En este sentido, una partícula neutra que resulta idónea es el neutralino (normalmente una mezcla de bino y wino), aunque también lo es el gravitino (muy ligero) o el sneutrino (no en MSSM sin incluir neutrinos estériles).

- La gran unificación de las fuerzas fuerte, eléctrica y débil a altas energías, que no se produce en el SM. Aunque a día de hoy no se haya encontrado la evidencia fundamental para probar esta unificación, la desintegración del protón en positrón y pión neutro, la gran unificación de las constantes de acoplamiento sigue siendo uno de los principios básicos a respetar más utilizado en la elaboración de teorías físicas de altas energías.

Pese a ello, SUSY ha sido fuertemente restringida de forma experimental. Aunque no se haya descartado completamente, la reducción de su espacio de parámetros la desfavorece. En la figura 1.1 podemos ver los actuales límites para stop y neutralino en las búsquedas de SUSY de los experimentos ATLAS y CMS del LHC, los cuales han descartado casi por completo un stop más ligero de 1 TeV junto a un neutralino ligero y posible candidato a LSP (partícula supersimétrica más ligera).

Partícula	Spin	Superpartícula	Spin
Leptón	1/2	Sleptón	0
Quark	1/2	Squark	0
Fotón	0	Fotino o bino	1/2
$W^{\pm}$	1	Wino$^{\pm}$	1/2
Z	1	Zino	1/2
Higgs	0	Higgsino	1/2
Gluon	0	Gluino	1/2
Graviton	2	Gravitino	3/2

Table 1.1: Patículas del modelo estándar con sus supercompañeros. Neutralinos y charginos, que no aparecen, son combinaciones lineales de winos, binos (supercompañero del campo de Gauge de la hipercarga) y higgsinos.

1.1.1 Búsqueda de un Higgs más ligero que el de 126 GeV

Una de las búsquedas más directas posibles una vez encontrado el bosón de Higgs de masa 126 GeV es la de los otros escalares que aparecen en el sector de Higgs del MSSM. Los dos dobletes de Higgs de MSSM contienen dos bosones escalares neutros, un pseudoescalar y dos escalares cargados. Normalmente, el tratamiento de este sector de Higgs es a nivel árbol, con conservación de CP. Hemos preferido darle un grado de libertad adicional permitiendo la violación de CP para poder obtener resultados de mayor generalidad.

Nuestra fuente de inspiración para acometer este estudio es el software CP-SuperH, que diagonaliza el lagrangiano MSSM a partir de introducir un número de parámetros que puede ampliarse más allá de los 4 habituales: $m_{1/2}$ (masa de gauginos y higgsinos a la escala de energía GUT (*Great Unification Theory* - Teoría de la Gran Unificación)), m_0 (masa de los escalares en GUT), A_0 (el acoplamiento trilineal), $\tan \beta$ (la relación entre los vevs (*vacuum expectation value* - valor esperado en el vacío) de los dos dobletes de Higgs) y el signo de la masa del higgsino. Este programa permite la violación de CP en el sector de Higgs y realiza barridos de parámetros dando como resultado masas y fases para todas las partículas del MSSM. Para llevar a cabo el análisis, preferimos utilizar CP-SuperH para determinar el rango de energías del sector de Higgs, ya que el software diagonaliza el lagrangiano. Se impuso que el Higgs de 126 GeV fuera el segundo del espectro en la primera publicación y el más ligera en la segunda. Tras ello, utilizamos un código propio para barrer los parámetros fundamentales en nuestro estudio (los habituales en fenomenología pMSSM pero con violación de CP). La validación de cada punto del espacio de parámetros se ha basado en la compatibilidad con los datos experimentales del LHC y también de los procesos de sabor que se referirán posteriormente. Aunque no parezca conveniente hacer todo el análisis evitando la diagonalización para cada conjunto de parámetros, sí supone una ventaja, ya que también se tienen en cuenta aquellos puntos que podrían quedar excluidos por necesidad de un ajuste más fino para conseguir que el lagrangiano pueda diagonalizarse.

Nuestro primer objetivo fue determinar las condiciones que reprodujesen el número de fotones encontrado por ATLAS y CMS en la desintegración ($pp \rightarrow H \rightarrow \gamma\gamma$), que fue la utilizada para anunciar el descubrimiento del Higgs. Este es un proceso a nivel loop, con lo que diferentes partículas entran en él realizando su aportación. En el MSSM se incluiría un número mayor de ellas, y se llegaría a pensar que al menos el stop (si lo suponemos el más ligero de los squarks) y el Higgs cargado tendrían una gran aportación,

pero los resultados demuestran que no es así. Tras comparar con el exceso de fotones experimental, se llega a la conclusión de que el Higgs de 126 GeV está dentro de los parámetros esperados en el SM. Por tanto, el propio proceso de descubrimiento no da ninguna pista de la existencia de nueva física. Como resultado de ello, obtuvimos que el Higgs observado experimentalmente era de tipo up con una mezcla marginal de escalar down y pseudoescalar, lo que es perfectamente compatible con el SM (figura 5.4) y favorece la desintegración a fotones, eliminando los canales a quarks b y leptones τ. Cabe esperar que los otros dos escalares neutros del sector de Higgs MSSM tengan mayoritariamente una mezcla del estado down y el pseudoescalar sin especificar. Es interesante recalcar dos cálculos necesarios para llegar a esto. Uno de ellos es la producción del Higgs descubierto, cuya procedencia demostramos dominada por fusión de gluones por encima de fusión de quarks b; el último ingrediente necesario para poder calcular el número de eventos es la producción del Higgs. Otro importante cálculo es la anchura de desintegración total del Higgs, presentada en la ecuación 3.72.

Según sea la mezcla de mayor o menor proporción en ellos, entre los canales de desintegración de Higgs que CMS y ATLAS analizan profundamente en el LHC (figuras 3.1 y 3.2), el proceso más determinante para certificar la existencia de estos otros bosones de Higgs es el $H \to \tau\tau$. Tanto una composición dominante de tipo down como una de naturaleza pseudoescalar se acopla fuertemente a los leptones, por lo que se esperaría que la relación de desintegración ("branching ratio", BR) de estos otros escalares yendo a dos leptones τ fuese grande. Efectivamente, determinamos que el BR de la desintegración crece con $\tan^2 \beta$.

Junto a este proceso, hay otros dos indirectos de gran utilidad para reducir el espacio de parámetros que permita la existencia de un Higgs ligero. Estos son los procesos de sabor $B_S \to \mu^+\mu^-$ y $B \to X_S\gamma$, estudiados en LHCb y en Belle, BaBar y CLEO respectivamente. Respecto a $B_S \to \mu^+\mu^-$, su BR se corresponde con lo expresado en la ecuación 3.44, y vemos que es aproximadamente proporcional a $\tan^2 \beta$, por lo que será restrictivo en la misma zona del espacio de parámetros que la desintegración $H \to \tau\tau$. En cuanto a $B \to X_S\gamma$ (o $b \to s\gamma$), este proceso tiene en su BR dos términos dominantes que proceden de la contribución del Higgs cargado: uno proporcional a $\tan^{-2} \beta$ y otro a $\tan^{-1} \beta$, con lo que suponen una restricción para valores bajos de este parámetro. Las contribuciones del stop-chargino ($\sim \tan^2 \beta$) son despreciables siempre que consideremos Higgs cargados relativamente ligeros, como es nuestro caso ($m_{H^\pm} < 350$ GeV) a causa de los límites inferiores en sus masas, muy altos. Debido a la fuerte dependencia inversamente proporcional a $\tan \beta$, estudiaremos el rango de $\tan \beta \in [3, 30]$, que será suficiente para determinar el comportamiento de los observables de forma completa.

Tras realizar un barrido sobre todos los parámetros ya comentados, al ir estudiando la influencia de cada uno de ellos podemos apreciar que aquel con influencia más visible es $\tan \beta$, algo esperable tras lo comentado en el párrafo anterior. En el capítulo 3 de esta tesis, que se corresponde nuestro primer artículo sobre el tema, intentábamos resolver la cuestión pendiente de si existía un Higgs más ligero que el de 126 GeV (pasando este a ser el segundo), algo todavía posible dado que los experimentos del LEP dejaban un pequeño resquicio del espacio de parámetros sin excluir. Según estudiamos las posibles masas del sector de Higgs mediante el software CPsuperH, que diagonaliza el lagrangiano, determinamos que las masas se van a mantener cercanas y más bajas de los 300 GeV, siendo la masa del Higgs cargado el parámetro que define la escala energética a la que se encontrarán. Lo habitual es definir esta escala a través de la masa del pseudoescalar, pero dado que trabajamos con modelos de violación de CP, es el Higgs cargado el que toma su papel.

Centrándonos en los resultados, podemos ver que para valores bajos de $\tan\beta$ (<8), un Higgs de $m_{H_1} = 110$ GeV (podríamos haber propuesto una masa mínima de 90 GeV, pero el valor presentado produce resultados más vistosos, ya que aquel se descarta con mayor rotundidad) sobreviviría de acuerdo a las restricciones experimentales del número de fotones provenientes de H_2, que se correspondería al descubierto, y el número de eventos del propio escalar H_1 yendo a dos leptones τ. Por tanto, se puede apreciar en la figura 3.5 que este último proceso es una potente herramienta para restringir el parámetro $\tan\beta$ en MSSM a valores bajos, ya que, como dijimos, la anchura de desintegración es proporcional a $\tan^2\beta$.

Además, conseguimos eliminar el espacio de parámetros al completo tras añadir sólo uno de los procesos de sabor propuestos, $B \to X_S\gamma$, que es especialmente restrictivo para valores bajos de $\tan\beta$, como ya predijimos (figura 3.6). La última posibilidad de que se encontrase un Higgs ligero residiría en forzar los límites experimentales sobre superpartículas (ya que no podemos cambiar el signo de la contribución stop-chargino), suponiendo la masa del stop entre la del chargino y la del chargino más la del top, lo que nos permite suponer una masa de stop menor a los 650 GeV. Pese a hacerlo, el proceso de violación de sabor no relaja la dominante restricción impuesta por las contribuciones del Higgs cargado lo suficiente a tangentes de beta intermedias y, como se puede ver en la figura 3.7, se excluye cualquier posibilidad de encontrar un Higgs más ligero que el de 126 GeV.

De esta primera publicación, aprendimos que el proceso $H \to \tau\tau$ es una herramienta muy potente para poder estudiar y confirmar, llegado el caso, el descubrimiento de un nuevo Higgs ya que, en MSSM, este decaería fuertemente a estos dos leptones y su BR es especialmente restrictivo a alta $\tan\beta$. También vimos que el proceso $B \to X_S\gamma$ es muy importante para poder eliminar de forma indirecta el espacio de parámetros a baja $\tan\beta$, formando ambos procesos una gran combinación. Gracias a ello podemos afirmar que, en caso de ser el MSSM una realidad, el bosón de Higgs más ligero sería en efecto el encontrado a 126 GeV.

1.1.2   Búsqueda de Higgs pesados

En el siguiente artículo nuestra intención ha sido reutilizar las herramientas desarrolladas en el anterior para hacer predicciones sobre el sector de Higgs de MSSM, pero esta vez intentando establecer qué posibilidades hay de encontrar los bosones más pesados y a qué masas los restringirían los datos experimentales.

Con el conocimiento ya adquirido sobre las características del Higgs de 126 GeV en cuanto a su composición en términos de Higgs up, down y pseudoescalar (recordemos que primordialmente up) y utilizando los procesos previamente señalados, dividimos nuestro trabajo en dos escalas: según si el Higgs cargado, cuya masa establece el límite superior del sector de Higgs, cuenta con una masa superior o inferior a la del quark top, abriendo el canal $H^\pm \to tb$. El principal motivo tras esto es bastante directo, ya que las medidas experimentales realizadas en el canal $H \to \tau\tau$ eran más precisas en ATLAS para masas bajas, con lo que conviene hacer el análisis por separado (figura 5.1). No obstante, no se pone el límite en 500 GeV, fin de las regiones de búsqueda experimental iniciales, porque consideramos que, dada la masa del Higgs más ligero, la masa del top es un buen límite para interpretar que los otros Higgs se han desacoplado, además de introducir los nuevos canales de desintegración en lo que clasificamos como masas elevadas.

En referencia a las masas de Higgs cargado ligeras, la figura 5.5 es muy representativa de la capacidad de exclusión que tiene el proceso de Higgs yendo a dos leptones τ para valores altos de $\tan\beta$. Como bien puede apreciarse, con una $\tan\beta = 7$ ya se excluiría una masa menor a 150 GeV para el segundo Higgs. Introduciendo ahora nuestro proceso

de violación de sabor de referencia, podemos ver en la figura 5.6 como sólo una cantidad ínfima de puntos puede superar las restricciones de $H \to \tau\tau$ y $B \to X_S\gamma$ simultáneamente, no permitiendo un segundo Higgs más ligero que 140 GeV en ningún caso. En la figura 5.7 ya se puede apreciar cómo la mejora estadística de 2013 en $H \to \tau\tau$ hace que este espacio de parámetros quede completamente eliminado de entre los posiblemente válidos.

Suponiendo ahora el resto del sector de Higgs más pesado, las posibilidades de encontrar un nuevo escalar se elevan. Una novedad respecto a los cálculos anteriores es la apertura del canal $H \to t\bar{t}$, que al ser una nueva vía de desintegración, bajará el número de eventos en el canal a dos τ mientras $\tan\beta$ no sea muy grande. No obstante, en la figura 5.7 podemos ver que para una $\tan\beta$ baja las masas del segundo Higgs más ligeras (hasta 350 GeV) son eliminadas por $B \to X_S\gamma$, y $H \to \tau\tau$ hace que para valores grandes de $\tan\beta$ se puedan llegar a eliminar masas de hasta 600 GeV, apreciándose también la diferencia en cuanto a restricciones provenientes de CMS y ATLAS. Sin embargo, en su momento afirmamos que era muy probable que nueva estadística en el canal $H \to \tau\tau$ supusiera unas restricciones mayores en la figura 5.8 que simulamos en ella.

Para finalizar esta publicación, decidimos aplicar nuestro estudio a un caso que en su momento era relevante, la aparición de un pico en producción de fotones para una masa de Higgs de 136.5 GeV. De entrada, ya era bastante complicado reproducir un exceso cercano a 3σ al asignarle una mezcla de tipo down y pseudoescalar a los elementos de la matriz de fase de este supuesto Higgs. Sin necesidad de agregar las restricciones originadas por la desintegración a dos τ ya es suficiente para descartar la existencia de un Higgs con esa masa, ya que las partículas que entran en el loop a fotones también verán incrementada la anchura de desintegración a su canal, con lo que el propio BR a fotones vuelve a verse disminuido. Una situación similar fue la del pico en 750 GeV, que pese a no aparecer en las publicaciones que conforman la tesis, cabe comentar que no era un candidato viable a Higgs en modelos MSSM según nuestro análisis.

1.1.3 Desintegraciones del Higgs con violación de sabor

Una vez analizado a fondo el sector de Higgs del MSSM, nuestra idea fue considerar otros caminos para poder probar la existencia de nueva física. Sin salir de modelos supersimétricos, nuestro interés viró a analizar el acoplamiento del Higgs ya descubierto en procesos de violación de sabor. El motivo tras esta decisión es no haber encontrado nuevas partículas a día de hoy, con lo que el propósito es poder evitar el método de ir elevando las colisiones a energías cada vez superiores con la esperanza de que aparezca un pico. Por tanto, la nueva estrategia es abandonar el incremento de la energía en centro de masas para invertir en estadística. La dificultad tecnológica de conseguir colisiones a escalas energéticas más elevadas siempre supondrá un gran obstáculo, así que parece una buena elección trabajar con el Higgs ya descubierto a mayor precisión, ya que, de existir estas desintegraciones, se trataría un canal con un BR muy bajo. Un hipotético segundo Higgs, más pesado, aunque ya sería una muestra de nueva física por su parte, también se caracterizaría por una estadística más favorable en estas desintegraciones, como se puede ver en el artículo.

Prohibidos en el SM, los procesos de cambio de sabor en desintegraciones del Higgs se permiten en el MSSM cuando se aplican correcciones radiativas a un loop. De acuerdo al teorema de desacoplo de Appelquist y Carazzone, los grados de libertad de partículas pesadas contribuirán como un operador de dimensión $d > 4$ o como correcciones logarítmicas. De este modo, las contribuciones son pequeñas en ambos casos (el primero porque el loop contribuirá elevado a una potencia $4 - d$). Los acoplamientos con violación de sabor del Higgs, al ser adimensionales (son un cociente de dos masas pesadas), desacoplan los efec-

tos de las partículas más pesadas sobre la coeficiente de desintegración aunque se subiese su masa hasta el infinito, con lo que suponen un buen indicador de la existencia de las superpartículas, que contribuirían a orden loop. Nuestros cálculos serán para el proceso $H \to b\bar{s} + s\bar{b}$.

Respecto a las restricciones que provienen de procesos estudiados en el LHC, estas no cambian respecto a las publicaciones anteriores. Dado que los parámetros que vamos a utilizar son una combinación de las fases CP, sigue siendo necesario ajustar tanto el número de fotones para el Higgs de 126 GeV como plantear un escenario plausible según las desintegraciones a dos τ y $B \to X_S \gamma$ para los otros. También haremos uso de los límites directos para las superpartículas. La novedad esta vez es la mayor relevancia de la desintegración $B_S \to \mu^+ \mu^-$ para valores de $\tan\beta$ intermedios y el uso de la diferencia de masa ΔB_S para valores de $\tan\beta$ altos.

Es interesante recalcar que en esta ocasión introducimos una reparametrización de la matriz de mezcla del sector de Higgs combinada con β de forma que obtenemos los parámetros δ_1 y η_1, como puede verse en la ecuación 6.4. Una vez definidos, se obtienen los acoplamientos del Higgs en función de estos parámetros. En la sección 6.2 puede seguirse de forma detallada cómo tratamos estos acoplamientos e introducimos inserciones de masa en los loops para simplificar el análisis de las corrientes neutras con violación de sabor (FCNC).

En la sección 6.4 se puede seguir la forma de introducir las matrices de violación de sabor donde se introducen los parámetros que contienen las contribuciones a nivel loop. Podemos ver que de entre estos parámetros, nuestros resultados van a depender básicamente de introducir inserciones de masa de rotura de supersimetría con cambio de sabor, levógiras o dextrógiras, como principales elementos de las perturbaciones. Considerando el formalismo del MSSM, tenemos una representación de la relación de desintegración (BR) del proceso $H \to b\bar{s} + s\bar{b}$, medible en un acelerador, respecto a los parámetros MSSM $\tan\beta$ y también δ_1, vemos que para una inserción de masa levógira sólo es necesario considerar el Yukawa que acopla a levógiros, de forma aproximada. No obstante, esto no es tan simple si se quiere introducir exclusivamente una inserción dextrógira, donde hay que considerar ambos.

En la figura 6.1 puede apreciarse como, para una inserción de masa levógira, en el mejor de los casos, necesitaríamos medir un BR de 10^{-6} para el Higgs de 126 GeV (BR proporcional a los cuadrados de δ_1 y η_1), aunque contaríamos con tres órdenes de magnitud de más si se encontrase un H_2 y realizásemos las mediciones en él (en su caso, el BR es independiente de su masa, δ_1 y η_1)[1]. Al ser un escalar de gran masa (como se mostró en publicaciones anteriores) las restricciones provenientes de procesos de sabor son menos efectivas. En el caso de una inserción de masa de tipo dextrógiro, los resultados, visibles en la figura 6.2, son peores por dos órdenes de magnitud tanto para H_1 como para H_2.

Tras esto optamos por relajar las restricciones que conlleva supersimetría o, lo que es lo mismo, a hacer un análisis independiente del modelo, lo que se traduce en no imponer la condición de unitariedad sobre las mezclas. A nivel teórico, el único cambio perceptible en este análisis es que, en esta ocasión, los parámetros δ_1 y η_1 sólo se ven limitados por los datos experimentales de desintegraciones del Higgs y otros procesos de sabor. Esta vez nos limitaremos sólo a la inserción de masa levógira, la cual ya vimos que es la más favorable, y apreciamos que sucede como expusimos: para un H_2 pesado no se debería

---

[1]Como muestra de la dificultad para lograr la estadística necesaria, tomando sección eficaz de producción del Higgs (por fusión de gluones) de 126 GeV en el Report4 del CERN ($\sqrt{s} = 14$ TeV), vemos que la sección eficaz para la inserción de masa levógira sería de $4.8 \cdot 10^{-5}$ pb, con lo que tendríamos un número de eventos de 1.9 considerando la luminosidad integrada lograda por ATLAS a esta energía.

encontrar diferencia alguna y no se encuentra, mientras que el Higgs de 126 GeV, que sí
depende de los parámetros de mezcla, vemos que el BR mejora hasta situarse en un valor
de 10^{-4}, que sin embargo todavía es bastante pequeño (figura 6.3).

La conclusión a la que llegamos en esta publicación es que los procesos en los que
se producen corrientes neutras de cambio de sabor son buenos candidatos para conseguir
de forma indirecta una medición de nueva física. Si bien son muy favorables para un
hipotético H_2, la existencia de este ya confirmaría que el SM debe ser extendido. El caso
de mayor interés en la actualidad sería la posible medición de estas corrientes en H_1. Sin
embargo, la precisión que se prevé teóricamente requiere de la construcción de un nuevo
acelerador de partículas, como podría ser el colisionador lineal ILC, que disponga de la
suficiente luminosidad para poder realizar este tipo de mediciones finas.

1.2 Búsqueda de no-Gaussianidades en estudios de estructuras a gran escala

Con el artículo anterior dejamos atrás el núcleo central de la tesis, dedicado al MSSM. El
próximo en ser presentado, dedicado al estudio del modelo cosmológico estándar, tiene en
común el propósito de buscar nueva física.

En Cosmología, se llama inflación al periodo de expansión rápida del espacio que sucede
al Big Bang. Propuesta por A. Guth y A. Linde en trabajos independientes, busca respon-
der a problemas tales como no haber encontrado curvatura del espacio (problema de la
planitud del universo), anisotropía e inhomogeneidades (constituyen el llamado problema
del horizonte), características que se esperaría poder medir y que gracias a la expansión
habrían sido suavizadas en el universo primigenio. Para poder explicar esto, el inflatón,
como se conoce al campo encargado de esta expansión, habría hecho que las densidades
de otros constituyentes presentes en ese periodo se diluyese (como los posibles monopolos
magnéticos) durante la expansión, dejando el universo práctimente plano y vacío, siendo la
densidad del inflatón constante hasta que se alcanzase la temperatura o escala energética
en la que se produce el recalentamiento, siendo este provocado por la desintegración del
inflatón, que llenó el universo de partículas del Modelo Estándar. Un problema por re-
solver es el de la formación de estructura, que vemos a diferentes escalas (desde cúmulos
estelares hasta cúmulos de galaxias). Este artículo indaga en una forma primordial de
generar estructura en el universo.

Se prevé que las perturbaciones del inflatón sigan una distribución gaussiana (como
campo libre que es el inflatón), pero desviaciones de la misma permitirían estudiar si este
campo interactuó y cómo lo hizo, siendo un buen discriminante para llegar a un modelo de
inflación correcto. Por tanto, unas funciones de correlación de órdenes mayores crearían
una no-Gaussianidad medible. Suponiendo que el inflatón es un campo libre, este no
debería haber interactuado y las condiciones iniciales que debería haber dejado tras el
periodo de inflación seguirían una distribución Gaussiana.

Si la dinámica del inflatón no fue la de un campo libre, deberían poder encontrarse
indicios observables de ello en funciones de correlación de órdenes altos. La más accesible
de ellas es la función de correlación de tres puntos (ecuación 7.2, el bispectro es uno de sus
términos), la cual no provee una no-Gaussianidad medible para modelos de inflación slow
roll de un solo campo en el límite en el que uno de los momentos de esta función es mucho
más pequeño que los otros ("squeezed limit"). En cambio, agregar nuevos inflatones, un
término cinético no trivial o ciertas características en el espectro de potencias sí daría
lugar a unas no-Gaussianidades que además son distintivas de cada modelo.

En el momento de la publicación del artículo, este prometía ser un tema candente al haber comenzado hacía poco la misión del satélite Planck, que se esperaba que aportase nuevas observaciones en el estudio de la función de correlación de tres puntos del Fondo Cósmico de Microondas (CMB), resultados que a día de hoy ya sabemos que han reforzado los modelos de inflación de un solo campo, descartando la mayoría de potenciales sencillos de más de un inflatón. No obstante, nuestro análisis se dirigió hacia el estudio de las estructuras a gran escala (LSS), que son otro mecanismo para estudiar las posibles no-Gausianidades en la polarización del halo ("halo bias"). Una no-Gaussianidad de tipo local generaría una escala, desplazamiento al rojo y dependencia de la masa características en el "halo bias".

La intención de nuestra publicación era estudiar el bispectro de modelos de inflación del tipo cuasi un solo campo, ya que en el límite "squeezed" generaría una no-Gaussianidad de tipo local. Este tipo de modelos inflacionarios consta de un inflatón ligero que cae en un potencial además de otra partícula llamada isocurvatón cuya masa es similar a la de la constante de Hubble durante la inflación. Estas dos partículas se acoplan formando una trayectoria circular en el espacio de campos, y es el movimiento ortogonal del isocurvatón el que genera las no-Gaussianidades, si se dan las condiciones expuestas. Tras el estudio, se esperaba poder ofrecer una idea de cuán determinantes serían las mediciones de un análisis LSS del espectro de potencias del ("halo bias") para dar por descubierta una no-Gaussianidad y asignarla a un tipo de plantilla concreto.

El uso de la dependencia respecto a los momentos del bispectro particular de cada modelo podría derivar en cálculos muy complicados. Debido a esto, se utilizan plantillas que tienen comportamientos similares a los bispectros particulares que reproducen el comportamiento aproximado de grupos de modelos con características similares. Dos de las plantillas más utilizadas son la equilátera y la ortogonal, útiles cuando se quieren emular los efectos de la inflación de un solo campo. El bispectro referido en la ecuación 7.6 se toma en la literatura como una buena aproximación del modelo de inflación que nosotros queremos estudiar y está normalizado a la plantilla local, útil en modelos con más de un inflatón, cuando sus momentos son iguales.

El parámetro más importante de este bispectro, ν, está relacionado con la masa del isocurvatón y su valor hace que el bispectro se aproxime más a un tipo u otro de las plantillas ya enumeradas para el límite "squeezed". Otro valor importante es la amplitud f_{NL}, relacionado con el propio ν y la derivada tercera del potencial de inflación. Este parámetro (o parámetros en plural, ya que nosotros sólo utilizamos el local), es producto del ajuste del bispectro estudiado a un bispectro plantilla (o varios de ellos), como se puede ver en la ecuación 7.8. En la figura 7.1 se puede ver una estimación de los rangos que, según WMAP, van a tener estos parámetros para los modelos a estudiar.

Tras el modelado del "halo bias" no-Gaussiano en la sección 7.3 y de los parámetros que definen su estudio experimental en la sección 7.4, se procedió a hacer predicciones sobre un modelo fiduciario con valores centrales de f_{NL} y ν determinados, calculando las posibles desviaciones del espectro de potencias dependiendo de estos parámetros al comparar el espectro de potencias fiduciario de cada plantilla (o cada $\bar{\nu}$) con el que aporta el bispectro propuesto. Las figuras 7.2 y 7.3 (esta se ha calculado de forma independiente del modelo) muestran que el cambio de plantilla ($\bar{\nu}$ o β, que es lo mismo con independencia del modelo) es enormemente restrictivo cuanto mayor sea el valor del parámetro fiduciario, dejando posibilidad a sólo muy pequeñas variaciones del parámetro ν respecto al central, con lo que una observación de no-Gaussianidad con unos valores de ν y f_{NL} similares a los valores fiduciarios daría una excelente estimación de los parámetros del modelo. Esto no pasaría para valores pequeños de $\bar{\nu}$, en los que apreciamos que se requeriría un valor

de f_{NL} muy alto para poder rebajar la incertidumbre de la medición.

1.3   Escalares compuestos tras condensación de neutrinos estériles

En esta última publicación se explora una posible dinámica de neutrinos estériles dextrógiros, muy pesados, que son aquellos sólo sensibles a la gravedad de entre las interacciones fundamentales. Su interacción con los neutrinos del Modelo Estándar debería ser a través de términos Yukawa, donde que el neutrino estéril adquiera masa hace que el neutrino levógiro también lo logre. La masa de los neutrinos está avalada por los experimentos de oscilación, con lo que es interesante considerar una teoría que incluya los neutrinos dextrógiros aunque se carezca de evidencias directas.

La conexión de este trabajo con los anteriores no sólo consiste en el estudio de un campo diferente de nueva física, sino que las conclusiones a las que llegamos podrían estar ligadas a la inflación cosmológica, ya que los escalares que aparecen naturalmente en este modelo pueden postularse como candidatos a inflatón, siguiendo un potencial generado dinámicamente. Además de ello, también exploraremos brevemente las consecuencias de esta teoría como generación de ondas gravitacionales.

La propuesta para el modelo teórico es asumir que, bajo cierta escala energética, los neutrinos estériles van condensar en escalares compuestos. Tras esta condensación, bien puede estar la interacción gravitatoria o bien otra que ahora desconocemos. Sin embargo, consideramos esta interacción incapaz de distinguir el "sabor" de los neutrinos, por lo que, para conseguir cierta generalidad sin una excesiva complejidad, suponemos dos familias de neutrinos estériles que condensarán en diferentes campos escalares, según combinatoria. Si bien podría parecer que la condensación debería afectar a otros fermiones, los condensados de neutrinos estériles son los únicos que no contarían con canales de desintegración debidos a su insensibilidad a otras interacciones, siendo los únicos físicamente relevantes.

Con estos ingredientes y la inspiración en el modelo BHL de condensación de quarks top, se genera un sistema de tres campos escalares, uno proveniente de neutrinos exclusivamente de la primera generación, otro análogamente con neutrinos de la segunda y un tercero formado por neutrinos de ambas. Con ello se forma un vector de escalares con el que se define el potencial de la ecuación 8.1.

Esta simetría nos permite eliminar parámetros no físicos haciendo un cambio de fase a la segunda componente del campo para dejarla real, una rotación para hacerla cero y otro cambio de fase para que la primera componente sea real, de modo que se el cálculo de la rotura espontánea de simetría se calcula de una manera más simple.

Es la rotura espontánea de simetría la que marca la segunda escala del problema, cuando el potencial alcanza el valor esperado en el vacío (v.e.v., ver definión en la sección 8.2) con un valor distinto de cero. El nuevo potencial tiene una simetría U(1) y se generan tres escalares masivos y tres bosones de Goldstone con masa.

La simetría U(1), que conserva el número leptónico, puede romperse explícitamente añadiendo el término presentado en la ecuación 8.7 al potencial, haciendo que uno de los bosones de Goldstone se vuelva masivo, mientras se preserva la simetría rotacional. Esta rotura espontánea supone una nueva escala energética para este modelo.

Los otros dos bosones de Goldstone adquirirán su masa gracias a la interacción de Yukawa, la cual define la escala más baja de este modelo. Por tanto, en el recuento nos quedan tres partículas asociadas a la rotura espontánea de simetría en la escala más alta bajo la masa de los neutrinos dextrógiros, una partícula originada en la rotura explícita

del número leptónico a una escala menor y dos partículas más causadas por la interacción Yukawa, en la escala más baja.

Dado que en 2016 se produjo el descubrimiento experimental de las ondas gravitacionales, nos propusimos agregar un apartado al artículo consistente en analizar una posible huella de este modelo en el espectro medible. Estas ondas se pueden generar, cuando hay una transición de fase, por colisiones de burbujas de vacío expandiéndose, ondas de sonido y turbulencias magnetohidrodinámicas de las burbujas de vacío que se encuentran en el plasma. Una transición de fase de primer orden es un buen candidato y, aunque la rotura espontánea de simetría podría considerarse de segundo orden, también podrían generarse ondas gravitacionales si parámetros como ϵ (ecuación 8.19) y β (ecuación 8.21) fuesen muy próximos a cero y del orden de mil (en valor absoluto) respectivamente.

A tal efecto, tomamos el potencial de la ecuación 8.1 en notación vectorial y renormalizado como se ve en el apéndice, dando valores aleatorios aunque convenientes a sus parámetros, valores que no pretenden explicar la dinámica del condensado de neutrinos sino servir de ejemplo para mostrar la generación de ondas gravitacionales. Un conjunto de parámetros diferente podría dar lugar a resultados similares, con lo que la rotura espontánea de simetría daría lugar a ondas gravitacionales sin requerir un excesivo ajuste fino de los parámetros.

En la figura 8.2 mostramos cómo el potencial tiene un mínimo en cero para una determinada temperatura (temperatura crítica) y cómo se produce la rotura espontánea de simetría que, tras calcular la acción a esta temperatura, cumple con los límites esperados en los parámetros ϵ y β, como antes enunciamos, procediendo a calcular el espectro de ondas gravitacionales de acuerdo a las ecuaciones presentadas en 8.22.

Tras representar las densidades de ondas gravitacionales del modelo para diferentes elecciones del valor esperado de vacío (figura 8.3), que situarían la rotura espontánea de simetría a diferentes escalas energéticas, podemos ver que, siempre según los parámetros que hemos elegido, una transición de fase a una escala energética alta ($10^{-9}M_P$) no sería medible por ninguno de los equipos experimentales tanto actuales como próximos, mientras que si nos movemos en escalas del TeV y unos 4 órdenes mayores, tendríamos una contribución visible por DECIGO y BBO.

Como conclusión de esta publicación, podemos decir que se ha propuesto una dinámica plausible para explicar el comportamiento de los elusivos neutrinos estériles, que condensarían, mediante gravedad u otra fuerza atractiva, en escalares compuestos. De ser cierta esta teoría, deberían encontrarse partículas a diferentes escalas energéticas, correspondiéndose con las sucesivas roturas de las simetrías del modelo y, además de estas partículas, proponemos otra posibilidad de búsqueda experimental en forma de señal de ondas gravitacionales.

2

Introduction

These last years have been quite fruitful in the field of High Energy Physics. When this thesis research started, the LHC and Planck experiments were about to deliver their first results, producing great expectation amongst the scientific community.

In 1964, P. Higgs and, separately, F. Englert and R. Brout defined theoretically the Higgs mechanism [1, 2]. It consists in defining a scalar field, the Higgs field, that has a potential with an $SU(2)$ symmetry that spontaneously breaks which, through the Nambu-Goldstone bosons associated to the breaking, gives mass to the particles, explaining why the weak interaction bosons $W^\pm$ and Z were massive unlike the photons and gluons.

It was in 2012 when the LHC claimed the experimental finding of the Higgs boson [1, 4]. Though theoretically expected, it was an extremely relevant discovery. It gave closure to the Standard Model (SM), completing its particles puzzle, but it opened many other doors at the same time, since there are still physics phenomena that need to be explained. Amongst them, the origin of dark matter and dark energy, the hierarchy problem and cosmological inflation are some that stand out.

Since the discovery of the Higgs scalar, its mass has become the reference for Beyond Standard Model (BSM) theories and searches, and a currently unsolved competition among models began. Two big contenders that can arguably be the next step in simplicity after the SM are the two-Higgs-doublet models (2HDM) [3] and Minimal SuperSymmetric Models (MSSM) [6]. Their simplicity and the similar treatment of the Higgs sector is responsible for this interest. Whereas in 2HDM there is an extension of the number of scalars present in the theory, adding a second doublet; MSSM comes with the supersymmetric partners of the known SM particles besides the introduction of a second similar scalar doublet. This thesis explores the second path from a phenomenological perspective.

Studying the viability of BSM physics is not a mere academic exercise, but it is rooted in strong motivations. As we stated before, the SM has no answer for the existence of dark matter or dark energy. An explanation for the neutrino masses origin is still missing, as well as the experimental confirmation of the existence of light sterile neutrinos. Cosmological inflation at the early universe does not have a theory providing an agent that outstands as a strong candidate for the explanation of its mysteries and there are theoretical challenges like the hierarchy problem that still need a solution.

As mentioned above, there are hints indicating that the SM is not the final theory that cannot be ignored. Only a 5% of the universe is composed by visible matter, a matter that is unable to explain the rotation velocity of galaxies or gravitational lensing among other phenomena. Thus, there must be an explanation for these phenomena, and the

best guess is that there is matter only sensible to gravitational interaction (a 27% of the total). Due to this abundance of matter, it is intuitive to expect a universe tending to a future contraction. Nonetheless, it is experiencing just the opposite. The expansion of the universe determines that, in addition to the regular matter and this dark matter, there is a 68% of it constituted by the exotic dark energy, which instigates gravitational repulsion or, as it is commonly stated, generation of space. The mechanism behind the current expansion is still unexplained. Despite not being able to solve the dark energy problem, Supersymmetry (SUSY) has been believed to deliver a partial solution to the cosmological puzzle, proposing a dark matter candidate with the Lightest Supersymmetric Particle (LSP). This particle, with the properties of a WIMP (Weakly Interacting Massive Particle), which justifies witnessing only gravity, would be stable (unless there is R-parity violation) and with neutral charge. Two SUSY particles can fit the role of the hypothetical LSP, the neutralino and the gravitino. Nevertheless, SUSY searches have put a high bound for them, diluting their privileged position as dark matter constituents.

As for the hierarchy problem, it is normally defined as the reason behind the gravitational interaction being so weak compared to the electroweak interaction, which can also be understood as why is M_W/M_{Planck} so small. It is necessary to protect the Higgs mass from quantum perturbations in BSM theories, despite not needing it in the SM because, being the square of its mass a UV-sensitive parameter (the only dimensional parameter of the SM), the SM has a single scale. Supersymmetry (SUSY) was born for several reasons (even mathematical elegance) but one of them was this (2HDM cannot solve it, it lacks the wide catalog of superpartners provided by SUSY). Cancellations between particles and their superpartners would allow the Higgs mass to be protected during renormalization. The LHC was built with the assumption of a SM cutoff at TeV scale, so it is natural to study the phenomenology linked to the supersymmetric framework as it has been done extensively in this thesis.

In order to do that, the core of this thesis is dedicated to cover the phenomenology of the Higgs sector for new scalar searches at LHC. The first two papers (and the proceeding between them) analyze the influence of direct Higgs decays and indirect flavour processes to propose the convenience of using both $H \to \tau\tau$ and $b \to s\gamma$ as the main processes for narrowing the MSSM parameter space. The viability of finding a Higgs lighter than the one discovered at CERN in 2012 will be discussed in the first paper and we will determine the conditions constraining the MSSM parameter space for finding a second Higgs in the second. In addition, we go futher than looking for a new scalar particle and study an indirect way to discover new physics, the flavor violating decays of the Higgs, that would be a proof of new physics without the need of finding a direct proof of it, just by the contribution the new particles would leave in these processes. This analysis of BSM Higgs phenomenology ends encouraging the building of a new accelerator able to deliver the accuracy needed for measuring these effects.

Regarding neutrino physics, the death of massless neutrinos was endorsed by neutrino oscillations, a phenomenon that granted the 2015 Nobel Prize in Physics to T. Kajita and A.B. McDonald for confirming these oscillations in atmospheric neutrinos [7] and solar neutrinos [8] respectively. Sterile neutrinos are elusive and it is complicated to find direct evidence of their existence, though MiniBooNE [9] excess in $\nu_\mu \to \nu_e$ below 475 MeV and the deficit of $\overline{\nu}_e$ in reactor production suggest that considering a light sterile partner of the SM neutrinos a reality would not be crazy. In addition to these light neutrinos, we have that, for constructing a four-dimensional mass term, heavy right-handed neutrinos are a theoretical requirement. However, the mass scale can be determined (lepton number conservation) or protected (Majorana). The last article of this thesis includes an proposal for

a sterile neutrino dynamics with two generations of right-handed neutrinos that condense in composite scalar bosons below a certain energy scale. The products of this theory, with the successive breakings associated with the appearance of particles at different scales may be of interest for neutrino physics, cosmology, etc.

We cited the Planck at the beginning of this introduction. It was launched with the hope of unveiling several astrophyisical secrets like non-Gaussianities in the primordial perturbations, after the deep study of the Cosmological Microwave Background (CMB). Non-Gaussianities in the CMB are a result that would strongly suggest a multifield inflation scenario. Nevertheless, by the end of Planck's analysis, there has not been a hint of isocurvature non-Gaussianity [10], being greatly constrained. Not completely ruled out, multifield inflation models are not that supported right now, with single field inflation, with its simplest depictions ruled out too, as the main focus of theoretical research. We decided to study the non-Gaussianities produced by a concrete multifield inflation bispectrum but, instead of dedicating to the Planck experiment (which had not delivered any result by that time), we made our analysis for the Large Scale Structure surveys. Studying the errors of the parameters defining the template of the bispectrum, we can forecast how reliable an experimental extimation of them and, in consequence, of the non-Gaussianities, would be.

There have been other experimental sources of interest in Astrophysics recently. In 2014, an unexpected guest retrieved all the attention of the community. BICEP2 claimed to have found the primordial B-mode polarization of the CMB. This result would have supposed both the confirmation for the primordial inflation of the universe and the existence of gravitational waves. Though it eventually was dust (literally), it boosted theoretical research in inflation for some time, and gravitational waves were avenged in 2016.

Some time before that, in September of 2015, the Laser Interferometer Gravitational-Wave Observatory (LIGO) [11] received a gravitational wave signal that came from a Binary Black Hole. The physical event were two black holes merging and transforming the equivalent of three solar masses into gravitational-wave energy. It was a double milestone, since it was the first direct evidence of both the merging and a gravitational wave signal. Of course, this great discovery is more related to Relativity than to Particle Physics, and LIGO will not disclose a quantum nature of gravity, although it gives another tool to physicists, either theoretical or experimental.

It is safe to say that gravitational wave detection will be a main source of interest in the forthcoming years and new interferometers will prove useful for confirming theories that currently may need direct accelerator evidence. As well as the CMB has been a blueprint for determining the evolution of the early universe, many physical phenomena will leave a signal in the gravitational waves spectrum waiting to be found. It seemed appropriate to finish this thesis with an example of this, testing the possibility of finding the signal left from a phase transition matching the potential of our Higgs-like composite neutrino condensate model and showing how convenient could it be to use gravitational waves as a source testing theoretical models indirectly.

Thus, the line of work of this thesis has been the study of phenomenology in the BSM physics framework. As it was stated before, these last years have had plenty of experimental input, and therefore, these articles could be considered as a small review of how to engage testing and putting boundaries to different theories that are amongst the most tracked nowadays, both experimentally and theoretically.

Of course, LHC SUSY searches, inflation, right-handed neutrino physics and gravitational waves phenomenology do not cover the whole landscape of the research being held by the High Energy Physics community, and it would be pretentious to state that this

thesis has the ultimate answer to their phenomenology. It has the humble purpose, beyond giving plausible answers to particular problems, of showing how powerful tools are both direct and indirect measurements, even of fields not directly related, to put boundaries and failproof theories.

Bibliography

[1] P. W. Higgs, Phys. Rev. Lett. **13**, 508 (1964). doi:10.1103/PhysRevLett.13.508

[2] F. Englert and R. Brout, Phys. Rev. Lett. **13**, 321 (1964). doi:10.1103/PhysRevLett.13.321

[3] G. Aad *et* al. [ATLAS Collaboration], Phys. Lett. B **7**16, 1 (2012) doi:10.1016/j.physletb.2012.08.020 [arXiv:1207.7214 [hep-ex]].

[4] S. Chatrchyan *et* al. [CMS Collaboration], Phys. Lett. B **7**16, 30 (2012) doi:10.1016/j.physletb.2012.08.021 [arXiv:1207.7235 [hep-ex]].

[5] G. C. Branco, P. M. Ferreira, L. Lavoura, M. N. Rebelo, M. Sher and J. P. Silva, Phys. Rept. **5**16, 1 (2012) doi:10.1016/j.physrep.2012.02.002 [arXiv:1106.0034 [hep-ph]].

[6] S. P. Martin, Adv. Ser. Direct. High Energy Phys. **2**1, 1 (2010) [Adv. Ser. Direct. High Energy Phys. **1**8, 1 (1998)] doi:10.1142/9789812839657_0001, 10.1142/9789814307505_0001 [hep-ph/9709356].

[7] Y. Fukuda *et* al. [Super-Kamiokande Collaboration], Phys. Rev. Lett. **8**1, 1562 (1998) doi:10.1103/PhysRevLett.81.1562 [hep-ex/9807003].

[8] Q. R. Ahmad *et* al. [SNO Collaboration], Phys. Rev. Lett. **8**9, 011301 (2002) doi:10.1103/PhysRevLett.89.011301 [nucl-ex/0204008].

[9] A. A. Aguilar-Arevalo *et* al. [MiniBooNE Collaboration], Phys. Rev. Lett. **1**05, 181801 (2010) doi:10.1103/PhysRevLett.105.181801 [arXiv:1007.1150 [hep-ex]].

[10] P. A. R. Ade *et* al. [Planck Collaboration], doi:10.1051/0004-6361/201525836 arXiv:1502.01592 [astro-ph.CO].

[11] B. P. Abbott *et* al. [LIGO Scientific and Virgo Collaborations], Phys. Rev. Lett. **1**16, no. 6, 061102 (2016) doi:10.1103/PhysRevLett.116.061102 [arXiv:1602.03837 [gr-qc]].

Eviction of a 125 GeV "heavy"-Higgs from the MSSM

G. Barenboim, C. Bosch, M.L. López-Ibáñez, O. Vives

Abstract

We prove that the present experimental constraints are already enough to rule out the possibility of the ~ 125 GeV Higgs found at LHC being the second lightest Higgs in a general MSSM context, even with explicit CP violation in the Higgs potential. Contrary to previous studies, we are able to eliminate this possibility analytically, using simple expressions for a relatively small number of observables. We show that the present LHC constraints on the diphoton signal strength, $\tau\tau$ production through Higgs and BR($B \to X_s\gamma$) are enough to preclude the possibility of H_2 being the observed Higgs with $m_H \simeq 125$ GeV within an MSSM context, without leaving room for finely tuned cancellations. As a by-product, we also comment on the difficulties of an MSSM interpretation of the excess in the $\gamma\gamma$ production cross section recently found at CMS that could correspond to a second Higgs resonance at $m_H \simeq 136$ GeV.

3.1   Introduction

In July 2012, both ATLAS and CMS, the two LHC general purpose experiments, announced the discovery of a bosonic resonance with a mass ~ 125 GeV that could be interpreted as the expected Higgs boson in the Standard Model (SM) [1, 2]. The observed production cross section and decay channels seem to be consistent, within errors, with a Higgs boson in the SM framework. However, at present, although CMS results are just below SM expectations, ATLAS shows a slight excess in the most sensitive channels that, if confirmed with more precise measurements, could be a sign of new physics beyond the single SM Higgs.

Besides, despite the extraordinary success of the SM in explaining all the experimental results obtained so far, both in the high energy as well as in the low energy region, there is a general belief that the SM is not the ultimate theory, but only a low energy limit of a

more fundamental one. This underling, more fundamental theory is expected to contain new particles and interactions opening new processes not possible in the SM but, above all, it is envisaged to go one step further in the long way to reach a theory which incorporates gravity to our quantum field description of Nature. In such an endeavor, symmetries, who have historically played an important role in our understanding of the laws of Nature, are expected to be a major player. This is one of the reasons why Supersymmetry (SUSY), the only possible extension of symmetry beyond internal Lie symmetries and the Poincare group [3, 4], is arguably the most popular extension of the SM. SUSY is a symmetry between fermions and bosons, and, in its minimal version, the Minimal Supersymmetric Standard Model (MSSM), assigns a supersymmetric partner to each SM particle [5, 6, 7, 8, 9, 10, 11, 12, 4, 5]. These particles must have a mass close to the electroweak scale, if SUSY is to solve the hierarchy problem of the SM. Moreover, the MSSM requires a second Higgs doublet in addition to the single doublet present in the SM and, therefore, Higgs phenomenology in the MSSM is much richer than the SM, with three neutral-Higgs states and a charged Higgs in the spectrum [16].

At tree level, the scalar potential of the MSSM is CP-conserving, and therefore mass eigenstates are also CP eigenstates. We have two neutral scalar bosons, h and H, and a neutral pseudoscalar, A. However, the MSSM contains several CP violating phases beyond the single SM phase in the CKM matrix[1], *e.g.* $M_i, i = 1, 2, 3$, A_t, μ are complex parameters, and then CP violation necessarily leaks into the Higgs sector at one-loop level [33, 32, 35, 41]. As a result, loop effects involving the complex parameters in the Lagrangian violate the tree-level CP-invariance of the MSSM Higgs potential modifying the tree-level masses, couplings, production rates and decay widths of Higgs bosons [35, 36, 37, 38, 21, 22]. In particular, the clear distinction between the two CP-even and the one CP-odd neutral boson is lost and the physical Higgs eigenstates become admixtures of CP-even and odd states. Therefore, significant deviations from the naive CP conserving scenario can be obtained in the regime where $M_{H^\pm}$ is low and Im (μA_t) is significant. Yet, the size of SUSY phases is strongly constrained by searches of electric dipole moments (EDM) of the electron and neutron. The phase of μ is bounded to be miserably small, $\lesssim 10^{-2}$, by the upper limits on EDMs if sfermion masses are below several TeV. Bounds on the phases of $A_{e,d,u}$, although somewhat weaker, are also strong, $\lesssim 10^{-1}$, under the same conditions. However, the phases of third generation trilinear couplings $A_{t,b,\tau}$ can still be sizeable[2] for soft masses $O(1 \text{ TeV})$ and, due to the large Yukawa couplings, these are precisely the couplings that influence the scalar potential more strongly [28]. In this work, we will take only third-generation trilinear couplings $A_{t,b,\tau}$ as complex to generate the scalar-pseudoscalar mixing in the Higgs potential.

Among all the possibilities opened up by this scenario, one particularly interesting is the case where the scalar observed at LHC is not the lightest but the second lightest one, having the lightest escaped detection at LEP/Tevatron/LHC due to its pseudoscalar or down-type content. As a result of the mixing, the couplings $H_1 - WW$, $H_1 - ZZ$ and $H_1 - t\bar{t}$ all get reduced simultaneously evading the current bounds. This idea of course is not new. Many studies have been carried out within this model [24, 33, 25, 26, 27, 28, 29, 30]. There are two public codes, CPsuperH [57, 68], specifically developed to analyze the Higgs phenomenology in the MSSM with explicit CP violation, and FeynHiggs [39, 40], that also calculates the spectrum and decay widths of the Higgses in the Complex MSSM. By using

---

[1]It is well-known that a single CKM phase is not enough to explain the observed matter-antimatter asymmetry of the universe. Additional phases (and therefore new physics) are required for that.

[2]These phases enter EDMs of the electron and proton at two loops through Barr-Zee diagrams[25, 26]. However, these contributions are suppressed for heavy squarks[27].

them, different regions of the parameters space have been explored through giant scans following the results of the colliders.

In this work, we will explore a different path. We will study this scenario, not by scanning its parameters space but rather by choosing a pair of key experimental signatures from both, high and low energy experiments, and analyzing (analytically or semi-analytically) whether their results can be simultaneously satisfied. This way we gain understanding on the physics of the model we are discussing and at the same time avoid the possibility of missing a fine-tuned region in the parameter space (even tiny to the point of being microscopic) where an unexpected cancellation or a lucky combination might occur. After all, whatever physics hides so effectively behind the SM will turn out to be just one point in our studies of the parameter space. In this sense it is clear that every region, independently of its size, has the same probability of being the right one and should be given enough attention.

Moreover, our analysis is performed in terms of the SUSY parameters at the electroweak scale, such that it encloses all possible MSSM setups (including explicit CP violation), as the CMSSM, NUHM, pMSSM or even a completely generic MSSM[41, 42, 43, 44, 45, 25, 46]. In fact, only a handful of MSSM parameters affect the Higgs sector and low-energy experiments that we study. As we will see, in the Higgs sector, we fix $m_{H_1} \leq m_{H_2} \simeq 125$ GeV $\leq m_{H_3} \simeq m_{H^\pm} \lesssim$ 200–220 GeV and use the experimental results to look for acceptable, 3×3, Higgs mixing matrices as a function of $\tan \beta$. Supersymmetric parameters affecting the Higgs sector, and also the indirect processes $B \to X_s \gamma$ and $B_s \to \mu^+ \mu^-$, are basically third generation masses and couplings, and gaugino masses. In our analysis, these parameters take general values consistent with the experimental constraints on direct and indirect searches.

This paper is organized as follows. We begin by summarizing the experimental situation in Section 3.2. In Section 7.2 we describe the basic ingredients of the model and analyze the direct and indirect signatures we will choose for our study. The parameter space is surveyed in Section 3.4 and results and conclusions are contained in Section 3.5.

3.2 Current experimental status.

3.2.1 Higgs signal at the LHC.

Both ATLAS and CMS experiments have recently updated the analysis of the Higgs-like signal using the full pp collision data sample. The ATLAS analysis [5] uses integrated luminosities of 4.8 fb^{-1} at $\sqrt{s} =$7 TeV plus 20.7 fb^{-1} at $\sqrt{s} =$8 TeV, for the most sensitive channels, $H \to \gamma\gamma$, $H \to ZZ^* \to 4l$ and $H \to WW^* \to l\nu l\nu$, plus 4.7 fb^{-1} at $\sqrt{s} =$7 TeV and 13 fb^{-1} at $\sqrt{s} =$8 TeV for the $H \to \tau\tau$ and $H \to b\bar{b}$. Similarly CMS study [4] uses 5.1 fb^{-1} at $\sqrt{s} =$7 TeV and 19.8 fb^{-1} at $\sqrt{s} =$8 TeV in all these channels.

The main channels contributing to the observed signal are the decays into photons and two Z-bosons. On the other hand, the most relevant channel constraining the presence of additional Higgs-bosons is the decay into two τ leptons. ATLAS and CMS agree on the mass of the observed state which is $m_h = 124.3 \pm 0.6$(stat)± 0.4(sist) GeV for ATLAS and $m_h = 125.7 \pm 0.3$(stat) ± 0.3(sist) GeV for CMS.

However, there are some differences on the signal strength in the different channels as measured by the two experiments. The signal strength μ_X, for a Higgs decaying to X is defined as,

$$\mu_X = \frac{\sigma(pp \to H) \times \text{BR}(H \to X)}{\sigma(pp \to H)_{\text{SM}} \times \text{BR}(H \to X)_{\text{SM}}}, \tag{3.1}$$

(a)   (b)
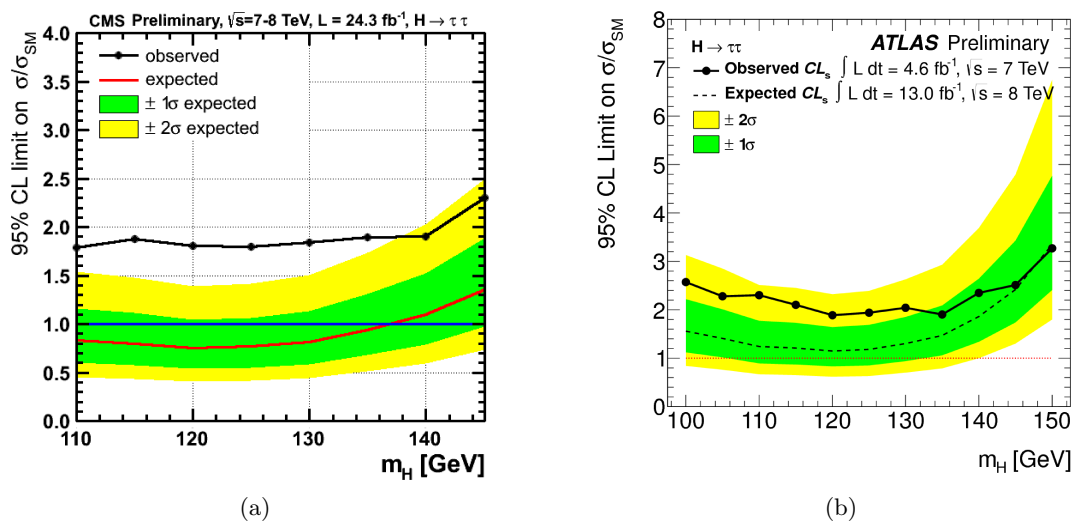
Figure 3.1: Higgs searches in the $H \to \tau\tau$ channel for $100 \text{ GeV} \le m_H \le 150 \text{ GeV}$ at CMS (a) and ATLAS (b).

such that $\mu = 0$ corresponds to the background-only hypothesis and $\mu = 1$ corresponds to a SM Higgs signal. The combined signal strength in the last results presented by ATLAS is $\mu^{\text{ATLAS}} = 1.3 \pm 0.2$ [3], while the signal strength measured by CMS is slightly below the SM expectations $\mu^{\text{CMS}} = 0.80 \pm 0.14$ [4].

For the diphoton channel, the measured signal strength in both experiments are $\mu_{\gamma\gamma}^{\text{ATLAS}} = 1.6 \pm 0.3$ and $\mu_{\gamma\gamma}^{\text{CMS}} = 0.78_{-0.26}^{+0.28}$. This signal is consistent with the SM, although ATLAS points to a slight excess over the SM expectations. In any case, both results agree on the fact that the diphoton signal must be of the order of the SM prediction. This fact is very important in the context of multi-Higgs models, as the MSSM, where the Higgs couplings to down quark and charged leptons are enhanced by additional $\tan\beta$ factors, which tend to decrease the $H \to \gamma\gamma$ branching ratio and therefore the signal strength. In this regard, here we will adopt a conservative approach and impose the weighted average of ATLAS and CMS results at 2σ,

$$0.75 \le \mu_{\gamma\gamma}^{\text{LHC}} \le 1.55 \,. \tag{3.2}$$

Similarly, the signal strength in the $H \to ZZ^*$ channel are, $\mu_{ZZ^*}^{\text{ATLAS}} = 1.5 \pm 0.4$ and $\mu_{ZZ^*}^{\text{CMS}} = 0.92 \pm 0.28$ and we will also use as a constraint,

$$0.78 \le \mu_{ZZ^*}^{\text{LHC}} \le 1.58 \,. \tag{3.3}$$

The main constraint on the presence of additional heavy Higgs states comes from the $H/A \to \tau\tau$ searches at ATLAS and CMS experiments. In this case, both experiments have searched for the SM Higgs boson decaying into a pair of τ-leptons and this provides a limit on $\sigma(pp \to H) \times \text{BR}(H \to \tau\tau)$ that can be applied to the extra Higgs states. ATLAS has analyzed the collected data samples of $4.6 \, \text{fb}^{-1}$ at $\sqrt{s} = 7$ TeV and $13.0 \, \text{fb}^{-1}$ at $\sqrt{s} = 8$ TeV [45] while CMS used $4.9 \, \text{fb}^{-1}$ at $\sqrt{s} = 7$ TeV and $19.4 \, \text{fb}^{-1}$ at $\sqrt{s} = 8$ TeV for Higgs masses up to 150 GeV [46]. These constraints on the $\tau\tau$-cross section normalized to the SM cross section as a function of the Higgs mass are shown in Figure 3.1. In this case, CMS sets the strongest bound for m_H below 150 GeV. For $m_H = 110$ GeV we obtain a bound at 95% CL of $\mu_{\tau\tau} = \sigma(H \to \tau\tau)/\sigma_{SM} \le 1.8$, and this limit remains nearly constant, $\mu_{\tau\tau} \le 2.0$,
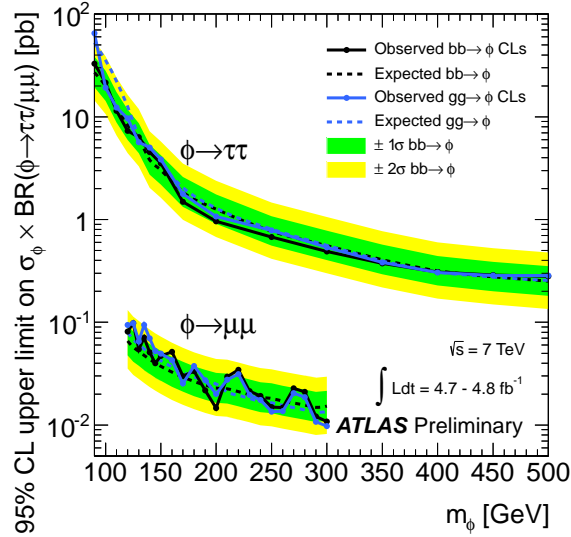
Figure 3.2: Upper limit on the $\tau\tau$ production cross section through heavy Higgs states from ATLAS with 4.8 fb^{-1} at $\sqrt{s} = 7$ TeV .

up to $m_H = 140$ GeV. For a neutral Higgs of mass $m_H = 150$ GeV we would have a bound of $\mu_{\tau\tau} \leq 2.3$. In our scenario, this limit would apply to H_1 with a mass below 125 GeV and to H_2 with $m_{H_2} \simeq 125$ GeV. In the case of H_3, this bound applies for masses below 150 GeV.

For heavier H_3 masses, there exist a previous analysis at LHC searching MSSM Higgs bosons with masses up to 500 GeV. In Figure 3.2, we present the analysis made in ATLAS with 4.9 fb^{-1} at $\sqrt{s} =$7 TeV [52]. In this case, the bound is presented as an upper limit on the $\tau\tau$, or $\mu\mu$ production cross section. As a reference, the SM cross section for a Higgs mass of 150 GeV is $\sigma(pp \to H)_{\rm SM} \times {\rm BR}(H \to X)_{\rm SM} \simeq 0.25$ pb and therefore, comparing with Figure 3.1, we can expect this bound to improve nearly an order of magnitude in an updated analysis with the new data [48]. Nevertheless, the production cross-section of τ-pairs through a heavy Higgs is enhanced by powers of $\tan\beta$ and therefore the present limits on $\sigma_\phi \times {\rm BR}(\phi \to \tau\tau)$ are already very important in the medium–large $\tan\beta$ region.

Finally, we include the bounds on charged Higgs produced in $t \to H^+ b$ with subsequent decay $H^+ \to \tau\nu$ [54, 55]. These analysis set upper bounds on $B(t \to H^+ b)$ in the range 2–3 % for charged Higgs bosons with masses between 80 and 160 GeV, under the assumption that $B(H^+ \to \tau^+\nu_\tau) = 1$, which is a very good assumption unless decay channels to the lighter Higgses and W-bosons are kinematically opened.

3.2.2   MSSM searches at LHC.

Simultaneously to the Higgs searches described above, LHC has been looking for signatures on new physics beyond the SM. A large effort has been devoted to search for Supersymmetric extensions of the SM. These studies, focused in searches of jets or leptons plus missing energy (possible evidence of the LSP), agree, so far, with the Standard Model expectations in all the explored region, and are used to set bounds on the mass of the supersymmetric particles.

The most stringent constraints from LHC experiments are set on gluinos and first generation squarks produced through strong interactions in pp collisions. Searches of

gluinos at CMS[56, 57, 58, 59] and ATLAS [60, 61] with ~ 20 fb^{-1} at 8 TeV have driven, roughly, to the exclusion of gluino masses up to 1.3 TeV for (neutralino) LSP masses below 500 GeV. The limits on first generation squarks directly produced are $m_{\tilde{q}} \gtrsim 740$ GeV for squarks decaying $\tilde{q} \to q\chi_1^0$ with $m_{\chi_1^0} = 0$ GeV[62][3].

The most important players in Higgs physics, because of their large Yukawa couplings, are third generation squarks. In this case mass bounds, from direct stop production, are somewhat weaker but still stop masses are required to be above ~ 650 GeV for $m_{\chi^0} \lesssim$ 200 GeV [63, 64, 65, 66] with the exception of small regions of nearly degenerate stop-neutralino. Limits on sbottom mass from direct production are also similar and sbottom masses up to 620 GeV are excluded at 95% C.L. for $m_{\chi^0} < 150$ GeV, with the exception of $m_{\tilde{b}_1} - m_{\chi^0} < 70$ GeV [65, 62, 59].

Finally, ATLAS and CMS have presented the limits on chargino masses from direct EW production [67, 68]. In both analysis, these limits depend strongly on the slepton masses and the branching ratios of chargino and second neutralino that are supposed to be degenerate. When the decays to charged sleptons are dominant, chargino masses are excluded up to ~ 600 GeV for large mass differences with χ^0. Even in the case when the slepton channels are closed, decays to weak bosons plus lightest neutralino can exclude[4] chargino masses up to ~ 350 GeV for $m_{\chi_1^0} \lesssim 120$ GeV.

Therefore, as we have seen, limits on SUSY particles from LHC experiments are already very strong with the exceptions of sparticle masses rather degenerate with the lightest supersymmetric particle.

3.2.3 Indirect bounds

Indirect probes of new physics in low energy experiments still play a very relevant role in the search for extensions of the SM [70, 71, 72]. Even in the absence of new flavour structures beyond the SM Yukawa couplings, in a Minimal Flavour Violation scheme, decays like $B_s^0 \to \mu^+\mu^-$ and, specially, $B \to X_s\gamma$ play a very important role, as we will see below, and put significant constraints for the whole $\tan\beta$ range.

The present experimental bounds on the decay $B_s^0 \to \mu^+\mu^-$ are obtained from LHCb measurements with 1.1 fb^{-1} of proton-proton collisions at $\sqrt{s} = 8$ TeV and 1.0 fb^{-1} at $\sqrt{s} = 7$ TeV. The observed value for the branching ratio at LHCb [73, 74] is,

$$\text{BR}\left(B_s^0 \to \mu^+\mu^-\right) = \left(2.9^{+1.1}_{-1.0}\right) \times 10^{-9}\,, \tag{3.4}$$

and at CMS [75],

$$\text{BR}\left(B_s^0 \to \mu^+\mu^-\right) = \left(3.0^{+1.0}_{-0.9}\right) \times 10^{-9}\,, \tag{3.5}$$

The limits on the decay $B \to X_s\gamma$ come from the BaBar and Belle B-factories and CLEO [76, 77, 78, 79, 80, 81]. The current world average for $E_\gamma > 1.6$ GeV given by HFAG [82, 83] is,

$$\text{BR}\left(B \to X_s\gamma\right) = (3.43 \pm 0.21 \pm 0.07) \times 10^{-4}\,. \tag{3.6}$$

We will see that this result provides a very important constraint on the charged Higgs mass in the low $\tan\beta$ region where other supersymmetric contributions are small.

---

[3]Limits on masses could be softer if these squarks are nearly degenerate with the LSP, but this does not affect our analysis below

[4]As pointed out in Ref. [69], these bounds with the slepton channel closed are only valid in a simplified model that assumes BR($\chi_2^0 \to Z\chi_1^0$)=1. This bound is strongly relaxed once the decay $\chi_2^0 \to h\chi_1^0$ is included. However, in our paper, this limit is only taken into account as a reference value for chargino masses and has no effect in our analysis of the feasibility of this scenario.

3.3 Theoretical model

As explained in the introduction, we intend to investigate whether the observed Higgs particle of $m_H \simeq 125$ GeV could correspond to the second Higgs in a general MSSM scenario, while the lightest Higgs managed to evade the LEP searches [24, 33, 25, 26, 27, 28, 29, 30]. The scenario we consider here is a generic MSSM defined at the electroweak scale. This means we do not impose the usual mass relations obtained through RGE from a high scale, that we obtain, for instance in the Constrained MSSM (CMSSM), but keep all MSSM parameters as free and independent at M_W. Furthermore, we are mainly interested in the Higgs sector of the model, which we analyze assuming generic Higgs masses and mixings in the presence of CP violation in the squark sector.

3.3.1 CP-violating MSSM Higgs sector

As it is well-known, the Higgs sector of the MSSM consists of a type II two-Higgs doublet model. In the MSSM, the scalar potential conserves CP at tree-level [16]. Nevertheless, in the presence of complex phases in the Lagrangian, CP violation enters the Higgs potential at the one-loop level, resulting in the mixing between the CP-even and CP-odd Higgses. Then, after electroweak symmetry breaking, we have three physical neutral scalar bosons, admixtures of the scalar and pseudoscalar Higgs bosons, plus a charged Higgs boson [33, 32, 35, 41].

The Higgs fields in the electroweak vacuum, with vevs v_1 and v_2 and $\tan\beta = v_2/v_1$, are

$$\Phi_1 = \begin{pmatrix} \frac{1}{\sqrt{2}} \left(v_1 + \phi_1 + i a_1 \right) \\ \phi_1^- \end{pmatrix} ; \quad \Phi_2 = e^{i\xi} \begin{pmatrix} \phi_2^+ \\ \frac{1}{\sqrt{2}} \left(v_2 + \phi_2 + i a_2 \right) \end{pmatrix} , \tag{3.7}$$

and, as mentioned above, the presence of CP-violating phases in the Lagrangian introduces off-diagonal mixing terms in the neutral Higgs mass matrix. In the weak basis, (ϕ_1, ϕ_2, a), with $\phi_{1,2}$ CP-even, scalar, and $a = a_1 \sin\beta + a_2 \cos\beta$ the CP-odd, pseudoscalar state, we write the neutral Higgs mass matrix as [35, 36, 38, 42],

$$M_H^2 = \begin{pmatrix} M_S^2 & M_{SP}^2 \\ M_{PS}^2 & M_P^2 \end{pmatrix} , \tag{3.8}$$

where the scalar-pseudoscalar mixings are non-vanishing in the presence of phases, M_{SP}^2, $M_{PS}^2 \propto \text{Im} \left[\mu A_{t,b} e^{i\xi} \right]$. Then, this 3×3 neutral Higgs mass matrix is diagonalized by

$$\mathcal{U} \cdot M_H^2 \cdot \mathcal{U}^T = \text{Diag} \left(m_{H_1}^2, m_{H_2}^2, m_{H_3}^2 \right) . \tag{3.9}$$

The Higgs sector of the MSSM is defined at the electroweak scale at tree-level by only two parameters that, in the limit of CP-conservation, are taken as $\left(m_A^2, \tan\beta \right)$. In the complex MSSM, the pseudoscalar Higgs is not a mass eigenstate and its role as a parameter defining the Higgs sector is played by the charged Higgs mass $m_{H^\pm}^2$. At higher orders, the different MSSM particles enter in the Higgs masses and mixings, although the main contributions are due to the top-stop and bottom–sbottom sectors. It is well-known that the one-loop corrections to M_S^2 can increase the lightest Higgs mass from $\lesssim M_Z$ to ~ 130 GeV [85, 86, 87], hence being $\lesssim M_Z$, with the leading part of order [88, 89],

$$\delta M_S^2 \simeq \frac{3 m_t^4}{2\pi^2 v^2 \sin^2\beta} \left[\log \frac{M_{SUSY}^2}{m_t^2} + \frac{X_t^2}{M_{SUSY}^2} \left(1 - \frac{X_t^2}{12 M_{SUSY}^2} \right) \right] , \tag{3.10}$$

with M_{SUSY} the geometric mean of the two stop masses and $X_t = A_t - \mu \cot\beta$.

Regarding the charged Higgs mass, we can relate it to the pseudoscalar mass M_P^2 in the neutral Higgs mass matrix [35],

$$M_{H^\pm}^2 = M_P^2 + \frac{1}{2}\lambda_4 v^2 - \mathrm{Re}\left(\lambda_5 e^{2i\xi}\right) v^2 , \qquad (3.11)$$

with $\lambda_{4,5}$ the two-loop corrected parameters of the Higgs potential [90, 35]. At tree level $\lambda_4 = g_w^2/2$, such that $\lambda_4 v^2/2 = M_W^2$, and $\lambda_5 = 0$. In any case, it looks reasonable to expected $\lambda_i \lesssim 1$. This implies that the squared charged Higgs mass can never be heavier that the largest neutral Higgs eigenvalue by a difference much larger than M_Z^2, which is equivalent to say that loop corrections are of the same order as $\sim \delta M_S^2$.

Similarly, we can expect the mass of the second neutral Higgs, which in our scenario is $m_{H_2} \simeq 125$ GeV, only to differ from the heavier eigenvalue by terms of order v^2. This can be seen from the trace of the neutral Higgs masses in the basis of CP eigenstates, where we would have, without loop corrections, $\mathrm{Tr}\left(M_H^2\right) = 2M_P^2 + M_Z^2$. As we have seen, loop corrections to the diagonal elements can be expected to be of the order of the corrections to the lightest Higgs mass which are also $O(M_Z^2)$. To obtain a light second Higgs we need, either low M_P or a large scalar-pseudoscalar mixing. The different contributions to scalar-pseudoscalar mixing, M_{SP}^2, are of order [35],

$$M_{SP}^2 = O\left(\frac{m_t^4 |\mu| |A_t|}{32\pi^2 \ v^2 M_{SUSY}^2}\right) \sin\phi_{CP} \times \left[6, \frac{|A_t|^2}{M_{SUSY}^2}, \frac{|\mu|^2}{\tan\beta M_{SUSY}^2}\right] , \qquad (3.12)$$

which again are of the same order as $\delta M_S^2 \simeq O(M_Z^2)$ for $\sin\phi_{CP} \sim O(1)$. Therefore, taking also into account that in the decoupling limit, and in the absence of scalar-pseudoscalar mixing, $M_H \simeq M_P$, we must require M_P^2 not to be much larger than M_Z^2. Taking $M_P^2 \lesssim 3M_Z^2$, the invariance of the trace tells us that $m_{H_1}^2 + m_{H_2}^2 + m_{H_3}^2 = 2M_P^2 + M_Z^2 + O(M_Z^2)$ in such a way that with 90 GeV $\lesssim m_{H_1} \lesssim m_{H_2} \simeq 125$ GeV, we get an upper limit[5] for $m_{H_3}^3 \lesssim 2M_P^2 + 2M_Z^2 - \left(m_{H_2}^2 + m_{H_1}^2\right) \lesssim (200 \text{ GeV})^2$. We must emphasize that in this work we do not consider the possibility of $m_{H_1} \lesssim 90$ GeV which would be possible in the presence of large CP-violating phases that could reduce the mass of the lightest Higgs through rather precise cancellations [91, 58]. Although this scenario could survive LEP limits around an "open hole" with $m_{H_1} \approx 45$ GeV and $\tan\beta \approx 8$ [93], it would never be able to reproduce the observed signal in $H_2 \to \gamma\gamma$, as the opening of the decay channel $H_2 \to H_1 H_1$ would render $B(H_2 \to \gamma\gamma)$ much smaller than the SM one (see the discussion related to the $H_2 \to b\bar{b}$ channel below).

In the following analysis of the direct and indirect constraints on the Higgs sector, we try to be completely general in the framework of a Complex MSSM defined at the electroweak scale. To attain this objective, and taking into account that the presence of CP violation and large radiative corrections strongly modifies the neutral Higgs mass matrix if we are outside the decoupling regime, we consider general neutral Higgs mixings and masses. In fact, in this work, we analyze the situation in which the second lightest neutral boson corresponds to the scalar resonance measured at LHC with a mass of 125 GeV. As we have seen, to achieve this, we need a relatively light charged Higgs (with approximately $M_{H^+} \lesssim 220$ GeV), and a similar mass for the heaviest neutral Higgs. The lightest neutral Higgs boson will have a mass varying in the range of 90 and 125 GeV. After fixing the Higgs masses in these ranges, we will consider generic mixing matrices $\mathcal{U}$ and look for mixings consistent with the present experimental results.

---

[5]Allowing the heaviest neutral Higgs to be 200 GeV with a second-heaviest Higgs of 125 GeV is a very conservative assumption. However, it looks very difficult to have such a heavy Higgs in any realistic MSSM construction.

$\mathbf{H_a \to f\bar{f}}$	$\mathbf{g_f}$	$\mathbf{g_{S,a}^{(0)}}$	$\mathbf{g_{P,a}^{(0)}}$
$H_a \to l\bar{l}$	$\frac{gm_l}{2M_W}$	$\frac{U_{a1}}{\cos(\beta)}$	$-\left(\frac{\sin(\beta)}{\cos(\beta)}\right)U_{a3}$
$H_a \to d\bar{d}$	$\frac{gm_d}{2M_W}$	$\frac{U_{a1}}{\cos(\beta)}$	$-\left(\frac{\sin(\beta)}{\cos(\beta)}\right)U_{a3}$
$H_a \to u\bar{u}$	$\frac{gm_u}{2M_W}$	$\frac{U_{a2}}{\sin(\beta)}$	$-\left(\frac{\cos(\beta)}{\sin(\beta)}\right)U_{a3}$
$H_a \to \tilde{\chi}_i^+ \tilde{\chi}_j^-$	$\frac{g}{\sqrt{2}}$	$g_s^{\tilde{\chi}^+}$	$g_p^{\tilde{\chi}^+}$

Table 3.1: Tree level Higgs–fermion couplings.

This analysis deals with the decays of the neutral Higgs bosons. Thus we need the Higgs couplings to the SM vector boson, fermions, scalars and gauginos. The conventions used in the following are described in Appendix 3.A. The couplings to the vector bosons are [57],

$$\mathcal{L}_{H_a V} = g\,M_W \left(W_\mu^+ W^{-\,\mu} + \frac{1}{2\cos^2\theta_W} Z_\mu Z^\mu \right) \sum_a g_{H_a VV}\,H_a\,. \tag{3.13}$$

with $g_{H_a VV} = \cos\beta\,\mathcal{U}_{a1} + \sin\beta\,\mathcal{U}_{a2}$.

The Lagrangian showing the fermion–Higgs couplings is

$$\mathcal{L}_{H_a f} = -\sum_f \frac{g\,m_f}{2M_W} \sum_a H_a \bar{f}\left(g_{S,a}^f + ig_{P,a}^f \gamma_5\right) f\,, \tag{3.14}$$

where the tree-level values of $(g_S^{(0)}, g_P^{(0)})$ are given in Table 3.1. Still, in the case of third generation fermions, these couplings receive very important threshold corrections due to gluino and chargino loops enhanced by $\tan\beta$ factors in the case of the down-type fermions [44, 46, 45, 52, 6, 8, 10, 56, 13]. The complete corrected couplings for third generation fermions, (g_S^f, g_P^f), can be found in Ref. [57, 58]. In our analysis, it is sufficient to consider the correction to the bottom couplings,

$$\begin{aligned} g_{S,a}^d =&\,\mathrm{Re}\left(\frac{1}{1+\kappa_d \tan\beta}\right)\frac{\mathcal{U}_{a1}}{\cos\beta} + \mathrm{Re}\left(\frac{\kappa_d}{1+\kappa_d \tan\beta}\right)\frac{\mathcal{U}_{a2}}{\cos\beta} \\ &+ \mathrm{Im}\left(\frac{\kappa_d\left(\tan^2\beta+1\right)}{1+\kappa_d \tan\beta}\right)\mathcal{U}_{a3} \end{aligned} \tag{3.15}$$

$$\begin{aligned} g_{P,a}^d =&-\mathrm{Re}\left(\frac{\tan\beta - \kappa_d}{1+\kappa_d \tan\beta}\right)\mathcal{U}_{a3} + \mathrm{Im}\left(\frac{\kappa_d \tan\beta}{1+\kappa_d \tan\beta}\right)\frac{\mathcal{U}_{a1}}{\cos\beta} \\ &-\mathrm{Im}\left(\frac{\kappa_d}{1+\kappa_d \tan\beta}\right)\frac{\mathcal{U}_{a2}}{\cos\beta} \end{aligned} \tag{3.16}$$

where $\kappa_d = (\Delta h_d/h_d)/(1 + \delta h_d/h_d)$ and the corrected Yukawa couplings are,

$$h_d = \frac{\sqrt{2}m_d}{v\cos\beta}\,\frac{1}{1 + \delta h_d/h_d + \Delta h_d/h_d \tan\beta}\,, \tag{3.17}$$

$$\delta h_d/h_d \ = \ -\frac{2\alpha_s}{3\pi}m_{\tilde{g}}^* A_d\, I(m_{\tilde{d}_1}^2, m_{\tilde{d}_2}^2, |m_{\tilde{g}}|^2) - \frac{|h_u|^2}{16\pi^2}|\mu|^2\, I(m_{\tilde{u}_1}^2, m_{\tilde{u}_2}^2, |\mu|^2)$$

$$\Delta h_d/h_d \ = \ \frac{2\alpha_s}{3\pi}m_{\tilde{g}}^* \mu^*\, I(m_{\tilde{d}_1}^2, m_{\tilde{d}_2}^2, |m_{\tilde{g}}|^2) + \frac{|h_u|^2}{16\pi^2}A_u^* \mu^*\, I(m_{\tilde{u}_1}^2, m_{\tilde{u}_2}^2, |\mu|^2)\,,$$

$$\tag{3.18}$$

and the loop function $I(a, b, c)$ is given by,

$$I(a, b, c) = \frac{a\, b\log(a/b) + b\, c\log(b/c) + a\, c\log(c/a)}{(a-b)(b-c)(a-c)}\,. \tag{3.19}$$

The Higgs-sfermion couplings are,

$$\mathcal{L}_{H_a \tilde{f}\tilde{f}} = \upsilon \sum_{\tilde{f}} g_{\tilde{f}\tilde{f}}^a \left(H_a \tilde{f}^* \tilde{f} \right)\,, \tag{3.20}$$

$$\upsilon\, g_{\tilde{f}_i \tilde{f}_j}^a = \left(\tilde{\Gamma}^{\alpha ff} \right)_{\beta\gamma} \mathcal{U}_{a\alpha}\, \mathcal{R}_{\beta i}^f \mathcal{R}_{\gamma j}^f\,, \tag{3.21}$$

with $\beta, \gamma = L, R$, $\mathcal{R}^f$, the sfermion mixing matrices and the couplings $\tilde{\Gamma}^{\alpha ff}$ given Ref. [57]. Other Higgs couplings that are needed to analyze the neutral Higgs decays are the couplings to charginos and charged Higgs, complete expressions can be found in Ref. [57] (taking into account their different convention on the Higgs mixing matrix, $\mathcal{U} = \mathcal{O}^T$).

After defining all these couplings, we show in the following the expressions for $H \to \gamma\gamma$ and $H \to gg$, that together with $H \to \bar{b}b, \tau\tau$ and $H \to WW^*, ZZ^*$ are the main Higgs decay channels for $m_H = 125$ GeV, and the Higgs production mechanisms at LHC.

3.3.2 Higgs decays.

3.3.2.1 Higgs decay into two photons.

The decay $H_a \to \gamma\gamma$ occurs only at the one-loop level and therefore we must include every contribution generated by sparticles in addition to the SM ones in our calculation. Taking into account the presence of CP violation, the Higgs decay has contributions of both the scalar and pseudoscalar components. Then its width becomes,

$$\Gamma\left(H_a \to \gamma\gamma\right) = \frac{M_{H_a}^3 \alpha^2}{256\pi^3 \upsilon^2} \left[|S_a^\gamma\left(M_{H_a}\right)|^2 + |P_a^\gamma\left(M_{H_a}\right)|^2 \right]\,, \tag{3.22}$$

where the scalar part is $S_a^\gamma\left(M_{H_a}\right)$ and the pseudoscalar $P_a^\gamma\left(M_{H_a}\right)$ and they are [57],

$$S_a^\gamma\left(M_{H_a}\right) \ = \ 2 \sum_{f=b,t,\tilde{\chi}_1^\pm,\tilde{\chi}_2^\pm} N_C\, J_f^\gamma\, Q_f^2 g_f\, g_{H_a \bar{f}f}^S \frac{\upsilon}{m_f} F_f^S\left(\tau_{af}\right)$$

$$-\sum_{\tilde{f}} N_C\, J_{\tilde{f}}^\gamma\, Q_f^2\, g_{H_a \tilde{f}_j \tilde{f}_j^*}^S \frac{\upsilon^2}{2m_{\tilde{f}_j}^2} F_0\left(\tau_{a\tilde{f}_j}\right)$$

$$-g_{H_a VV} F_1\left(\tau_{aW}\right) \ - \ g_{H_a H^- H^+} \frac{\upsilon^2}{2M_{H_a}^2} F_0\left(\tau_{aH}\right) \tag{3.23}$$

$$P_a^\gamma\left(M_{H_a}\right) \ = \ 2 \sum_{f=b,t,\tilde{\chi}_1^\pm,\tilde{\chi}_2^\pm} N_C\, J_f^\gamma\, Q_f^2 g_f\, g_{H_a \bar{f}f}^P \frac{\upsilon}{m_f} F_f^P\left(\tau_{af}\right) \tag{3.24}$$

With $\tau_{aj} = M_{H_a}^2/(4m_i^2)$ and the loop functions being:

$$F_f^S\left(\tau\right) = \tau^{-1}\left[1 + \left(1 - \tau^{-1}\right)f\left(\tau\right)\right]\,; \quad F_f^P\left(\tau\right) = \tau^{-1}f\left(\tau\right)\,;$$
$$F_0\left(\tau\right) = \tau^{-1}\left[-1 + \tau^{-1}f\left(\tau\right)\right]\,; \quad F_1\left(\tau\right) = 2 + 3\tau^{-1} + 3\tau^{-1}\left(2 - \tau^{-1}\right)f\left(\tau\right)\,; \tag{3.25}$$

$$f(\tau) = -\frac{1}{2}\int_0^1 \frac{dx}{x}\ln[1-4\tau x(1-x)] = \begin{cases} \arcsin^2(\sqrt{\tau}) : & \tau \leq 1 \\ \\ -\frac{1}{4}\left[\ln\left(\frac{\sqrt{\tau}+\sqrt{\tau-1}}{\sqrt{\tau}-\sqrt{\tau-1}}\right)-i\pi\right]^2 : & \tau \geq 1 \end{cases} \tag{3.26}$$

And we included the QCD corrections [103, 104],

$$J_\chi^\gamma = 1; \ J_q^\gamma = 1 - \frac{\alpha_s(M_{H_a}^2)}{\pi}; \qquad J_{\tilde{q}}^\gamma = 1 + \frac{\alpha_s(M_{H_a}^2)}{\pi} \tag{3.27}$$

3.3.2.2 Higgs decay into two gluons.

Similarly, the decay width for $H_a \to gg$ is given by:

$$\Gamma_{H_a \to gg} = \frac{M_{H_a}^2 \alpha_s^2}{32\pi^3 v^2}\left[K_H^g |S_a^g|^2 + K_A^g |P_a^g|^2\right] \tag{3.28}$$

where $K_{H,A}^g$ is again the QCD correction enhancement factor while S_a^g and P_a^g are the scalar and pseudoscalar form factors, respectively. $K_{H,A}^g$ is [103, 104],

$$K_H^g = 1 + \frac{\alpha_s(M_{H_a}^2)}{\pi}\left(\frac{95}{4}-\frac{7}{6}N^F\right), \qquad K_A^g = 1 + \frac{\alpha_s(M_{H_a}^2)}{\pi}\left(\frac{97}{4}-\frac{7}{6}N^F\right), \tag{3.29}$$

being N^F the number of quark flavours that remains lighter than the Higgs boson in consideration. On the other hand, the expressions that define S_a^g and P_a^g are:

$$S_a^g = \sum_{f=b,t} g_f\, g_{sff}^a \frac{v}{m_f}F_f^S(\tau_{af}) \ - \ \sum_{\tilde{f}_i=\tilde{b}_1,\tilde{b}_2,\tilde{t}_1,\tilde{t}_2} g_{\tilde{f}\tilde{f}}^a \frac{v^2}{4m_{\tilde{f}_i}^2}F_0(\tau_{a\tilde{f}_i}) \tag{3.30}$$

$$P_a^g = \sum_{f=b,t} g_f\, g_{pff}^a \frac{v}{m_f}F_f^P(\tau_{af}) \tag{3.31}$$

3.3.3 Higgs production.

The Higgs production processes are basically the same as in the SM [105, 16], although the couplings in these processes change to the MSSM couplings. The two main production processes are gluon fusion and, specially for large $\tan\beta$, the $b\bar{b}$ fusion. Other production mechanisms, like vector boson fusion will always be sub-dominant and we do not consider them here.

At parton level, the leading order cross section for the production of Higgs particles through the gluon fusion process is given by [106, 107, 108, 16]:

$$\sigma_{gg \to H_a}^{LO} = \hat{\sigma}_{gg \to H_a}^{LO}\,\delta\left(1-\frac{M_{H_a}^2}{\hat{s}}\right) = \frac{\pi^2}{8M_{H_a}}\Gamma_{H_a \to gg}^{LO}\,\delta\left(1-\frac{M_{H_a}^2}{\hat{s}}\right) \tag{3.32}$$

$$\hat{\sigma}_{gg \to H_a}^{LO} = \frac{\alpha_s^2(Q)}{256\pi}\frac{M_{H_a}^2}{v^2}\left[\left|\sum_{f=t,b}\frac{g_f g_{S,a}^f v}{m_f}F_f^S(\tau_{af}) + \frac{1}{4}\sum_{\tilde{f}_i=\tilde{b}_1,\tilde{b}_2,\tilde{t}_1,\tilde{t}_2}\frac{g_{\tilde{f}\tilde{f}}^a v^2}{m_{\tilde{f}}^2}F_0\left(\tau_{a\tilde{f}}\right)\right|^2\right.$$

$$\left. + \left|\sum_{f=t,b}\frac{g_f g_{P,a}^f v}{m_f}F_f^P(\tau_{af})\right|^2\right] = \frac{\alpha_s^2(Q)}{256\pi}\frac{M_{H_a}^2}{v^2}\left[|S_a^g|^2 + |P_a^g|^2\right],$$

with $\hat{s}$ the partonic center of mass energy squared. The hadronic cross section from gluon fusion processes can be obtained in the narrow-width approximation as,

$$\sigma(pp \to H_a)^{LO} = \hat{\sigma}_{gg \to H_a}^{LO} \tau_{H_a} \frac{d\mathcal{L}_{LO}^{gg}}{d\tau_{H_a}} \ . \tag{3.33}$$

The gluon luminosity $d\mathcal{L}_{LO}^{gg}/d\tau$ at the factorization scale M, with $\tau_{H_a} = M_{H_a}^2/s$, is given by,

$$\frac{d\mathcal{L}_{LO}^{gg}}{d\tau} = \int_\tau^1 \frac{dx}{x} \, g(x, M^2) \, g(\tau/x, M^2) \ . \tag{3.34}$$

In the numerical analysis below, we use the MSTW2008 [63] parton distribution functions.

The $bb \to H_a$ production process can also play an important role for the high and intermediate $\tan\beta$ region, roughly for $\tan\beta \geq 7$ [110, 64, 112, 113, 114, 115, 116]. The leading order partonic cross section is directly related to the fermionic decay width,

$$\hat{\sigma}_{bb \to H_a} \quad = \quad \frac{4\pi^2}{9M_{H_a}} \Gamma_{H_a \to b\bar{b}} = \frac{\pi}{6} \frac{g^2 m_b^2}{4M_W^2} \beta_b \left(\beta_b^2 \left| g_s^b \right|^2 + \left| g_p^b \right|^2 \right) \tag{3.35}$$

Again the proton-proton cross section is obtained in the narrow-width approximation in terms of the $b\bar{b}$ luminosity. Notice that associated Higgs production with heavy quarks $gg/q\bar{q} \to b\bar{b} + H_a$ is equivalent to the $b\bar{b} \to H_a$ inclusive process if we do not require to observe the final state b-jets and one considers the b-quark as a massless parton in a five active flavour scheme [110, 16, 89]. In this way, large logarithms $\log(s/m_b^2)$ are resummed to all orders. As before, we are using the MSTW2008 five flavour parton distribution functions. Regarding the QCD corrections to this process, for our purposes it is enough to take into account the QCD enhancing factor K_a^f used in the decay $H_a \to b\bar{b}$, with the bottom mass evaluated at m_{H_a}, and to use the threshold-corrected bottom couplings in Eqs. (3.15,3.16).

$$\hat{\sigma}_{bb \to H_a}^{QCD} = \frac{4\pi^2}{9M_{H_a}} \Gamma_{H_a \to b\bar{b}} = \frac{\pi}{6} \frac{g^2 m_b^2}{4M_W^2} K_a^b \left(\frac{m_b(m_{H_a})}{m_b(m_t)} \right)^2 \beta_b \left(\beta_b^2 \left| g_s^b \right|^2 + \left| g_p^b \right|^2 \right) \tag{3.36}$$

The total hadronic cross section can be obtained at NLO using the so-called K-factors [104, 117, 118, 108] to correct the LO gluon fusion, and it is given by,

$$\sigma(pp \to H_a) = K \ \hat{\sigma}_{gg \to H_a}^{LO} \tau_{H_a} \frac{d\mathcal{L}_{LO}^{gg}}{d\tau_{H_a}} \ + \ \hat{\sigma}_{bb \to H_a}^{QCD} \tau_{H_a} \frac{d\mathcal{L}_{LO}^{bb}}{d\tau_{H_a}} \tag{3.37}$$

where the K-factor parametrizes the ratio of the higher order cross section to the leading order one. It is important to include this term as it is known that the next to leading order QCD effects, which affect both quark and squark contributions similarly [118, 119], are very large and cannot be neglected. Such effects are essentially independent of the Higgs mass but exhibit a $\tan\beta$ dependence. In the low $\tan\beta$ region, K can be approximated by 2 while for large $\tan\beta$ its value gets closer to unity [116]. In our study we have taken K to be constant for fixed $\tan\beta$ in the considered range of Higgs masses.

3.3.4   Indirect constraints

As explained in the introduction, indirect searches of new physics in low-energy precision experiments play a very important role in Higgs boson searches. The main players in this game are $b \to s\gamma$ and $B_s \to \mu^+\mu^-$.

3.3.4.1 $b \to s\gamma$ decay.

Following references [120, 121, 122, 123], the branching ratio of the decay given in terms of the Wilson coefficients can be written as:

$$\mathrm{BR}(B \to X_s\gamma) \simeq \left[a\ + a_{77}\ \delta\mathcal{C}_7^2 + a_{88}\ \delta\mathcal{C}_8^2 + \mathrm{Re}\left[a_7\ \delta\mathcal{C}_7 \right] + \mathrm{Re}\left[a_8\ \delta\mathcal{C}_8 \right] + \\ + \mathrm{Re}\left[a_{78}\ \delta\mathcal{C}_7 \delta\mathcal{C}_8^* \right] \right] \tag{3.38}$$

where $a \sim 3.0 \times 10^{-4}$, $a_{77} \sim 4.7 \times 10^{-4}$, $a_{88} \sim 0.8 \times 10^{-4}$, $a_7 \sim (-7.2 + 0.6\,i) \times 10^{-4}$, $a_8 \sim (-2.2 - 0.6\,i) \times 10^{-4}$ and $a_{78} \sim (2.5 - 0.9\,i) \times 10^{-4}$ and the main contributions to the Wilson coefficients, beyond the W–boson contribution, are chargino and charged-Higgs contributions, $\delta\mathcal{C}_{7,8} = \mathcal{C}_{7,8}^{H^\pm} + \mathcal{C}_{7,8}^{\chi^\pm}$.

Chargino contributions are given by,

$$\mathcal{C}_{7,8}^{\chi^\pm} = \frac{1}{\cos\beta} \sum_{a=1,2} \left\{ \frac{U_{a2}V_{a1}M_W}{\sqrt{2}m_{\tilde\chi_a^\pm}} \mathcal{F}_{7,8}\left(x_{\tilde q \tilde\chi_a^\pm}, x_{\tilde t_1 \tilde\chi_a^\pm}, x_{\tilde t_2 \tilde\chi_a^\pm} \right) + \frac{U_{a2}V_{a2}\overline{m}_t}{2m_{\tilde\chi_a^\pm}\sin\beta} \mathcal{G}_{7,8}\left(x_{\tilde t_1 \tilde\chi_a^\pm}, x_{\tilde t_2 \tilde\chi_a^\pm} \right) \right\} \tag{3.39}$$

where $x_{\alpha\beta} = m_\alpha^2/m_\beta^2$ and the functions $\mathcal{F}_{7,8}(x,y,z) = f_{7,8}^{(3)}(x) - \left|\mathcal{R}_{11}^{\tilde t}\right|^2 f_{7,8}^{(3)}(y) - \left|\mathcal{R}_{21}^{\tilde t}\right|^2 f_{7,8}^{(3)}(z)$ and $\mathcal{G}_{7,8}(x,y) = \mathcal{R}_{11}^{\tilde t}\mathcal{R}_{12}^{*\tilde t} f_{7,8}^{(3)}(x) - \mathcal{R}_{21}^{\tilde t}\mathcal{R}_{22}^{*\tilde t} f_{7,8}^{(3)}(y)$ with $f_{7,8}^{(3)}(x)$,

$$f_7^{(3)}(x) = \frac{5 - 7x}{6(x-1)^2} + \frac{x(3x-2)}{3(x-1)^2}\ln x; \quad f_8^{(3)}(x) = \frac{1+x}{2(x-1)^2} - \frac{x}{(x-1)^3}\ln x; \tag{3.40}$$

Now, using the expansion in Appendix 3.B, we can see that the dominants terms in $\tan\beta$ are:

$$\mathcal{C}_{7,8}^{\chi^\pm} \simeq M_W^2 \frac{\mu M_2 \tan\beta}{m_{\tilde\chi_1^\pm}^2 - m_{\tilde\chi_2^\pm}^2} \left(\frac{f_{7,8}^{(3)}\left(x_{\tilde q \tilde\chi_1^\pm}\right) - f_{7,8}^{(3)}\left(x_{\tilde t_1 \tilde\chi_1^\pm}\right)}{m_{\tilde\chi_1^\pm}^2} - \frac{f_{7,8}^{(3)}\left(x_{\tilde q \tilde\chi_2^\pm}\right) - f_{7,8}^{(3)}\left(x_{\tilde t_1 \tilde\chi_2^\pm}\right)}{m_{\tilde\chi_2^\pm}^2} \right)$$

$$+\ M_W^2 \frac{m_t^2}{m_{\tilde t_1}^2 - m_{\tilde t_2}^2} \frac{\mu A_t \tan\beta}{m_{\tilde\chi_1^\pm}^2 - m_{\tilde\chi_2^\pm}^2} \left(\frac{f_{7,8}^{(3)}\left(x_{\tilde t_1 \tilde\chi_1^\pm}\right) - f_{7,8}^{(3)}\left(x_{\tilde t_2 \tilde\chi_1^\pm}\right)}{m_{\tilde\chi_1^\pm}^2} - \right.$$

$$\left. - \frac{f_{7,8}^{(3)}\left(x_{\tilde t_1 \tilde\chi_2^\pm}\right) - f_{7,8}^{(3)}\left(x_{\tilde t_2 \tilde\chi_2^\pm}\right)}{m_{\tilde\chi_2^\pm}^2} \right)$$

and in the limit $m_{\tilde\chi_1} \simeq M_2 \ll m_{\tilde\chi_2} \simeq \mu$, we have,

$$\mathcal{C}_{7,8}^{\chi^\pm} \simeq\ -\ \frac{M_2}{\mu} \tan\beta \frac{M_W^2}{M_2^2} \left(f_7^{(3)}\left(x_{\tilde q \tilde\chi_1^\pm}\right) - f_7^{(3)}\left(x_{\tilde t_1 \tilde\chi_1^\pm}\right) \right) \tag{3.41}$$

$$-\ \frac{A_t}{\mu} \tan\beta \frac{M_W^2}{M_2^2} \frac{m_t^2}{m_{\tilde t_1}^2 - m_{\tilde t_2}^2} \left(f_8^{(3)}\left(x_{\tilde t_1 \tilde\chi_1^\pm}\right) - f_8^{(3)}\left(x_{\tilde t_2 \tilde\chi_1^\pm}\right) \right)$$

Then, the charged-Higgs contribution, including the would-be Goldstone-boson corrections to the W-boson contribution [123], is given by,

$$\mathcal{C}_{7,8}^{H^\pm} = \frac{1}{3\tan^2\beta} f_{7,8}^{(1)}(y_t) + \frac{f_{7,8}^{(2)}(y_t) + \left(\Delta h_d/h_d(1+\tan\beta) - \delta h_d/h_d(1-\cot\beta)\right) f_{7,8}^{(2)}(x_t)}{1 + \delta h_d/h_d + \Delta h_d/h_d \tan\beta} \tag{3.42}$$

with $y_t = m_t^2/M_{H^{\pm}}^2$, $x_t = m_t^2/M_W^2$ and

$$f_7^{(1)}(x) = \frac{x\left(7 - 5x - 8x^2\right)}{24\left(x-1\right)^3} + \frac{x^2\left(3x-2\right)}{4\left(x-1\right)^4}\ln x; \qquad f_7^{(2)}(x) = \frac{x(3-5x)}{12(x-1)^2} + \frac{x(3x-2)}{6(x-1)^3}\ln x;$$

$$f_8^{(1)}(x) = \frac{x\left(2 + 5x - x^2\right)}{8\left(x-1\right)^3} - \frac{3x^2}{4\left(x-1\right)^4}\ln x; \qquad f_8^{(2)}(x) = \frac{x(3-x)}{4(x-1)^2} - \frac{x}{2(x-1)^3}\ln x;$$

$$(3.43)$$

3.3.4.2 $B_s \to \mu^- \mu^+$ decay.

The branching ratio associated to this decay can be adequately approximated by the following expression [13]:

$$\mathrm{BR}(B_s \to \mu^- \mu^+) = 2.32 \cdot 10^{-6}\ \frac{\tau_{B_s}}{1.5ps}\left(\frac{F_{B_s}}{230MeV}\right)^2\left(\frac{|V_{ts}|}{0.04}\right)^2\left[|\tilde{c}_S|^2 + |\tilde{c}_P + 0.04(c_A - c_A')|^2\right]$$

$$(3.44)$$

where the dimensionless Wilson coefficients are given by $\tilde{c}_S = m_{B_s}c_S$, $\tilde{c}_P = m_{B_s}c_P$ and the coefficients c_A and c_A' can be neglected in comparison with c_S and c_P since they are related with contributions from box diagrams and Z^0-penguin diagrams. In our analysis, we use the approximate expressions for c_S and c_P in Ref. [13]:

$$c_S \simeq \frac{m_\mu \overline{m}_t^2}{4M_W}\frac{16\pi^2 \tan^3\beta\ \epsilon_Y}{(1 + \delta h_d/h_d + \Delta h_d/h_d \tan\beta)(1 + \epsilon_0 \tan\beta)}\left[\frac{|U_{11}|^2}{m_{H_1}^2} + \frac{|U_{21}|^2}{m_{H_2}^2} + \frac{|U_{31}|^2}{m_{H_3}^2}\right]$$

$$(3.45)$$

$$c_P \simeq \frac{m_\mu \overline{m}_t^2}{4M_W}\frac{16\pi^2 \tan^3\beta\ \epsilon_Y}{(1 + \delta h_d/h_d + \Delta h_d/h_d \tan\beta)(1 + \epsilon_0 \tan\beta)}\left[\frac{|U_{13}|^2}{m_{H_1}^2} + \frac{|U_{23}|^2}{m_{H_2}^2} + \frac{|U_{33}|^2}{m_{H_3}^2}\right]$$

$$(3.46)$$

with

$$\epsilon_0 = \frac{2\alpha_s}{3\pi}\ \mu^* m_{\tilde{g}}^*\ I\left(m_{\tilde{d}_1}^2, m_{\tilde{d}_2}^2, m_{\tilde{g}}^2\right) \qquad \epsilon_Y = -\frac{1}{16\pi^2}\ A_t^* \mu^*\ I\left(m_{\tilde{t}_1}^2, m_{\tilde{t}_2}^2, |\mu|^2\right). \quad (3.47)$$

And, given that in Eq. (3.44) we are including only the $\tan\beta$-enhanced Higgs contributions, in the following, we use the experimental result as a 3σ upper limit on this contribution.

3.4   Model analysis.

In the previous section we have defined the MSSM model we are going to analyze and presented the different production mechanisms and the main decay channels for neutral Higgses at LHC. In this section we study, in this general MSSM scenario with the possible presence of CP violating phases, whether it is still possible to interpret the Higgs resonance observed at LHC with a mass of ~ 125 GeV as the second Higgs having a lighter Higgs below this mass and a third neutral Higgs with a mass $m_{H_3} \leq 200$ GeV. As we will see in the following, the present experimental results that we use to this end are the measurement of $pp \to H_2 \to \gamma\gamma$, $pp \to H_a \to \tau\tau$ at LHC and the indirect constraints on charged Higgs from $\mathrm{BR}(b \to s\gamma)$. We divide our analysis in two $\tan\beta$ regions: low $\tan\beta$ defined as $\tan\beta \lesssim 8$ and medium-large $\tan\beta$, for $\tan\beta \gtrsim 8$.

3.4.1   Medium–large $\tan\beta$ regimen.

Now, we take $\tan\beta \gtrsim 8$, which implies that $\sin\beta \simeq 1$ and $\cos\beta \simeq (1/\tan\beta) \ll 1$. We analyze the different processes in this regime of medium–large $\tan\beta$. First, we analyze the model predictions for the process $pp \to H_2 \to \gamma\gamma$ that is requested to satisfy the new experimental constraints with a signal strength $0.75 \le \mu_{\gamma\gamma}^{\mathrm{LHC}} \le 1.55$. Then, we analyze the constraints from $pp \to H_a \to \tau\tau$ and see whether the two results can be compatible in the regime of medium–large $\tan\beta$ for $m_{H_2} = 125$ GeV.

3.4.1.1   Two photon cross section.

The two photon cross section through a Higgs boson can be divided, in the narrow-width approximation, in two parts: Higgs production cross section and Higgs decay to the two photon final state, $\sigma_{\gamma\gamma} = \sigma(pp \to H_2) \times \mathrm{BR}(H_2 \to \gamma\gamma) = \sigma(pp \to H_2) \times \Gamma(H_2 \to \gamma\gamma)/\Gamma_{H_2}$. Thus we have to analyze these three elements, *i.e.* $\sigma(pp \to H_2)$, $\Gamma(H_2 \to \gamma\gamma)$ and Γ_{H_2}.

In first place, we are going to analyze the decay width of the Higgs boson into two photons in our MSSM model. As a reference value, we can compare our prediction with the Standard Model value,

$$S_H^\gamma = \frac{2}{3}F_b^S\left(\tau_{Hb}\right) + \frac{8}{3}F_t^S\left(\tau_{Ht}\right) - F_1\left(\tau_{HW}\right) \simeq (-0.025 + i\,0.034) + 1.8 - 8.3 \simeq -6.54; \quad (3.48)$$

In the MSSM, this decay width is given by the Eq. (3.22) and it has both a scalar and a pseudoscalar part, receiving each one contributions from different virtual particles:

$$S_{H_2^0}^\gamma = S_{H_2^0,b}^\gamma + S_{H_2^0,t}^\gamma + S_{H_2^0,W}^\gamma + S_{H_2^0,\tilde{b}}^\gamma + S_{H_2^0,\tilde{t}}^\gamma + S_{H_2^0,\tilde{\tau}}^\gamma + S_{H_2^0,\tilde{\chi}}^\gamma + S_{H_2^0,H^\pm}^\gamma; \quad (3.49)$$

$$P_{H_2^0}^\gamma = P_{H_2^0,b}^\gamma + P_{H_2^0,t}^\gamma + P_{H_2^0,\tilde{\chi}}^\gamma; \quad (3.50)$$

Once we fix the mass of the Higgs particle, $M_{H_2} \simeq 125$ GeV, the contributions from W-bosons and SM fermions are completely fixed, at least at tree level, with the only exception of the Higgs mixings, that we take as free, and $\tan\beta$. In the case of third generation fermions, as we have already seen, it is very important to take into account the non-holomorphic threshold corrections from gluino and chargino loops to the Higgs–fermionic couplings, (g_f^S, g_f^P) and therefore we introduce an additional dependence on sfermion masses. Nevertheless these contributions remain very simple,

$$S_{H_2^0,W}^\gamma = -g_{H_2WW}\,F_1\left(\tau_{2W}\right) = -\left(\mathcal{U}_{21}\cos\beta + \mathcal{U}_{22}\sin\beta\right)F_1\left(\tau_{2W}\right) \simeq -8.3\left(\mathcal{U}_{22} + \frac{\mathcal{U}_{21}}{\tan\beta}\right), \quad (3.51)$$

where we have used that $F_1\left(\tau_{2W}\right) = F_1\left(0.61\right) \simeq 8$.

The top and bottom quark contributions enter both in the scalar and pseudoscalar pieces, which are both similar. The scalar contribution, from Eq. (3.24) and taking into account again the $\tan\beta$ regime in consideration, is given by the following approximate expression:

$$\begin{aligned}
S_{H_2^0,b+t}^\gamma \simeq \frac{1}{3}\Bigg[&2\left(\mathrm{Re}\left\{\frac{\mathcal{U}_{21} + \mathcal{U}_{22}\kappa_d}{1 + \kappa_d\tan\beta}\right\}\tan\beta + \mathrm{Im}\left\{\frac{\kappa_d\left(\tan^2\beta + 1\right)}{1 + \kappa_d\tan\beta}\right\}\mathcal{U}_{23}\right)F_b^S\left(\tau_{2b}\right) \\
&+ 8\mathcal{U}_{22}\,F_t^S\left(\tau_{2t}\right)\Bigg];
\end{aligned} \quad (3.52)$$

where κ_b is a parameter associated to the finite loop-induced threshold corrections that modify the couplings of the neutral Higgses to the scalar and pseudoscalar fermion bilinears, as defined in Eqs. (3.15,3.16). These parameters are always much lower than 1,

whereas for $m_t = 173, 1$ GeV (pole mass) and $m_b = 4.33$ GeV (mass at m_t scale) the loop functions are just about $F_b^S \simeq -0.04 + i\,0.05$ and $F_t^S \simeq 0.7$. In this way, Eq. (3.52) can be finally approximated by:

$$S_{H_2^0,b+t}^\gamma \simeq 1.8\,\mathcal{U}_{22} + (-0.025 + i\,0.034)\left[\mathrm{Re}\left\{\frac{\tan\beta}{1+\kappa_d\tan\beta}\right\}\mathcal{U}_{21} + \mathrm{Im}\left\{\frac{\kappa_d\tan^2\beta}{1+\kappa_d\tan\beta}\right\}\mathcal{U}_{23}\right].$$
(3.53)

The first contribution beyond the Standard Model that we are going to consider is the charged Higgs boson. As we can see from Eq. (3.24), it only takes part in the scalar part of the decay width. Its contribution is given by:

$$S_{H_2^0,H^\pm}^\gamma = -g_{H_2^0 H^\pm}\frac{v^2}{2m_{H^\pm}^2}F_0\left(\tau_{2H^\pm}\right),$$
(3.54)

where the self-coupling to the second neutral Higgs can be approximated as follows for medium-large $\tan\beta$, keeping only the leading terms in $\cos\beta$:

$$\begin{aligned}g_{H_2^0 H^\pm} &\simeq \quad (2\lambda_1\cos\beta - \lambda_4\cos\beta - 2\cos\beta\,\mathrm{Re}\{\lambda_5\} + \mathrm{Re}\{\lambda_6\})\,\mathcal{U}_{21} \\ &+ \quad (\lambda_3 + \cos\beta\,\mathrm{Re}\{\lambda_6\} - 2\cos\beta\,\mathrm{Re}\{\lambda_7\})\,\mathcal{U}_{22} + (2\cos\beta\,\mathrm{Im}\{\lambda_5\} - \mathrm{Im}\{\lambda_6\})\,\mathcal{U}_{23};\end{aligned}$$
(3.55)

The loop function, $F_0\left(\tau\right)$ is quite stable for small τ, for 150 GeV $\leq m_{H^\pm} \leq 200$ GeV, $0.17 \simeq (125/300)^2 \leq \tau_{2H^\pm} \leq 0.097 \simeq (125/400)^2$, we have $F_0\left(\tau_{2H^\pm}\right) \simeq 0.34$ and then, taking,

$$\begin{aligned}S_{H_2^0,H^\pm}^\gamma &\lesssim \quad -0.45\left[\left(\frac{2\lambda_1 - \lambda_4 - 2\,\mathrm{Re}\{\lambda_5\}}{\tan\beta} + \mathrm{Re}\{\lambda_6\}\right)\mathcal{U}_{21}\right. \\ &+ \quad \left.\left(\lambda_3 + \frac{\mathrm{Re}\{\lambda_6\} - 2\,\mathrm{Re}\{\lambda_7\}}{\tan\beta}\right)\mathcal{U}_{22} + \left(\frac{2\,\mathrm{Im}\{\lambda_5\}}{\tan\beta} - \mathrm{Im}\{\lambda_6\}\right)\mathcal{U}_{23}\right]\end{aligned}$$
(3.56)

Now, we take into account that the Higgs potential couplings $\lambda_i = \lambda_i\left(g,\beta, M_{susy}, A_t,\mu\right)$, can be safely considered $\lambda_i \lesssim 1$. Numerically, we find a maximum $\lambda_i^{max} \sim 0.25$ for some of them and taking only the couplings not suppressed by $\tan\beta$ factors, we have $\lambda_3 \simeq -0.074$ at tree-level with the value at one-loop typically smaller due to the opposite sign of the fermionic corrections and $\lambda_6 \simeq -0.14\,e^{i\alpha}$. Thus, we can expect the charged Higgs contribution to be always negligible when compared to the above SM contributions, even for $m_{H^\pm} \simeq 150$ GeV, and can not modify substantially the diphoton amplitude.

The squarks involved in the two photon decay width are the ones with large Yukawa couplings, that is, the sbottom and the stop. The scalar contribution of these squarks is given in Eq. (3.24) and writing explicitly their couplings to the Higgs, it can be expressed as follows:

$$S_{H_2^0,\tilde{b}}^\gamma = -\sum_{i=1,2}\frac{1}{3}g_{H_2\tilde{b}_i^*\tilde{b}_i}\frac{v^2}{2m_{\tilde{b}_i}^2}F_0\left(\tau_{2\tilde{b}_i}\right) = -\sum_{i=1,2}\frac{v^2}{6m_{\tilde{b}_i}^2}\left(\tilde{\Gamma}^{\alpha bb}\right)_{\beta\gamma}\mathcal{U}_{2\alpha}\mathcal{R}_{\beta i}^{\tilde{b}*}\mathcal{R}_{\gamma i}^{\tilde{b}}F_0\left(\tau_{2\tilde{b}_i}\right)$$
(3.57)

$$S_{H_2^0,\tilde{t}}^\gamma = -\sum_{i=1,2}\frac{4}{3}g_{H_2\tilde{t}_i^*\tilde{t}_i}\frac{v^2}{2m_{\tilde{t}_i}^2}F_0\left(\tau_{2\tilde{t}_i}\right) = -\sum_{i=1,2}\frac{2v^2}{3m_{\tilde{t}_i}^2}\left(\tilde{\Gamma}^{\alpha tt}\right)_{\beta\gamma}\mathcal{U}_{2\alpha}\mathcal{R}_{\beta i}^{\tilde{t}*}\mathcal{R}_{\gamma i}^{\tilde{t}}F_0\left(\tau_{2\tilde{t}_i}\right)$$
(3.58)

In the sbottom contribution, we make the expansion described in Appendix 3.B, taking into account that the off-diagonal terms in its mass matrix are much smaller than the

diagonal ones. This approximation leads us to the expression:

$$
\begin{aligned}
S^\gamma_{H^0_2,\tilde{b}} &\simeq 0.12 \tan^2\beta \, \frac{m_b^2}{m_{\tilde{b}_1}^2} \left[\frac{\mathrm{Re}\{A_b^*\mu\}}{m_{\tilde{b}_2}^2} \mathcal{U}_{21} - \frac{\mu^2}{m_{\tilde{b}_2}^2} \mathcal{U}_{22} + \frac{\mathrm{Im}\{A_b^*\mu\}}{m_{\tilde{b}_2}^2 \tan\beta} \mathcal{U}_{23} \right] \\
&\simeq 1.2 \times 10^{-5} \tan^2\beta \left(\frac{300\ \mathrm{GeV}}{m_{\tilde{b}_1}} \right)^2 \left[\frac{\mathrm{Re}\{A_b^*\mu\}}{m_{\tilde{b}_2}^2} \mathcal{U}_{21} - \frac{\mu^2}{m_{\tilde{b}_2}^2} \mathcal{U}_{22} + \frac{\mathrm{Im}\{A_b^*\mu\}}{m_{\tilde{b}_2}^2 \tan\beta} \mathcal{U}_{23} \right]
\end{aligned}
\tag{3.59}
$$

where we have used that $F_0\left(\tau_{2\tilde{b}_i}\right) \simeq 0.34$ for both right and left-handed sbottoms. Assuming that $A_b/m_{\tilde{b}_2}, \mu/m_{\tilde{b}_2} \simeq O(1)$, it is clear that the sbottom contribution can be safely neglected, as even for $\tan\beta \sim 50$ would be two orders of magnitude below the top-quark contribution. Incidentally, the stau contribution can be obtained with the replacement $b \leftrightarrow \tau$, and we can also expect it to be negligible for stau masses above 100 GeV, except for the very large $\tan\beta$ region[6].

On the other hand, we have the top squark case where there are large off-diagonal terms in the mass matrix which can not be neglected in comparison with the diagonal ones, specially if we intend to analyze small stop masses. This does not allow us to use the Appendix 3.B approximation in such a straightforward way. Nevertheless, we can still expand the chargino mass-matrix, keeping the stop mixing matrices, $\mathcal{R}$, and we can write Eq. (3.58) as,

$$
\begin{aligned}
S^\gamma_{H^0_2,\tilde{t}} \simeq 0.45 &\left[\frac{m_t^2}{m_{\tilde{t}_1}^2} \left(|\mathcal{R}_{11}|^2 + |\mathcal{R}_{12}|^2 \right) + \frac{m_t^2}{m_{\tilde{t}_2}^2} \left(|\mathcal{R}_{22}|^2 + |\mathcal{R}_{21}|^2 \right) \right] \mathcal{U}_{22} \; + \; 0.45 \left(1 - \frac{m_{\tilde{t}_1}^2}{m_{\tilde{t}_2}^2} \right) \\
&\left[-\mathrm{Re}\left\{ \frac{\mu m_t}{m_{\tilde{t}_1}^2} \mathcal{R}_{11}^* \mathcal{R}_{21} \right\} \mathcal{U}_{21} + \mathrm{Im}\left\{ \frac{\mu m_t}{m_{\tilde{t}_1}^2} \mathcal{R}_{11}^* \mathcal{R}_{21} \right\} \mathcal{U}_{23} + \mathrm{Re}\left\{ \frac{A_t^* m_t}{m_{\tilde{t}_1}^2} \mathcal{R}_{11}^* \mathcal{R}_{21} \right\} \mathcal{U}_{22} \right]
\end{aligned}
\tag{3.60}
$$

where we take that $F_0\left(\tau_{2\tilde{t}_1}\right) \simeq F_0\left(\tau_{2\tilde{t}_2}\right) \simeq 0.34$. Regarding the stop mass, the limit provided by ATLAS and CMS sets $m_{\tilde{t}} \geq 650$ GeV for the general case where the lightest neutralino mass is $m_{\tilde{\chi}^0_1} \lesssim 250$ GeV [63, 64, 65, 66]. Therefore if we typically consider upper values for $A_t, \mu \lesssim 3m_{\widetilde{Q}_3} \sim 3000$ GeV for $m_{\widetilde{Q}_3} \lesssim 1000$ GeV (higher values may have naturalness and charge and color breaking problems) the size of the coefficients associated to the equation above will be $m_t^2/m_{\tilde{t}_2}^2$, $m_t^2/m_{\tilde{t}_1}^2 < 0.1$, $A_t m_t/m_{\tilde{t}_1}^2$, $\mu m_t/m_{\tilde{t}_1}^2 \lesssim 1.2$ and taking into account that $\mathcal{R}_{11}^* \mathcal{R}_{21} \leq \frac{1}{2}$, $|\mathcal{R}_{ij}|^2 \leq 1$ and $(1 - m_{\tilde{t}_1}^2/m_{\tilde{t}_2}^2) < 1$ we obtain

$$
S^\gamma_{H^0_2,\tilde{t}} \lesssim 0.26 \left[-\mathcal{U}_{21} + 1.7\,\mathcal{U}_{22} + \mathcal{U}_{23} \right] ,
\tag{3.61}
$$

and therefore typically an order of magnitude smaller than the top quark and the W-boson contribution and without $\tan\beta$ enhancement. Nevertheless, we keep this stop contribution to take into account the possibility of a light stop, $m_{\tilde{t}_1} \leq 650$ GeV with a small mass difference to the LSP.

Finally, the chargino contribution is given by:

$$
S^\gamma_{H^0_2,\tilde{\chi}^\pm} = \sqrt{2} g \sum_{i=1,2} \mathrm{Re}\left\{ V_{i1}^* U_{i2}^* G_2^{\phi_1} + V_{i2}^* U_{i1}^* G_2^{\phi_2} \right\} \frac{v}{m_{\chi_i^\pm}} F_f^S\left(\tau_{2\tilde{\chi}_i}\right) ,
\tag{3.62}
$$

$$
\text{with} \quad G_2^{\phi_1} = \left(\mathcal{U}_{21} - i\sin\beta\,\mathcal{U}_{23} \right) , \qquad G_2^{\phi_2} = \left(\mathcal{U}_{22} - i\cos\beta\,\mathcal{U}_{23} \right) .
$$

---

[6]In a recent analysis on this issue [62], enhancements of the diphoton decay width of order 40% could be obtained for $\tan\beta \geq 60$ and $m_{\tilde{\tau}} \simeq 95$ GeV.

Using again the expansion of chargino mass matrices, Appendix 3.B, we have the expression:

$$S^{\gamma}_{H^0_2, \tilde{\chi}^{\pm}} \simeq 2.8 \left[\cos\beta \frac{M_W^2}{\mu^2} \mathcal{U}_{21} + \frac{M_W^2}{M_2^2} \mathcal{U}_{22} \right] \tag{3.63}$$

where we have supposed that $m_{\chi_1^{\pm}} \simeq M_2 \ll m_{\chi_2^{\pm}} \simeq \mu$, $\sin\beta \simeq 1$, $F_f^S \left(\tau_{H_2 \chi_2^{\pm}} \right) \simeq F_f^S \left(\tau_{H_2 \chi_1^{\pm}} \right) \simeq 0.7$, and neglected $(F_f^S \left(\tau_{H_2 \chi_1^{\pm}} \right) - F_f^S \left(\tau_{H_2 \chi_2^{\pm}} \right))/(m_{\chi_1^{\pm}}^2 - m_{\chi_2^{\pm}}^2)$. If we take $M_W^2/M_2^2 \lesssim 0.05$ for $m_{\chi_1^{\pm}} < 350$ GeV from LHC limits [67, 68], we have,

$$S^{\gamma}_{H^0_2, \tilde{\chi}^{\pm}} \lesssim 0.15 \left[\mathcal{U}_{22} + \frac{M_2^2}{\mu^2} \mathcal{U}_{21} \right] \tag{3.64}$$

and again we see we can safely neglect the chargino contribution compared to the W-boson, top and bottom contributions.

Therefore, in summary, we can safely neglect the charged Higgs, chargino and sbottom contributions to the 2-photon decay width and we can approximate the scalar amplitude by,

$$S^{\gamma}_{H^0_2} \simeq \mathcal{U}_{21} \left(-\frac{8.3}{\tan\beta} (-0.025 + i\, 0.034)\, \mathrm{Re} \left\{ \frac{\tan\beta}{1 + \kappa_d \tan\beta} \right\} - 0.45 \left(\frac{m_{\tilde{t}_2}^2}{m_{\tilde{t}_1}^2} - 1 \right) \mathrm{Re} \left\{ \frac{\mu m_t \mathcal{R}_{11}^* \mathcal{R}_{21}}{m_{\tilde{t}_2}^2} \right\} \right) +$$

$$+ \mathcal{U}_{22} \left(-6.5 + 0.45 \left(\frac{m_{\tilde{t}_2}^2}{m_{\tilde{t}_1}^2} - 1 \right) \mathrm{Re} \left\{ \frac{A_t^* m_t \mathcal{R}_{11}^* \mathcal{R}_{21}}{m_{\tilde{t}_2}^2} \right\} + 0.45 \left(\frac{m_t^2 |\mathcal{R}_{11}|^2}{m_{\tilde{t}_1}^2} + \frac{m_t^2 |\mathcal{R}_{22}|^2}{m_{\tilde{t}_2}^2} \right) \right) +$$

$$+ \mathcal{U}_{23} \left((-0.025 + i\, 0.034)\, \mathrm{Im} \left\{ \frac{\kappa_d \tan^2\beta}{1 + \kappa_d \tan\beta} \right\} + 0.45\, \mathrm{Im} \left\{ \frac{\mu m_t \mathcal{R}_{11}^* \mathcal{R}_{21}}{m_{\tilde{t}_2}^2} \right\} \right) \tag{3.65}$$

Thus, it looks very difficult to obtain a scalar amplitude to two photons significantly larger than the SM value taking into account that the stop contribution can be, at most, order one. The same discussion applies to the pseudoscalar amplitude that receives only fermionic contributions, only top and bottom are relevant and thus is much smaller than the scalar contribution above. The possibility of large SUSY contributions, as advocated in Refs. [60, 61, 62] seems closed, at least in the MSSM with $m_{H_2} \simeq 125$ GeV. In particular, large stau contributions would require $\tan\beta \geq 50$ that we show below to be incompatible with the bounds from $H_1, H_3 \to \tau\tau$.

Next, we analyze the Higgs production cross section, presented at section 3.3.3. At the partonic level, this cross section receives contributions from gluon fusion and $b\bar{b}$-fusion.

The $b\bar{b}$–fusion is tree-level at the partonic level and proportional to the bottom Yukawa coupling. Considering only the main threshold corrections to the bottom couplings, we have,

$$\begin{aligned} \hat{\sigma}_{b\bar{b} \to H_2} &\simeq \frac{\pi}{6} \frac{g^2 m_b^2}{4 M_W^2} \left(\frac{\tan^2\beta}{(1 + \kappa_d \tan\beta)^2} \left(|\mathcal{U}_{21}|^2 + |\mathcal{U}_{23}|^2 \right) \right) \\ &\simeq 6.8 \times 10^{-5} \frac{\tan^2\beta}{(1 + \kappa_d \tan\beta)^2} \left(|\mathcal{U}_{21}|^2 + |\mathcal{U}_{23}|^2 \right). \end{aligned} \tag{3.66}$$

This dimensionless partonic cross section must be multiplied by the $b\bar{b}$ luminosity in the proton, $\tau\, d\mathcal{L}^{b\bar{b}}/d\tau$, for $\tau = m_{H_2}^2/s$. Taking $m_{H_2} = 125$ GeV and for $\sqrt{s} = 8$ TeV, we

have $\tau \, d\mathcal{L}^{b\bar{b}}/d\tau \simeq 2300$ pb from the MSTW2008 parton distributions at LO. Thus, the $b\bar{b}$ contribution to the pp cross section:

$$\sigma(pp \to H_2)_{bb} \simeq 0.16 \frac{\tan^2 \beta}{(1 + \kappa_d \tan \beta)^2} \left(|\mathcal{U}_{21}|^2 + |\mathcal{U}_{23}|^2 \right) \text{pb} . \qquad (3.67)$$

On the other hand, gluon fusion cross section is a loop process,

$$\hat{\sigma}^{LO}_{gg \to H_2} = \frac{\alpha_s^2 (M_{H_2})}{256\pi} \frac{m_{H_2}^2}{v^2} \left[|S_2^g|^2 + [|P_2^g|^2 \right] \simeq 4 \times 10^{-6} \left[|S_2^g|^2 + [|P_2^g|^2 \right] \qquad (3.68)$$

where the scalar coupling, S_2^g, gets contributions from both quarks and squarks, while the pseudoscalar one, P_2^g, receives contributions only from quarks. With regard to the squark contributions, they can be easily obtained from Eqs. (3.59,3.60), taking into account that, for $J_{\tilde{f}}^\gamma = 1$, $S_{2,\tilde{b}}^g = 3/2 \, S_{2,\tilde{b}}^\gamma$ and $S_{2,\tilde{t}}^g = 3/8 \, S_{2,\tilde{t}}^\gamma$. Therefore, it is easy to see that analogously to the photonic amplitudes, we can safely neglect the sbottom and stop contributions to gluon fusion production. Thus, the scalar and pseudoscalar contributions to gluon fusion production can be approximated by,

$$S_{2,b+t}^g \simeq 0.7\mathcal{U}_{22} + (-0.04 + i\,0.05) \left[\text{Re} \left\{ \frac{\tan \beta}{1 + \kappa_d \tan \beta} \right\} \mathcal{U}_{21} + \text{Im} \left\{ \frac{\kappa_d \tan^2 \beta}{1 + \kappa_d \tan \beta} \right\} \mathcal{U}_{23} \right]; \qquad (3.69)$$

$$P_{2,b+t}^g \simeq (-0.04 + i\,0.05) \left[\text{Im} \left\{ \frac{\kappa_d \tan \beta}{1 + \kappa_d \tan \beta} \right\} \mathcal{U}_{22} + \text{Im} \left\{ \frac{\kappa_d \tan^2 \beta}{1 + \kappa_d \tan \beta} \right\} \mathcal{U}_{21} \right]$$

$$+ \left[(-0.04 + i\,0.05) \, \text{Re} \left\{ \frac{\tan \beta}{1 + \kappa_d \tan \beta} \right\} - \frac{1}{\tan \beta} \right] \mathcal{U}_{23}; \qquad (3.70)$$

The gluon fusion contribution to the pp cross section is obtained by multiplying the gluon luminosity, $\tau_{H_2} \, d\mathcal{L}_{LO}^{gg}/d\tau_{H_2} \simeq 3 \times 10^6$ pb and the K-factor, which we take $K \simeq 2.2$, corresponding to low $\tan \beta$. Then, with κ_d real for simplicity, the gluon fusion contribution to pp cross section would be,

$$\sigma(pp \to H_2)_{gg} \simeq 27.5 \left[|S_2^g|^2 + [|P_2^g|^2 \right] \text{ pb} \simeq \left[13\mathcal{U}_{22}^2 - \frac{1.5 \tan \beta}{1 + \kappa_d \tan \beta} \mathcal{U}_{21}\mathcal{U}_{22} + \qquad (3.71) \right.$$

$$\left. + \frac{0.1 \tan^2 \beta}{(1 + \kappa_d \tan \beta)^2} \mathcal{U}_{21}^2 + \left(\frac{2}{(1 + \kappa_d \tan \beta)} + \frac{0.1 \tan^2 \beta}{(1 + \kappa_d \tan \beta)^2} + \frac{27}{\tan^2 \beta} \right) \mathcal{U}_{23}^2 \right] \text{ pb} .$$

This equation with the approximate values of S_2^g, P_2^g is compared with the full result in Figure 3.3. We can see that this approximate expression reproduces satisfactorily the gluon fusion contribution to H_2 production in the whole explored region. From this equation, we see that the gluon fusion production is dominated by the top quark contribution if $\mathcal{U}_{21}, \mathcal{U}_{22} = O(1)$ up to $\tan \beta \gtrsim 10$. Moreover, the SM contribution corresponds simply to take $\kappa = 0$, $\tan \beta = 1$, $\mathcal{U}_{21} = \mathcal{U}_{22} = 1$ and $\mathcal{U}_{23} = 0$ and therefore, we see the gluon fusion cross section will be typically smaller than the SM cross section for medium-low $\tan \beta$. Also, comparing Eqs. (3.67) and (3.71), we see that gluon fusion still dominates over $b\bar{b}$–fusion except for large $\tan \beta$ or small $\mathcal{U}_{22}$.

Finally, we have to check the total width, Γ_{H_2}. The main decay channels for $m_{H_2} \simeq 125$ GeV, are $H_2 \to b\bar{b}$, $H_2 \to WW^*$ and $H_2 \to \tau\tau$ ($H_2 \to gg$ can of the same order as $H_2 \to \tau\tau$ in some cases, but, being comparatively small with respect to $b\bar{b}$ and WW, it is not necessary to consider it in the following discussion). The decay width is usually dominated by the $b\bar{b}$-channel which can be enhanced by $\tan \beta$ factors with respect to the SM width (as the $\tau\tau$ channel). The main contribution to the decay width to $b\bar{b}$ is captured by the
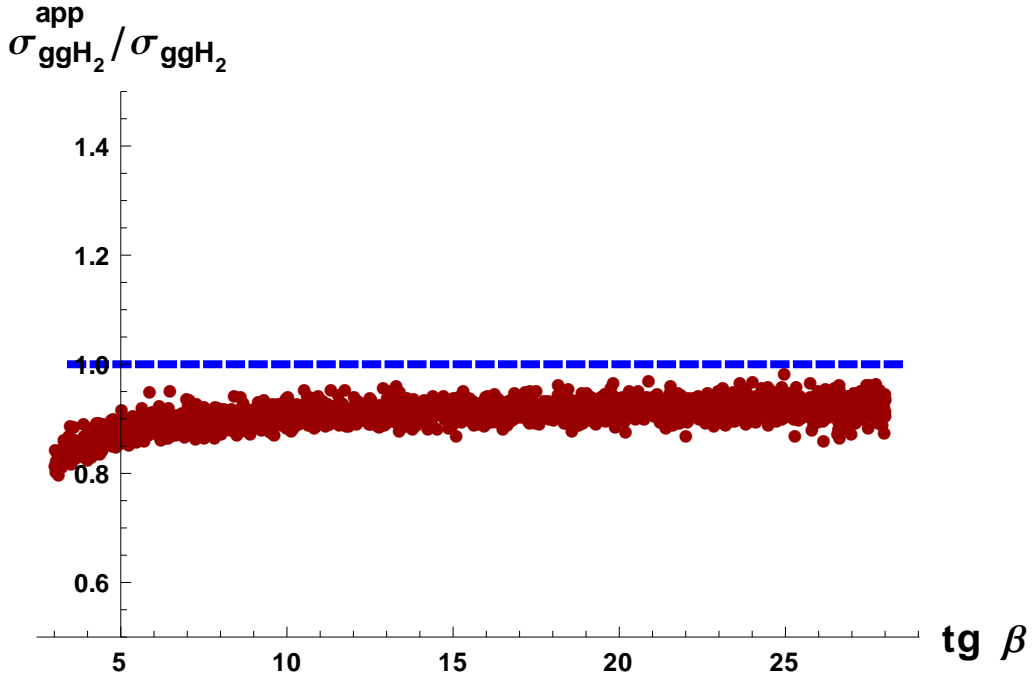
Figure 3.3: Comparison of the approximation to $\sigma(pp \to H_2)_{gg}$ in Eq. (3.71) with the full result as a function of $\tan\beta$.

tree-level Higgs-bottom couplings, in the limit $\kappa_d \to 0$ (although threshold corrections are important and always taken into account in our numerical analysis),

$$
\Gamma_{H_2} \simeq \frac{g^2 m_{H_2}}{32\pi M_W^2} \left[\tan^2\beta \left(|\mathcal{U}_{21}|^2 + |\mathcal{U}_{23}|^2 \right) \left(3m_b^2 + m_\tau^2 \right) + \left(\mathcal{U}_{22} + \frac{\mathcal{U}_{21}}{\tan\beta} \right)^2 m_{H_2}^2 I_{PS} \right],
$$
(3.72)

where $I_{PS} \simeq 6.7 \times 10^{-4}$ represents the phase space integral in the $H_2 \to WW^*$ decay width as can be found in Ref. [57] for $m_H \simeq 125$ GeV. This must be compared with the SM decay width, which would correspond to the usual MSSM decoupling limit if we replace $H_1 \leftrightarrow H_2$: $\tan\beta \to 1$, $\mathcal{U}_{21}, \mathcal{U}_{22} \to 1$ and $\mathcal{U}_{23} = 0$. This implies that for sizable $\mathcal{U}_{21}, \mathcal{U}_{23} > \tan^{-1}\beta$, the total width will be much larger than the SM width. Then, taking into account that we have shown that $\Gamma_{H_2 \to \gamma\gamma} \simeq \Gamma_{h \to \gamma\gamma}^{SM}$ we have that, for $\mathcal{U}_{22} \leq 1$, the diphoton branching ratio will be smaller than the SM one. The only way to keep a large branching ratio is to take $\mathcal{U}_{21}, \mathcal{U}_{23} \lesssim \tan^{-1}\beta$, when the total width is reduced keeping $\Gamma_{H_2 \to \gamma\gamma}$ similar to the SM. On the other hand, we have seen that the H_2 production cross section is typically smaller than the SM unless we have $\mathcal{U}_{22} \simeq 1$ and H_2 is produced through the gluon-fusion process, or $\tan\beta \gtrsim 20$ with sizeable $\mathcal{U}_{21}, \mathcal{U}_{23}$ and the production is dominated by $b\bar{b}$ fusion. Even for this last case, $b\bar{b}$ fusion, the $\tan\beta$ enhancement of the production cross section is exactly compensated by the suppression on the $H_2 \to \gamma\gamma$ branching ratio. For gluon fusion, there is no $\tan\beta$ enhancement and thus in both cases the $\gamma\gamma$-production cross section is smaller than the SM one. Therefore, we arrive to the conclusion that the only way to increase the $\gamma\gamma$-production cross section to reproduce the LHC results in our scenario is to **decrease the total width by suppressing the b-quark and the τ-lepton decay widths**. This implies having a second Higgs, H_2, predominantly H_u^0, so that we decrease the couplings associated to these fermions and consequently increase the two photons branching ratio.

This condition means, in terms of the mixing matrix elements:

$$\mathcal{U}_{22} \sim 1, \qquad \mathcal{U}_{21} \simeq \mathcal{U}_{23} \leq \frac{1}{\tan\beta} \ll \mathcal{U}_{22} \tag{3.73}$$

3.4.1.2 Tau-tau cross section.

The above analysis has led us to the conclusion that, to reproduce the $\gamma\gamma$-production cross section, we need the second lightest Higgs to be almost purely up type. As a consequence, H_2 nearly decouples from tau fermions and then it is unavoidable that the other neutral Higgses inherit large down-type components, increasing thus their decays into two τ-fermions. Once more, to compute the $\tau\tau$-production cross section through a Higgs, we must compute $\sigma(pp \to H_i)$, $\Gamma(H_i \to \gamma\gamma)$ and Γ_{H_i}.

The decay width $H_i \to \tau\tau$ is given by the following equation:

$$\Gamma_{H_a \to \tau\tau} = \frac{g_{\tau\tau}^2 m_{H_a} \beta_\tau}{8\pi} \left(\beta_\tau^2 |g_{\tau,a}^S|^2 + |g_{\tau,a}^P|^2 \right) , \tag{3.74}$$

where $\tau_i = m_\tau^2/m_{H_i}^2$ and $\beta_\tau = \sqrt{1 - 4\tau_i}$. The values of the τ scalar and pseudoscalar couplings are given by:

$$g_{\tau i}^S \simeq \frac{\tan\beta}{1 + \epsilon_\tau \tan\beta} \mathcal{U}_{i1} + \frac{\epsilon_\tau \tan\beta}{1 + \epsilon_\tau \tan\beta} \mathcal{U}_{i2}; \qquad g_{\tau i}^P \simeq -\frac{\tan\beta - \epsilon_\tau}{1 + \epsilon_\tau \tan\beta} \mathcal{U}_{i3} \tag{3.75}$$

In this case $\epsilon_\tau \simeq g^2/16\pi^2 \, (\mu M_1/m_{\tilde{\tau}_2}^2) \simeq 2 \times 10^{-3}$, and we are taking it real. Then, we have $\epsilon_\tau \simeq \epsilon_b/20$ being only a sub-leading correction in this case which can be safely neglected. Therefore we get, for $i = 1, 3$,

$$\Gamma_{i,\tau\tau} \simeq \frac{m_{H_i}}{8\pi} \left(\frac{g m_\tau}{2 M_W} \right)^2 \left[\tan^2\beta \left(|\mathcal{U}_{i1}|^2 + |\mathcal{U}_{i3}|^2 \right) \right] \simeq \frac{g^2 m_{H_i} m_\tau^2}{32\pi M_W^2} \tan^2\beta \, , \tag{3.76}$$

where we used that $\mathcal{U}_{22} \simeq 1$ and $\mathcal{U}_{12}, \mathcal{U}_{32} \ll 1$.

Now we need the production cross section for H_1 and H_3. We can use Eqs. (3.67) and (3.71) with the replacement $\mathcal{U}_{2j} \to \mathcal{U}_{ij}$. Then, using $|\mathcal{U}_{i1}|^2 + |\mathcal{U}_{i3}|^2 \simeq 1$ and $\mathcal{U}_{i2} \simeq 1/\tan\beta$, we have,

$$\sigma(pp \to H_i)_{gg} \simeq 27.5 \left[|S_2^g|^2 + [|P_2^g|^2 \right] \text{ pb} \simeq \left[13 \mathcal{U}_{i2}^2 - \frac{1.5 \tan\beta}{1 + \kappa_d \tan\beta} \mathcal{U}_{i1} \mathcal{U}_{i2} + \right.$$

$$\left. + \frac{0.1 \tan^2\beta}{(1 + \kappa_d \tan\beta)^2} \mathcal{U}_{i1}^2 + \left(\frac{2}{(1 + \kappa_d \tan\beta)} + \frac{0.1 \tan^2\beta}{(1 + \kappa_d \tan\beta)^2} + \frac{27.5}{\tan^2\beta} \right) \mathcal{U}_{i3}^2 \right] \text{ pb}$$

$$\simeq \left[\frac{0.1 \tan^2\beta}{(1 + \kappa_d \tan\beta)^2} + \frac{13 + 27.5 \mathcal{U}_{i3}^2}{\tan^2\beta} + \frac{2 \mathcal{U}_{i3}^2 - 1.5 \mathcal{U}_{i1}}{1 + \kappa_d \tan\beta} \right] \text{ pb} \tag{3.77}$$

$$\sigma(pp \to H_i)_{bb} \simeq 0.16 \frac{\tan^2\beta}{(1 + \kappa_d \tan\beta)^2} \left(|\mathcal{U}_{i1}|^2 + |\mathcal{U}_{i3}|^2 \right) \text{pb} \simeq 0.16 \frac{\tan^2\beta}{(1 + \kappa_d \tan\beta)^2} \text{ pb} \tag{3.78}$$

Therefore, we see that for $\tan\beta \gtrsim 5$ in our scenario, always with $\mathcal{U}_{i2} \lesssim 1/\tan\beta$, the bottom contribution to gluon fusion is larger than the top contribution and only slightly
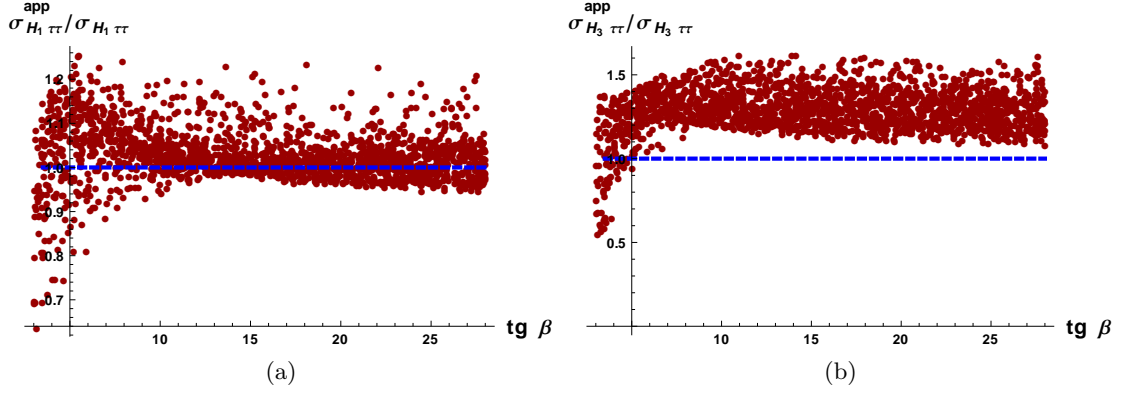
Figure 3.4: Comparison of the the approximation to $\sigma(pp \to H_i \to \tau\tau)$ in Eq. (3.4.1.2) with the full result as a function of $\tan\beta$.

smaller than the $b\bar{b}$–fusion. Then we approximate the total production cross section for $H_{1,3}$,

$$\sigma(pp \to H_i) \simeq \left[0.16 \left(\frac{\tau_{H_i} \, d\mathcal{L}^{bb}/d\tau_{H_i}}{2300 \text{ pb}} \right) + 0.11 \left(\frac{\tau_{H_i} \, d\mathcal{L}^{gg}_{LO}/d\tau_{H_i}}{3 \times 10^6 \text{ pb}} \right) \right] \frac{\tan^2\beta}{(1 + \kappa_d \tan\beta)^2} \text{ pb} \tag{3.79}$$

The last ingredient we need is the total width of the H_i, we can still consider that the dominant contributions will come from $b\bar{b}$, $\tau\tau$ and WW^* for Higgs masses below 160 GeV. For masses above 160 GeV, the width is usually dominated by real W-production and ZZ or ZZ^*. Therefore, below 160 GeV, the total width can be directly read from Eq. (3.72) replacing $H_2 \to H_i$ and the mixing $\mathcal{U}_{2a} \to \mathcal{U}_{ia}$. For Higgs masses above 160 GeV, always below 200 GeV in our scenario, the total width will be larger than Eq. (3.72) and thus taking only $b\bar{b}$, $\tau\tau$ and WW^* we obtain a lower limit to Γ_i. In the case of H_1 and H_3, we have $\mathcal{U}_{i2} \ll 1$ and $|\mathcal{U}_{i1}|^2 + |\mathcal{U}_{i3}|^2 \simeq 1$. Then the total width is,

$$\Gamma_i \gtrsim \frac{g^2 m_{H_i}}{32\pi M_W^2} \left(\frac{3m_b^2}{1 + \kappa_d \tan\beta} + m_\tau^2 \right) \tan^2\beta \,, \tag{3.80}$$

And thus, the branching ratio is,

$$\text{BR}\,(H_i \to \tau\tau) \lesssim \frac{m_\tau^2 \,(1 + \kappa_d \tan\beta)^2}{3m_b^2 + m_\tau^2 \,(1 + \kappa_d \tan\beta)^2} \tag{3.81}$$

So, for the $\tau\tau$-production cross section of H_1 and H_3 we have,

$$\sigma(pp \xrightarrow{H_i} \tau\tau) \lesssim \frac{\tan^2\beta}{(1 + \kappa_d \tan\beta)^2} \frac{m_\tau^2 (1 + \kappa_d \tan\beta)^2}{3m_b^2 + m_\tau^2 (1 + \kappa_d \tan\beta)^2} \left[0.16 \left(\frac{\tau_{H_i} \, d\mathcal{L}^{bb}/d\tau_{H_i}}{2300 \text{ pb}} \right) + 0.11 \left(\frac{\tau_{H_i} \, d\mathcal{L}^{gg}_{LO}/d\tau_{H_i}}{3 \times 10^6 \text{ pb}} \right) \right] \text{ pb}$$

$$\simeq \frac{\tan^2\beta}{8.4 + 2\kappa_d \tan\beta + \kappa_d^2 \tan^2\beta} \left[0.16 \left(\frac{\tau_{H_i} \, d\mathcal{L}^{bb}/d\tau_{H_i}}{2300 \text{ pb}} \right) + 0.11 \left(\frac{\tau_{H_i} \, d\mathcal{L}^{gg}_{LO}/d\tau_{H_i}}{3 \times 10^6 \text{ pb}} \right) \right] \text{ pb} \tag{3.82}$$

which should be compared with the SM cross section $\sigma(pp \to H \to \tau\tau) \simeq 1.4$ pb for $m_H \simeq$

110 GeV. The comparison of this approximate expression with the full result is shown in Figure 3.4. In fact, this approximate expression works very well for $m_{H_1} = 110$ GeV and is slightly larger than the exact result for $m_{H_3} = 155$ GeV. This is due to the fact that we did not include the $H_i \to WW^*$ channel in Eq. (3.4.1.2) and this channel is important for H_3, which means that the approximate branching ratio is larger than one in the full expression. Nevertheless, we can safely use this expression to understand the qualitative behaviour in this process.

Next, we combine the bounds on the two photon production cross section and the $\tau\tau$ production cross section in our model with medium-large $\tan\beta$. In Figure 3.5 we present the $\tau\tau$ production cross sections at LHC for $m_{H_1} \simeq 110$ GeV and $m_{H_3} \simeq 160$ GeV with (squares in blue) or without (circles in red) fulfilling the requirement $0.75 \le \mu_{\gamma\gamma}^{\mathrm{LHC}} \le 1.55$. The green line is the CMS limit on the $\tau\tau$ production cross section for Higgs masses below 150 GeV and the green points are the points where, in addition, the $\tau\tau$ cross-section limit on the observed Higgs, H_2 in our scenario, at a mass $m_{H_2} \simeq 125$ GeV is also fulfilled. Even though we fixed $m_{H_1} = 110$ GeV in this plot, we have checked that the situation does not change at all for $m_{H_1} = 100$ GeV or $m_{H_1} = 120$ GeV. Notice that, the present constraints
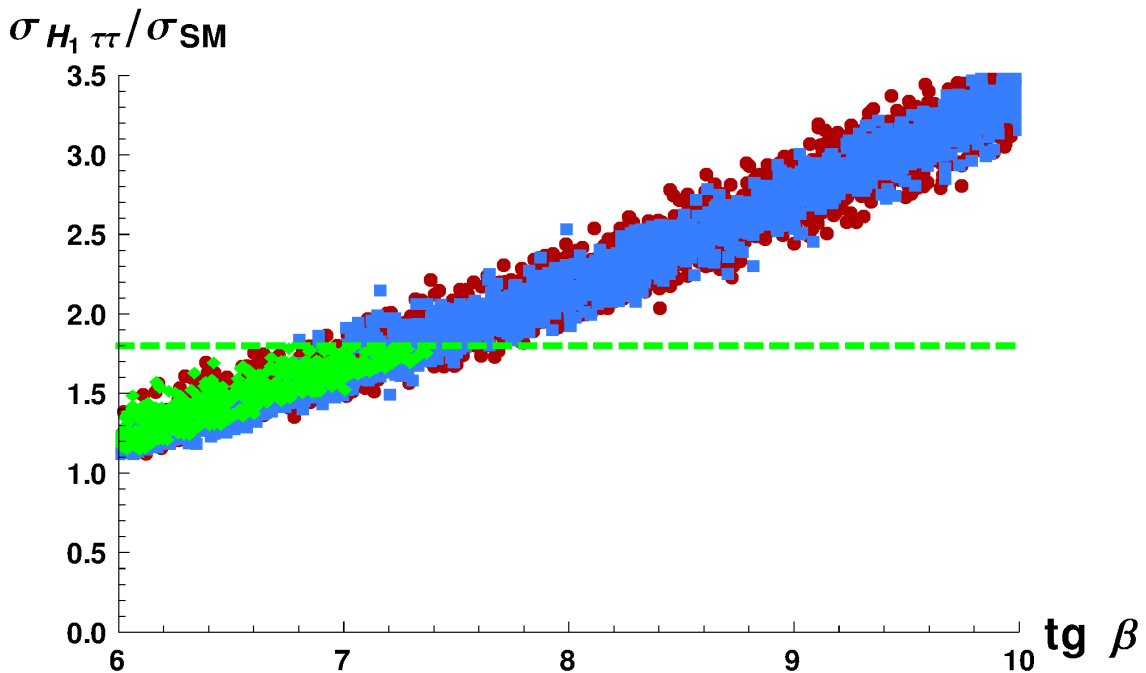
Figure 3.5: $\tau\tau$ production cross-section at $m_{H_1} = 110$ GeV as a function of $\tan\beta$, with the CMS limit on $\tau\tau$ production in green.

on heavy Higgses for $\sigma(pp \to H_3 \to \tau\tau)$ for masses 150 GeV $\le m_{H_3} \lesssim 200$ GeV can only eliminate the region of $\tan\beta \gtrsim 25$, but we expect the future analysis of the stored data to reduce this parameter space significantly [48].

Hence, we see that there are no points consistent with the LHC constraints on $\sigma(pp \to H_1 \to \tau\tau)$ for $\tan\beta \ge 7.8$ and 100 GeV $< m_{H_1} < 125$ GeV and, as we will see in the next section, all the surviving points are inconsistent with BR$(B \to X_s\gamma)$.

3.4.2 Low $\tan\beta$ regime.

As we have just seen, LHC constraints on $\sigma(pp \to H_1 \to \tau\tau)$ rule out the possibility of $m_{H_2} \simeq 125$ GeV for $\tan\beta \geq 7.8$, still, the situation for $\tan\beta \lesssim 8$ is very different. For low $\tan\beta$, it is much easier to satisfy the constraint from the $\gamma\gamma$-signal strength at LHC, $\mu_{\gamma\gamma} \gtrsim 0.5$.

Analogously to the discussion in the case of medium-large $\tan\beta$, we can see that the $\gamma\gamma$-decay width for low $\tan\beta$ remains of the same order as the SM one, $\Gamma_{H_2\to\gamma\gamma} \simeq \Gamma_{h\to\gamma\gamma}^{SM}$. The production cross section is typically of the order of the SM one, as the $b\bar{b}$-fusion process and the b-quark contribution to gluon fusion, being proportional to $\tan\beta$, are now smaller and the top contribution is very close to the SM for $\mathcal{U}_{22} \simeq O(1)$. In fact, the total decay width is still larger than the SM value if $\mathcal{U}_{21,21}$ are sizeable, as the $b\bar{b}$ and $\tau\tau$ widths are enhanced by $\tan^2\beta$. So, the same requirements on Higgs mixings, Eq. (3.73), hold true now, although are less suppressed correspondingly to the smaller $\tan\beta$ values. On the other hand, the $\tau\tau$ production cross section through the three neutral Higgses remains an important constraint, but it is much easier to satisfy for low $\tan\beta$ values, as we can see in Fig. 3.5.

However, in our scenario, we have a rather light charged Higgs, $m_{H^\pm} \lesssim 220$ GeV, and the main constraint for $\tan\beta \lesssim 8$ now comes from the BR($B \to X_s\gamma$).

3.4.2.1 Constraints from BR($B \to X_s\gamma$)

The decay $B \to X_s\gamma$ is an important constraint on the presence of light charged Higgs particles as we have in our scenario. However, although the charged Higgs interferes always constructively with the SM W-boson contribution to the Wilson coefficients, in the MSSM this contribution can be compensated by an opposite sign contribution from the stop-chargino loop if $\text{Re}\,(\mu A_t)$ is negative. The charged Higgs contribution is given by Eq. (3.42). The size of $\mathcal{C}_7^{H^\pm}$ can be approximated by the dominant contribution, given by $f_7^{(2)}(m_t^2/m_{H^\pm}^2)$,

$$\mathcal{C}_7^{H^\pm} \simeq \frac{f_7^{(2)}(y_t)}{1 + \delta h_d/h_d + \Delta h_d/h_d \tan\beta}\,, \tag{3.83}$$

and for $m_{H^\pm} \in [150, 200]$ GeV we get $f_7^{(2)}(y_t) \in [-0.22, -0.18]$. Incidentally, we see that this charged Higgs contribution decreases with $\tan\beta$, and thus it is more difficult to satisfy the constraints at low $\tan\beta$ unless this contribution is compensated by a different sign contribution. Then for the stop-chargino contribution, using Eq. (3.42),

$$
\begin{aligned}
\mathcal{C}_{7,8}^{\chi^\pm} \simeq\ & -\frac{M_W^2}{M_2^2}\frac{M_2}{\mu}\tan\beta\left(f_{7,8}^{(3)}\left(x_{\tilde{q}\tilde{\chi}_1^\pm}\right) - f_{7,8}^{(3)}\left(x_{\tilde{t}_1\tilde{\chi}_1^\pm}\right)\right) \\
& -\frac{A_t}{\mu}\tan\beta\frac{M_W^2}{M_2^2}\frac{m_t^2}{m_{\tilde{t}_1}^2 - m_{\tilde{t}_2}^2}\left(f_{7,8}^{(3)}\left(x_{\tilde{t}_1\tilde{\chi}_1^\pm}\right) - f_{7,8}^{(3)}\left(x_{\tilde{t}_2\tilde{\chi}_1^\pm}\right)\right)
\end{aligned}
\tag{3.84}
$$

Taking now $f_7^{(3)}\,(x \simeq 1) \simeq 0.44$, and therefore, with the limits on stop and chargino masses, $m_{\tilde{t}_1} \geq 650$ GeV and $m_{\chi^\pm} \geq 350$ GeV, we estimate $\mathcal{C}_7^{\chi^\pm} \simeq 0.02\, M_2/\mu\,\tan\beta \ll \mathcal{C}_{7,8}^{H^\pm}$. Thus it looks very difficult to compensate the charged Higgs contribution for low $\tan\beta$ and this is confirmed in the numerical analysis. In Figure 3.6, we present the obtained BR($B \to X_s\gamma$), the blue squares fulfil the requirements of, $0.75 \leq \mu_{\gamma\gamma}^{\text{LHC}} \leq 1.55$, $\sigma_{H_1\tau\tau}/\sigma_{\text{SM}} \leq 1.8$ and $\sigma_{H_2\tau\tau}/\sigma_{\text{SM}} \leq 1.8$ while the red dots violate some of these requirements. The experimentally allowed region at the one-σ and two-σ level is shown in green and yellow
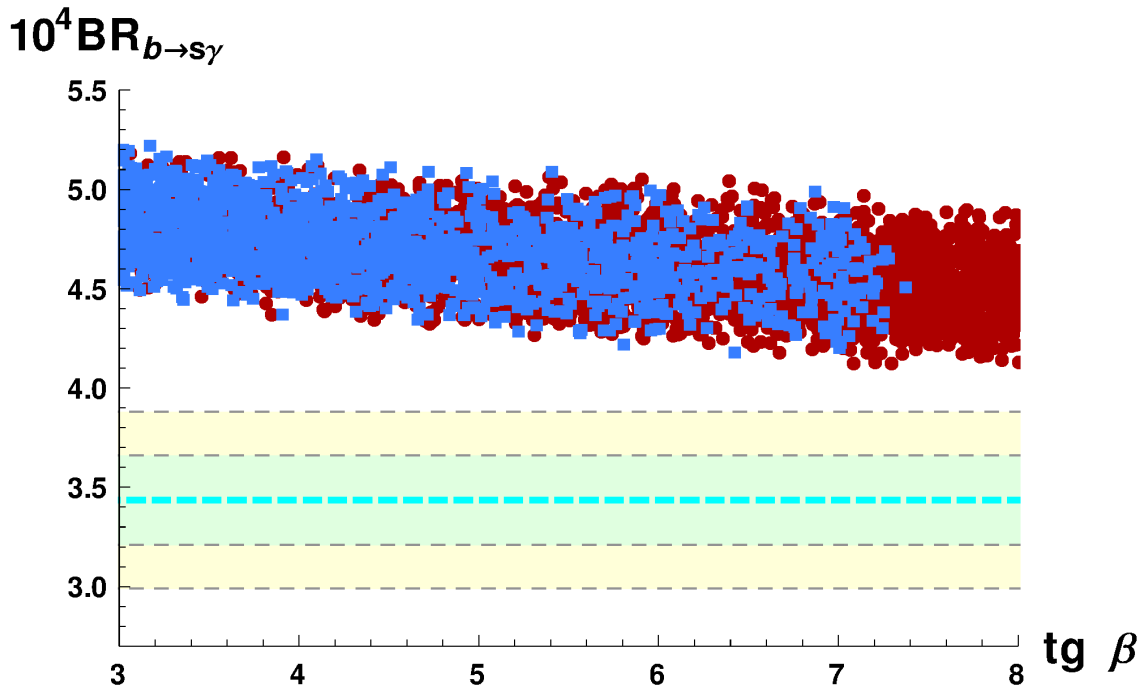
Figure 3.6: Branching ratio of the $B \rightarrow X_s \gamma$ decay as a function of $\tan \beta$. Blue squares fulfil the $\mu_{\gamma\gamma}^{\mathrm{LHC}}$ and $\sigma_{H_i\tau\tau}/\sigma_{\mathrm{SM}}$ constraints, as explained in the text. Green and yellow regions are the one and two-σ experimentally allowed regions.

respectively [7]. In passing, please note that the reduction of the BR with $\tan \beta$ is mainly due to the reduction of the charged Higgs contribution, as shown in Eq. (3.83), and not to the negative interference with the chargino diagram.

Therefore, the only remaining option is to have a light stop with a small mass difference with respect to the lightest neutralino that has escaped detection so far at LHC. To explore numerically this possibility, we select the lightest stop mass to be $m_{\chi_1^0} \leq m_{\tilde{t}_1} \leq m_t + m_{\chi_1^0}$. The result is shown in Fig. 3.7, where we plot again $\mathrm{BR}(B \rightarrow X_s \gamma)$ as a function of $\tan \beta$. Now, we can see that the range of $\mathrm{BR}(B \rightarrow X_s \gamma)$ for a given $\tan \beta$ has decreased, as expected, due to a possible destructive interference of the stop-chargino diagram. Nevertheless, we can see that there are no points allowed by collider constraints that reach the two-σ allowed region[8].

As a by-product, we can already see from here that it will be very difficult, if not completely impossible, to accommodate two sizeable Higgs-like peaks in the $\gamma\gamma$ production cross section, as recently announced by the CMS collaboration [9], within an MSSM context. The CMS analysis of an integrated luminosity of 5.1 (19.6) fb^{-1} at a center of mass energy of 7 (8) TeV reveals a clear excess near $m_H = 136.5$ GeV, aside from the 125–126 GeV Higgs boson that has already been discovered, with a local significance for this extra peak of 2.73 σ combining the data from Higgs coming from vector-boson fusion and vector-boson associated production (each of which shows the excess individually).

As we have shown in this work, the 125 GeV Higgs found at the LHC ought to be the lightest, therefore this new resonance, despite its light mass, is bounded to be the second

---

[7]Even allowing a three-σ range, we find no allowed points when $m_{\tilde{t}_1} \geq 650$ GeV and $m_{\chi^\pm} \geq 350$ GeV

[8]If we allowed points within a three-σ region, $\mathrm{BR}(B \rightarrow X_s \gamma) \leq 4.1 \times 10^{-4}$, several points would still survive. However, for all the three-σ allowed points we have very large $\sigma_{H_3\tau\tau}$ and even these points will be forbidden when ATLAS analysis on heavy MSSM Higgses is updated [52, 48].

10^{4}BR$_{b\rightarrow s\gamma}$
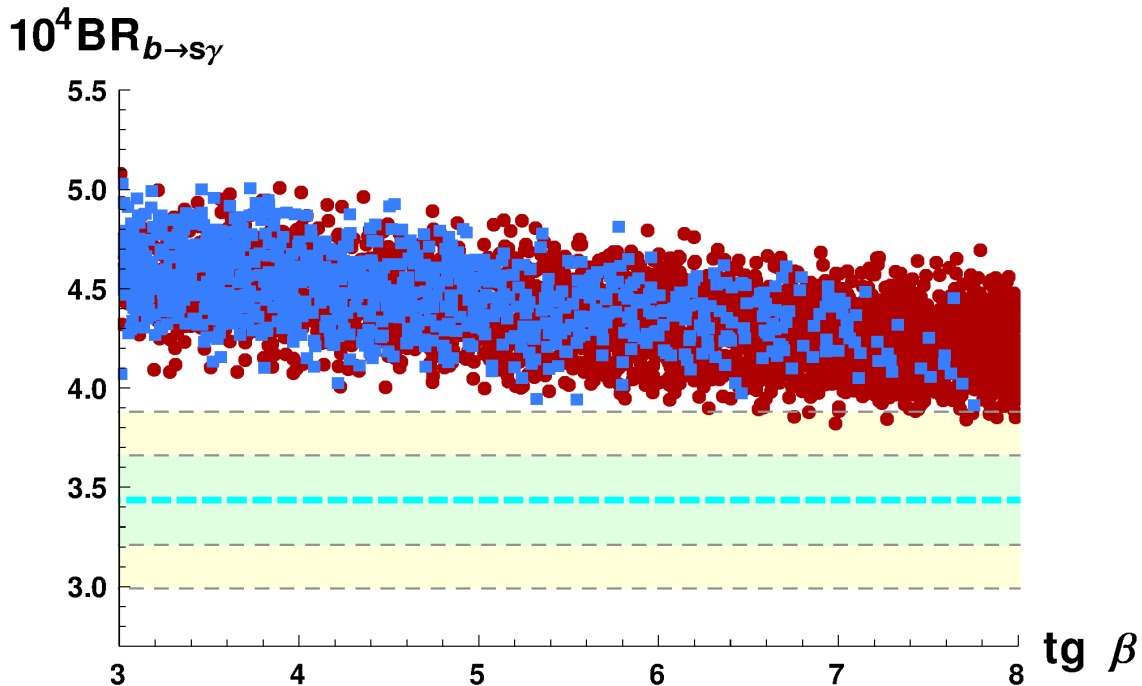
Figure 3.7: Branching ratio of the $B \rightarrow X_s\gamma$ decay as a function of $\tan\beta$, for $m_{\tilde{t}_1} \leq 650$ and $m_{\chi_1^0} \leq m_{\tilde{t}_1} \leq m_t + m_{\chi_1^0}$. The color coding is the same as in Fig. 3.6

lightest Higgs, meaning that the third neutral Higgs (and its charged sibling) are to be found nearby. This can be easily seen following our line of reasoning in section 7.2, where we obtain $m_{H_3} < 180$ GeV and $m_{H^+} < 200$ GeV. However, to reproduce the observed signal strength in $H_1 \longrightarrow \gamma\gamma$ of the ~ 126 GeV peak for medium–large $\tan\beta$, we must force all the pseudoscalar and down-type content out of the lightest state. In this case, we have $\mathcal{U}_{12} \approx 1$ and $\mathcal{U}_{11}, \mathcal{U}_{13} \ll 1$, so that the the two heavier Higgses will necessarily couple, with $\tan\beta$-enhancement, to down-type fermions and the branching ratio of these Higgses to $\gamma\gamma$ will be brutally inhibited. At the same time, the $H_i \longrightarrow \tau\tau$ channel, for $i = 2, 3$ is $\propto (U_{i1}^2 + U_{i3}^2) \approx (1 - U_{i2}^2) \approx U_{12}^2 \simeq 1$. Meaning that any MSSM setting would predict a $H_i \longrightarrow \tau\tau$ at a level that is already excluded [45, 46, 52].

The only possible escape to this situation would be to stay in the (very) low $\tan\beta$ region, but then, given the low mass of the charged Higgs, the constraints from BR($B \rightarrow X_s\gamma$) eliminate completely this possibility. Therefore, we can not see any way to accommodate two Higgs peaks in the $\gamma\gamma$ spectrum with a signal strength of the order of the SM model one. Nevertheless this possibility will be fully explored in a subsequent paper [128].

3.5   Conclusions.

In this work we have investigated the possibility of the Higgs found at LHC with a mass $m_H \sim 125$ GeV not being the lightest but the second lightest Higgs in an MSSM context, having the actual lightest Higgs escaped detection due to its pseudoscalar and/or down-type content. In this scheme, such a content suppresses simultaneously its couplings to gauge bosons and up-type quarks and paves the way to evade LEP constraints.

Although similar studies, with previous LHC constraints, are already present in the literature, most of these studies proceed through giant scans of the model's parameter space and the later analysis of the scanning results. Our approach in this work has

been different, and we have chosen to study analytically, with simple expressions under reasonable approximations, three or four key phenomenological signatures, including the two photon signal strength and the $\tau\tau$ production cross sections at LHC and the indirect constraints on $\text{BR}(B \to X_s\gamma)$. To the best of our knowledge, this is the first study carried out in this way in an MSSM context using the LHC data. Our approach has the advantage that can rule out the model altogether without risking having missed a region where unexpected cancellations or combinations can take place.

This analysis is accomplished in a completely generic MSSM, in terms of SUSY parameters at the electroweak scale, such that it encloses all possible MSSM setups. To be as general as possible, we have allowed for the presence of CP violating phases in the Higgs potential such that the three neutral-Higgs eigenstates become admixtures with no definite CP–parity. Our study starts with the $\gamma\gamma$ signal observed at LHC at $m_H \simeq 125$ GeV. The experimental results show a signal slightly larger or of the order of the SM expectations, and this is a strong constraint on models with extended Higgs sectors. We have shown than in the MSSM with $m_{H_2} \simeq 125$ GeV the width $\Gamma(H_2 \to \gamma\gamma)$ cannot be substantially modified from its SM value. On the other hand, the total width of H_2 tends to be significantly larger if the down-type or pseudoscalar components of H_2 are sizeable. Simply requiring that $\text{BR}(H_2 \to \gamma\gamma)$ or, more exactly, $\sigma(pp \to H_2) \times \text{BR}(H_2 \to \gamma\gamma)$ is not much smaller than the SM severely restricts the possible mixings in the Higgs sector and determines the bottom and τ decay rates of the three Higgses.

Next, we have analyzed the $\tau\tau$ production cross sections for the three Higgs eigenstates, splitting the parameter space in two regions of large and small $\tan\beta$, being the dividing line $\tan\beta \simeq 8$. We have shown that, for large $\tan\beta$, present constraints on $\sigma(pp \to H_1 \to \tau\tau)$ forbid all points in the model parameter space irrespective of the supersymmetric mass spectrum.

On the other hand, in the low $\tan\beta$ region, the presence of a relatively light charged Higgs, $m_{H^\pm} \lesssim 220$ GeV, provides a large charged-Higgs contribution to $\text{BR}(B \to X_s\gamma)$ which can not be compensated by an opposite sign chargino contribution, precisely due to the smallness of $\tan\beta$ and this eliminates completely the possibility of the observed Higgs at $M_H \simeq 125$ GeV, being the next-to-lightest Higgs in an MSSM context.

In summary, we have shown that a carefully chosen combination of three or four experimental signatures can be enough to entirely rule out a model without resorting to gigantic scans while simultaneously provides a much better understanding on the physics of the model studied. The power of this technique should not be underestimated specially when studying models with large parameter spaces where monster scans can be quite time consuming and not precisely enlightening. Special interest raises the case in which the Higgs found at the LHC is the lightest where this type of combined analysis can close significant regions of the parameters space [128].

In this respect, the straightforward application of this kind of study to the recently published CMS data with a second Higgs-like resonance at ~ 136 GeV, aside from the 125–126 GeV Higgs, shows it is not possible to accommodate both resonances in the $\gamma\gamma$ spectrum with a signal strength of the order of the SM model one.

APPENDICES

3.A   MSSM Conventions

We follow the MSSM conventions in the classical review of Haber and Kane [5], see also [129]. In this section we review the mass matrices entering in our analysis,

Charginos:

In our convention the chargino mass matrix is,

$$\mathcal{M}_C = \begin{pmatrix} M_2 & \sqrt{2}M_W \sin\beta \\ \sqrt{2}M_W \cos\beta & \mu \end{pmatrix} \tag{3.85}$$

and can be diagonalized by two unitary matrices so that $U^* \mathcal{M}_C V^\dagger = \text{Diag.}\left\{ m_{\chi_1^\pm}, \, m_{\chi_2^\pm} \right\}$ with $m_{\chi_1^\pm} \le m_{\chi_2^\pm}$. The mass eigenstates, $\chi_i^\pm$, are related to the electroweak eigenstates, $\hat{\chi}_i^\pm$, by

$$\chi_i^+ = V_{ij}\hat{\chi}_j^+, \qquad \chi_i^- = U_{ij}\hat{\chi}_j^- . \tag{3.86}$$

Sfermions:

The squark mass matrix is given by,

$$\mathcal{M}_q^2 = \begin{pmatrix} M_{\tilde{Q}_3}^2 + m_q^2 + \cos(2\beta) M_Z^2 \left(R_z^q - Q_q \sin^2\theta_W \right) & h_q^* v_q \left(A_q^* - \mu T_q \right)/\sqrt{2} \\ h_q v_q \left(A_q - \mu^* T_q \right)/\sqrt{2} & M_{\tilde{R}_3}^2 + m_q^2 + \cos(2\beta) M_Z^2 Q_q \sin^2\theta_W \end{pmatrix} \tag{3.87}$$

With $R_z^t = -R_z^b = \frac{1}{2}$, Q_q the quark charge, $T_b = \tan\beta = \frac{v_u}{v_d} = T_t^{-1}$ and h_q the Yukawa coupling corresponding to the quark. This matrix is diagonalized $\mathcal{R}_q \mathcal{M}_{\tilde{q}}^2 \mathcal{R}_q^\dagger = \text{Diag.}\left\{ m_{\tilde{q}_1}^2, \, m_{\tilde{q}_2}^2 \right\}$

Similarly, the stau mass matrix,

$$\mathcal{M}_\tau^2 = \begin{pmatrix} M_{\tilde{L}_3}^2 + m_\tau^2 + \cos(2\beta) M_Z^2 \left(\sin^2\theta_W - \frac{1}{2} \right) & h_\tau^* v_1 \left(A_\tau^* - \mu \tan\beta \right)/\sqrt{2} \\ h_\tau v_1 \left(A_\tau - \mu^* \tan\beta \right)/\sqrt{2} & M_{\tilde{E}_3}^2 + m_\tau^2 + \cos(2\beta) M_Z^2 \sin^2\theta_W \end{pmatrix} \tag{3.88}$$

3.B   Expansion of Hermitian matrices

Following Refs. [130, 131], we have that given a $n \times n$ hermitian matrix $A = A^0 + A^1$ with $A^0 = Diag(a_1^0, ..., a_n^0)$ and A^1 completely off diagonal that is diagonalized by $\mathcal{U} \cdot A \cdot \mathcal{U}^\dagger = Diag(a_1, ..., a_n)$, we have a first order in A^1:

$$\mathcal{U}_{ki}^* f(a_k) \mathcal{U}_{kj} \simeq \delta_{ij} f(a_i^0) + A_{ij}^1 \frac{f(a_i^0) - f(a_j^0)}{a_i^0 - a_j^0} \tag{3.89}$$

We use this formula to expand the chargino Wilson coefficients, $\mathcal{C}_{7,8}$, with respect to the chargino mass matrix elements. In this case we have to be careful because the chargino

mass matrix is not hermitian. However due to the necessary chirality flip in the chargino line $\mathcal{C}_{7,8}$ is a function of odd powers of M_{χ^+} [132], and then

$$\sum_{j=1}^{2} U_{j2} V_{j1} m_{\chi_j^+} A(m_{\chi_j^+}^2) = \sum_{j,k,l=1}^{2} U_{jk} m_{\chi_j^+} V_{j1} U_{l2} A(m_{\chi_l^+}^2) U_{lk}^* \qquad (3.90)$$

where we introduced $\sum_k U_{jk} U_{lk}^* = \delta_{jl}$. Then, we obtain,

$$\mathcal{C}_{7,8}^{\chi^\pm(a)} = \frac{1}{\cos\beta} \sum_{a=1,2} \frac{U_{a2} V_{a1} M_W}{\sqrt{2} m_{\tilde\chi_a^\pm}} \mathcal{F}_{7,8}\left(x_{\tilde q \tilde\chi_a^\pm}, x_{\tilde t_1 \tilde\chi_a^\pm}, x_{\tilde t_2 \tilde\chi_a^\pm}\right) \sim \frac{M_W}{\sqrt{2}\cos\beta}\left[(\mathcal{M}_\chi)_{21} \frac{\mathcal{F}_{7,8}\left(x_{\tilde q \tilde\chi_2^\pm}, x_{\tilde t_1 \tilde\chi_2^\pm}, x_{\tilde t_2 \tilde\chi_2^\pm}\right)}{m_{\tilde\chi_2^\pm}^2} + \right.$$

$$\left. + (\mathcal{M}_\chi)_{11} \left(\mathcal{M}_\chi \mathcal{M}_\chi^\dagger\right)_{21} \frac{m_{\tilde\chi_1^\pm}^2 \mathcal{F}_{7,8}\left(x_{\tilde q \tilde\chi_2^\pm}, x_{\tilde t_1 \tilde\chi_2^\pm}, x_{\tilde t_2 \tilde\chi_2^\pm}\right) - m_{\tilde\chi_2^\pm}^2 \mathcal{F}_{7,8}\left(x_{\tilde q \tilde\chi_1^\pm}, x_{\tilde t_1 \tilde\chi_1^\pm}, x_{\tilde t_2 \tilde\chi_1^\pm}\right)}{m_{\tilde\chi_1^\pm}^2 m_{\tilde\chi_2^\pm}^2 \left(m_{\tilde\chi_2^\pm}^2 - m_{\tilde\chi_1^\pm}^2\right)} \right] \qquad (3.91)$$

$$\mathcal{C}_{7,8}^{\chi^\pm(b)} = \frac{1}{\cos\beta} \sum_{a=1,2} \frac{U_{a2} V_{a2} \overline{m}_t}{2 m_{\tilde\chi_a^\pm} \sin\beta} \mathcal{G}_{7,8}\left(x_{\tilde t_1 \tilde\chi_a^\pm}, x_{\tilde t_2 \tilde\chi_a^\pm}\right) \sim \frac{\overline{m}_t}{2\cos\beta\sin\beta}\left[(\mathcal{M}_\chi)_{22} \frac{\mathcal{G}_{7,8}\left(x_{\tilde q \tilde\chi_2^\pm}, x_{\tilde t_1 \tilde\chi_2^\pm}, x_{\tilde t_2 \tilde\chi_2^\pm}\right)}{m_{\tilde\chi_2^\pm}^2} + \right.$$

$$\left. + (\mathcal{M}_\chi)_{12} \left(\mathcal{M}_\chi \mathcal{M}_\chi^\dagger\right)_{21} \frac{m_{\tilde\chi_1^\pm}^2 \mathcal{G}_{7,8}\left(x_{\tilde q \tilde\chi_2^\pm}, x_{\tilde t_1 \tilde\chi_2^\pm}, x_{\tilde t_2 \tilde\chi_2^\pm}\right) - m_{\tilde\chi_2^\pm}^2 \mathcal{G}_{7,8}\left(x_{\tilde q \tilde\chi_1^\pm}, x_{\tilde t_1 \tilde\chi_1^\pm}, x_{\tilde t_2 \tilde\chi_1^\pm}\right)}{m_{\tilde\chi_1^\pm}^2 m_{\tilde\chi_2^\pm}^2 \left(m_{\tilde\chi_2^\pm}^2 - m_{\tilde\chi_1^\pm}^2\right)} \right] \qquad (3.92)$$

and using again the same approximation we can expand the stop mixings in the $\mathcal{F}_{7,8}$ and $\mathcal{G}_{7,8}$, we obtain:

$$\mathcal{F}_{7,8}\left(x_{\tilde q \tilde\chi_a^\pm}, x_{\tilde t_1 \tilde\chi_a^\pm}, x_{\tilde t_2 \tilde\chi_a^\pm}\right) \simeq f_{7,8}^{(3)}\left(x_{\tilde q \tilde\chi_a^\pm}\right) - f_{7,8}^{(3)}\left(x_{\tilde t_1 \tilde\chi_a^\pm}\right); \qquad (3.93)$$

$$\mathcal{G}_{7,8}\left(x_{\tilde t_1 \tilde\chi_a^\pm}, x_{\tilde t_2 \tilde\chi_a^\pm}\right) \simeq (\mathcal{M}_{\tilde t})_{21} \frac{f_{7,8}^{(3)}\left(x_{\tilde t_1 \tilde\chi_a^\pm}\right) - f_{7,8}^{(3)}\left(x_{\tilde t_2 \tilde\chi_a^\pm}\right)}{m_{\tilde t_1}^2 - m_{\tilde t_2}^2}; \qquad (3.94)$$

So, putting all together, we have:

$$\mathcal{C}_{7,8}^{\chi^\pm(a)} \sim \frac{M_W}{\sqrt{2}\cos\beta}\left[(\mathcal{M}_\chi)_{21} \frac{f_{7,8}^{(3)}\left(x_{\tilde q \tilde\chi_2^\pm}\right) - f_{7,8}^{(3)}\left(x_{\tilde t_1 \tilde\chi_2^\pm}\right)}{m_{\tilde\chi_2^\pm}^2} + \right.$$

$$\left. + \frac{(\mathcal{M}_\chi)_{11} \left(\mathcal{M}_\chi \mathcal{M}_\chi^\dagger\right)_{21}}{m_{\tilde\chi_1^\pm}^2 - m_{\tilde\chi_2^\pm}^2} \left(\frac{f_{7,8}^{(3)}\left(x_{\tilde q \tilde\chi_1^\pm}\right) - f_{7,8}^{(3)}\left(x_{\tilde t_1 \tilde\chi_1^\pm}\right)}{m_{\tilde\chi_1^\pm}^2} - \frac{f_{7,8}^{(3)}\left(x_{\tilde q \tilde\chi_2^\pm}\right) - f_{7,8}^{(3)}\left(x_{\tilde t_1 \tilde\chi_2^\pm}\right)}{m_{\tilde\chi_2^\pm}^2} \right) \right] \qquad (3.95)$$

$$\mathcal{C}_{7,8}^{\chi^\pm(b)} \sim \frac{\overline{m}_t}{2\cos\beta\sin\beta}\left[(\mathcal{M}_\chi)_{22} \frac{(\mathcal{M}_{\tilde t})_{21}}{m_{\tilde t_1}^2 - m_{\tilde t_2}^2} \left(\frac{f_{7,8}^{(3)}\left(x_{\tilde t_1 \tilde\chi_2^\pm}\right) - f_{7,8}^{(3)}\left(x_{\tilde t_2 \tilde\chi_2^\pm}\right)}{m_{\tilde\chi_2^\pm}^2} \right) + \right.$$

$$
+ \frac{(\mathcal{M}_\chi)_{12} \left(\mathcal{M}_\chi \mathcal{M}_\chi^\dagger \right)_{21}}{m_{\tilde{\chi}_1^\pm}^2 - m_{\tilde{\chi}_2^\pm}^2} \left(\frac{f_{7,8}^{(3)} \left(x_{\tilde{t}_1 \tilde{\chi}_1^\pm} \right) - f_{7,8}^{(3)} \left(x_{\tilde{t}_2 \tilde{\chi}_1^\pm} \right)}{m_{\tilde{\chi}_1^\pm}^2} - \frac{f_{7,8}^{(3)} \left(x_{\tilde{t}_1 \tilde{\chi}_2^\pm} \right) - f_{7,8}^{(3)} \left(x_{\tilde{t}_2 \tilde{\chi}_2^\pm} \right)}{m_{\tilde{\chi}_2^\pm}^2} \right) \frac{(\mathcal{M}_{\tilde{t}})_{21}}{m_{\tilde{t}_1}^2 - m_{\tilde{t}_2}^2} \Bigg]
$$

$$(3.96)$$

Bibliography

[1] G. Aad *et al.* [ATLAS Collaboration], Phys. Lett. B **716**, 1 (2012) [arXiv:1207.7214 [hep-ex]].

[2] S. Chatrchyan *et al.* [CMS Collaboration], Phys. Lett. B **716**, 30 (2012) [arXiv:1207.7235 [hep-ex]].

[3] S. R. Coleman and J. Mandula, Phys. Rev. **159**, 1251 (1967).

[4] R. Haag, J. T. Lopuszanski and M. Sohnius, Nucl. Phys. B **88**, 257 (1975).

[5] P. Fayet, Nucl. Phys. B **90**, 104 (1975).

[6] P. Fayet, Phys. Lett. B **69**, 489 (1977).

[7] G. R. Farrar and P. Fayet, Phys. Lett. B **76**, 575 (1978).

[8] E. Witten, Nucl. Phys. B **188**, 513 (1981).

[9] S. Dimopoulos and H. Georgi, Nucl. Phys. B **193**, 150 (1981).

[10] N. Sakai, Z. Phys. C **11**, 153 (1981).

[11] L. E. Ibanez and G. G. Ross, Phys. Lett. B **105**, 439 (1981).

[12] R. K. Kaul, Phys. Lett. B **109**, 19 (1982).

[13] H. P. Nilles, Phys. Rept. **110**, 1 (1984).

[14] H. E. Haber and G. L. Kane, Phys. Rept. **117**, 75 (1985).

[15] A. Djouadi, Phys. Rept. **459**, 1 (2008) [hep-ph/0503173].

[16] A. Pilaftsis, Phys. Lett. B **435**, 88 (1998) [hep-ph/9805373].

[17] A. Pilaftsis, Phys. Rev. D **58**, 096010 (1998) [hep-ph/9803297].

[18] A. Pilaftsis and C. E. M. Wagner, Nucl. Phys. B **553**, 3 (1999) [hep-ph/9902371].

[19] D. A. Demir, Phys. Rev. D **60**, 055006 (1999) [hep-ph/9901389].

[20] M. S. Carena, J. R. Ellis, A. Pilaftsis and C. E. M. Wagner, Nucl. Phys. B **586**, 92 (2000) [hep-ph/0003180].

[21] S. Y. Choi, M. Drees and J. S. Lee, Phys. Lett. B **481**, 57 (2000) [hep-ph/0002287].

[22] M. S. Carena, J. R. Ellis, A. Pilaftsis and C. E. M. Wagner, Nucl. Phys. B **625**, 345 (2002) [hep-ph/0111245].

[23] S. Y. Choi, K. Hagiwara and J. S. Lee, Phys. Rev. D **64**, 032004 (2001) [hep-ph/0103294].

[24] S. Y. Choi, M. Drees, J. S. Lee and J. Song, Eur. Phys. J. C **25**, 307 (2002) [hep-ph/0204200].

[25] S. M. Barr and A. Zee, Phys. Rev. Lett. **65**, 21 (1990) [Erratum-ibid. **65**, 2920 (1990)].

[26] D. Chang, W. -F. Chang and W. -Y. Keung, Phys. Lett. B **478**, 239 (2000) [hep-ph/9910465].

[27] J. R. Ellis, J. S. Lee and A. Pilaftsis, JHEP **0810**, 049 (2008) [arXiv:0808.1819 [hep-ph]].

[28] A. Pilaftsis, Phys. Lett. B **471**, 174 (1999) [hep-ph/9909485].

[29] S. Heinemeyer, O. Stal and G. Weiglein, Phys. Lett. B **710**, 201 (2012) [arXiv:1112.3026 [hep-ph]].

[30] K. Hagiwara, J. S. Lee and J. Nakamura, JHEP **1210**, 002 (2012) [arXiv:1207.0802 [hep-ph]].

[31] A. Arbey, M. Battaglia, A. Djouadi and F. Mahmoudi, JHEP **1209**, 107 (2012) [arXiv:1207.1348 [hep-ph]].

[32] P. Bechtle, S. Heinemeyer, O. Stal, T. Stefaniak, G. Weiglein and L. Zeune, Eur. Phys. J. C **73**, 2354 (2013) [arXiv:1211.1955 [hep-ph]].

[33] J. Ke, H. Luo, M. -x. Luo, K. Wang, L. Wang and G. Zhu, Phys. Lett. B **723**, 113 (2013) [arXiv:1211.2427 [hep-ph]].

[34] J. Ke, H. Luo, M. -x. Luo, T. -y. Shen, K. Wang, L. Wang and G. Zhu, arXiv:1212.6311 [hep-ph].

[35] S. Moretti, S. Munir and P. Poulose, arXiv:1305.0166 [hep-ph].

[36] S. Scopel, N. Fornengo and A. Bottino, arXiv:1304.5353 [hep-ph].

[37] J. S. Lee, A. Pilaftsis, M. S. Carena, S. Y. Choi, M. Drees, J. R. Ellis and C. E. M. Wagner, Comput. Phys. Commun. **156**, 283 (2004) [hep-ph/0307377].

[38] J. S. Lee, M. Carena, J. Ellis, A. Pilaftsis and C. E. M. Wagner, Comput. Phys. Commun. **184**, 1220 (2013) [arXiv:1208.2212 [hep-ph]].

[39] S. Heinemeyer, W. Hollik and G. Weiglein, Comput. Phys. Commun. **124**, 76 (2000) [hep-ph/9812320].

[40] T. Hahn, W. Hollik, S. Heinemeyer and G. Weiglein, eConf C **050318**, 0106 (2005) [hep-ph/0507009].

[41] J. R. Ellis, K. A. Olive and Y. Santoso, Phys. Lett. B **539**, 107 (2002) [hep-ph/0204192].

[42] J. R. Ellis, T. Falk, K. A. Olive and Y. Santoso, Nucl. Phys. B **652**, 259 (2003) [hep-ph/0210205].

[43] J. R. Ellis, K. A. Olive and P. Sandick, Phys. Rev. D **78**, 075012 (2008) [arXiv:0805.2343 [hep-ph]].

[44] C. F. Berger, J. S. Gainer, J. L. Hewett and T. G. Rizzo, JHEP **0902**, 023 (2009) [arXiv:0812.0980 [hep-ph]].

[45] S. S. AbdusSalam, B. C. Allanach, F. Quevedo, F. Feroz and M. Hobson, Phys. Rev. D **81**, 095012 (2010) [arXiv:0904.2548 [hep-ph]].

[46] A. Arbey, M. Battaglia, A. Djouadi and F. Mahmoudi, Phys. Lett. B **720**, 153 (2013) [arXiv:1211.4004 [hep-ph]].

[47] [ATLAS Collaboration], ATLAS-CONF-2013-034.

[48] [CMS Collaboration], CMS-PAS-HIG-13-005.

[49] G. Aad *et al.* [ATLAS Collaboration], arXiv:1307.1427 [hep-ex].

[50] G. Aad *et al.* [ATLAS Collaboration], JHEP **1209**, 070 (2012) [arXiv:1206.5971 [hep-ex]].

[51] [CMS Collaboration], CMS-PAS-HIG-13-004.

[52] G. Aad *et al.* [ATLAS Collaboration], JHEP **1302**, 095 (2013) [arXiv:1211.6956 [hep-ex]].

[53] L. Fiorini, private communication.

[54] G. Aad *et al.* [ATLAS Collaboration], JHEP **1206**, 039 (2012) [arXiv:1204.2760 [hep-ex]].

[55] [CMS Collaboration], CMS-PAS-HIG-12-052

[56] S. Chatrchyan *et al.* [CMS Collaboration], JHEP **1303**, 037 (2013) [arXiv:1212.6194 [hep-ex]].

[57] S. Chatrchyan *et al.* [CMS Collaboration], arXiv:1305.2390 [hep-ex].

[58] [CMS Collaboration], PAS-SUS-13-007

[59] [CMS Collaboration], PAS-SUS-13-008

[60] [ATLAS Collaboration], ATLAS-CONF-2012-145.

[61] [ATLAS Collaboration], ATLAS-CONF-2013-007.

[62] S. Chatrchyan *et al.* [CMS Collaboration], arXiv:1303.2985 [hep-ex].

[63] [ATLAS Collaboration], ATLAS-CONF-2013-024.

[64] [ATLAS Collaboration], ATLAS-CONF-2013-037.

[65] [ATLAS Collaboration], ATLAS-CONF-2013-053

[66] [CMS Collaboration], PAS-SUS-13-011

[67] [ATLAS Collaboration], ATLAS-CONF-2013-035.

[68]   [CMS Collaboration], PAS-SUS-12-022

[69]   A. Bharucha, S. Heinemeyer and F. von der Pahlen, arXiv:1307.4237 [hep-ph].

[70]   A. Masiero and O. Vives, Ann. Rev. Nucl. Part. Sci. **51**, 161 (2001) [hep-ph/0104027].

[71]   M. Raidal, A. van der Schaaf, I. Bigi, M. L. Mangano, Y. K. Semertzidis, S. Abel, S. Albino and S. Antusch *et al.*, Eur. Phys. J. C **57**, 13 (2008) [arXiv:0801.1826 [hep-ph]].

[72]   L. Calibbi, R. N. Hodgkinson, J. Jones Perez, A. Masiero and O. Vives, Eur. Phys. J. C **72**, 1863 (2012) [arXiv:1111.0176 [hep-ph]].

[73]   RAaij *et al.* [LHCb Collaboration], Phys. Rev. Lett. **110**, 021801 (2013) [arXiv:1211.2674 [hep-ex]].

[74]   RAaij *et al.* [LHCb Collaboration], Phys. Rev. Lett. 111, **101805** (2013) [arXiv:1307.5024 [hep-ex]].

[75]   S. Chatrchyan *et al.* [CMS Collaboration], arXiv:1307.5025 [hep-ex].

[76]   S. Chen *et al.* [CLEO Collaboration], Phys. Rev. Lett. **87**, 251807 (2001) [hep-ex/0108032].

[77]   K. Abe *et al.* [Belle Collaboration], Phys. Lett. B **511**, 151 (2001) [hep-ex/0103042].

[78]   A. Limosani *et al.* [Belle Collaboration], Phys. Rev. Lett. **103**, 241801 (2009) [arXiv:0907.1384 [hep-ex]].

[79]   J. P. Lees *et al.* [BaBar Collaboration], Phys. Rev. D **86**, 052012 (2012) [arXiv:1207.2520 [hep-ex]].

[80]   J. P. Lees *et al.* [BaBar Collaboration], Phys. Rev. D **86**, 112008 (2012) [arXiv:1207.5772 [hep-ex]].

[81]   B. Aubert *et al.* [BaBar Collaboration], Phys. Rev. D **77**, 051103 (2008) [arXiv:0711.4889 [hep-ex]].

[82]   Y. Amhis *et al.* [Heavy Flavor Averaging Group Collaboration], arXiv:1207.1158 [hep-ex].

[83]   HFAG: Rare B decay parameterss, http://www.slac.stanford.edu/xorg/hfag/rare/

[84]   K. Funakubo, S. Tao and F. Toyoda, Prog. Theor. Phys. **109**, 415 (2003) [hep-ph/0211238].

[85]   Y. Okada, M. Yamaguchi and T. Yanagida, Prog. Theor. Phys. **85**, 1 (1991).

[86]   J. R. Ellis, G. Ridolfi and F. Zwirner, Phys. Lett. B **257**, 83 (1991).

[87]   H. E. Haber and R. Hempfling, Phys. Rev. Lett. **66**, 1815 (1991).

[88]   H. E. Haber, R. Hempfling and A. H. Hoang, Z. Phys. C **75** (1997) 539 [hep-ph/9609331].

[89]   A. Djouadi and J. Quevillon, arXiv:1304.1787 [hep-ph].

[90] M. S. Carena, J. R. Espinosa, M. Quiros and C. E. M. Wagner, Phys. Lett. B **355**, 209 (1995) [hep-ph/9504316].

[91] M. S. Carena, J. R. Ellis, A. Pilaftsis and C. E. M. Wagner, Phys. Lett. B **495** (2000) 155 [hep-ph/0009212].

[92] M. S. Carena, J. R. Ellis, S. Mrenna, A. Pilaftsis and C. E. M. Wagner, Nucl. Phys. B **659**, 145 (2003) [hep-ph/0211467].

[93] K. E. Williams and G. Weiglein, Phys. Lett. B **660**, 217 (2008) [arXiv:0710.5320 [hep-ph]].

[94] L. J. Hall, R. Rattazzi and U. Sarid, Phys. Rev. D **50**, 7048 (1994) [hep-ph/9306309].

[95] M. S. Carena, M. Olechowski, S. Pokorski and C. E. M. Wagner, Nucl. Phys. B **426**, 269 (1994) [hep-ph/9402253].

[96] T. Blazek, S. Raby and S. Pokorski, Phys. Rev. D **52**, 4151 (1995) [hep-ph/9504364].

[97] M. S. Carena, D. Garcia, U. Nierste and C. E. M. Wagner, Nucl. Phys. B **577**, 88 (2000) [hep-ph/9912516].

[98] C. Hamzaoui, M. Pospelov and M. Toharia, Phys. Rev. D **59**, 095005 (1999) [hep-ph/9807350].

[99] K. S. Babu and C. F. Kolda, Phys. Rev. Lett. **84**, 228 (2000) [hep-ph/9909476].

[100] G. Isidori and A. Retico, JHEP **0111**, 001 (2001) [hep-ph/0110121].

[101] A. Dedes and A. Pilaftsis, Phys. Rev. D **67**, 015012 (2003) [hep-ph/0209306].

[102] A. J. Buras, P. H. Chankowski, J. Rosiek and L. Slawianowska, Nucl. Phys. B **659**, 3 (2003) [hep-ph/0210145].

[103] M. Spira, A. Djouadi, D. Graudenz and P. M. Zerwas, Nucl. Phys. B **453**, 17 (1995) [hep-ph/9504378].

[104] M. Spira, Fortsch. Phys. **46**, 203 (1998) [hep-ph/9705337].

[105] A. Djouadi, Phys. Rept. **457**, 1 (2008) [hep-ph/0503172].

[106] A. Dedes and S. Moretti, Phys. Rev. Lett. **84**, 22 (2000) [hep-ph/9908516].

[107] A. Dedes and S. Moretti, Nucl. Phys. B **576**, 29 (2000) [hep-ph/9909418].

[108] S. Y. Choi and J. S. Lee, Phys. Rev. D **61**, 115002 (2000) [hep-ph/9910557].

[109] A. D. Martin, W. J. Stirling, R. S. Thorne and G. Watt, Eur. Phys. J. C **63**, 189 (2009) [arXiv:0901.0002 [hep-ph]].

[110] D. A. Dicus and S. Willenbrock, Phys. Rev. D **39**, 751 (1989).

[111] J. M. Campbell, R. K. Ellis, F. Maltoni and S. Willenbrock, Phys. Rev. D **67**, 095002 (2003) [hep-ph/0204093].

[112] F. Maltoni, Z. Sullivan and S. Willenbrock, Phys. Rev. D **67**, 093005 (2003) [hep-ph/0301033].

[113] R. V. Harlander and W. B. Kilgore, Phys. Rev. D **68**, 013001 (2003) [hep-ph/0304035].

[114] S. Dittmaier, M. Kramer, 1 and M. Spira, Phys. Rev. D **70**, 074010 (2004) [hep-ph/0309204].

[115] S. Dawson, C. B. Jackson, L. Reina and D. Wackeroth, Phys. Rev. D **69**, 074027 (2004) [hep-ph/0311067].

[116] J. Baglio and A. Djouadi, JHEP **1103**, 055 (2011) [arXiv:1012.0530 [hep-ph]].

[117] D. Graudenz, M. Spira and P. M. Zerwas, Phys. Rev. Lett. **70**, 1372 (1993).

[118] S. Dawson, A. Djouadi and M. Spira, Phys. Rev. Lett. **77**, 16 (1996) [hep-ph/9603423].

[119] A. Djouadi and M. Spira, Phys. Rev. D **62**, 014004 (2000) [hep-ph/9912476].

[120] G. Degrassi, P. Gambino and G. F. Giudice, JHEP **0012**, 009 (2000) [hep-ph/0009337].

[121] M. Misiak, H. M. Asatrian, K. Bieri, M. Czakon, A. Czarnecki, T. Ewerth, A. Ferroglia and P. Gambino *et al.*, Phys. Rev. Lett. **98**, 022002 (2007) [hep-ph/0609232].

[122] E. Lunghi and J. Matias, JHEP **0704**, 058 (2007) [hep-ph/0612166].

[123] M. E. Gomez, T. Ibrahim, P. Nath and S. Skadhauge, Phys. Rev. D **74**, 015015 (2006) [hep-ph/0601163].

[124] M. Carena, S. Gori, N. R. Shah, C. E. M. Wagner and L. -T. Wang, JHEP **1308** (2013) 087 [arXiv:1303.4414 [hep-ph]].

[125] M. Carena, S. Gori, N. R. Shah and C. E. M. Wagner, JHEP **1203**, 014 (2012) [arXiv:1112.3336 [hep-ph]].

[126] M. Carena, S. Gori, N. R. Shah, C. E. M. Wagner and L. -T. Wang, JHEP **1207**, 175 (2012) [arXiv:1205.5842 [hep-ph]].

[127] [CMS Collaboration], CMS PAS HIG-13-016.

[128] G. Barenboim, C. Bosch, M.L. López-Ibáñez and O. Vives, work in progress.

[129] D. J. H. Chung, L. L. Everett, G. L. Kane, S. F. King, J. D. Lykken and L. -T. Wang, Phys. Rept. **407**, 1 (2005) [hep-ph/0312378].

[130] A. J. Buras, A. Romanino and L. Silvestrini, Nucl. Phys. B **520**, 3 (1998) [hep-ph/9712398].

[131] A. Masiero, S. K. Vempati and O. Vives, arXiv:0711.2903 [hep-ph].

[132] L. Clavelli, T. Gajdosik and W. Majerotto, Phys. Lett. B **494**, 287 (2000) [hep-ph/0007342].

ICHEP 2014 oral contribution: Discarding a 125 GeV heavy Higgs in an MSSM model with explicit CP-violation

C. Bosch

Abstract

Current experimental constraints prove being enough to rule out the possibility of the $m_h \sim 125$ GeV Higgs found at LHC being a heavy Higgs in a general MSSM context, even with explicit CP violation in the Higgs potential. Differently than what has been done in prior studies, we perform this job analitically, with expressions related to a few observables. Te relevance of $\tau\tau$ production through Higgs and $\mathrm{BR}(B \to X_s \gamma)$ processes is emphasized, since they are enough to erase the possibility of finding an MSSM neutral Higgs lighter than the scalar discovered at LHC.

4.1 Theoretical considerations

In our publication about this topic [58], we study those models characterized by fitting the Minimal Supersymmetric (MSSM) description [2]. For the sake of generalization, we consider a CP-violating Higgs sector formed by two-Higgs doublets including all the possible mixings between the three scalars that are contained in it, besides a charged Higgs, with fields:

$$\Phi_1 = \begin{pmatrix} \frac{1}{\sqrt{2}}\left(v_1 + \phi_1 + ia_1\right) \\ \phi_1^- \end{pmatrix}; \;\; \Phi_2 = e^{i\xi} \begin{pmatrix} \phi_2^+ \\ \frac{1}{\sqrt{2}}\left(v_2 + \phi_2 + ia_2\right) \end{pmatrix}$$

$$(4.1)$$
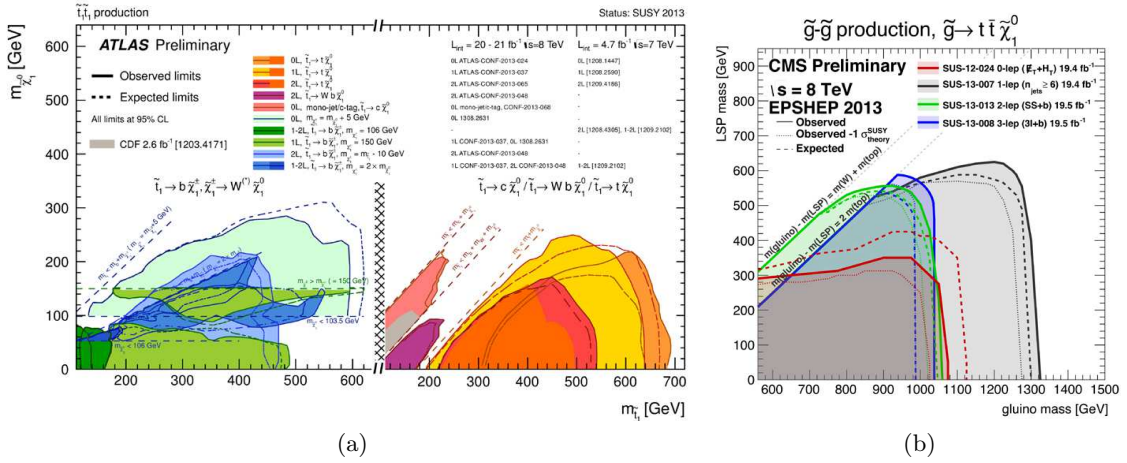
Figure 4.1: SUSY particle searches at (a) ATLAS (neutralino and stop) and (b) CMS (LSP and gluino).

We place the possible light Higgs in the mass range between 90 GeV $< m_h <$ 110 GeV, identifying the scalar found at the LHC as the next one according to mass, being $m_H =$125.5 GeV the value we used for our analysis. The heaviest neutral scalar mass will be restricted to an upper limit of 200 GeV due to the fact of having small CP violation, and thus avoiding a big splitting of the Higgs mass spectrum.

The mixing between up, down and pseudoscalar nature in the Higgs sector will find its origin in the one-loop corrections of the scalar potential, which leaves the pseudoscalar state as $a = a_1 \sin\beta + a_2 \cos\beta$ and a neutral Higgs mass matrix defined according to:

$$M_H^2 = \begin{pmatrix} M_S^2 & M_{SP}^2 \\ M_{PS}^2 & M_P^2 \end{pmatrix}, \qquad (4.2)$$

Our analysis will be developed using a small number of parameters, being them $\tan\beta \equiv {}^{v_2}\!/_{v_1}$, the Higgsino mass μ, the stop trilinear coupling A_t, its phase $\alpha(A_t)$, the sparticle mass scale M_{SUSY}, the gaugino mass M_2 and $m_{H^\pm}$ (since the pseudoscalar mass cannot be fixed, and they are related by $m_{H^\pm}^2 = M_P^2 + \frac{1}{2}\lambda_4 v^2 - Re(\lambda_5 e^2 i\xi)v^2$).

4.2 Experimental status

4.2.1 Bounds on SUSY particles

The LHC determination [3, 8] of allowed regions in which we can run the neutralino, stop and gluino masses is shown by the experimental plots of Figure 4.1a. In there, we can see that the neutrino mass is mostly forbidden to be below 500 GeV and, according to Figure 4.1b, the gluino mass below 1.3 TeV.

It is important that we consider the stop mass in a more sublte way, though the most visual lower bond is of $m_{\tilde{t}} =$650 GeV. In case there is stop-neutralino degeneracy, the lower bound for the mass can go down to 250 GeV, and taking into account every possibility for the stop mass is crucial for one of the observables we are going to use for the parameter space analysis.
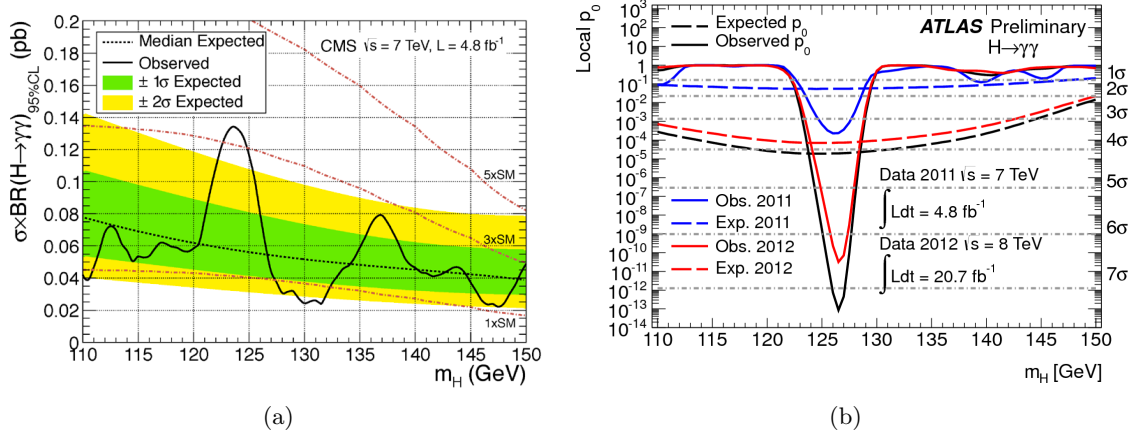
Figure 4.2: LHC plots indicating the discovery of a neutral scalar in the diphoton channel at (a) CMS and (b) ATLAS.

4.2.2 LHC Higgs Data: diphoton channel

LHC anounced the discovery [9, 10] of the $m_H =125.5$ GeV scalar based on the data found at the diphoton channel, which is a loop mediated decay.

In Figure 4.2 we can see how the peak of this plot fits in an excess corresponding to a signal of $0.90 \leq \mu_{\gamma\gamma}^{\text{LCH}} \leq 1.58$, taking the data in a conservative way, and according to the statistics availabe by the time our analysis was done.

4.3 Theoretical estimation of the diphoton channel events

For MSSM models with the number of parameters we are considering, the diphoton channel decay appears as [11]:

$$\Gamma(H_i \to \gamma\gamma) = \frac{M_{H_i}^3 \alpha^2}{256\pi^3 v^2}[|S_i^\gamma(M_{H_i}^3)|^2 + |P_i^\gamma(M_{H_i}^3)|^2] \tag{4.3}$$

which includes contributions coming from both scalar and pseudoscalar nature. The scalar contributions come from quarks, W bosons, squarks, charginos and the charged Higgs; whilst the pseudoscalar contributions only come from quarks, squarks and charginos.

Regarding the scalar Standard Model contributions to the Higgs decay (the pseudoscalar have an equivalent development), their values are:

$$W \to S_{H_i,W}^\gamma = -(\mathcal{U}_{i1}\cos\beta + \mathcal{U}_{i2}\sin\beta)F_1(\tau_{iW}); \qquad F_1(\tau_{iW}) \simeq 8; \quad \tau_{ij} = \frac{M_{H_i}^2}{4m_j^2}$$

$$t \to S_{H_i,t}^\gamma = \frac{8}{3}\mathcal{U}_{i2}F_t^S(\tau_{it}); \qquad\qquad\qquad F_t^S(\tau_{it}) \simeq 0.7$$

$$b \to S_{H_i,b}^\gamma = \frac{2}{3}\left(\text{Re}\left\{\frac{\mathcal{U}_{i1}+\mathcal{U}_{i2}\kappa_d}{1+\kappa_d\tan\beta}\right\}\tan\beta + \text{Im}\left\{\frac{\kappa_d(1+\tan\beta^2)}{1+\kappa_d\tan\beta}\right\}\right)\mathcal{U}_{i3}F_b(\tau_{ib});$$
$$F_b^S(\tau_{it}) \simeq 0.7$$

$$t+b \to S_{H_i,t+b}^\gamma \simeq 1.8\mathcal{U}_{i2} + (-0.025+i0.034)\left(\text{Re}\left\{\frac{\tan\beta}{1+\kappa_d\tan\beta}\right\}\mathcal{U}_{i1} + \text{Im}\left\{\frac{\kappa_d\tan^2\beta}{1+\kappa_d\tan\beta}\right\}\right)\mathcal{U}_{i3}$$

The SUSY contributions prove to be negligible compared to those previously exposed, since they are approximately:

$$S^\gamma_{H_i, \tilde{t}} \lesssim 0.26 \left[-\mathcal{U}_{i1} + 1.7 \mathcal{U}_{i2} + \mathcal{U}_{i3} \right]$$

$$S^\gamma_{H_i, \tilde{b}} \propto 1.2 \times 10^{-5} \tan^2 \beta$$

$$S^\gamma_{H_i, \tilde{\chi}^\pm} \lesssim 0.15 \left(\mathcal{U}_{i2} + \frac{M_2^2}{\mu^2} \right)$$

$$S^\gamma_{H_i, H^\pm} \lesssim -0.456 \left[\left(\frac{\mathcal{O}\left(\lesssim 1 \right)}{\tan \beta} + \mathcal{O}\left(\lesssim 1 \right) \right) + \left[\pm \mathcal{U}_{i1} \pm \mathcal{U}_{i2} \pm \mathcal{U}_{i3} \right] \right]$$

In addition, the calculation of the number of the events needs the computation of the Higgs production, according to:

$$\sigma(pp \to H_i) = K \hat{\sigma}^{\mathrm{LO}}_{gg \to H_i} \tau_{H_i} \frac{d\mathcal{L}^{gg}_{\mathrm{LO}}}{d\tau_{H_i}} + \hat{\sigma}^{\mathrm{QCD}}_{bb \to H_i} \tau_{H_i} \frac{d\mathcal{L}^{bb}_{\mathrm{LO}}}{d\tau_{H_i}} \tag{4.4}$$

Its contributions are defined as:

$$\sigma(pp \to H_i)_{bb} = 0.16 \frac{\tan^2 \beta}{(1 + \kappa_d \tan \beta)^2} \left[|\mathcal{U}_{i1}|^2 + |\mathcal{U}_{i3}|^2 \right] \quad \mathrm{pb} \tag{4.5}$$

for bb-fusion. Besides, the contribution coming from gluon fusion is:

$$\sigma(pp \to H_i)_{gg} = 13 \mathcal{U}_{i2}^2 - \frac{1.5 \tan \beta}{1 + \kappa_d \tan \beta} \mathcal{U}_{i1} \mathcal{U}_{i2} + \frac{0.1 \tan^2 \beta}{(1 + \kappa_d \tan \beta)^2} \mathcal{U}_{i1}^2 + \left(\frac{2}{1 + \kappa_d \tan \beta} + \frac{0.1 \tan^2 \beta}{(1 + \kappa_d \tan \beta)^2} + \frac{27}{\tan^2 \beta} \mathcal{U}_{i3}^2 \right) \quad \mathrm{pb} \tag{4.6}$$

The last piece we need to start our study is an estimation of the Higgs total width, which is approximately given by:

$$\Gamma_{H_i} \simeq \frac{g^2}{32 \pi M_W^2} \left[\tan^2 \beta \left(|\mathcal{U}_{i1}^2| + |\mathcal{U}_{i3}^2| \right) \left(3 m_b^2 + m_t^2 \right) + 6.7 \times 10^{-4} \left(\mathcal{U}_{i2}^2 + \frac{\mathcal{U}_{i1}^2}{\tan \beta} \right)^2 m_{H_i}^2 \right] \tag{4.7}$$

4.4   Analysis of diphoton channel data

Given the expressions of the previous section, we can infer that, if H_2 corresponds to the Higgs found at the LHC, $\tan \beta \to 1$ and the CP-mixing matrix takes the limits $\mathcal{U}_{21} = \mathcal{U}_{22} = 1$ and $\mathcal{U}_{23} = 0$, we will have a gluon fusion cross section and a total width equal to that predicted by the Standard Model (SM).

However, we have seen as well that the diphoton decay practically has no supersymmetrical contribution despite not taking any SM limit, thus forcing us to find a different explanation for the excess present in Figure 4.2, the loop-induced decay channel that drove to claiming the discovery of the Higgs boson.
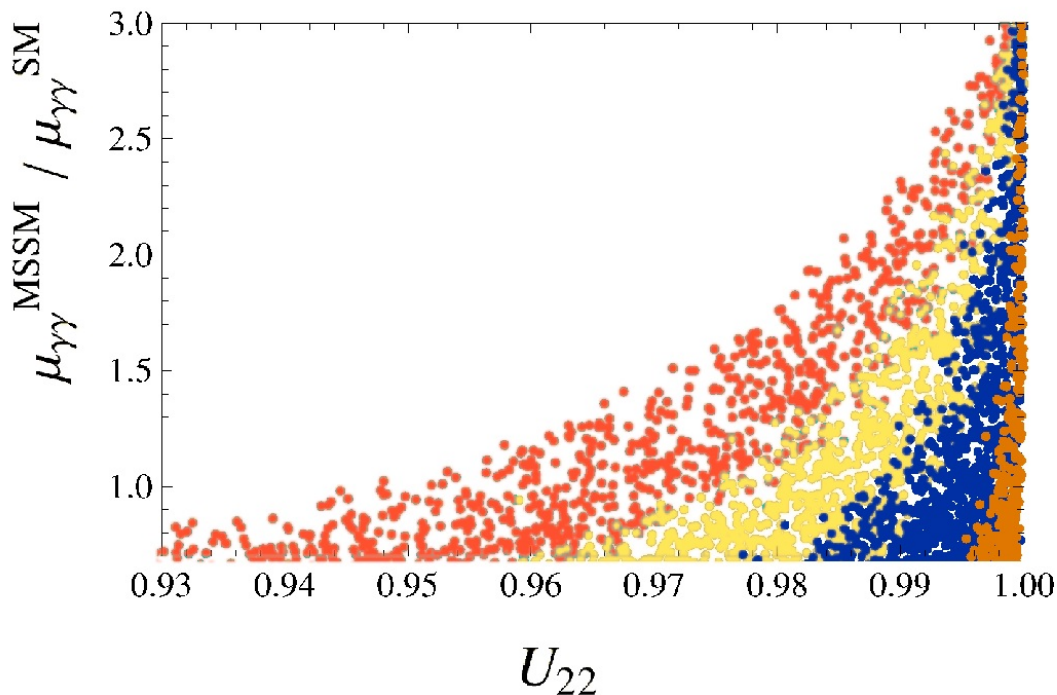
Figure 4.3: Number of events in the $\gamma\gamma$-channel according to the up mixing mmatrix element. Colors imply different values of $\tan\beta$, being orange the highest and brown the lowest.

First of all, we observe that the contributions to the $\gamma\gamma$-channel coming from both the W boson and the top quark (the two most important of them) have a strong dependence on the up-type mixing element $\mathcal{U}_{22}$. The gluon fusion cross section is also enhanced by this matrix element. Therefore, if we plot how the number of events in the diphoton channel changes according to the up-type component, we obtain the growing behavior appearing at Figure 4.3.

Consequently, we choose our mixing matrix to possess this feature, imposing $\mathcal{U}_{22} \simeq 1$ and taking the other components as decreasing according to $\tan\beta$, since we have to keep unitarity and we observe that there is a dependence in $\tan\beta$ for our result (Figure 4.3).

This is the first milestone of our work. In this situation, we need the neutral Higgs identified as that discovered at the LHC being an up-type Higgs for any MSSM model. The lightest and heaviest neutral Higgs bosons will have a mixture of down-type and pseudoscalar nature.

4.5 Other experimental constraints

Along this section we focus in determining if the scalar mass spectrum assuming the second Higgs to be the currently accepted as the SM Higgs is plausible. For that matter, we will begin with another LHC experimental result, the $H_i \to \tau\tau$ decay [12, 15].

The $\tau\tau$-channel relevance comes from the origin of this decay in the MSSM. Its enhancement will be associated with the particular CP character of the scalar decaying, which must be down-type or pseudoscalar. Taking this into account, the decay rate is,
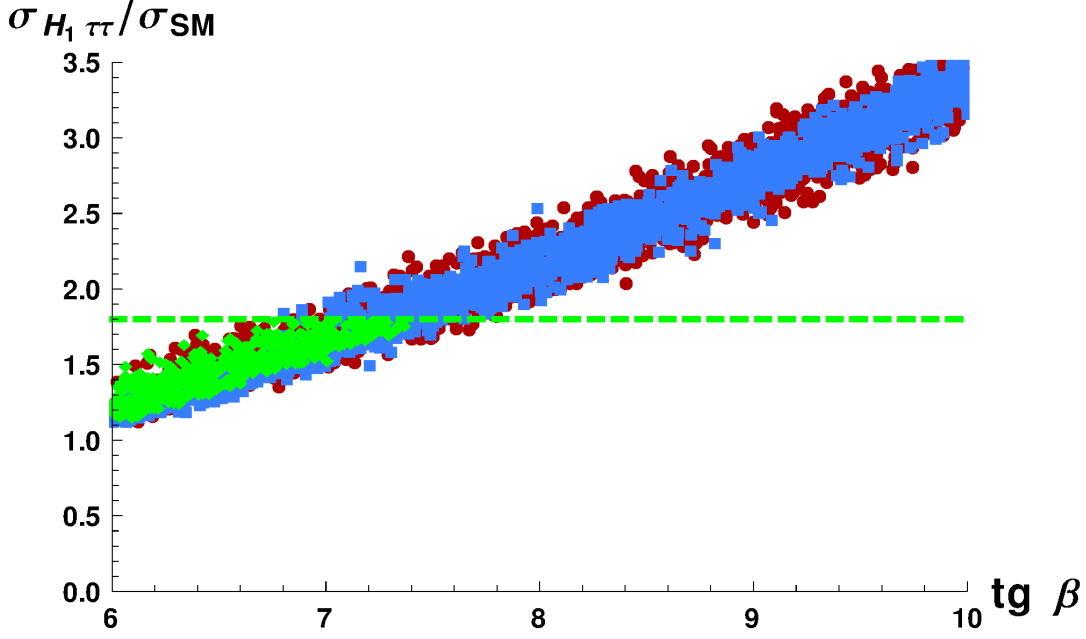
Figure 4.4: Scan results for the lightest Higgs decay into τ leptons, showing the allowed region in green. In red, points that do not accomplish this bound and neither the diphoton decay. In blue, points that fulfil the diphoton decay for the second Higgs.

approximately:

$$\Gamma_{j,\,\tau\bar{\tau}} \simeq \frac{g^2 m_{H_j} m_\tau^2}{32\pi M_W^2} \tan^2 \beta \qquad (4.8)$$

And its production will be mostly originated now by the bb-fusion:

$$\sigma\left(H_j \to pp\right) \simeq 0.16 \frac{\tan^2 \beta}{\left(1 + \kappa_d \tan \beta\right)^2} \quad \text{pb} \qquad (4.9)$$

in which we have considered the $\mathcal{U}_{j2}$ negligible and the sum of the square of the other components equal to one, thus preserving unitarity in the mixing matrix.

Performing now a scan with $m_{H_1} = 110\text{GeV}$ and $m_{H_3} = 160\text{GeV}$, both masses being valid guesses that do not affect generality, is found that only those models with low $\tan \beta$ are good candidates for being in agreement with LHC data, as it is presented in Figure 4.4.

This allowed region needs to be put to test. For this purpose, we make use of a flavour indirect bound, the $B \to X_S \gamma$ decay. This process is supposed to be quite constraining for low values of $\tan \beta$, and it includes the contribution of sparticles. This decay and $B_S^0 \to \mu^+ \mu^-$ are the references for low and high values of $\tan \beta$ respectively, though the analysis for its high values is already covered.

Experimentally, the branching ratio of the process (HFAG) [16, 17] is BR $(B \to X_S \gamma) = (3.43 \pm 0.21 \pm 0.07) \times 10^{-4}$. Theoretically, I will offer a qualitative approach to the sparticles contributions, though we used exact expressions for our scans [18, 22].

The term coming from the charged Higgs is always additive, defining the Wilson coefficient:

$$\mathcal{C}_7^{H^\pm} \simeq \frac{-0.2}{\tan \beta} \qquad (4.10)$$
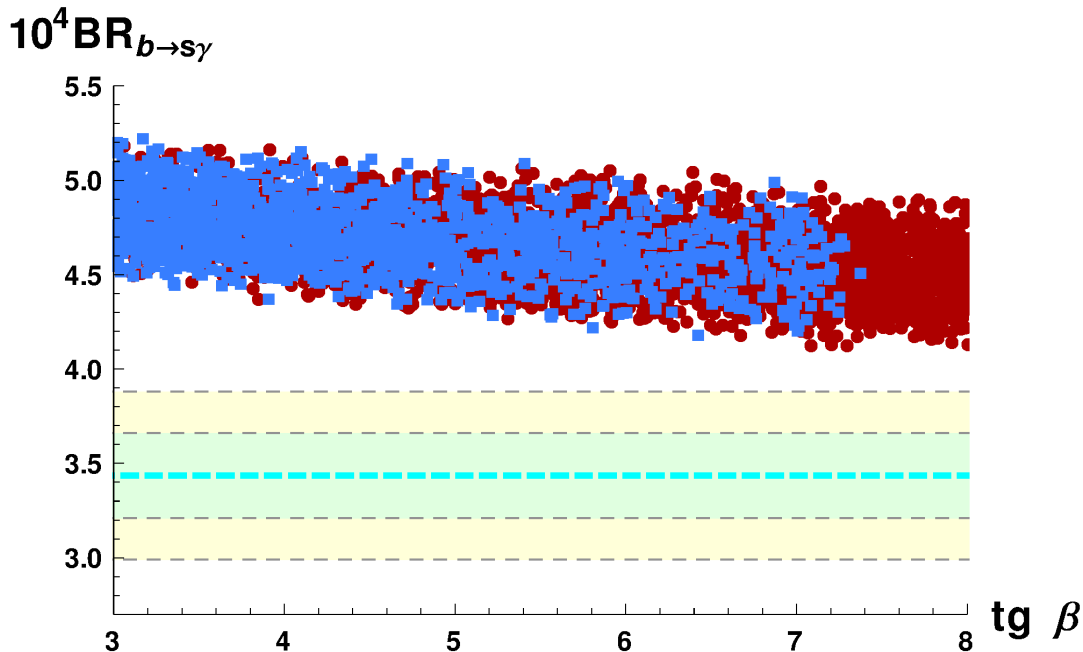
Figure 4.5: Scan results for $B \to X_S \gamma$. Blue squares survive any previous constraint, red squares have fallen before this. There is no allowed region within 2σ.

which shows to be indirectly proportional to $\tan \beta$. In addition, there is a contribution coming from the stop-chargino loop that can compensate it, depending on the sign of our parameters $\mathrm{Re}\,(\mu A_t)$, defined as:

$$\mathcal{C}_{7,8}^{\chi^{\pm}} \simeq 0.02 \frac{M_2}{\mu} \tag{4.11}$$

which is only valid for values of the stop mass with an inferior limit $m_{\tilde{t}_1} \geq 650$ GeV. Given this, we can find no compensation whatsoever, as presented in Figure 4.5. Therefore, every MSSM model that includes a Higgs boson lighter than 125.5 GeV would be vanished.

Nevertheless, we stated in Section 4.2 that there is an experimental region with a light stop that is mostly degenerate with the neutralino, avoiding detection. If this is the case, the Wilson coefficient correspondent to this contribution will not only change its sign, but gain strength with increasing values of $\tan \beta$ too, as shown in:

$$\mathcal{C}_{7,8}^{\chi^{\pm}} \propto -\tan \beta \frac{m_t^2}{m_{\tilde{t}_1}^2 - m_{\tilde{t}_2}^2} \tag{4.12}$$

Having considered this, we can see in Figure 4.6 that, though data ara closer to the 2σ threshold of this decay value, it is impossible to find any plausible MSSM with a light Higgs at all.

4.6 Conclusions

Our results give some relevant implications both for the purpose of disproving the existence of a MSSM neutral scalar lighter than 125.5 GeV and for searching these neutral bosons independently of their masses.

First of all, the study of the Higgs decaying into two photons gives us enough information for the determination of the CP mixing matrix. Concretely, for any MSSM model, the
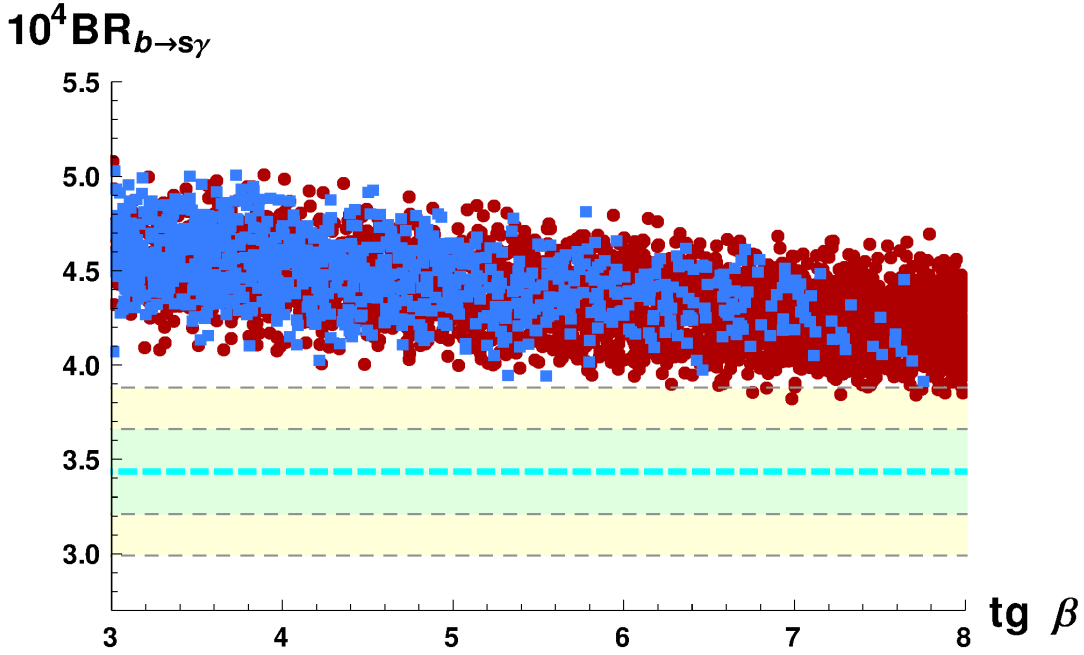
Figure 4.6: Scan results for $B \to X_S \gamma$ in the light stop regime. Color code is the same as in Figure 4.5.

neutral scalar representing the Higgs boson found at LHC should have an up-type matrix element. The other two neutral scalars are mixed states of down-type and pseudoscalar.

A fundamental decay channel for analysing the validity of the MSSM Higgs sector at high $\tan \beta$ is the Higgs decaying to two tau leptons. As it has been shown, this decay is enhanced when the decaying scalar has an associated CP matrix element with strong down and pseudoscalar components. Therefore, this decay channel deserves being a focus of experimental interest.

In the case of proposing MSSM models with a neutral Higgs lighter than the one found at 125.5 GeV, the $\tau\tau$ decay channel forbids any of them having a value of $\tan \beta \gtrsim 7.5$. If this channel was not enough to cover this range of $\tan \beta$, we should add $B_S^0 \to \mu^+ \mu^-$ as a constraint for our scan.

In order to swipe the $\tan \beta$ parameter space completely, a powerful constraint for its low values is given by $B \to X_S \gamma$ and its contributions coming from sparticles.

Including this decay in the analysis, which is very strict, we have been able to discard completely the existence of a Higgs boson lighter than that found in the LHC if it comes from any MSSM model, since there is no $\tan \beta$ value that allows this to happen.

These tools can be used for the analysis of different scalar mass spectra, and we have subsequently done it to study MSSM with a lightest neutral Higgs of $m_h = 125.5 \, \text{GeV}$, since it is the only possibility left by experimental data after our thorough study of it.

Bibliography

[1] G. Barenboim, C. Bosch, M. L. López-Ibañez and O. Vives, JHEP **1311** (2013) 051 [arXiv:1307.5973 [hep-ph]].

[2] A. Djouadi, Phys. Rept. **459**, 1 (2008) [hep-ph/0503173].

[3] S. Chatrchyan *et al.* [CMS Collaboration], JHEP **1303**, 037 (2013) [arXiv:1212.6194 [hep-ex]].

[4] S. Chatrchyan *et al.* [CMS Collaboration], arXiv:1305.2390 [hep-ex].

[5] [CMS Collaboration], PAS-SUS-13-007

[6] [CMS Collaboration], PAS-SUS-13-008

[7] [ATLAS Collaboration], ATLAS-CONF-2012-145.

[8] [ATLAS Collaboration], ATLAS-CONF-2013-007.

[9] G. Aad *et al.* [ATLAS Collaboration], Phys. Lett. B **716**, 1 (2012) [arXiv:1207.7214 [hep-ex]].

[10] S. Chatrchyan *et al.* [CMS Collaboration], Phys. Lett. B **716**, 30 (2012) [arXiv:1207.7235 [hep-ex]].

[11] J. S. Lee, A. Pilaftsis, M. S. Carena, S. Y. Choi, M. Drees, J. R. Ellis and C. E. M. Wagner, Comput. Phys. Commun. **156**, 283 (2004) [hep-ph/0307377].

[12] G. Aad *et al.* [ATLAS Collaboration], arXiv:1307.1427 [hep-ex].

[13] G. Aad *et al.* [ATLAS Collaboration], JHEP **1209**, 070 (2012) [arXiv:1206.5971 [hep-ex]].

[14] [CMS Collaboration], CMS-PAS-HIG-13-004.

[15] G. Aad *et al.* [ATLAS Collaboration], JHEP **1302**, 095 (2013) [arXiv:1211.6956 [hep-ex]].

[16] Y. Amhis *et al.* [Heavy Flavor Averaging Group Collaboration], arXiv:1207.1158 [hep-ex].

[17] HFAG: Rare B decay parameterss, http://www.slac.stanford.edu/xorg/hfag/rare/

[18] K. Funakubo, S. Tao and F. Toyoda, Prog. Theor. Phys. **109**, 415 (2003) [hep-ph/0211238].

[19] G. Degrassi, P. Gambino and G. F. Giudice, JHEP **0012**, 009 (2000) [hep-ph/0009337].

[20] M. Misiak, H. M. Asatrian, K. Bieri, M. Czakon, A. Czarnecki, T. Ewerth, A. Ferroglia and P. Gambino *et al.*, Phys. Rev. Lett. **98**, 022002 (2007) [hep-ph/0609232].

[21] E. Lunghi and J. Matias, JHEP **0704**, 058 (2007) [hep-ph/0612166].

[22] M. E. Gomez, T. Ibrahim, P. Nath and S. Skadhauge, Phys. Rev. D **74**, 015015 (2006) [hep-ph/0601163].

Improved τ-weapons for Higgs hunting

G. Barenboim, C. Bosch, M.L. López-Ibáñez, O. Vives

Abstract

In this work, we use the results from Higgs searches in the $\gamma\gamma$ and $\tau\tau$ decay channels at LHC and indirect bounds as $\mathrm{BR}(B \to X_s\gamma)$ to constrain the parameter space of a generic MSSM Higgs sector. In particular, we include the latest CMS results that look for additional Higgs states with masses up to 1 TeV. We show that the $\tau\tau$ channel is the best and most accurate weapon in the hunt for new Higgs states beyond the Standard Model. We obtain that present experimental results rule out additional neutral Higgs bosons in a generic MSSM below 300 GeV for any value of $\tan\beta$ and, for instance, values of $\tan\beta$ above 30 are only possible for Higgs masses above 600 GeV. ATLAS stored data have the potential to render this bound obsolete in the near future.

5.1   Introduction

The main purpose of the LHC, *i.e.* to find the Higgs boson and complete the Standard Model (SM) construction, was recently fulfilled with the discovery, at ATLAS and CMS, of a bosonic resonance with a mass ~ 126 GeV [1, 2]. The relevance of this discovery can not be understimated because of the key role the Higgs boson plays in the structure of the SM, as it provides the mechanism of electroweak symmetry breaking and generates the masses for gauge bosons and fermions. Likewise, in all the SM extensions other scalar bosons associated to the breaking of the electroweak symmetry are present and play an equaly important role.

However, to confirm that this resonance corresponds indeed to the SM Higgs boson or it belongs to one of the SM extensions, it is necessary to measure in LHC experiments its properties and couplings with high precision [3, 4, 5, 6, 7, 8, 9, 10, 11, 12, 13]. At present, the observed production cross section and decay channels seem to be consistent, within errors, with a Higgs boson in the SM framework. But the current experimental

precision leaves the possibility of this resonance being a Higgs boson of one of the different extensions of the SM open [3, 4]. To clarify this issue, further experimental studies on the resonance properties are needed, together with complementary studies looking for new scalar particles that are usually present in these extensions of the SM.

The prototype SM extension in the Higgs sector is the so-called two Higgs doublet model (2HdM). In a 2HdM, the Higgs sector is expanded with the inclusion of a second scalar doublet of opposite hypercharge. This enlargement of the scalar sector leads to an increase in the number of physical Higgs states in the spectrum, that is then composed by two scalar states, one pseudoscalar state and a charged Higgs boson. In particular, it is well-known that the Higgs sector of the MSSM is a type II 2HdM [4, 5, 16]. The type II qualifier refers to the fact that, at tree level, only one of the doublets couples to down-type fermions while the second one couples to up-type fermions. This is one of the classical mechanisms to avoid the appearance of flavour changing neutral currents (FCNC) at tree-level. The requirement of holomorficity of the superpotential together with gauge invariance forces the Higgs sector in a supersymmetric model to be precisely a type II 2HdM, and this is the scenario where we will perform our analysis. The MSSM is the minimal supersymmetric extension of the Standard Model with respect to particle content. In particular the Higgs sector of the MSSM is a type II 2HdM and it is CP-conserving at tree-level [4, 5, 16]. However, loop effects involving the complex parameters in the MSSM Lagrangian violate the tree-level CP-invariance of the MSSM Higgs potential modifying the tree-level masses, couplings, production rates and decay widths of Higgs bosons [35, 36, 37, 38, 21, 22]. In this way, the physical Higgs eigenstates become admixtures of CP-even and odd states and its couplings to SM particles are modified accordingly.

In a recent paper [58], we carried out an analysis in a generic MSSM under the assumption that the observed Higgs state corresponded to the second-lightest Higgs. We were able to eliminate this possibility analytically, using only the diphoton signal strength, $\tau\tau$ production through Higgs and $\mathrm{BR}(B \to X_s \gamma)$. In this work, we follow a similar strategy to scrutinize the allowed areas of parameter space in a complex MSSM in the case the Higgs measured at LHC is the lightest MSSM Higgs boson. We look for the best observables to identify the nature of the Higgs sector and, specially, where it is more appropriate to search for additional Higgs states.

As our analysis concentrates mainly on the Higgs sector of the MSSM and this sector is affected only by a handful of MSSM parameters, it is possible to perform a general phenomenological analysis in terms of these parameters encompassing all the different MSSM setups. In this context, we fix $m_{H_1} \simeq 126$ GeV $\leq m_{H_2}, m_{H_3}, m_{H^\pm}$ and use the experimental results to look for acceptable values for these Higgs masses and 3×3 Higgs mixing matrices as a function of $\tan\beta$. It is important to emphasize that we keep Higgs masses and mixings as free, constrained only by the experimental results, and we do not determine them by minimizing the Higgs potential imposing the correct breaking of the electroweak symmetry. This implies that some of the considered points may not be possible to achieve in a complete model, although most of them can be reproduced with appropriate parameters in the SUSY sector. The main supersymmetric parameters affecting the Higgs sector, and also the indirect processes $B \to X_s \gamma$ and $B_s \to \mu^+ \mu^-$, are basically third generation masses and couplings, because of their large Yukawa couplings, and gaugino masses. In our analysis, these parameters take general values consistent with the experimental constraints on direct and indirect searches.

In the literature there have been several works constraining the parameter space of different MSSM variants with LHC data [24, 25, 26, 27, 28, 29, 30] with special emphasis in light Higgs masses and the non-decoupling MSSM limit [31, 32, 33, 34, 35, 36, 37, 38].

As described in the previous paragraph, our analysis in a generic MSSM model includes all these MSSM variants and updates them with the latest data on searches in the $\tau\tau$ channel from ATLAS and CMS at LHC. Furthermore, our analytic approach with a few key phenomenological observables, the two photon signal strength, the $\tau\tau$ production cross sections at LHC and the indirect constraints on $\text{BR}(B \to X_s\gamma)$, can neatly exclude wide regions of the parameter space without the risk of missing a small region where unexpected cancellations or combinations can take place and simultaneously allows us to identify clearly the observables responsible of this exclusion.

This work is organized as follows. We begin by describing the basic ingredients of the model in Section 7.2 and recount the latest results on extra-Higgs searches in Section 5.3. In section 5.4 we analyze the present constraints on the model and the future prospects for the searches of additional Higgs states. We discuss the possibility of a second peak in the diphoton spectrum in Section 5.5. Finally, results and conclusions are summarized in Section 5.6.

5.2   Higgs sector in a complex MSSM

As explained above, we aim to establish the identity of the observed scalar resonance found at $m_H \simeq 126$ GeV in LHC experiments and, in particular, to check whether this is one of the Higgs states in an MSSM setup. The MSSM is the most simple supersymmetric extension of the SM. In this work, we carry our analysis in a generic MSSM in the presence of CP-violating phases. Even though the Higgs sector is CP-conserving at tree-level [16], the presence of CP-violating phases in the theory induces at loop level CP violation in the Higgs potential [33, 32, 35, 41, 36, 37, 38, 21, 22]. These loop corrections produce a mixing between scalar and pseudoscalar states, turning this way the physical mass eigenstates into admixtures of CP even and CP odd states, with no definite CP parity. Thus, the introduction of CP phases set us a far cry from the CP conserving MSSM where the neutral scalars, h^0 and H^0, and the pseudoscalar, A^0 do not mix.

Including CP violating phases into the MSSM requires to write the two scalar doublets as [35, 36, 38, 42],

$$\Phi_1 = \begin{pmatrix} \frac{1}{\sqrt{2}}(v_1 + \phi_1 + ia_1) \\ \phi_1^- \end{pmatrix}; \quad \Phi_2 = e^{i\xi} \begin{pmatrix} \phi_2^+ \\ \frac{1}{\sqrt{2}}(v_2 + \phi_2 + ia_2) \end{pmatrix}, \tag{5.1}$$

where v_1 and v_2 are the Higgs vacuum expectation values in the electroweak vacuum and $\tan\beta = v_2/v_1$. Now, the mass matrix for the physical neutral scalars, in the basis, (ϕ_1, ϕ_2, a) with $a = a_1 \sin\beta + a_2 \cos\beta$, becomes

$$M_H^2 = \begin{pmatrix} M_S^2 & M_{SP}^2 \\ M_{PS}^2 & M_P^2 \end{pmatrix}, \tag{5.2}$$

where M_S^2 is 2×2 and $M_{SP}^2 = (M_{PS}^2)^T$ is a 1×2 block. This mass matrix is diagonalized by a 3×3 matrix, $\mathcal{U}$,

$$\mathcal{U} \cdot M_H^2 \cdot \mathcal{U}^T = \text{Diag}\left(m_{H_1}^2, m_{H_2}^2, m_{H_3}^2\right). \tag{5.3}$$

The scalar-pseudoscalar mixing, which is absent in the CP conserving case, arises at the one-loop level in the CP violating MSSM and is of order [35],

$$M_{SP}^2 = O\left(\frac{m_t^4 |\mu||A_t|}{32\pi^2 \ v^2 M_{SUSY}^2}\right) \sin\phi_{CP} \times \left[6, \frac{|A_t|^2}{M_{SUSY}^2}, \frac{|\mu|^2}{\tan\beta M_{SUSY}^2}\right], \tag{5.4}$$

where $\phi_{CP} = \arg(\mu A_{t,b} e^{i\xi})$ and $M_{SUSY}^2 = (m_{\tilde{t}_1}^2 + m_{\tilde{t}_2}^2)/2$. From this expression, we see that large effects in the Higgs sector due to the presence of this CP violating phase are obtained for $\mathrm{Im}\left[\mu A_{t,b} e^{i\xi}\right] \gtrsim M_{SUSY}^2$ and M_P^2 not much larger than v^2. This situation is still possible phenomenologically outside the decoupling limit and thus in the following we analyze this complex MSSM which, obviously, includes the usual real scalar potential as a particular case.

In our analysis, we consider a generic MSSM defined at the electroweak scale with the lightest Higgs mass $m_{H_1} \simeq 126$ GeV. We take the other two neutral Higgses and the charged Higgs masses as free with generic mixing matrices $\mathcal{U}$, which we constrain with the present experimental results. The rest of MSSM parameters are also free and independent at M_W and only constrained by experimental results without further theoretical restrictions. Nevertheless, some of the parameters of the Higgs sector of the MSSM, and in particular the μ term in the superpotential, are very important in other sectors of the theory like sfermion masses and left–right mixings and play a very important role in several of the analyzed flavour changing decays. In this work, we are not fixing the value of the μ term through the requirement of correct electroweak symmetry breaking, but we take it to vary in a wide range from $M_2 \leq \mu \leq 3m_{H^\pm}$, taking into account that, at tree-level, the scale of the charged and heavy Higgses is fixed by the μ parameter.

The remaining SUSY masses and mixings are fixed by the SUSY soft breaking terms and are only subject to the experimental constraints from direct LHC searches and contributions to FCNC, as summarized in [57, 58] [1]. In our analysis of the Higgs sector and FCNC constraints, the most important SUSY parameters are gaugino masses and third generation sfermion masses and mixings. The complete expressions for Higgs production and decays taking into account the couplings of the new Higgs states to fermions, scalars and gauge bosons, can be found in [58].

5.3   Extra-Higgs searches in the $pp \to \tau\tau$ process

The experimental constraints we impose on the Higgs sector of our generic MSSM were already described in our previous paper, [58]. The $H \to \gamma\gamma$ bounds and the indirect constraints, $\mathrm{BR}(B \to X_s\gamma)$ and $\mathrm{BR}(B_s \to \mu\mu)$, are still the same and we refer to [58] for details.

Still, the results in the channel $H_i \to \tau\tau$, which play a very important role in the searches for additional heavy Higgs states, has been recently updated by the CMS collaboration [60]. Both ATLAS and CMS experiments had previously carried dedicated analysis in this channel. Both experiments have searched for the SM Higgs boson decaying into a pair of τ-leptons and this provides a limit on $\sigma(pp \to H) \times \mathrm{BR}(H \to \tau\tau)$ at 95% C.L. that can be applied to all three neutral Higgs states in the MSSM. ATLAS has analyzed the collected data samples of $4.6\,\mathrm{fb}^{-1}$ at $\sqrt{s} = 7$ TeV and $13.0\,\mathrm{fb}^{-1}$ at $\sqrt{s} = 8$ TeV [45] while CMS used $4.9\,\mathrm{fb}^{-1}$ at $\sqrt{s} = 7$ TeV and $19.4\,\mathrm{fb}^{-1}$ at $\sqrt{s} = 8$ TeV for Higgs masses up to 150 GeV [46]. For this range of masses, CMS sets the strongest bound: for $m_H = 110$ GeV we obtain a bound at 95% CL of $\mu_{\tau\tau} = \sigma(H \to \tau\tau)/\sigma_{SM} \leq 1.8$, and this limit remains nearly constant, $\mu_{\tau\tau} \leq 2.0$, up to $m_H = 140$ GeV. For a neutral Higgs of mass $m_H = 150$ GeV we would have a bound of $\mu_{\tau\tau} \leq 2.3$. In our generic MSSM, this limit would apply to the lightest Higgs with $m_{H_1} \simeq 126$ GeV and to the two heavier neutral Higgs states when their masses are below 150 GeV.

---

[1]In particular, we allow the trilinear couplings A_i to take values in the range $0 \leq A_i \leq 3m_{\tilde{i}}$, to avoid charge and color-breaking minima.
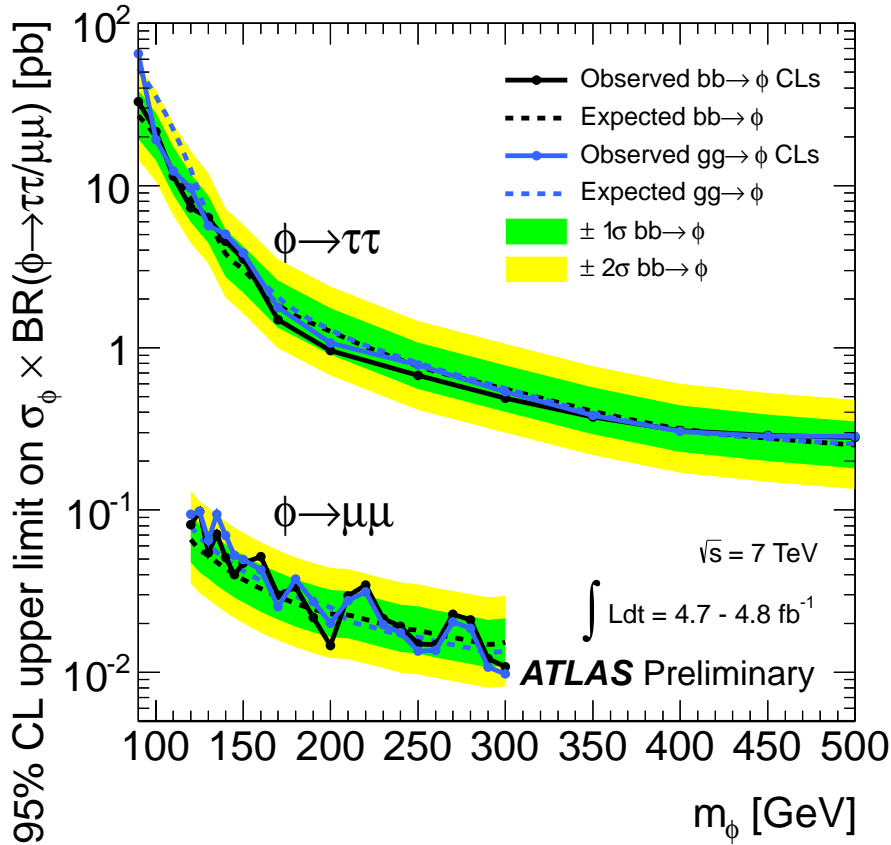
Figure 5.1: Upper limit on the $\tau\tau$ production cross section through heavy Higgs states from ATLAS with 4.8 fb^{-1} at $\sqrt{s} = 7$ TeV .

For heavier H_i masses, there exist a previous ATLAS analysis at LHC searching MSSM Higgs bosons with masses up to 500 GeV with 4.9 fb^{-1} at $\sqrt{s} = 7$ TeV [47]. In this case, the bound as an upper limit on the $\tau\tau$, or $\mu\mu$ production cross section also at 95 % C.L. that is shown in Figure 3.2. We can expect this bound to improve nearly an order of magnitude in an updated analysis with the new data [48]. Nevertheless, recently the CMS collaboration has presented an analysis of the full data set with an integrated luminosity of 24.6 fb^{-1}, with 4.9 fb^{-1} at 7 TeV and 19.7 fb^{-1} at 8 TeV searching for additional neutral Higgs states in the $\tau\tau$ channel up to masses of 1 TeV [60]. The analysis discriminates between Higgses produced through gluon fusion and $b\bar{b}$ fusion with two extra b-jets. These latest CMS results are presented in Figure 5.2. As we will see later, these new experimental results set very stringent constraints for the neutral Higgs spectrum. In the following, we apply all these bounds at 95 % C.L. on the theoretical cross sections obtained in our generic MSSM.

5.4 Model analysis

The purpose of this section is to present the outcome of our complex MSSM model predictions in different Higgs decay channels and compare them to the current experimental results at LHC. The main Higgs search channels that we use to constrain the parameters in our model are $pp \rightarrow H_1 \rightarrow \gamma\gamma$ and $pp \rightarrow H_i \rightarrow \tau^+\tau^-$. However, we will see that indirect
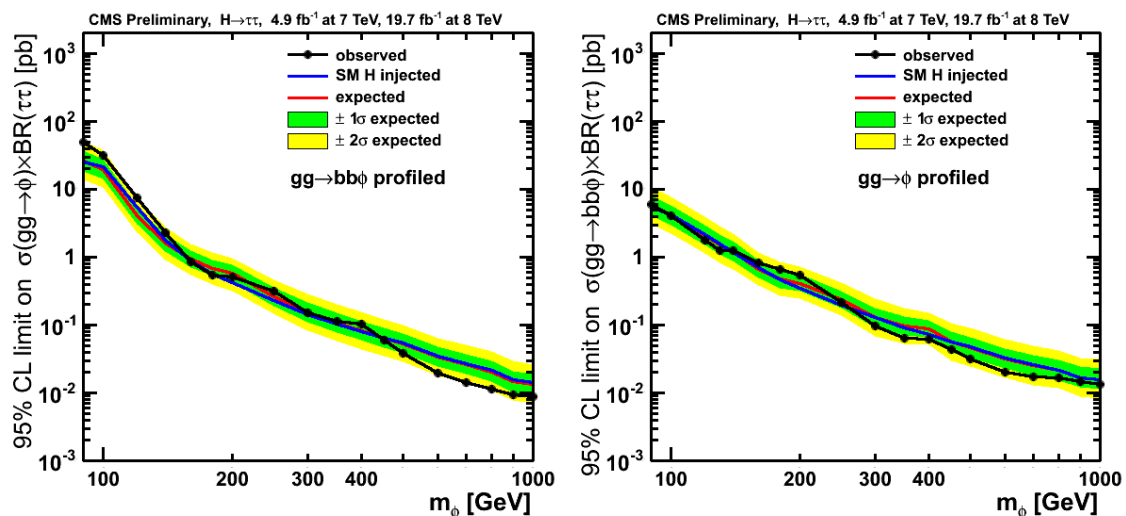
Figure 5.2: Latest CMS results on the $\tau\tau$ production cross section through heavy Higgs states with 24.6 fb^{-1} at $\sqrt{s}$=7–8 TeV. On the left the bound obtained from gluon-fusion produced Higgs while on the right the bound from the $b\bar{b}$ production mode with two additional b-jets is shown.

new physics searches also play a very important role in constraining the model due the charged and neutral Higgs contributions to $b \to s\gamma$ and $B_s \to \mu^+\mu^-$.

In the following, after setting the lightest neutral Higgs mass at $m_{H_1} = 126$ GeV, we impose the constraints derived from the LHC results on $pp \to H_1 \to \gamma\gamma$ and indirect bounds from low energy experiments. Then, we divide our analysis in two different regions to study the $\tau\tau$ production cross section: i) a light MSSM Higgs sector, defined by $m_{H^+} < m_t$, that can be considered the non-decoupling regime, and ii) heavy Higgs masses, when $m_{H^+} > m_t$, as would correspond to the decoupling limit in the sense discussed below Eq. (5.4) of $M_P^2 > v^2$.

5.4.1   Two photon cross section

The decay $H \to \gamma\gamma$ has been the main channel in the discovery of a scalar resonance at $m_H \simeq 126$ GeV at LHC experiments. ATLAS finds an excess of 2.8 σ local significance at a mass of $m_H = 126.5$ GeV while CMS finds a contribution at a mass of $m_H = 126.5$ GeV with a p-value of 4.1 σ. The measured signal strength in this channel, defined as the ratio of the measured $\gamma\gamma$ production cross section to the SM expected value, combining both ATLAS and CMS results at two sigma is $0.75 \le \mu_{\gamma\gamma}^{\text{LHC}} \le 1.55$ and we impose the accepted points in the parameter space to be within this range. The $\gamma\gamma$ production through the Higgs in the narrow width approximation depends on the Higgs production cross section and the $H \to \gamma\gamma$ branching ratio, which in turn depends both on the decay width into two photons and on the total decay width. Thus, we will have to analyze these three elements to constrain our model.

First of all, we focus on the Higgs decay amplitude into photons, $\Gamma(H_1 \to \gamma\gamma)$, which has both scalar and pseudoscalar amplitudes that receive contributions from gauge bosons, fermions, sfermions and charged Higgs in our MSSM model, *i.e.*,

$$\Gamma(H_a \to \gamma\gamma) = \frac{M_{H_a}^3 \alpha^2}{256\pi^3 v^2} \left[|S_a^\gamma(M_{H_a})|^2 + |P_a^\gamma(M_{H_a})|^2 \right]. \tag{5.5}$$

The full expressions for the different contributions to the scalar S_a^γ, and pseudoscalar, P_a^γ, amplitudes are presented in [58]. The dominant contributions to the scalar amplitude are given by the W-boson and top quark, with the bottom-quark contributing only for very large $\tan\beta$,

$$S_{H_1^0,W}^\gamma \simeq -8.3 \left(\mathcal{U}_{12} + \frac{\mathcal{U}_{11}}{\tan\beta} \right)$$

$$S_{H_1^0,b+t}^\gamma \simeq 1.8\,\mathcal{U}_{12} + (-0.025 + i\,0.034) \left[\mathrm{Re}\left\{ \frac{\tan\beta}{1+\kappa_d\tan\beta} \right\} \mathcal{U}_{11} + \mathrm{Im}\left\{ \frac{\kappa_d\tan^2\beta}{1+\kappa_d\tan\beta} \right\} \mathcal{U}_{13} \right] \tag{5.6}$$

where $\kappa_d = (\Delta h_d/h_d)/(1 + \delta h_d/h_d)$ encodes the loop corrections to the down Yukawas, with $(h_d + \delta h_d)$ the one-loop corrected Yukawa coupling of down quarks to H_1 and Δh_d the non-holomorphic coupling of down quarks to H_2^* [44, 46, 45, 52, 6, 8, 10, 56, 13, 57, 58].

Next, we have to consider the MSSM contributions to the amplitude, that include the charged Higgs and third generation sfermions. In the analysis of Ref. [58] we showed that the charged Higgs contribution can always be neglected in comparison to the contributions in Eq. (5.6). In the case of the stop, if we impose the LHC bound on the stop mass for large mass difference to the LSP $m_{\tilde{t}} \gtrsim 650\,\mathrm{GeV}$, its contribution is also much smaller than the dominant SM contributions. However, this contribution can be somewhat larger for lighter stops with a small mass difference with the LSP, although there exists an absolute lower bound of $m_{\tilde{t}} \gtrsim 250\,\mathrm{GeV}$ from single jet searches [59]. For low stop masses, the stop contribution can be important and we keep it in our approximate expression for the scalar amplitude.

Finally, we have to consider sbottom and stau contributions. These contributions are negligible at medium-low $\tan\beta$, say $\tan\beta \lesssim 8$, compared to those coming from the SM particles due to the smallness of the Yukawa couplings in this regime. However, they can be sizeable for very large $\tan\beta$ or very light sparticles. In fact, in Refs. [60, 61, 62] the stau contribution was proposed as a way to increase the diphoton decay rate without affecting the Higgs production cross section[2] and therefore not modifying the successful predictions in other channels. However, this would require large $\tan\beta$ values and, as we show below, this is incompatible with the bounds from $H_2, H_3 \to \tau\tau$ for $m_{H_{2,3}} \leq 1$ TeV. Nevertheless, for such heavy Higgs masses, a light stau could contribute considerably to the scalar amplitude for large $\tan\beta$. The stau contribution to $S_{H_1^0}^\gamma$ can be approximated by

$$
\begin{aligned}
S_{H_1^0,\tilde{\tau}}^\gamma &\simeq 0.36\tan^2\beta\, \frac{m_\tau^2}{m_{\tilde{\tau}_1}^2} \left[\frac{\mathrm{Re}\{A_\tau^*\mu\}}{m_{\tilde{\tau}_2}^2}\mathcal{U}_{11} - \frac{\mu^2}{m_{\tilde{\tau}_2}^2}\mathcal{U}_{12} + \frac{\mathrm{Im}\{A_\tau^*\mu\}}{m_{\tilde{\tau}_2}^2\tan\beta}\mathcal{U}_{13} \right] \\
&\simeq 3\times 10^{-5}\tan^2\beta \left(\frac{200\mathrm{GeV}}{m_{\tilde{\tau}_1}} \right)^2 \left[\frac{\mathrm{Re}\{A_\tau^*\mu\}}{m_{\tilde{\tau}_2}^2}\mathcal{U}_{11} - \frac{\mu^2}{m_{\tilde{\tau}_2}^2}\mathcal{U}_{12} + \frac{\mathrm{Im}\{A_\tau^*\mu\}}{m_{\tilde{\tau}_2}^2\tan\beta}\mathcal{U}_{13} \right],
\end{aligned}
\tag{5.7}
$$

where we used that the loop function is approximately 0.35 (and tends to 1/3) for $m_{\tilde{\tau}} \gtrsim 200\,\mathrm{GeV}$. From here it is clear that an $O(1)$ stau contribution, which would be required to enhance the diphoton rate, is only possible for $\tan\beta \geq 80$ and $m_{\tilde{\tau}} \leq 100$ GeV if $A_\tau^*/m_{\tilde{\tau}_2}, \mu/m_{\tilde{\tau}_2} \simeq O(1)$. Even in an extreme case, $A_\tau^*/m_{\tilde{\tau}_2}, \mu/m_{\tilde{\tau}_2} \lesssim 3$, would require

---

[2]Notice that a large sbottom contribution would enhance both the Higgs production and the diphoton decay width, and thus modify also the successful ZZ and WW predictions.
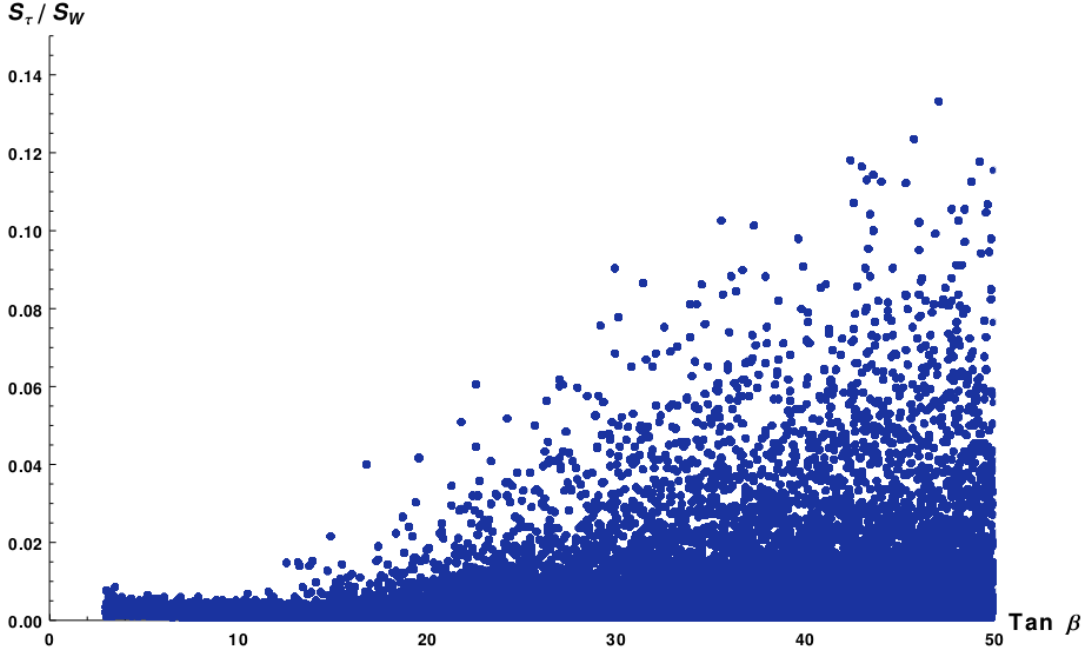
Figure 5.3: $\tilde{\tau}$ scalar contribution to the two photons decay width compared to the W-boson contribution as a function of $\tan\beta$

$\tan\beta \geq 50$ and $m_{\tilde{\tau}} \leq 150$ GeV to get an $O(1)$ contribution. This can be seen in Figure 5.3, where we compare the stau and the W-boson contributions up to $\tan\beta$ values of 50. In any case, these large $\tan\beta$ values can increase the diphoton width at most a 10–30% and, as we show below, such large $\tan\beta \gtrsim 50$ values are strongly constrained by $H_i \to \tau\tau$ channel. Moreover, this large $\tan\beta$ values would not be enough to increase the $H_1 \to \gamma\gamma$ branching ratio, as they would simultaneously increase the H_1 total width. Therefore, in this work, we do not consider such large $\tan\beta$ values and we neglect stau and sbottom contributions. Also, as we show in [58], chargino contributions are always negligible.

Thus, finally, keeping only the dominant W-boson, quark and stop contributions, we can approximate the scalar amplitude by,

$$
\begin{aligned}
S_{H_1^0}^{\gamma} \quad \simeq \quad & \mathcal{U}_{11}\left(-\frac{8.3}{\tan\beta} + (-0.025 + i\,0.034)\,\mathrm{Re}\left\{\frac{\tan\beta}{1 + \kappa_d\tan\beta}\right\}\right. \qquad (5.8)\\
& \left. -0.45\left(\frac{m_{\tilde{t}_2}^2}{m_{\tilde{t}_1}^2} - 1\right)\mathrm{Re}\left\{\frac{\mu m_t \mathcal{R}_{11}^* \mathcal{R}_{21}}{m_{\tilde{t}_2}^2}\right\}\right) + \\
& \mathcal{U}_{12}\left(-6.5 + 0.45\left(\frac{m_{\tilde{t}_2}^2}{m_{\tilde{t}_1}^2} - 1\right)\mathrm{Re}\left\{\frac{A_t^* m_t \mathcal{R}_{11}^* \mathcal{R}_{21}}{m_{\tilde{t}_2}^2}\right\}\right. \\
& \left. +0.45\left(\frac{m_t^2 |\mathcal{R}_{11}|^2}{m_{\tilde{t}_1}^2} + \frac{m_t^2 |\mathcal{R}_{12}|^2}{m_{\tilde{t}_2}^2}\right)\right) + \\
& \mathcal{U}_{13}\left((-0.025 + i\,0.034)\,\mathrm{Im}\left\{\frac{\kappa_d\tan^2\beta}{1 + \kappa_d\tan\beta}\right\}\right. \\
& \left. +0.45\left(\frac{m_{\tilde{t}_2}^2}{m_{\tilde{t}_1}^2} - 1\right)\mathrm{Im}\left\{\frac{\mu m_t \mathcal{R}_{11}^* \mathcal{R}_{21}}{m_{\tilde{t}_2}^2}\right\}\right).
\end{aligned}
$$

This amplitude has to be compared with the SM value $S_{H_{SM}}^{\gamma} \simeq -6.55$. The pseudoscalar

amplitude, absent in the SM, is typically much smaller, as it receives contributions only from fermions, i.e. mainly top and bottom quarks, and these contributions are of the same order as fermionic contributions to the scalar amplitude.

Then, the total Higgs decay width receives contributions mainly from $H_1 \to WW^*$ and the down-type fermion, $H_1 \to b\bar{b}$ and $H_1 \to \tau\tau$ which, compared to the SM predictions, are enhanced by $\tan^2\beta$. Then $H_1 \to gg$ decay can be of the same order of $H_1 \to \tau\tau$ for low $\tan\beta$, but can be safely neglected as it is always subdominant with respect to $b\bar{b}$ and WW^* and does not influence significantly the total width:

$$\Gamma_{H_1} \simeq \frac{g^2 m_{H_1}}{32\pi M_W^2} \left[\tan^2\beta \left(\mathcal{U}_{11}^2 + \mathcal{U}_{13}^2 \right) \left(3m_b^2 + m_\tau^2 \right) + I_{PS} \left(\mathcal{U}_{12} + \frac{\mathcal{U}_{11}}{\tan\beta} \right)^2 m_{H_1}^2 \right] \quad (5.9)$$

with $I_{PS} \simeq 6.7 \times 10^{-4}$ being the phase space integral.

Using Eqs. (5.5) and (5.9) we can estimate BR($H_1 \to \gamma\gamma$) as,

$$\begin{aligned} \mathrm{BR}(H_1 \to \gamma\gamma) &\simeq \frac{\alpha^2}{32\pi^2 \left(3x_b + x_\tau\right)} \frac{|S^\gamma|^2 + |P^\gamma|^2}{\left(\mathcal{U}_{11}^2 + \mathcal{U}_{13}^2\right)\tan^2\beta + \left(\mathcal{U}_{12} + \frac{\mathcal{U}_{11}}{\tan\beta}\right)^2 \frac{I_{PS}}{(3x_b+x_\tau)}} \\ &\simeq 4.65 \times 10^{-3} \frac{|S^\gamma/6.5|^2 + |P^\gamma/6.5|^2}{\left(\mathcal{U}_{11}^2 + \mathcal{U}_{13}^2\right)\tan^2\beta + 0.38 \left(\mathcal{U}_{12} + \frac{\mathcal{U}_{11}}{\tan\beta}\right)^2}. \quad (5.10) \end{aligned}$$

From here we can see that it is very difficult to obtain a diphoton branching ratio larger than the SM value, $\sim 3 \times 10^{-3}$. In fact, the branching ratio is inversely proportional to $\tan^2\beta$ for $\mathcal{U}_{11} \sim O(1)$, and from the diphoton decay width, Eq. (5.8), we see that there is no way to compensate this enhancement in the total width through a $\tan\beta$-enhanced contribution or through the stop contribution to S^γ in the numerator consistently with present bounds on sfermion masses [58].

Finally, the last ingredient we need is the Higgs production cross section. This cross section is dominated by gluon fusion and $b\bar{b}$–fusion (a complete derivation can be found in [58]). As before, the Higgs mixings and $\tan\beta$ are the main parameters determining the final result. The partonic tree-level $b\bar{b}$–fusion cross section together with the $b\bar{b}$ luminosity of the 5-flavour MSTW2008 parton distributions [63] give a pp cross section of the form:

$$\sigma\left(pp \to H_1\right)_{b\bar{b}} \simeq 0.16 \frac{\tan^2\beta}{(1 + \kappa_d \tan\beta)^2} \left(|\mathcal{U}_{11}|^2 + |\mathcal{U}_{13}|^2 \right) \text{ pb}. \quad (5.11)$$

Whereas the gluon fusion contribution, with the gluon luminosity from MSTW2008, will be:

$$\begin{aligned} \sigma\left(pp \to H_1\right)_{gg} \simeq &\left[13\, \mathcal{U}_{12}^2 + \frac{0.1\tan^2\beta}{(1+\kappa_d\tan\beta)^2}\, \mathcal{U}_{11}^2 - \frac{1.4\tan\beta}{1+\kappa_d\tan\beta}\, \mathcal{U}_{11}\mathcal{U}_{12} + \right. \\ &\left. \left(\frac{2}{(1+\kappa_d\tan\beta)} + \frac{0.1\tan^2\beta}{(1+\kappa_d\tan\beta)^2} + \frac{27}{\tan^2\beta} \right) \mathcal{U}_{23}^2 \right] \text{ pb}, \quad (5.12) \end{aligned}$$

where we can see that the top quark contribution is the most relevant one in the gluon fusion amplitude, except for large $\tan\beta$ and $\mathcal{U}_{11}, \mathcal{U}_{13} \sim O(1)$ where bottom fusion and the bottom contributions to gluon fusion become important and overcome the top contribution. Nevertheless, we must keep the Higgs production cross section close to the SM values, as this is required by the experimental results in other Higgs search channels.

In summary, we have seen that the production cross section must be similar to the SM one, while the total decay width is larger than the SM one if $\mathcal{U}_{11}, \mathcal{U}_{13} > \tan^{-1}\beta$. Thus,
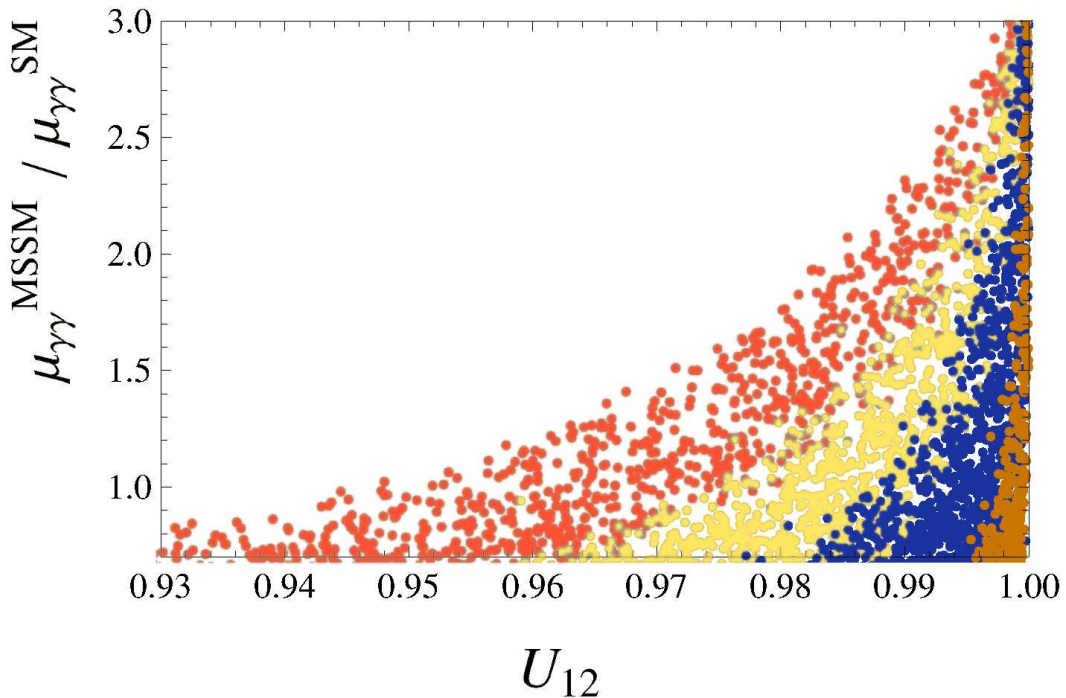
Figure 5.4: Number of events (normalized to SM) in $H_1 \rightarrow \gamma\gamma$ respect to the Higgs up mixing component in a generic MSSM as described in the text.

we would need $\mathcal{U}_{11}, \mathcal{U}_{13} \lesssim \tan^{-1}\beta$ to reduce the total width and increase BR($H_1 \rightarrow \gamma\gamma$) to keep it of the order of the SM value. On the other hand, for small $\mathcal{U}_{11}, \mathcal{U}_{13}$, the Higgs production is dominated by gluon fusion and then it is possible to reproduce the observed signal strength in the different Higgs decay channels. Therefore, the following Higgs mixing components appear naturally as a consequence of enlarging the value of BR $(H_1 \rightarrow \gamma\gamma)$:

$$\mathcal{U}_{12} \simeq 1; \; \mathcal{U}_{11}, \mathcal{U}_{13} < \frac{1}{\tan\beta} \tag{5.13}$$

In Figure 5.4 we show the allowed U_{12} values as a function of the diphoton signal strength. The different colours correspond to different $\tan\beta$ values with $\tan\beta < 5$ orange, $5 < \tan\beta < 9$ yellow, $9 < \tan\beta < 30$ blue and $30 < \tan\beta$ brown. From here, it is clear that $\mathcal{U}_{12}$ is required to be close to one, as $1 - (1/\tan\beta)^2$. Notice that this result simply generalizes the usual real MSSM result in the decoupling limit, which implies that $\mathcal{U}_{12} = \cos\alpha \simeq \sin\beta$. Once our model satisfies the requirement of the observed signal strength in the diphoton channel, we impose next the limits on $H_a \rightarrow \tau\tau$ and BR($B \rightarrow X_s\gamma$). As we will see, the first and second constraints are more relevant for medium–high or low $\tan\beta$ values respectively. Then, we divide the analysis in two areas depending on the masses of the extra Higgses: i) light Higgs masses, $m_{H^\pm} \leq m_t$, where we have strong constraints from the experimental searches of the SM Higgs and ii) heavy Higgs masses, $m_{H^\pm} \geq m_t$, where at the moment, we can use the searches of MSSM neutral Higgses with 4.8 fb^{-1} from ATLAS [47] and 24.6 fb^{-1} from CMS experiment [60].

5.4.2 $H_a \rightarrow \tau\tau$ production cross section

The $pp \rightarrow H \rightarrow \tau\tau$ production cross section is one of the main channels used to search for Higgs boson states at LHC. For Higgs masses below 150 GeV, ATLAS and CMS

put stringent bounds on this cross section with 13.0 fb^{-1} and 19.4 fb^{-1} respectively at $\sqrt{s} = 8$ TeV. Larger Higgs masses are constrained by the search for MSSM Higgs bosons at ATLAS, but only with 4.8 fb^{-1} at $\sqrt{s} = 7$ TeV [47] . Recently the CMS colaboration has released a complete analysis with the full collected datat set at $\sqrt{s} = 7$ and 8 TeV, which looks for extra neutral Higgses with masses up to 1 TeV [60].

As we have seen, the lightest Higgs with $m_{H_1} = 126$ GeV must be mainly up-type to reproduce the observed signal strength. Thus, the $\tan\beta$ enhancement of the decay width of H_1 into tau fermions is controlled by this small mixing. However, for the heavier neutral Higgses, we have the opposite effect and the down-type or pseudoscalar content of the heavier Higgses is high and, thus, the $H_{2,3} \to \tau^+\tau^-$ decay width will be, at tree level and neglecting the relatively small non-holomorphic corrections to the tau Yukawa, proportional to $\tan^2\beta$ in the form:

$$\Gamma_{i,\tau\tau} \simeq \frac{g^2 m_{H_i} m_\tau^2}{32\pi M_W^2} \tan^2\beta \,. \tag{5.14}$$

Here, we have to remember that the relevant quantity in the $pp \to \tau\tau$ production cross section is the H_i branching ratio to $\tau^+\tau^-$, and in this case, due to similar $\tan\beta$ enhancement of the dominant decay width into the $b\bar{b}$ channel, it will be basically independent of $\tan\beta$.

On the other hand, for medium–large $\tan\beta$, the production of these Higgs bosons will also be mainly due to $b\bar{b}$–fusion and the $b\bar{b}$ contribution to the gluon-fusion loop[3] and can be approximated by:

$$\sigma(pp \to H_i) \simeq \left[0.07 \left(\frac{\tau_{H_i}\, d\mathcal{L}^{bb}/d\tau_{H_i}}{1000 \text{ pb}}\right) + 0.04 \left(\frac{\tau_{H_i}\, d\mathcal{L}^{gg}_{LO}/d\tau_{H_i}}{1.1\times10^6 \text{ pb}}\right)\right] \frac{\tan^2\beta}{(1+\kappa_d \tan\beta)^2} \text{ pb} \tag{5.15}$$

where we have taken $U_{2,2}^2 + U_{2,3}^2 \simeq U_{3,2}^2 + U_{3,3}^2 \simeq 1$ and used the gluon and $b\bar{b}$ luminosities at $m_{H_1} = 150$ GeV at $\sqrt{s} = 7$ TeV. Therefore, we can see that the $\tau\tau$ production cross section of H_2 and H_3 will be

$$\sigma(pp \xrightarrow{H_i} \tau\tau) \lesssim \frac{\tan^2\beta}{8.4 + 10.4\kappa_d \tan\beta + \kappa_d^2 \tan^2\beta}$$
$$\left[0.07 \left(\frac{\tau_{H_i}\, d\mathcal{L}^{bb}/d\tau_{H_i}}{1000 \text{ pb}}\right) + 0.04 \left(\frac{\tau_{H_i}\, d\mathcal{L}^{gg}_{LO}/d\tau_{H_i}}{1.1 \times 10^6 \text{ pb}}\right)\right] \text{ pb}\,, \tag{5.16}$$

where we used the partonic luminosities for $m_{H_i} = 150$ GeV.

The latest CMS constraints discriminate between Higgs bosons produced through gluon fusion and through $b\bar{b}$ fusion in association with two b-jets. A p_T-cut of 30 GeV is imposed in at least one b-jet in order to identify the $b\bar{b}$ origin. The theoretical production cross section with b-jets is obtained using the MSTW2008 pdf in the 5-flavour scheme [63] with the $bg \to h_i b$ cross section and a 30 GeV p_T cut on the final b-jet. For this, we use the differential partonic cross section [64],

$$\frac{d\hat{\sigma}_{gb\to h_i b}}{dt} = -\frac{1}{s^2} \frac{\alpha_S(\mu)}{24} \left(\frac{y_b(\mu)}{\sqrt{2}}\right)^2 \frac{m_{h_i}^4 + u^2}{st}\,, \tag{5.17}$$

where s, t, u are the Mandelstan variables. The total pp cross section is then obtained as,

$$\sigma(pp \to h_i b) = 4\,\hat{\sigma}_{gb\to h_i b} \int_\tau^1 \frac{dx}{x}\, b(x, M^2)\, g(\tau/x, M^2)\,, \tag{5.18}$$

---

[3]In our numerical analysis, we include also the gluon-b production channel, although it is always subdominant if b-jets are not tagged.

where now $\tau = (p_g + p_b)^2/s$ and the factor 4 is due to the b-quark coming from one of the two protons and the conjugated process $g\bar{b} \to h_i \bar{b}$.

On the other hand, the gluon fusion cross section without tagged b-jets is obtained as before.

5.4.3   Indirect bounds from $B \to X_s \gamma$

After applying the constraints on the Higgs mixings from the $H_1 \to \gamma\gamma$ decay and the $H_i \to \tau^+ \tau^-$ decay, the most important constraint will come now from an indirect flavour bound, $B \to X_s \gamma$. However, in our calculation we include other indirect constraints on additional Higgs states, as the top quark decay $t \to b\, H^+$ for light charged Higgs, the $B^+ \to \tau^+ \nu$ decay and specially the rare decay $B_s \to \mu^+ \mu^-$, which plays a significant role for large $\tan\beta$.

The BR $(B \to X_s \gamma)$ has, as shown in [58], a sizeable contribution coming from the light charged-Higgs for low $\tan\beta$,

$$\mathcal{C}_{7,8}^{H^\pm} = \frac{f_{7,8}^{(1)}(y_t)}{3\tan^2\beta} + \frac{f_{7,8}^{(2)}(y_t) + (\Delta h_d/h_d\,(1+\tan\beta) - \delta h_d/h_d\,(1-\cot\beta))\; f_{7,8}^{(2)}(y_t)}{1 + \delta h_d/h_d + \Delta h_d/h_d \tan\beta} \quad (5.19)$$

with $y_t = m_t^2/M_{H^\pm}^2$ and the loop functions $f_{7,8}^{(i)}(x)$ are defined in Ref. [58]. We can see in this equation that the charged Higgs contribution at large $\tan\beta$ is given by the second term, which is only mildly dependent on $\tan\beta$ due to the loop corrections to the b-quark mass. At low $\tan\beta$ values, $C_{7,8}^{H^\pm}$ increases due to a larger contribution from the first term and the reduction of denominator in the second term, and it can become sizeable for low $m_{H^\pm}$ values. This large charged-Higgs contribution cannot be compensated by the stop–chargino contribution. This is due to the $\tan\beta$ proportionality of this contribution and the small $\tan\beta$ values that make this contribution too small even if we force the stop mass into the region below $m_{\tilde{t}_1} = 650\,\mathrm{GeV}$, still experimentally allowed for small stop–neutralino mass differences.

5.4.4   Light MSSM Higgs masses

We define the light Higgs region as $m_{H^+} < m_t$, being the charged Higgs heavier than the neutral scalars of our model. In this regime, Higgs states are strongly constrained by the present experimental results, in particular by the process $pp \to H_i \to \tau^+ \tau^-$ which has been analyzed with 13.0 fb^{-1} and 19.4 fb^{-1} at $\sqrt{s} = 8$ TeV in ATLAS and CMS respectively for Higgs masses below 150 GeV and with 4.8 fb^{-1} at $\sqrt{s} = 7$ TeV by ATLAS for $m_H \geq 150$ GeV. However, recently the CMS collaboration has presented an analysis with 4.9 fb^{-1} at $\sqrt{s} = 7$ TeV and 19.7 fb^{-1} at $\sqrt{s} = 8$ TeV [60]. Furthermore, such light charged-Higgs produce a rather large contribution to flavour changing observables as the $B \to X_s \gamma$ decay and this constraint is very relevant in the low $\tan\beta$ region.

Thus, the $\tau\tau$ production cross section is proportional to $\tan^2\beta$ and we can expect the presence of additional Higgs bosons to be strongly constrained by the current searches, that are sensitive to cross sections of the order of the SM cross section for $m_H \lesssim 150$ GeV. In Figure 5.5 we present the allowed Higgs masses as a function of $\tan\beta$, using only the ATLAS and CMS searches up to 150 GeV plus ATLAS MSSM Higgs searches up to 500 GeV on the channel $H_i \to \tau\tau$. As we can see in this figure, these bounds eliminate completely the possibility of having additional Higgs states with masses below 145 GeV for $\tan\beta \gtrsim 7$. This is due to the strong bounds from the SM Higgs searches in the $\tau\tau$ channel at CMS with 19 fb^{-1}. However, for masses 145 GeV $\leq m_{H_i} \leq 175$ GeV, ATLAS

Figure 5.5: Allowed Higgs masses in the plane $(\tan\beta, M_{H_2})$ in the light Higgs scenario. All points satisfy the ATLAS and CMS $pp \to \tau\tau$ bounds in SM Higgs searches (for $m_{H_i} \le 150$ GeV), plus the bounds from the ATLAS search of MSSM neutral Higgses.

constraints on $\sigma(pp \to H \to \tau\tau)$, shown in Figure 5.1, are not able to exclude additional Higgs states for $\tan\beta \lesssim 24$.

Besides, if we add the constraints from the rare decay $B \to X_s\gamma$, most of these points are also excluded, as can be seen in Figure 5.6. All the points in this figure satisfy current $\tau\tau$ bounds, but blue points satisfy in addition $B \to X_s\gamma$ while red points do not satisfy this constraint. From this figure we can see that the combination of current $B \to X_s\gamma$ and ATLAS $\tau\tau$ bounds is able to nearly eliminate the possibility of additional Higgs states with masses below 175 GeV with the exception of a few points in the $10 \le \tan\beta \le 23$ range, where the charged Higgs contribution is reduced and can be compensated by a sizeable stop-chargino opposite sign contribution.

However, when the present analysis was about to be completed, the CMS collaboration relased an analysis of the full data set with 24.6 fb^{-1} searching for neutral MSSM Higgs states up to 1 TeV [60]. In light of these results, this narrow region is completely ruled out, closing the door on the possibility of having extra Higgs states below m_t.

5.4.5 Heavy MSSM Higgs masses

Next, we consider second and third neutral Higgs masses much larger than the lightest Higgs mass wich is fixed at the experimental value of $m_{H_1} = 126$ GeV. In this limit, already approaching the decoupling limit in the MSSM, the heaviest mass of the scalar sector is the charged-Higgs mass, that we take now $m_{H^\pm} > m_t$.

As we did in the previous case, we require the lightest Higgs to reproduce the observed signal strength in the $\gamma\gamma$ channel. As we have seen, this implies that H_1 must have a dominant up-type component and therefore, the heavier Higgs states must be dominantly down-type or pseudoscalar. So, we can expect the $H_{2,3} \to \tau\tau$ decay width to be important.
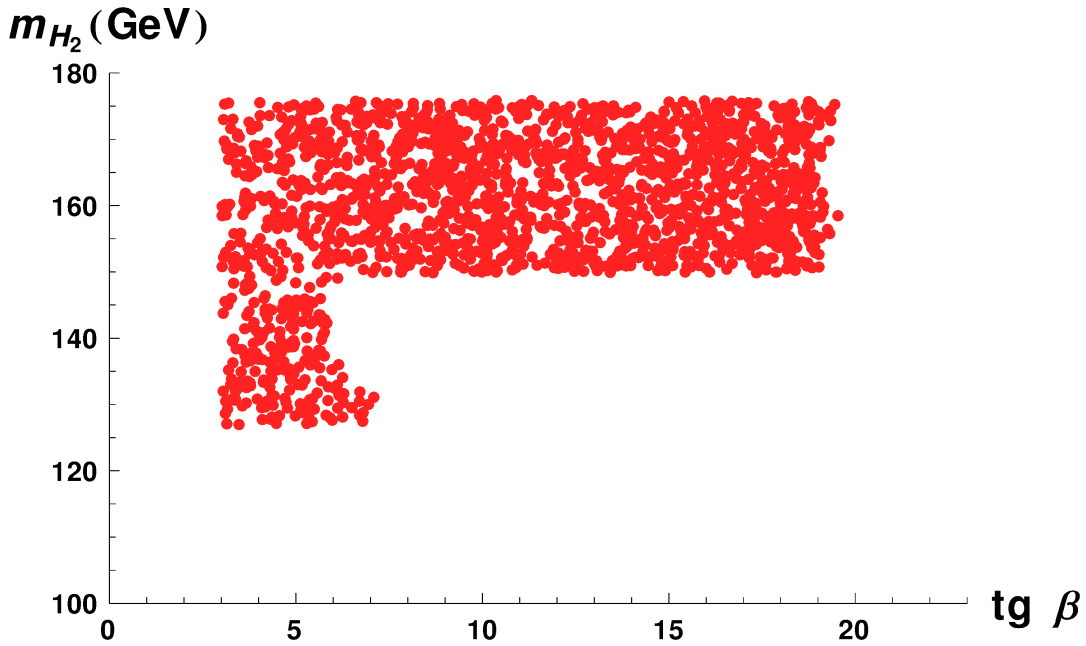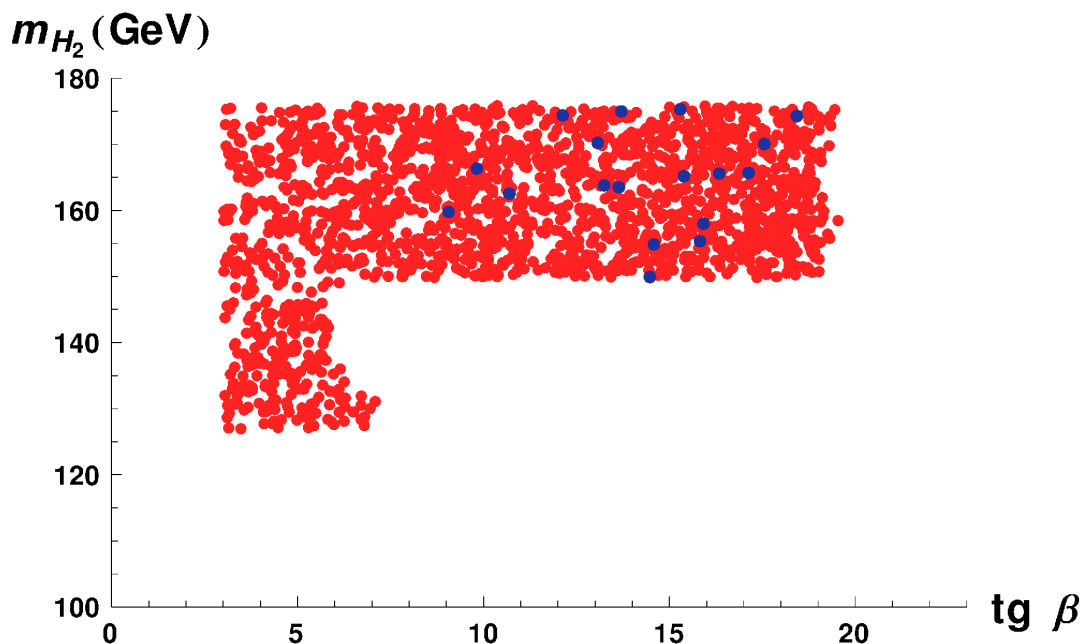
Figure 5.6: Allowed Higgs masses in the plane $(\tan \beta, M_{H_2})$ in the light Higgs scenario. Red (dark grey) points satisfy the ATLAS and CMS $pp \to \tau\tau$ bounds in SM Higgs searches plus ATLAS MSSM neutral Higgs searches, whereas blue (black) points satisfy $B \to X_s \gamma$ in addition. However, if we consider improved CMS $pp \to \tau\tau$ bounds through $b\bar{b}$-produced or gluon-fusion produced Higgs all the parameter space is ruled out.

On the other hand, once the neutral and charged Higgs have large masses, new decay channels are opened, which can reduce the branching ratio of $H_{2,3} \to \tau\bar{\tau}$. However, in the limit of large $\tan \beta$, both the (mostly) down-type Higgs and the pseudoscalar Higgs decay dominantly to $b\bar{b}$ and $\tau^+\tau^-$ and we have that $\mathrm{BR}(H_{2,3} \to \tau^+\tau^-)$ is typically ~ 0.1. In the low $\tan \beta$ region, and once $m_{H_i} \geq 2m_t$, the $t\bar{t}$ channel is sizeable too and can dominate the total Higgs width reducing in this way the $H_{2,3} \to \tau^+\tau^-$ branching ratio. Nevertheless we will see that in this low $\tan \beta$ region, the constraints from $B \to X_s \gamma$ on charged Higgs masses are important and reduce significantly the allowed parameter space.

On this framework, we add now the constraints from ATLAS and CMS searches of MSSM neutral Higgs bosons in the $\tau\tau$ channel. ATLAS searches were done only with 4.8 fb^{-1} at $\sqrt{s} = 7$ TeV, but at the moment the collaboration has, in addition to this data, more than 20 fb^{-1} at $\sqrt{s} = 8$ TeV and therefore we can expect these bounds to improve nearly an order of magnitude in an updated analysis with the new data [48]. On the other hand, the more recent CMS analysis uses 4.9 fb^{-1} at $\sqrt{s} = 7$ TeV and 19.7 fb^{-1} at $\sqrt{s} = 8$ TeV and it is, at present, the key constraint on additional neutral Higgs searches.

As we have seen in the previous section, $\tau\tau$ constraints are very effective in the large $\tan \beta$ region. As an example, the $\tau\tau$ production cross section at $\sqrt{s} = 7$ TeV for high Higgs masses is given by,

$$\sigma(pp \xrightarrow{H_i} \tau\tau) \lesssim \frac{\tan^2 \beta}{8.4 + 2\kappa_d \tan \beta + \kappa_d^2 \tan^2 \beta} \left[0.011 \left(\frac{\tau_{H_i} d\mathcal{L}^{bb}/d\tau_{H_i}}{155 \text{ pb}} \right) + 0.004 \left(\frac{\tau_{H_i} d\mathcal{L}^{gg}_{LO}/d\tau_{H_i}}{1.2 \times 10^5 \text{ pb}} \right) \right] \text{ pb}$$

$$(5.20)$$
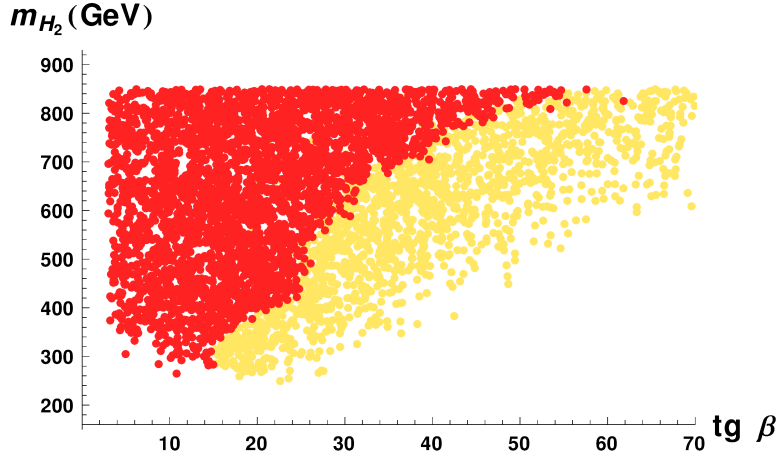
Figure 5.7: Allowed Higgs masses in the plane $(\tan\beta, M_{H_2})$ taking into account the diphoton signal strength, $\tau\tau$ bounds and $\mathrm{BR}(B \to X_s\gamma)$. Yellow (light grey) points are those that satisfy the present ATLAS bounds at 95% C.L., whereas red (dark grey) points that fulfill the recent CMS constraints at 95% C.L.

where we used the luminosities corresponding to a Higgs mass of 250 GeV. Comparing this equation with ATLAS constraints in Fig. 5.1 at $m_H = 250$ GeV, we see that this cross section would be lower than ~ 1.5 pb at 95 % CL. Thus we would obtain, from this approximate formula and using a typical value for $\kappa_b \simeq 0.05$, a bound on $\tan\beta \lesssim 30$ at a mass $m_H = 250$ GeV. Then, we impose also the recent CMS bounds on the $pp \to H \to \tau\tau$ and $pp \to H + b\bar{b} \to \tau\tau + b\bar{b}$ cross section. The result from these bounds is shown in Figure 5.7 in the plane $(\tan\beta, M_{H_2})$. The yellow points in this figure are allowed by ATLAS $\tau\tau$ constraints while red points satisfy also the stronger CMS bounds. All the points in this figure satisfy $\mathrm{BR}(B \to X_s\gamma)$ bounds and other indirect constraints, as $B \to \tau\nu$ and $B_s \to \mu^+\mu^-$.

Indeed, we see that the combination of direct and indirect constraints is very effective in the search for additional neutral Higgs bosons at low Higgs masses and/or large $\tan\beta$. In fact, we can see that the recent CMS constraints, which discriminate different production mechanisms, reduce the area allowed by the previous ATLAS searches strongly. At present, the second neutral Higgs in a generic MSSM must be heavier than 250 GeV, and such low values for the Higgs mass are possible only for $\tan\beta \simeq 16$. In fact, lower values of $\tan\beta$ require a somewhat heavier neutral Higgs, $m_{H_2} \gtrsim 300$ GeV, due to the large charged Higgs contribution to $\mathrm{BR}(B \to X_s\gamma)$. Larger values of $\tan\beta$ are strongly constrained by the CMS searches in the $H_i \to \tau\tau$ channel and require much heavier Higgs states. For instance, a value of $\tan\beta = 30$ would be only possible for $m_{H_2} \gtrsim 600$ GeV. By comparing with the previous estimate from ATLAS results, the improvement becomes aparent. Thus, these bounds are able to constrain very effectively the allowed parameter space in the $(\tan\beta, M_{H_2})$ plane for a generic MSSM, even in the presence of CP violation.

Still, as we said in the previous section, it is reasonable to expect ATLAS bounds to improve significantly when the stored data are analyzed. In Figure 5.8, we present the effect on the allowed values of $(\tan\beta, M_{H_2})$ that an improvement of the ATLAS bound on the $\tau\tau$ production cross section by a factor of 5 or 10 would have. The different colours correspond to applying the present ATLAS bound on $\sigma_{H_i} \times \mathrm{BR}(H_i \to \tau\tau)$, red circles, or assuming an improvement of this bound by a factor of five, yellow circles, or ten, blue circles. These results can also be applied to the heaviest neutral Higgs, H_3, which, in this
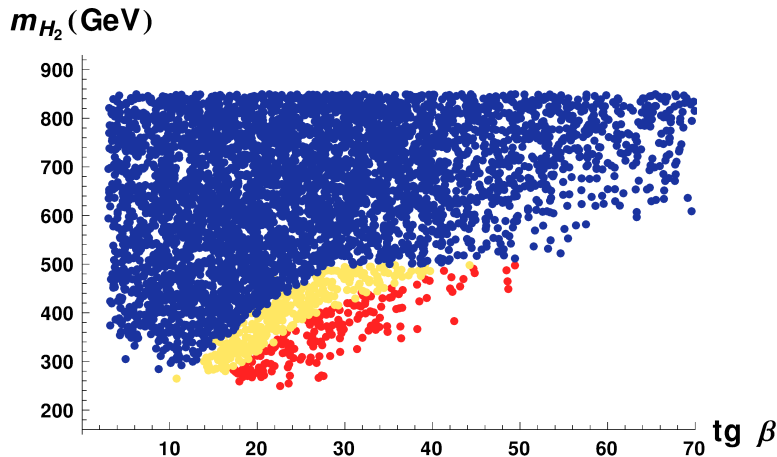
Figure 5.8: Allowed Higgs masses in the plane ($\tan\beta$, M_{H_2}) for present and improved ATLAS constraints. Red (dark grey) points satisfy present ATLAS $H_i \to \tau\tau$ bounds whereas yellow (light grey) and blue (black) points show the effect of improving these bounds on the $\tau\tau$ production cross section by a factor of 5 or 10, respectively. It is clear, that an extension of the analysis up to masses of 1 TeV would be very welcome.

limit, is nearly degenerate to H_2. We can see here that the present ATLAS $\tau\tau$ bound is very restrictive for large values of $\tan\beta$, although the bound is relaxed for heavier Higgs masses and for $m_{H_2} \gtrsim 400$ GeV, $\tan\beta \simeq 50$ is still allowed, while there is no constraint for Higgs masses above 500 GeV. Improving the ATLAS bound by a factor of 5 or 10 reduces strongly the allowed parameter space. For instance, an improvement by a factor of 10 would restrict $\tan\beta < 30$, for $m_{H_2} \leq 500$ GeV. Needless to say, an extension of the analysis up to masses of 1 TeV, at least, is not only welcome but absolutely necessary.

On the other hand, at low $\tan\beta$, the constraints from $B \to X_s\gamma$ eliminate light Higgs masses due to the smallness of the stop-chargino contribution which can not compensate the large charged Higgs contribution. The combination of $\tau\tau$ and $B \to X_s\gamma$ constraints implies that $H_{2,3}$ masses below 250 GeV are already ruled out. An improvement of the $\tau\tau$ bound by a factor of 10, which could be possible with the analysis of the stored LHC data [48], would eliminate the possibility of $m_{H_2} \leq 300$ GeV for all $\tan\beta$ values. Thus, we can see that the combination of both constraints is very important in the searches for additional Higgs states at LHC.

5.5   Second Higgs at $m_{H_2} = 136.5$ GeV

In his recent study on Higgs resonance properties using the diphoton channel [9], the CMS collaboration analyzed an integrated luminosity of 5.1 (19.6) fb^{-1} at a centre of mass energy of 7 (8) TeV. This analysis searched for a second Higgs-like state, aside from the signal at 125–126 GeV previously reported and widely interpreted as the SM Higgs boson, in the range $110 < m_H < 150$ GeV. The result of this analysis reveals a clear excess at $m_H = 136.5$ GeV with a local significance of 2.73 σ combining the data from gluon fusion and vector-boson associated production (each of which shows the excess individually). Even though there is no other channel (as $H \to WW^*$, $H \to ZZ^*$, $H \to \tau\tau$ ...) backing this result, the statistical analysis has proven to be incapable of eliminating this particular excess. However, as we have shown in this paper, the combination of $\tau\tau$ and BR($B \to X_s\gamma$) constraints restricts any additional neutral Higgs in the MSSM to be

above 250 GeV. Nevertheless, we will show here that it is not possible to accommodate two peaks of sizeable strength in the $\gamma\gamma$ channel in an MSSM model, even disregarding the $\tau\tau$ and $\mathrm{BR}(B \to X_s\gamma)$ constraints.

In section 5.4, we have seen that it is difficult to reproduce the observed $O(1)$ signal strength of the diphoton signal for $\tan\beta \geq 1$. This is due to the fact that the amplitude for the process $H_i \to \gamma\gamma$ is basically set by the SM particles running in the loop, mainly W-boson and top quark, while heavy SUSY particles are typically subdominant. The only way to increase the diphoton amplitude would be to use large values of $\tan\beta$, when the down-type couplings, both for fermions and scalars, are enhanced with respect to their SM value. The stau contributions, which have been advocated in the literature as a possible solution to this problem, are only effective for very large $\tan\beta$ values and light stau masses. However, although in this case the diphoton amplitude is increased, the tree-level decays to bottom and tau-lepton also increase, so that the diphoton branching ratio typically decreases. This effect can not be compensated by an enhancement of the Higgs production cross section which would also modify the successful predictions in other Higgs decay channels. Then, the only possibility to reproduce the first peak at $m_{H_1} = 126$ GeV is to reduce the down-type and pseudoscalar component of H_1, and to constrain the value of U_{12}, i.e. the up-type Higgs component of H_1, to be close to unity, as shown in Figure 5.4. In this way, it is possible to reproduce the observed signal strength for H_1, but this implies that the other two neutral Higgs states in the MSSM have necessarily large down-type and pseudoscalar components.

Then, using this solution to reproduce the first peak in $\gamma\gamma$ at ~ 126 GeV, it is clear that we can not repeat the same strategy to have a second peak of an intensity similar to the SM one at $m_{H_2} \simeq 136$ GeV. This second Higgs state necessarily has a small up-type component, which will go as $U_{22} \sim 1/\tan\beta$, and then $(U_{21}^2 + U_{23}^2) \sim 1 - 1/\tan^2\beta$. Moreover, $\Gamma(H_2 \to \gamma\gamma)$ has to be compared with the SM Higgs cross section for $m_H = 126$ GeV and the W-boson contribution to the decay width, dominant for the SM Higgs, would be much smaller for H_2 with these mixings, as $S^\gamma_{H_2^0,W} \simeq -8.3\,(\mathcal{U}_{22} + \mathcal{U}_{21}/\tan\beta)$. So, the W-boson contribution to the H_2 decay width is suppressed by a factor $\tan\beta$ and this reduction of the amplitude can not be compensated by an increase in the contributions from down-type fermions or sfermions to the diphoton triangle with large $\tan\beta$. For instance, we could think that the b-quark contribution to the scalar amplitude, given by $S^\gamma_{H_2^0,b} \sim (-0.025 + i\,0.034)\;\tan\beta\;(\mathcal{U}_{11} + \tan\beta\;\mathrm{Im}\,\{\kappa_d\}\mathcal{U}_{13})$, could compensate the W-boson contribution. However, for typical values $\kappa_d \simeq 0.05$, this would require values of $\tan\beta \geq 80$, while, on the other side, the $H_2 \to b\bar{b}$ tree-level decay width would also increase with $\tan^2\beta$ so that the diphoton branching ratio would be decreased. The same reasoning is valid for the case of light staus, which can not contribute significantly to the diphoton scalar amplitude as shown in Figure 5.3.

In summary, reproducing two SM-size peaks in the diphoton spectrum is not possible in a generic MSSM setup, even before considering the additional constraints from the $\tau\tau$ and $\mathrm{BR}(B \to X_s\gamma)$ searches. Adding then the present $\tau\tau$ constraints reinforces this conclusion and we can completely discard an MSSM explanation of this second peak in the $\gamma\gamma$ spectrum.

5.6 Conclusions

In this work we have used the latest LHC results on the two photon signal strength and the $\tau\tau$ production cross sections, together with the indirect low-energy constraints on

BR($B \to X_s \gamma$), to restrict the allowed parameter space of the Higgs sector in a generic MSSM.

Our study starts with the $\gamma\gamma$ signal observed at LHC at $m_H \simeq 126$ GeV. The experimental results show a signal slightly larger or of the order of the SM expectations, and this is a strong constraint on models with extended Higgs sectors. For large $\tan\beta$ values, when the partial width $\Gamma(H_1 \to \gamma\gamma)$ can be increased, the branching ratio BR($H_1 \to \gamma\gamma$) tends to be smaller than the SM if the down-type or pseudoscalar components of H_2 are sizeable. Requiring $\sigma(pp \to H_1) \times$ BR($H_1 \to \gamma\gamma$) to be of the order of the SM severely restricts the possible mixings in the Higgs sector, so that the down-type or pseudoscalar components of H_1 are required to be $\lesssim 1/\tan\beta$.

Next, we have analyzed the $\tau\tau$ production cross sections for the three Higgs eigenstates. We have shown the present constraints on a generic MSSM coming from $\sigma(pp \to H_i \to \tau\tau)$, including for the first time to the best of our knowledge, the new CMS constraints of neutral MSSM Higgs bosons up to 1 TeV which discriminate different Higgs production mechanisms. As it became apparent in our analysis, the combination of the recent CMS $\tau\tau$ searches and indirect constraints is an excellent weapon in any strategy to search for additional Higgs states at LHC. In this respect, both an update and an extension up to 1 TeV of the present ATLAS analysis is mandatory. If the theory that is hiding so effectively behind the SM is in fact the MSSM, the $\tau\tau$ searches are the ideal tool to bail it out.

Bibliography

[1] G. Aad *et al.* [ATLAS Collaboration], Phys. Lett. B **716** (2012) 1 [arXiv:1207.7214 [hep-ex]].

[2] S. Chatrchyan *et al.* [CMS Collaboration], Phys. Lett. B **716** (2012) 30 [arXiv:1207.7235 [hep-ex]].

[3] G. Aad *et al.* [ATLAS Collaboration], Phys. Lett. B **726** (2013) 88 [arXiv:1307.1427 [hep-ex]].

[4] CMS Collaboration [CMS Collaboration], CMS-PAS-HIG-13-005.

[5] [ATLAS Collaboration], ATLAS-CONF-2013-034.

[6] [ATLAS Collaboration], ATLAS-CONF-2013-030.

[7] [ATLAS Collaboration], ATLAS-CONF-2013-013.

[8] [ATLAS Collaboration], ATLAS-CONF-2013-012.

[9] CMS Collaboration [CMS Collaboration], CMS-PAS-HIG-13-016.

[10] CMS Collaboration [CMS Collaboration], CMS-PAS-HIG-13-020.

[11] CMS Collaboration [CMS Collaboration], CMS-PAS-HIG-13-022.

[12] CMS Collaboration [CMS Collaboration], CMS-PAS-HIG-13-019

[13] CMS Collaboration [CMS Collaboration], CMS-PAS-HIG-12-024

[14] H. P. Nilles, Phys. Rept. **110** (1984) 1.

[15] H. E. Haber and G. L. Kane, Phys. Rept. **117** (1985) 75.

[16] A. Djouadi, Phys. Rept. **459** (2008) 1 [hep-ph/0503173].

[17] A. Pilaftsis and C. E. M. Wagner, Nucl. Phys. B **553** (1999) 3 [hep-ph/9902371].

[18] M. S. Carena, J. R. Ellis, A. Pilaftsis and C. E. M. Wagner, Nucl. Phys. B **586** (2000) 92 [hep-ph/0003180].

[19] S. Y. Choi, M. Drees and J. S. Lee, Phys. Lett. B **481** (2000) 57 [hep-ph/0002287].

[20] M. S. Carena, J. R. Ellis, A. Pilaftsis and C. E. M. Wagner, Nucl. Phys. B **625** (2002) 345 [hep-ph/0111245].

[21] S. Y. Choi, K. Hagiwara and J. S. Lee, Phys. Rev. D **64** (2001) 032004 [hep-ph/0103294].

[22] S. Y. Choi, M. Drees, J. S. Lee and J. Song, Eur. Phys. J. C **25** (2002) 307 [hep-ph/0204200].

[23] G. Barenboim, C. Bosch, M. L. López-Ibañez and O. Vives, JHEP **1311** (2013) 051 [arXiv:1307.5973 [hep-ph]].

[24] S. Heinemeyer, O. Stal and G. Weiglein, Phys. Lett. B **710** (2012) 201 [arXiv:1112.3026 [hep-ph]].

[25] A. Arbey, M. Battaglia, A. Djouadi and F. Mahmoudi, JHEP **1209** (2012) 107 [arXiv:1207.1348 [hep-ph]].

[26] P. Bechtle, S. Heinemeyer, O. Stal, T. Stefaniak, G. Weiglein and L. Zeune, Eur. Phys. J. C **73** (2013) 2354 [arXiv:1211.1955 [hep-ph]].

[27] J. Ke, H. Luo, M. -x. Luo, K. Wang, L. Wang and G. Zhu, Phys. Lett. B **723** (2013) 113 [arXiv:1211.2427 [hep-ph]].

[28] J. Ke, H. Luo, M. -x. Luo, T. -y. Shen, K. Wang, L. Wang and G. Zhu, arXiv:1212.6311.

[29] S. Moretti, S. Munir and P. Poulose, arXiv:1305.0166 [hep-ph].

[30] S. Scopel, N. Fornengo and A. Bottino, Phys. Rev. D **88** (2013) 023506 [arXiv:1304.5353 [hep-ph]].

[31] G. Barenboim, P. Paradisi, O. Vives, E. Lunghi and W. Porod, JHEP **0804** (2008) 079 [arXiv:0712.3559 [hep-ph]].

[32] F. Mahmoudi, J. Rathsman, O. Stal and L. Zeune, Eur. Phys. J. C **71** (2011) 1608 [arXiv:1012.4490 [hep-ph]].

[33] K. Hagiwara, J. S. Lee and J. Nakamura, JHEP **1210** (2012) 002 [arXiv:1207.0802 [hep-ph]].

[34] E. Arganda, J. L. Diaz-Cruz and A. Szynkman, Eur. Phys. J. C **73** (2013) 2384 [arXiv:1211.0163 [hep-ph]].

[35] N. D. Christensen, T. Han and T. Li, Phys. Rev. D **86** (2012) 074003 [arXiv:1206.5816 [hep-ph]].

[36] T. Han, T. Li, S. Su and L. -T. Wang, JHEP **1311** (2013) 053 [arXiv:1306.3229 [hep-ph]].

[37] R. Barbieri, D. Buttazzo, K. Kannike, F. Sala and A. Tesi, Phys. Rev. D **88** (2013) 055011 [arXiv:1307.4937 [hep-ph]].

[38] E. Arganda, J. L. Diaz-Cruz and A. Szynkman, Phys. Lett. B **722** (2013) 100 [Phys. Lett. B **722** (2013) 100] [arXiv:1301.0708 [hep-ph]].

[39] A. Pilaftsis, Phys. Lett. B **435** (1998) 88 [hep-ph/9805373].

[40] A. Pilaftsis, Phys. Rev. D **58** (1998) 096010 [hep-ph/9803297].

[41] D. A. Demir, Phys. Rev. D **60** (1999) 055006 [hep-ph/9901389].

[42] K. Funakubo, S. Tao and F. Toyoda, Prog. Theor. Phys. **109** (2003) 415 [hep-ph/0211238].

[43] J. S. Lee, A. Pilaftsis, M. S. Carena, S. Y. Choi, M. Drees, J. R. Ellis and C. E. M. Wagner, Comput. Phys. Commun. **156** (2004) 283 [hep-ph/0307377].

[44] CMS Collaboration [CMS Collaboration], CMS-PAS-HIG-13-021.

[45] G. Aad *et al.* [ATLAS Collaboration], JHEP **1209** (2012) 070 [arXiv:1206.5971 [hep-ex]].

[46] [CMS Collaboration], CMS-PAS-HIG-13-004.

[47] G. Aad *et al.* [ATLAS Collaboration], JHEP **1302** (2013) 095 [arXiv:1211.6956 [hep-ex]].

[48] L. Fiorini, private communication.

[49] L. J. Hall, R. Rattazzi and U. Sarid, Phys. Rev. D **50**, 7048 (1994) [hep-ph/9306309].

[50] M. S. Carena, M. Olechowski, S. Pokorski and C. E. M. Wagner, Nucl. Phys. B **426**, 269 (1994) [hep-ph/9402253].

[51] T. Blazek, S. Raby and S. Pokorski, Phys. Rev. D **52**, 4151 (1995) [hep-ph/9504364].

[52] M. S. Carena, D. Garcia, U. Nierste and C. E. M. Wagner, Nucl. Phys. B **577**, 88 (2000) [hep-ph/9912516].

[53] C. Hamzaoui, M. Pospelov and M. Toharia, Phys. Rev. D **59**, 095005 (1999) [hep-ph/9807350].

[54] K. S. Babu and C. F. Kolda, Phys. Rev. Lett. **84**, 228 (2000) [hep-ph/9909476].

[55] G. Isidori and A. Retico, JHEP **0111**, 001 (2001) [hep-ph/0110121].

[56] A. Dedes and A. Pilaftsis, Phys. Rev. D **67**, 015012 (2003) [hep-ph/0209306].

[57] A. J. Buras, P. H. Chankowski, J. Rosiek and L. Slawianowska, Nucl. Phys. B **659**, 3 (2003) [hep-ph/0210145].

[58] M. S. Carena, J. R. Ellis, S. Mrenna, A. Pilaftsis and C. E. M. Wagner, Nucl. Phys. B **659**, 145 (2003) [hep-ph/0211467].

[59] A. Delgado, G. F. Giudice, G. Isidori, M. Pierini and A. Strumia, Eur. Phys. J. C **73** (2013) 2370 [arXiv:1212.6847 [hep-ph]].

[60] M. Carena, S. Gori, N. R. Shah and C. E. M. Wagner, JHEP **1203** (2012) 014 [arXiv:1112.3336 [hep-ph]].

[61] M. Carena, S. Gori, N. R. Shah, C. E. M. Wagner and L. -T. Wang, JHEP **1207** (2012) 175 [arXiv:1205.5842 [hep-ph]].

[62] M. Carena, S. Gori, N. R. Shah, C. E. M. Wagner and L. -T. Wang, JHEP **1308** (2013) 087 [arXiv:1303.4414 [hep-ph]].

[63] A. D. Martin, W. J. Stirling, R. S. Thorne and G. Watt, Eur. Phys. J. C **63**, 189 (2009) [arXiv:0901.0002 [hep-ph]].

[64] J. M. Campbell, R. K. Ellis, F. Maltoni and S. Willenbrock, Phys. Rev. D **67** (2003) 095002 [hep-ph/0204093].

Flavour-changing Higgs decays into bottom and strange quarks in supersymmetry

G. Barenboim, C. Bosch, J.S. Lee, M.L. López-Ibáñez, O. Vives

Abstract

In this work, we explore the flavour changing decays $H_i \to bs$ in a general supersymmetric scenario. In these models, the flavour changing decays arise at loop-level but, originating from a dimension-four operator, do not decouple and may provide a first sign of new physics for heavy masses beyond collider reach. In the framework of the minimal supersymmetric extension of the Standard Model (MSSM), we find that the largest branching ratio of the lightest Higgs (H_1) is $\mathcal{O}(10^{-6})$ after imposing present experimental constraints, while heavy Higgs states may still present branching ratios $\mathcal{O}(10^{-3})$. In a more general supersymmetric scenario, where additional Higgs states may modify the Higgs mixings, the branching ratio $\mathrm{BR}(H_1 \to bs)$ can reach values $\mathcal{O}(10^{-4})$, while heavy Higgses still remain at $\mathcal{O}(10^{-3})$. Although these values are clearly out of reach for the LHC, a full study in a linear collider environment could be worth.

6.1 Introduction

Since the discovery of a scalar boson with mass $\sim$126 GeV, at the LHC in 2012 [1, 2], the Standard Model (SM) picture may have been completed. Indeed, if this scalar particle corresponds to the SM Higgs boson, the SM could be the correct description of nature up to scales close to the Planck mass. So far, all the experimental evidence seems to be pointing in the direction of confirming that it is really the missing piece of the SM puzzle. Nevertheless the exploration of features of this particle is just beginning and further studies are needed to confirm its identity.

From now on, our efforts to probe the SM and to search for physics beyond it may follow two complementary paths: i) push the energy frontier in the search for new particles and

interactions and ii) increase the precision on the couplings of the first (so far) fundamental scalar ever discovered. Indirect searches, which would include the latter path, searches of rare processes or higher order corrections to low energy couplings, have been very successful in the past and have led to the discovery of new particles such as the third generation quarks. They have also been instrumental in exploring the scale of new physics beyond the collider reach.

In the case of the Higgs boson, the study of its couplings can be the way to go. Scrutinizing non-standard Higgs couplings is a way to test the presence of additional scalar bosons even when their direct production is closed. In the models beyond the SM in which there exists more than one Higgs doublet, as in a two Higgs doublet model (2HDM)[3] or the MSSM [4, 5], the couplings of the candidate for the discovered scalar boson may not be flavour diagonal and thus it can have flavour changing decays [6, 7, 8, 9, 10, 11, 12, 13, 14, 15, 16, 17, 18, 19, 20, 21, 22, 23]. Furthermore, these flavour changing couplings are dimensionless and therefore the effects of additional heavy particles may not decouple even when the masses of such particles are taken to infinity, providing a unique opportunity to find an assuring indirect evidence for such a high scale non-easily accessible in the near future.

Even more, as we have no clue of the new energy scale (if any) associated with the new particles and interactions we are looking for, considering rare Higgs decays is a wise way to go. Thus, our proposal consists of searching for the Flavour-Changing (FC) Higgs decays. In the SM these FC decays do not exist and therefore their presence would undoubtedly signal the presence of new physics beyond the SM.

As mentioned before, in the past, rare decays, including processes like $b \to s\,\gamma$ and $B_s \to \mu^+\,\mu^-$, have been extensively used to search for new physics. Their precise experimental measurements were useful for the exploration of the parameter space of different SM extensions. Likewise, FC Higgs decays are very useful to search for new physics since they are present in almost any extension of the SM containing additional scalars that mix with the lighter Higgs. For instance they are unavoidable in type-II 2HDMs, like the MSSM, pseudo-dilaton models [24, 25], models with extra dimensions [26, 27] or composite Higgs models [28]. To be specific, in this work we will explore a generic supersymmetric scenario, as well as the MSSM framework, both in the presence of non-minimal flavour structures.

Our analysis will be focused on the process $H \to b\,s$, since one would expect on general grounds that, among FC Higgs decays, those involving third generation particles whose Yukawa couplings are larger are the most experimentally accessible. Besides, loop-induced FC processes in the quark sector are typically larger by a factor α_3^2/α_2^2 (where α_3 and α_2 are the coupling constants associated to the groups $SU(3)$ and $SU(2)$ respectively) for similar flavour changing entries in the lepton sector.

The main goal in this analysis is to find out the largest FC branching ratios for the different Higgs states attainable in a general supersymmetric scenario. As we will show, in the MSSM, the decoupling of the heavy Higgses, enforced by present constraints, makes the FC branching ratio (BR) of the observed light-Higgs to be below the level of 10^{-6}, while heavy Higgs states could reach $\sim 10^{-3}$. In a more general supersymmetric standard model, the light Higgs BR could still reach values of $\sim 10^{-4}$. Thus, these rare decays are very challenging for the LHC but they can be searched for at lepton colliders as the International Linear Collider (ILC). As will be shown, the branching ratio can reach a level of 10^{-3} under special circumstances in the generic SUSY case. These branching ratios could be reached at a linear collider. In fact, we can see that already at LEP, a limit of $\mathrm{BR}(Z \to b\bar{s}) < O(10^{-3})$ was obtained with only $O(10^6)$ Z-bosons in Ref. [29]. We

can expect the larger statistics and improved experimental techniques to improve these limits (see also [30]). In the case of the Higgs decays, we can produce between $O(10^5)$ and $O(10^6)$ Higgs bosons for $m_H = 125$ GeV [31], and therefore we can expect similar values for the lightest Higgs branching ratio. Thus, FC Higgs decays may provide an indirect hint for the existence of new physics at higher energies even when these higher scales are beyond the LHC or ILC reach.

This paper is organized as follows: in section 6.2, we introduce the framework in which the analysis will be carried out. Some compelling variations of it will also be addressed because of their interest when trying to observe FC processes. Still in this section, the theoretical expressions for the FC Higgs decays into down-type quarks will be provided. Section 6.3 summarizes the latest experimental data corresponding to collider probes and indirect bounds from low-energy experiments. Finally, section 6.4 collects the main features of the numerical analysis, concluding in section 6.5 with the main results.

6.2 Higgs Flavour Changing in the MSSM

Our analysis is performed within a generic CP-violating MSSM framework and its extensions, in which the minimal Higgs sector is a type-II 2HDM, *i.e.* one of the two scalar doublets couples only to the up-type quarks at tree-level while the other couples only to down-type quarks. When electroweak symmetry breaking (EWSB) occurs, the neutral components of the two Higgs fields acquire vacuum expectation values (VEVs) and five physical Higgs states appear: three with neutral electric charge and two charged bosons. The two Higgs doublets can be parameterized as

$$\Phi_1 = \begin{pmatrix} \Phi_1^0 \\ \phi_1^- \end{pmatrix}, \qquad \Phi_2 = e^{i\xi} \begin{pmatrix} \phi_2^+ \\ \Phi_2^0 \end{pmatrix} \qquad (6.1)$$

where $\Phi_i^0 = \frac{1}{\sqrt{2}}(v_i + \phi_i + i\, a_i)$, with $v_1 = v \cos\beta$, $v_2 = v \sin\beta$ and $v \simeq 246$ GeV. At tree level the mass eigenstates (H_i) are CP eigenstates, but this situation changes once loop corrections are taken into account [32, 33, 34, 35, 36, 37, 38]. In the MSSM, the possibility of having CP-violating phases increases due to the growing number of complex parameters in the so-called soft SUSY breaking terms, and indeed these CP phases contribute at loop-level to Higgs masses and mixings. Consequently, weak-state fields ($\phi_{1,2}$ and a) give rise to CP-mixed mass eigenstates (H_i) and these states are related through a unitary transformation represented by the 3×3 orthogonal mixing matrix $\mathcal{O}$:

$$\phi_1 = \mathcal{O}_{1i} H_i, \qquad \phi_2 = \mathcal{O}_{2i} H_i, \qquad a = \mathcal{O}_{3i} H_i. \qquad (6.2)$$

The mass eigenvalues will be obtained by means of diagonalising the mass squared matrix:

$$\mathcal{O}^T \cdot \mathcal{M}_H^2 \cdot \mathcal{O} = \text{Diag}\left(m_{H_1}^2, m_{H_2}^2, m_{H_3}^2\right) \qquad (6.3)$$

To study Higgs flavour changing decays, it is helpful to introduce a convenient parametrization of the Higgs mixings. During the analysis, we will use

$$\delta_1 \equiv \left(\frac{\mathcal{O}_{11}}{\cos\beta} - \frac{\mathcal{O}_{21}}{\sin\beta}\right) \qquad \eta_1 \equiv \frac{\mathcal{O}_{31}}{\sin\beta \cos\beta}, \qquad (6.4)$$

where δ_1 quantifies the distance of the lightest Higgs mixings from $\cos\beta$ and $\sin\beta$ and η_1 is directly related to the pseudoscalar content of H_1.

In our analysis below, we will distinguish two different situations in regard to the Higgs mixing:

- Full MSSM framework: Here, we consider the usual MSSM Higgs potential [5] which breaks the electroweak symmetry radiatively. The minimization of this potential gives us the Higgs masses and mixings.

  Using $\mathcal{O}_{11}^2 + \mathcal{O}_{21}^2 + \mathcal{O}_{31}^2 = 1$, one may express the mixing angles $\mathcal{O}_{\alpha 1}$ in terms of δ_1 and η_1 as follows

$$
\begin{aligned}
\mathcal{O}_{11} &= \cos\beta \left[\sqrt{1 - (\delta_1^2 + \eta_1^2)\cos^2\beta\sin^2\beta} + \delta_1\sin^2\beta \right], \\
\mathcal{O}_{21} &= \sin\beta \left[\sqrt{1 - (\delta_1^2 + \eta_1^2)\cos^2\beta\sin^2\beta} - \delta_1\cos^2\beta \right], \\
\mathcal{O}_{31} &= \eta_1 \cos\beta \sin\beta .
\end{aligned}
\tag{6.5}
$$

Then, the coupling of the lightest Higgs to a pair of massive vector bosons is given by

$$
g_{H_1 VV} = \cos\beta\,\mathcal{O}_{11} + \sin\beta\,\mathcal{O}_{21} = \sqrt{1 - (\delta_1^2 + \eta_1^2)\cos^2\beta\sin^2\beta} .
\tag{6.6}
$$

The current LHC Higgs data constrain $g_{H_1 VV}$ to be close to its SM value, $g_{H_1 VV} = 1$. In fact, the present best-fit values and uncertainties are $\kappa_V = g_{H_1 VV} = 1.15 \pm 0.08$ if we assume there is no change in the Higgs total width, *i.e.* $\kappa_H^2 = \Gamma_H/\Gamma_H^{\mathrm{SM}} = 1$, and $\kappa_{VV} = \kappa_V \cdot \kappa_V/\kappa_H = 1.28^{+0.16}_{-0.15}$ if we allow for a change in the total decay width [39]. At present, the errors are still large, but requiring, for example, $g_{H_1 VV} \gtrsim 0.9$, one needs to have $(\delta_1^2 + \eta_1^2)\cos^2\beta\sin^2\beta \lesssim 0.2$. As we will show later, BR $\left(H_1 \to \bar{b}s + \bar{s}b \right)$ is directly proportional to the quantity $(\delta_1^2 + \eta_1^2)$ which can be larger for larger $\tan\beta$ values while satisfying this constraint. On the other hand, large $\tan\beta$ values are constrained by the $\Delta B = 1$ and $\Delta B = 2$ processes such as $b \to s\gamma$, $B_s^0 \to \mu^+\mu^-$, $B_s^0 - \bar{B}_s^0$ mixing, etc. Taking into account all these constraint, we find that, BR $\left(H_1 \to \bar{b}s + \bar{s}b \right)$ can be as large as 10^{-6} in an MSSM framework.

- Generic supersymmetric SM: Given that no signs of supersymmetry have been found so far in collider experiments, and taking into account the strong constraints on the parameter space of minimal models, it is interesting to consider more general models. In fact, the situation could be different if we consider SUSY models beyond the MSSM which contain additional Higgs states. In this case, the Higgs mass eigenstates H_i are given by

$$
H_i = \sum_{\alpha=1,2} \mathcal{O}_{\alpha i}\,\phi_\alpha + \mathcal{O}_{3i}\,a + \sum_{\beta \geq 4} \mathcal{O}_{\beta i}\,\varphi_\beta
\tag{6.7}
$$

where φ_β represent the additional CP-even and CP-odd Higgs states which can be charged or neutral under SU(2)$_L$. We note that only the SU(2)$_L$-charged CP-even states contribute to the tree-level $g_{H_i VV}$ couplings and, due to the additional states, we generically have $\mathcal{O}_{11}^2 + \mathcal{O}_{21}^2 + \mathcal{O}_{31}^2 < 1$. As in the MSSM framework, these couplings are constrained by the experimental results on Higgs decays, but in the presence of other Higgs states close to the 125-GeV state, the mixing pattern could be different from that in the MSSM and δ_1 and/or η_1 can be sizeable. In this case, one may treat δ_1 and η_1 as free parameters effectively. We find that, in this case, BR $\left(H_1 \to \bar{b}s + \bar{s}b \right)$ can be as large as 10^{-4}.

Processes mediated by flavor changing neutral currents (FCNCs) involving down-type quarks have been largely studied in the context of 2HDM where significant contributions can be accommodated due to the $\tan\beta$-enhancement of their Yukawa couplings. This

type of processes are very useful for investigating the dynamics of quark-flavour mixing, especially the possible non-standard phenomena. Here, our main purpose is studying transitions such as $H_i \to bs$, keeping always under control other processes that will impose additional experimental constraints, for instance, the B-meson decay $B_s \to \mu^+\mu^-$ and the mass difference ΔM_{B_s} [1].

6.2.1 FC couplings

It is well-known that, in the MSSM, the superpotential holomorphicity prevents the appearance of Higgs-boson FCNCs by coupling the Higgs-doublet superfield Φ_1 to the down-quark sector and Φ_2 to the up-quark sector. However, this property is violated when considering finite radiative (threshold) corrections due to soft SUSY-breaking interactions [42, 43, 44, 45, 46, 47, 48, 49, 50, 51, 52, 53, 54]. As a consequence, Higgs-mediated FCNCs show up at the one-loop level. The general effective Yukawa Lagrangian for down-type quarks may be simply written as [55]:

$$-\mathcal{L}_Y^d = \bar{d}_R^0\, \mathbf{h_d} \left[\left(1 + \boldsymbol{\Delta}_d^{\phi_1}\right) \frac{v_1 + \phi_1}{\sqrt{2}} - i\left(1 + \boldsymbol{\Delta}_d^{a_1}\right) \frac{a_1}{\sqrt{2}}\right] d_L^0 + \bar{d}_R^0\, \mathbf{h_d} \left[\boldsymbol{\Delta}_d^{\phi_2}\, \frac{v_2 + \phi_2}{\sqrt{2}} - i\, \boldsymbol{\Delta}_d^{a_2}\, \frac{a_2}{\sqrt{2}}\right] d_L^0 + \text{H.c.}$$
(6.8)

where $\mathbf{h_d}$ is the tree-level Yukawa matrix and $d_{L,R}^0$ refer to the weak eigenstates. After EWSB, this Lagrangian gives rise to the d-quarks mass terms and also to the Higgs-mediated FC terms. For the former, we have:

$$-\mathcal{L}_{\text{mass}}^d = \frac{v_1}{\sqrt{2}} \bar{d}_R^0\, \mathbf{h_d} \left(1 + \boldsymbol{\Delta}_d^{\phi_1}\right) d_L^0 + \frac{v_2}{\sqrt{2}} \bar{d}_R^0\, \mathbf{h_d}\, \boldsymbol{\Delta}_d^{\phi_2}\, d_L^0 + \text{H.c.} \equiv \frac{v_1}{\sqrt{2}} \bar{d}_R^0\, \mathbf{h_d} \left(1 + \boldsymbol{\Delta}_d\right) d_L^0 + \text{h.c.}$$
(6.9)

where $\boldsymbol{\Delta}_d = \boldsymbol{\Delta}_d^{\phi_1} + (v_2/v_1)\,\boldsymbol{\Delta}_d^{\phi_2}$ contains the loop corrections. Transforming the states to the mass basis:

$$d_R^0 = \mathcal{U}_R^d\, d_R\,; \qquad\qquad d_L^0 = \mathcal{U}_L^d\, d_L = \mathcal{U}_L^Q\, \mathbf{V}\, d_L\,; \qquad\qquad (6.10)$$

$$u_R^0 = \mathcal{U}_R^u\, u_R\,; \qquad\qquad u_L^0 = \mathcal{U}_L^u\, u_L = \mathcal{U}_L^Q\, u_L\,, \qquad\qquad (6.11)$$

we have:

$$-\mathcal{L}_{\text{mass}}^d = \bar{d}_R\, \widehat{\mathbf{M}}_d\, d_L + \text{h.c.} \qquad \text{with} \quad \widehat{\mathbf{M}}_d = \frac{v_1}{\sqrt{2}} \left(\mathcal{U}_R^d\right)^\dagger \mathbf{h_d}\, [\mathbf{1} + \boldsymbol{\Delta}_d]\, \mathcal{U}_L^Q\, \mathbf{V} \qquad (6.12)$$

where $\widehat{\mathbf{M}}_d = \text{diag}\,(m_d, m_s, m_b)$ is the physical diagonal mass matrix for the down-type quarks. Using the flavour basis where $\mathcal{U}_L^Q = \mathcal{U}_R^u = \mathcal{U}_R^d = \mathbf{1}$ and introducing $\mathbf{R}_d = \mathbf{1} + \boldsymbol{\Delta}_d$, we can relate the physical masses to the Yukawa couplings through the following expression:

$$\mathbf{h_d} = \frac{\sqrt{2}}{v_1} \widehat{\mathbf{M}}_d\, \mathbf{V}^\dagger\, \mathbf{R}_d^{-1}\,. \qquad (6.13)$$

Using this expression in Eq. (6.8), we obtain the FC effective Lagrangian for the interactions of the physical neutral Higgses with the down-type quarks [55, 56]:

$$\mathcal{L}_{\text{FC}} = -\frac{g}{2M_W} \left[H_i\, \bar{d} \left(\widehat{\mathbf{M}}_d\, \mathbf{g}_{H_i \bar{d}d}^L\, P_L + \mathbf{g}_{H_i \bar{d}d}^R\, \widehat{\mathbf{M}}_d\, P_R\right) d\right]\,. \qquad (6.14)$$

---

[1]In the presence of CP phases, limits from electric dipole moments (EDMs) should also be considered. However, in our scenario we have decoupled sfermions, and heavy Higgs masses are above the TeV. In these conditions, the main contributions to EDMs are due to scalar-pseudoscalar Higgs mixing from the two-loop Barr-Zee diagrams with H_1. As shown in [40, 41], the relevant constraint on our couplings would be, $|\eta_1| \lesssim (0.1 \tan\beta)^2$ which does not playing any relevant role in most of the considered parameter space.

A simplified expression for the Higgs couplings can be obtained working in the single-Higgs-insertion (SHI) approximation [55] where:

$$
\begin{aligned}
\mathbf{\Delta}_d^{\phi_1} &= \mathbf{\Delta}_d^{a_1} = \mathbf{F}_d^0 \,; \\
\mathbf{\Delta}_d^{\phi_2} &= \mathbf{\Delta}_d^{a_2} = \mathbf{G}_d^0 \, : \\
\mathbf{\Delta}_d &= \mathbf{F}_d^0 + \tfrac{v_2}{v_1}\mathbf{G}_d^0 = \mathbf{F}_d^0 + \tan\beta\,\mathbf{G}_d^0
\end{aligned}
$$

(6.15)

(6.16)

For large $\tan\beta$ values, the $\mathbf{F}_d^0$ term can be neglected and therefore $\mathbf{R}_d$ may be approximated as:

$$
\mathbf{R}_d = \mathbf{1} + \tan\beta\,\mathbf{G}_d^0.
$$

(6.17)

Then the Higgs couplings in the Lagrangian of Eq. (6.14) will be simplified to:

$$
\mathbf{g}_{H_i\bar{d}d}^L = \frac{\mathcal{O}_{1i}}{\cos\beta}\mathbf{V}^\dagger\mathbf{R}_d^{-1}\mathbf{V} + \frac{\mathcal{O}_{2i}}{\cos\beta}\mathbf{V}^\dagger\mathbf{R}_d^{-1}\mathbf{G}_d^0\mathbf{V} + i\mathcal{O}_{3i}\tan\beta\left[\frac{1}{\sin^2\beta}\mathbf{V}^\dagger\mathbf{R}_d^{-1}\mathbf{V} - \frac{1}{\tan^2\beta}\right]
$$

(6.18)

$$
\mathbf{g}_{H_i\bar{d}d}^R = \left(\mathbf{g}_{H_i\bar{d}d}^L\right)^\dagger
$$

(6.19)

By noting $\mathbf{V}^\dagger\mathbf{R}_d^{-1}\mathbf{G}_d^0\mathbf{V} = \left(\mathbf{1} - \mathbf{V}^\dagger\mathbf{R}_d^{-1}\mathbf{V}\right)/\tan\beta$, we observe that the size of flavour violation is dictated by the off-diagonal components of the matrix $\mathbf{V}^\dagger\mathbf{R}_d^{-1}\mathbf{V} = \mathbf{V}^\dagger\left(\mathbf{1} + \tan\beta\,\mathbf{G}_d^0\right)^{-1}\mathbf{V}$. Therefore the Higgs couplings to the down-type quarks will be determined once $\mathbf{G}_d^0$ is known.

The detailed expression for this quantity $\mathbf{G}_d^0$ in terms of soft SUSY-breaking parameters can be found in Appendix 6.A. Observe that in this formalism, flavour violation from off-diagonal components of the sfermion mass matrices as well as its diagonal parts has been included.

6.2.2 FC Higgs decays

For the computation of the decay width $\Gamma(H_i \to \bar{b}s + \bar{s}b)$, we consider the relevant terms involving b and s quarks in Eq. (6.14). Introducing the effective couplings $y_{L_i} \equiv m_b\mathbf{g}_{H_i\bar{b}s}^L/v$ and $y_{R_i} \equiv m_s\mathbf{g}_{H_i\bar{b}s}^R/v$, we may write:

$$
\mathcal{L}_{H_ibs} = -H_i\,\bar{b}\Big[y_{L_i}\,P_L + y_{R_i}\,P_R\Big]s + \text{H.c.}
$$

(6.20)

This expression can be rewritten as:

$$
\mathcal{L}_{H_ibs} = -H_i\,\bar{b}\Big[g_i^S + ig_i^P\gamma_5\Big]s + \text{H.c.}
$$

(6.21)

with $g_i^S = (y_{L_i} + y_{R_i})/2$ and $g_i^P = i(y_{L_i} - y_{R_i})/2$. Then, using Eq. (28) of [57], the decay width can be obtained as:

$$
\begin{aligned}
\Gamma\left(H_i \to \bar{b}s + \bar{s}b\right) = {}& 2 \times \frac{N_c\,m_{H_i}}{16\pi}\lambda^{1/2}\left(1, x_b, x_s\right)\kappa_{QCD} \times \\
& \Big[(1 - x_b - x_s)\left(|y_{L_i}|^2 + |y_{R_i}|^2\right) - 4\sqrt{x_bx_s}\,\Re e\left(y_{L_i}y_{R_i}^*\right)\Big]
\end{aligned}
$$

(6.22)

where $\kappa_{QCD} = 1 + 5.67\,\alpha_S\left(m_{H_i}^2\right)/\pi$ including the QCD correction, $x_f = m_f^2/m_{H_i}^2$ and $\lambda\left(1, a, b\right) = (1 - a - b)^2 - 4ab$. Note that in y_{L_i,R_i} the masses involved are $m_{b,s} = m_{b,s}\left(m_{H_i}\right)$.

6.3 Experimental Constraints

In our analyses, we use two main sets of experimental data: collider constraints on Higgs and supersymmetric particles and constraints on flavour changing processes. Collider constraints come mainly from CMS and ATLAS, the two general purpose experiments in the LHC that claimed the observation of a new 125 GeV particle in 2012 [1, 2]. Regarding indirect processes, we use the current flavour experimental data associated with B-meson decays and mass differences.

6.3.1 Collider Constraints

ATLAS and CMS are the two general purpose LHC experiments which provide the most accurate data concerning the Higgs boson and SUSY. In particular, we will consider the Higgs $\gamma\gamma$ signal, the $\tau\tau$-channel limits, and direct limits on supersymmetric particle masses. All these constraints have been already used in previous works [58, 59], so we refer to them for details. Here, we will summarize the basic requirements taken into account during the analysis. First, according to the experimental data so far, we require a diphoton signal in the range:

$$0.75 \leq \mu_{\gamma\gamma}^{LHC} \leq 1.55\,, \tag{6.23}$$

where μ_X is the signal strength for a Higgs decaying to X: $\mu_X = [\sigma(pp \to H) \times \mathrm{BR}(H \to X)]/[\sigma(pp \to H)_{\mathrm{SM}} \times \mathrm{BR}(H \to X)_{\mathrm{SM}}]$.

On the other hand, we apply the limits set by CMS [60] and ATLAS [61] in the $H \to \tau\tau$-channel. Specifically, we use the 95 % Confidence Level (CL) limits on the gluon-fusion and b-associated Higgs boson production cross sections times the branching ratio into τ pairs, presented in Fig. 4 in Ref. [60] and Fig. 11 in Ref. [61]. In these analysis, extended searches for extra Higgs states have been carried out for masses up to 1 TeV at 95% CL. In our case, these limits will be imposed to all three neutral Higgs states: H_1, H_2 and H_3.

Finally, we must take into account direct bounds on SUSY masses. Taking into account that the effects of SUSY particles on Higgs couplings are non-decoupling, we can apply conservative limits on the masses. For the gluino, we set the mass limit at $m_{\tilde{g}} \gtrsim 1.4$ TeV when the neutralino mass is below ~ 700 GeV, in agreement with the exclusion limits from ATLAS [62] and CMS [63]. The mass limits for the third generation squarks are taken from ATLAS data [62] as: $m_{\tilde{t}_1} \gtrsim 650$ GeV when the neutralino mass is below 250 GeV, or $m_{\tilde{t}_1} - m_{\chi_1^0} \lesssim 175$ GeV when it is nearly degenerate with the LSP. Finally, according to ATLAS searches [62], the chargin mass limits are: $m_{\tilde{\chi}_1^\pm} \gtrsim 700$ GeV for dominant decays into charged leptons, or $m_{\chi_1^\pm} \gtrsim 450$ GeV when the decays into weak bosons prevail.

6.3.2 FC Constraints

Apart from these data coming from the collider experiments, there is another kind of processes that can play a significant part in the search for SM extensions. As presented in the previous works [58, 59], flavour constraints may be a powerful weapon to restrict the parameter space, especially the parameter $\tan\beta$, even in the absence of complex flavour structures beyond the SM Yukawa couplings. Therefore, for our analysis, we will make use of indirect bounds coming from B-meson decays and mass differences. In particular, we will consider: $B_s^0 \to \mu^+\mu^-$, ΔM_{B_s} and $B \to X_s\gamma$. In the case of the rare decay $B_s^0 \to \mu^+\mu^-$, the latest experimental value for its branching fraction is the combined

analysis of CMS and LHCb data at 7 TeV and 8 TeV, with integrated luminosities of 25 fb^{-1} and 3 fb^{-1} respectively [64]:

$$\mathrm{BR}\left(B_s^0 \to \mu^+\mu^-\right) = \left(2.8^{+0.7}_{-0.6}\right) \cdot 10^{-9} \tag{6.24}$$

Hence, our analysis bound at 2σ will be:

$$\mathrm{BR}\left(B_s^0 \to \mu^+\mu^-\right) \leq 4.2 \cdot 10^{-9} \tag{6.25}$$

Another valuable flavour decay is $B \to X_s\gamma$, which becomes the most restrictive constraint for medium and low $\tan\beta$ values. Combining the BaBar, Belle and CLEO analysis, the world average value given by HFAG [65] is:

$$\mathrm{BR}\left(B \to X_s\gamma\right) = (3.43 \pm 0.21 \pm 0.07) \cdot 10^{-4} \tag{6.26}$$

For the opposite $\tan\beta$ regime, that is large $\tan\beta$ values, the main experimental result turns out to be the B_s-meson mass difference ΔM_{B_s}. The present experimental value is [65]:

$$\Delta M_{B_s} = (17.757 \pm 0.021) \quad \mathrm{ps}^{-1} \tag{6.27}$$

We will require in our analysis:

$$15.94\,\mathrm{ps}^{-1} \leq \Delta M_{B_s} \leq 19.83\,\mathrm{ps}^{-1} \tag{6.28}$$

where we included the theoretical error on $f_{B_s}\sqrt{B_s} = 262 \pm 10$ [66].

6.4 Numerical Analysis

Before we present the results of our numerical analysis, we present first some approximate analytic expressions for $\mathbf{G}_d^0$, $\mathbf{R}_d^{-1}$ and, finally, $\left(\mathbf{V}^\dagger\mathbf{R}_d^{-1}\mathbf{V}\right)_{32,23}$, which are most relevant to the FC Higgs decay into b and s quarks. Note that the FC structure is common to the two situations under consideration: the full MSSM framework and the generic Supersymmetric SM.

From Eq. (6.18) and using $\mathbf{V}^\dagger\mathbf{R}_d^{-1}\mathbf{G}_d^0\mathbf{V} = \left(\mathbf{1} - \mathbf{V}^\dagger\mathbf{R}_d^{-1}\mathbf{V}\right)/\tan\beta$, we observe that the size of flavour violation is dictated by the off-diagonal components of the matrix $\mathbf{V}^\dagger\mathbf{R}_d^{-1}\mathbf{V}$ which can be determined once $\mathbf{G}_d^0$ is known.

As shown in Appendix 6.A, one may need the explicit forms of the flavour violating matrices $\delta\widetilde{\mathbf{M}}^2_{Q,U,D}$ and $\delta\mathbf{a}_u$ to derive $\mathbf{G}_d^0$. Assuming universality for the first two generations, we introduce the following flavour parametrization [2]

$$\widetilde{\mathbf{M}}^2_X = \begin{pmatrix} \rho & 0 & 0 \\ 0 & \rho & \delta_X \\ 0 & \delta_X & 1 \end{pmatrix} \widetilde{M}^2_{X_3}\,, \qquad \mathbf{h}_u^{-1}\mathbf{a}_u = \begin{pmatrix} \rho & 0 & 0 \\ 0 & \rho & \delta_{A_u} \\ 0 & \delta_{A_u} & 1 \end{pmatrix} A_{u_3} \tag{6.29}$$

where $X = Q, U, D$ and then $\delta\widetilde{\mathbf{M}}^2_{Q,U,D}$ and $\delta\mathbf{a}_u$ are given by

$$\delta\widetilde{\mathbf{M}}^2_{Q,U,D} = \widetilde{\mathbf{M}}^2_{Q,U,D} - \widetilde{M}^2_{Q,U,D}\mathbf{1}\,, \qquad\qquad \delta\mathbf{a}_u = \mathbf{a}_u - \mathbf{h}_u A_u \tag{6.30}$$

---

[2]We are assuming, for simplicity, symmetric Yukawa and trilinear matrices at tree-level. In general, $\left(\mathbf{h}_u^{-1}\mathbf{a}_u\right)_{23}$ and $\left(\mathbf{h}_u^{-1}\mathbf{a}_u\right)_{32}$ can be different from each other and complex.

with $\widetilde{M}^2_{Q,U,D} = \frac{1}{3}\text{Tr}\left(\widetilde{\mathbf{M}}^2_{Q,U,D}\right) = \frac{1}{3}\left(2\rho+1\right)\widetilde{M}^2_{Q_3,U_3,D_3}$ and $A_u = \frac{1}{3}\text{Tr}\left(\mathbf{h}_u^{-1}\mathbf{a}_u\right) = \frac{1}{3}\left(2\rho+1\right)A_{u_3}$. In the basis where the up-type Yukawa quarks are diagonal $\mathbf{h}_u = \text{diag}\left(y_u, y_c, y_t\right)$, we have,

$$\delta\widetilde{\mathbf{M}}^2_X = \begin{pmatrix} \frac{\rho-1}{3} & 0 & 0 \\ 0 & \frac{\rho-1}{3} & \delta_X \\ 0 & \delta_X & -\frac{2}{3}\left(\rho-1\right) \end{pmatrix} \widetilde{M}^2_{X_3}, \qquad \delta\mathbf{a}_u = \begin{pmatrix} \frac{\rho-1}{3}\,y_u & 0 & 0 \\ 0 & \frac{\rho-1}{3}\,y_c & \delta_{A_u}\,y_c \\ 0 & \delta_{A_u}\,y_t & -\frac{2}{3}\left(\rho-1\right)y_t \end{pmatrix} A_{u_3}.$$
(6.31)

Inserting the above expression for $\delta\widetilde{\mathbf{M}}^2_{Q,U,D}$ and $\delta\mathbf{a}_u$ into Eqs. (6.63) and (6.64), we obtain

$$\mathbf{G}^0_d \simeq \begin{pmatrix} \epsilon & 0 & 0 \\ 0 & \epsilon & \delta\epsilon_{23} \\ 0 & \delta\epsilon_{32} & \epsilon+\eta \end{pmatrix}$$
(6.32)

where ϵ, η, $\delta\epsilon_{32}$ and $\delta\epsilon_{23}$ are parameters containing the main loop contributions of Eq. (6.63) and Eq. (6.64). Here, it is worth mentioning that EW corrections in those two equations have been neglected, while the down-type Yukawa couplings have been approximated as $\mathbf{h}_d \simeq \frac{\sqrt{2}}{v_1}\widehat{\mathbf{M}}_d\mathbf{V}^\dagger$. The explicit forms of the diagonal entries ϵ and η are given in Appendix 6.A, while the off-diagonal elements, which are the key ones for us as will be seen later, are given by the following expressions:

$$\delta\epsilon_{23} = \delta_L\left[\frac{2\alpha_s}{3\pi}\mu^* M_3^*\,\tilde{M}^2_{Q_3}\,K\left(\tilde{M}^2_Q,\tilde{M}^2_D,|M_3|^2\right) + \frac{|y_t|^2}{16\pi^2}\mu^* A_t^*\,\tilde{M}^2_{Q_3}\,K\left(\tilde{M}^2_Q,\tilde{M}^2_D,|\mu|^2\right)\right] \quad (6.33)$$

$$+\,\delta_{A_u}\left[\frac{|y_t|^2}{16\,\pi^2}\mu^* A_t^* I\left(\tilde{M}^2_Q,\tilde{M}^2_U,|\mu|^2\right)\right] + \delta_R\left[\frac{2\alpha_s}{3\pi}\frac{V^*_{33}\,y_b}{V^*_{22}\,y_s}\mu^* M_3^*\,\tilde{M}^2_{D_3}K\left(\tilde{M}^2_D,\tilde{M}^2_Q,|M_3|^2\right)\right]$$

$$+\,(\rho-1)\left[\frac{2\alpha_s}{3\pi}\frac{V^*_{32}}{V^*_{22}}\mu^* M_3^*\,\tilde{M}^2_{D_3}K\left(\tilde{M}^2_D,\tilde{M}^2_Q,|M_3|^2\right)\right]$$

$$\delta\epsilon_{32} = \delta_L\left[\frac{2\alpha_s}{3\pi}\mu^* M_3^*\,\tilde{M}^2_{Q_3}\,K\left(\tilde{M}^2_Q,\tilde{M}^2_D,|M_3|^2\right)\right] + \delta_{A_u}\left[\frac{|y_c|^2}{16\pi^2}\mu^* A_t^* I\left(\tilde{M}^2_Q,\tilde{M}^2_U,|\mu|^2\right)\right] \quad (6.34)$$

$$+\,\delta_R\left[\frac{2\alpha_s}{3\pi}\left(\frac{V^*_{22}\,y_s}{V^*_{33}\,y_b} - \frac{V^{*2}_{23}\,y_b}{V^*_{22}\,V^*_{33}\,y_s}\right)\mu^* M_3^*\,\tilde{M}^2_{D_3}\,K\left(\tilde{M}^2_D,\tilde{M}^2_Q,|M_3|^2\right)\right]$$

$$-\,(\rho-1)\left[\frac{2\alpha_s}{3\pi}\frac{V^*_{23}}{V^*_{33}}\mu^* M_3^*\,\tilde{M}^2_{D_3}\,K\left(\tilde{M}^2_D,\tilde{M}^2_Q,|M_3|^2\right)\right]$$

where $\delta_Q \equiv \delta_L$ and $\delta_U = \delta_D \equiv \delta_R$. We note that there are four types of flavour-violating terms proportional to δ_L, δ_{A_u}, δ_R, and $(\rho-1)$ [3]. Then, we obtain

$$\mathbf{R}_d^{-1} \simeq \begin{pmatrix} \frac{(1+\epsilon\tan\beta)(1+(\epsilon+\eta)\tan\beta)-\delta\epsilon_{23}\delta\epsilon_{32}\tan^2\beta}{\text{Det}(\mathbf{R}_d)} & 0 & 0 \\ 0 & \frac{(1+\epsilon\tan\beta)(1+(\epsilon+\eta)\tan\beta)}{\text{Det}(\mathbf{R}_d)} & -\frac{\delta\epsilon_{23}(1+\epsilon\tan\beta)\tan\beta}{\text{Det}(\mathbf{R}_d)} \\ 0 & -\frac{\delta\epsilon_{32}(1+\epsilon\tan\beta)\tan\beta}{\text{Det}(\mathbf{R}_d)} & \frac{(1+\epsilon\tan\beta)^2}{\text{Det}(\mathbf{R}_d)} \end{pmatrix}$$
(6.35)

from

$$\mathbf{R}_d = \mathbf{1} + \tan\beta\,\mathbf{G}^0_d \simeq \begin{pmatrix} 1+\epsilon\tan\beta & 0 & 0 \\ 0 & 1+\epsilon\tan\beta & \delta\epsilon_{23}\tan\beta \\ 0 & \delta\epsilon_{32}\tan\beta & 1+(\epsilon+\eta)\tan\beta \end{pmatrix}.$$
(6.36)

As we will see, the most relevant flavour-violating matrix element in the FC Higgs decay

---

[3] Please note that our definition of δ_{A_u} in Eq (6.31) makes it different from the δ_{LR} usually defined in the literature.

$H_i \to bs$ is $\left(\mathbf{V}^\dagger \mathbf{R_d^{-1}} \mathbf{V}\right)_{32,23}$. In principle, this matrix element $\left(\mathbf{V}^\dagger \mathbf{R_d^{-1}} \mathbf{V}\right)_{32}$ is:

$$
\begin{aligned}
\left(\mathbf{V}^\dagger \mathbf{R}_d^{-1} \mathbf{V}\right)_{32} &= \sum_{i,j=1}^{3} \mathbf{V}_{i3}^* \left(\mathbf{R}_d^{-1}\right)_{ij} \mathbf{V}_{j2} \\
&= \sum_{i=1}^{3} \left[\mathbf{V}_{i3}^* \left(\mathbf{R}_d^{-1}\right)_{ii} \mathbf{V}_{i2}\right] + \mathbf{V}_{23}^* \left(\mathbf{R}_d^{-1}\right)_{23} \mathbf{V}_{32} + \mathbf{V}_{33}^* \left(\mathbf{R}_d^{-1}\right)_{32} \mathbf{V}_{22} .
\end{aligned}
$$
(6.37)

Using Eq. (6.35) for $\mathbf{R}_d^{-1}$ and taking into account the unitarity of the CKM matrix, we can write:

$$
\sum_{i=1}^{3} \left[\mathbf{V}_{i3}^* \left(\mathbf{R}_d^{-1}\right)_{ii} \mathbf{V}_{i2}\right] = \left(\mathbf{V}_{13}^* \mathbf{V}_{12} + \mathbf{V}_{23}^* \mathbf{V}_{22}\right) \frac{(1 + \epsilon \tan\beta)\,\eta\,\tan\beta}{\mathrm{Det}\,(\mathbf{R}_d)} - \mathbf{V}_{13}^* \mathbf{V}_{12} \frac{\delta\epsilon_{23}\delta\epsilon_{32}\tan^2\beta}{\mathrm{Det}\,(\mathbf{R}_d)}.
$$
(6.38)

In this expression, we can neglect all the terms proportional to $\mathbf{V}_{13}^* \mathbf{V}_{12} \sim 8 \times 10^{-4}$ with respect to $\mathbf{V}_{23}^* \mathbf{V}_{22} \sim 4 \times 10^{-2}$, even for the last term proportional to $\delta\epsilon_{23}\delta\epsilon_{32}$, which, as can be seen from Eqs. (6.33,6.34) and (6.67,6.68), is, for sizeable mass insertion (MI), of the same order as $\epsilon \times \eta$.

Then, in Eq. (6.37), if we have similar values of the off-diagonal elements $\left(\mathbf{R}_d^{-1}\right)_{23}$ and $\left(\mathbf{R}_d^{-1}\right)_{32}$, the former can also be neglected with respect to later, being suppressed by an additional $|\mathbf{V}_{23}^* \mathbf{V}_{32}| \sim 2.10^{-3}$. Therefore, in the presence of sizeable mass insertions $\delta_{L,R} \geq \mathbf{V}_{23}^* \mathbf{V}_{22}$, we have $\delta\epsilon_{32} \geq \eta \times \mathbf{V}_{23}^* \mathbf{V}_{22}$ and then we can safely take,

$$
\left(\mathbf{V}^\dagger \mathbf{R_d^{-1}} \mathbf{V}\right)_{32} \simeq \mathbf{V}_{33}^* \mathbf{V}_{22} \left(\mathbf{R_d^{-1}}\right)_{32} + \mathbf{V}_{23}^* \mathbf{V}_{22} \frac{(1 + \epsilon \tan\beta)\,\eta\,\tan\beta}{\mathrm{Det}\,(\mathbf{R}_d)} \simeq \left(\mathbf{R_d^{-1}}\right)_{32} . \quad (6.39)
$$

Repeating the same exercise with $\left(\mathbf{V}^\dagger \mathbf{R_d^{-1}} \mathbf{V}\right)_{23}$, we obtain,

$$
\left(\mathbf{V}^\dagger \mathbf{R_d^{-1}} \mathbf{V}\right)_{23} \simeq \mathbf{V}_{22}^* \mathbf{V}_{33} \left(\mathbf{R_d^{-1}}\right)_{23} + \mathbf{V}_{22}^* \mathbf{V}_{23} \frac{(1 + \epsilon \tan\beta)\,\eta\,\tan\beta}{\mathrm{Det}\,(\mathbf{R}_d)} \simeq \left(\mathbf{R_d^{-1}}\right)_{23} . \quad (6.40)
$$

The study of these matrix elements is very interesting because of their dependence on δ_L, δ_R and δ_{A_u}. Looking at Eq. (6.34) for $\delta\epsilon_{32}$ and comparing the δ_L and δ_R contributions, we can see that the δ_R term is suppressed by the difference $\left(y_s/y_b - \mathbf{V}_{23}^{*}{}^2 y_b/y_s\right) \simeq -0.013$ with respect to the δ_L term. Therefore, these matrix elements, and especially $\left(\mathbf{R}_d^{-1}\right)_{32}$, will have very different values for these two mass insertions. Also from these equations, it is evident that, if $\delta_L \simeq \delta_{A_u}$, we would obtain similar results from both types of mass insertions to $\delta\epsilon_{23}$, but its contributions to $\delta\epsilon_{32}$ would be suppressed by an additional factor $(y_c/y_t)^2$. In any case, the δ_{A_u} contributions to $\delta\epsilon_{23}$ and $\delta\epsilon_{32}$ are always smaller than the δ_R contributions. For this reason, we will only consider the cases of the δ_L and δ_R insertions

All the results of the numerical analysis presented in the following sections and the corresponding figures are done with the `CPsuperH2.3` code [57, 67, 68].

6.4.1   Full MSSM framework

In the full MSSM framework, the effective FC Higgs couplings are given by:

$$y_{L_i} \equiv \frac{m_b}{v} \mathbf{g}^L_{H_i \bar{b}s} = \frac{m_b}{v} \left(\frac{\mathcal{O}_{1i}}{\cos \beta} - \frac{\mathcal{O}_{2i}}{\sin \beta} + i \tan \beta \frac{\mathcal{O}_{3i}}{\sin^2 \beta} \right) \left(\mathbf{V}^\dagger \mathbf{R}_d^{-1} \mathbf{V} \right)_{32}, \quad (6.41)$$

$$y_{R_i} \equiv \frac{m_s}{v} \mathbf{g}^R_{H_i \bar{b}s} = \frac{m_s}{v} \left(\frac{\mathcal{O}_{1i}}{\cos \beta} - \frac{\mathcal{O}_{2i}}{\sin \beta} - i \tan \beta \frac{\mathcal{O}_{3i}}{\sin^2 \beta} \right) \left(\mathbf{V}^\dagger \mathbf{R}_d^{-1} \mathbf{V} \right)^*_{23}, \quad (6.42)$$

and the decay width, Eq. (6.22), is:

$$\Gamma \left(H_i \to \bar{b}s + \bar{s}b \right) \simeq \frac{3 m_{H_i}}{8\pi} \kappa_{QCD} \left(|y_{L_i}|^2 + |y_{R_i}|^2 \right) \quad (6.43)$$

$$\simeq \frac{3 m_{H_i} m_b^2}{8\pi v^2} \kappa_{QCD} \left[\left(\frac{\mathcal{O}_{1i}}{\cos \beta} - \frac{\mathcal{O}_{2i}}{\sin \beta} \right)^2 + \left(\tan \beta \frac{\mathcal{O}_{3i}}{\sin^2 \beta} \right)^2 \right]$$

$$\times \left(\left| \left(\mathbf{V}^\dagger \mathbf{R}_d^{-1} \mathbf{V} \right)_{32} \right|^2 + \frac{m_s^2}{m_b^2} \left| \left(\mathbf{V}^\dagger \mathbf{R}_d^{-1} \mathbf{V} \right)_{23} \right|^2 \right),$$

In the case of δ_L insertions, from the discussion in the previous section, we observe $|y_{R_i}| \ll |y_{L_i}|$ due to the m_s/m_b suppression with $\left(\mathbf{V}^\dagger \mathbf{R}_d^{-1} \mathbf{V} \right)_{32} \sim \left(\mathbf{V}^\dagger \mathbf{R}_d^{-1} \mathbf{V} \right)^*_{23}$. In the presence of δ_R insertions the situation is more involved and both terms must be considered.

Now, considering the total decay widths of the Higgs bosons, we will obtain the corresponding branching ratios. In the case of the lightest Higgs, its total decay width is dominated by the decay into two b-quarks, two W-bosons and two τ-leptons. Thus:

$$\Gamma_{H_1} = \frac{m_{H_1} m_b^2}{8\pi v^2} \left[\left(3 \kappa_{QCD} + \frac{m_\tau^2}{m_b^2} \right) \tan^2 \beta \left(\mathcal{O}_{11}^2 + \mathcal{O}_{31}^2 \right) + I_{PS} \frac{m_{H_1}^2}{m_b^2} \left(\mathcal{O}_{21} + \frac{\mathcal{O}_{11}}{\tan \beta} \right)^2 \right] (6.44)$$

where in the large-$\tan \beta$ limit we have used $\left(\mathcal{O}_{11}^2 / \cos^2 \beta + \tan^2 \beta \, \mathcal{O}_{31}^2 \right) \simeq \tan^2 \beta \left(\mathcal{O}_{11}^2 + \mathcal{O}_{31}^2 \right)$ and $(\sin \beta \, \mathcal{O}_{21} + \cos \beta \, \mathcal{O}_{11})^2 \simeq (\mathcal{O}_{21} + \mathcal{O}_{11} / \tan \beta)^2$. I_{PS} in the second term refers to the phase-space integral in the Higgs decay into two W bosons [57] and can be approximated by $I_{PS} \simeq 6.7 \times 10^{-4}$ when $m_{H_1} = 125$ GeV. Then, the branching ratio will be:

$$\mathrm{BR} \left(H_1 \to \bar{b}s + \bar{s}b \right) = \left| \left(\mathbf{V}^\dagger \mathbf{R}_d^{-1} \mathbf{V} \right)_{32} \right|^2 \frac{3 \kappa_{QCD} \left[\left(\frac{\mathcal{O}_{11}}{\cos \beta} - \frac{\mathcal{O}_{21}}{\sin \beta} \right)^2 + \left(\frac{\mathcal{O}_{31}}{\sin \beta \cos \beta} \right)^2 \right]}{\left(3 \kappa_{QCD} + \frac{m_\tau^2}{m_b^2} \right) \tan^2 \beta \left(\mathcal{O}_{11}^2 + \mathcal{O}_{31}^2 \right) + I_{PS} \frac{m_{H_1}^2}{m_b^2} \left(\mathcal{O}_{21} + \frac{\mathcal{O}_{11}}{\tan \beta} \right)^2}.$$
$$(6.45)$$

For the heavier Higgses, and for $\tan \beta \gtrsim 30$, the total decay width is dominated by the bottom and tau widths:

$$\Gamma_{H_2} \simeq \frac{m_{H_2} m_b^2}{8\pi v^2} \left(3 \kappa_{QCD} + \frac{m_\tau^2}{m_b^2} \right) \tan^2 \beta \left(\mathcal{O}_{12}^2 + \mathcal{O}_{32}^2 \right) \quad (6.46)$$

using $\left(\mathcal{O}_{12}^2 / \cos^2 \beta + \tan^2 \beta \, \mathcal{O}_{32}^2 \right) \simeq \tan^2 \beta \left(\mathcal{O}_{12}^2 + \mathcal{O}_{32}^2 \right)$ and the branching ratio is:

$$\mathrm{BR} \left(H_2 \to \bar{b}s + \bar{s}b \right) = 3 \kappa_{QCD} \left| \left(\mathbf{V}^\dagger \mathbf{R}_d^{-1} \mathbf{V} \right)_{32} \right|^2 \frac{\left(\frac{\mathcal{O}_{12}}{\cos \beta} - \frac{\mathcal{O}_{22}}{\sin \beta} \right)^2 + \left(\frac{\mathcal{O}_{32}}{\sin \beta \cos \beta} \right)^2}{\left(3 \kappa_{QCD} + \frac{m_\tau^2}{m_b^2} \right) \tan^2 \beta \left(\mathcal{O}_{12}^2 + \mathcal{O}_{32}^2 \right)}.$$
$$(6.47)$$

In a previous work [59], we showed that the latest LHC data for the Higgs signal in the diphoton channel strongly constrains the Higgs mixing within a general CP-violating model. In particular, if we consider the lightest Higgs as the recently discovered boson at

126 GeV, its mixing conditions are $\left(\mathcal{O}_{11}^2 + \mathcal{O}_{31}^2\right) \sim 1/\tan^2\beta$ and $\mathcal{O}_{21}^2 \sim 1$. Additionally, using the parametrization presented in Eq. (6.4), we have:

$$\text{BR}\left(H_1 \to \bar{b}s + \bar{s}b\right) = \left|\left(\mathbf{V}^\dagger \mathbf{R_d^{-1}} \mathbf{V}\right)_{32}\right|^2 \frac{3\,\kappa_{QCD}\,(\delta_1^2 + \eta_1^2)}{\left(3\,\kappa_{QCD} + \frac{m_\tau^2}{m_b^2}\right) + I_{PS}\frac{m_{H_1}^2}{m_b^2}}. \quad (6.48)$$

Still following [59], it was also showed that the diphoton condition establishes for the heavier Higgs mixings that: $\left(\mathcal{O}_{1i}^2 + \mathcal{O}_{3i}^2\right) \sim 1$ and $\mathcal{O}_{2i} \lesssim 1/\tan\beta$, $i = 2,3$. Hence:

$$\text{BR}\left(H_2 \to \bar{b}s + \bar{s}b\right) \simeq \left|\left(\mathbf{V}^\dagger \mathbf{R_d^{-1}} \mathbf{V}\right)_{32}\right|^2 \frac{3\,\kappa_{QCD}}{3\,\kappa_{QCD} + \frac{m_\tau^2}{m_b^2}} \quad (6.49)$$

where we have considered $\tan\beta \geq 3$ and, therefore, $1/\cos\beta \simeq \tan\beta$ and $\sin\beta \simeq 1$ in a good approximation.

6.4.1.1 Left-handed (L) insertion

First, we analyze the case with $\delta_L \neq 0$ and $\delta_R = 0$:

$$\delta\epsilon_{32(L)} \simeq \delta_L \frac{2\alpha_s}{3\pi} \mu^* M_3^* \tilde{M}_{Q_3}^2 K\left(\tilde{M}_Q^2, \tilde{M}_D^2, |M_3|^2\right) \sim -3 \cdot 10^{-3}\delta_L \quad (6.50)$$

where we can see that $\delta\epsilon_{32(L)}$ has a non-decoupling behaviour as it depends only on ratios of sparticle masses and we have used $\tilde{M}_{Q,D,Q_3} \sim 5$ TeV, $M_3 \sim 7$ TeV and $\mu \sim 6$ TeV. Consequently, for the maximum values of $\tan\beta$ and δ_L considered during the scan, $\delta_L \sim 0.5$ [4] and $\tan\beta \sim 60$, we would obtain:

$$\left(\mathbf{R_d^{-1}}\right)_{32(L)}^{\max} \simeq -\frac{\delta\epsilon_{32(L)}\,(1 + \epsilon\tan\beta)\tan\beta}{\text{Det}\,(\mathbf{R_d})} \sim \frac{3 \cdot 10^{-3} \times 1.5 \times 60}{4} \sim 0.03 \quad (6.51)$$

where ϵ, Eq. (6.67), and $\text{Det}(\mathbf{R_d})$ for the masses specified above take the values $\epsilon \simeq 0.01$ and $\text{Det}(\mathbf{R}_d) \simeq 4.7$. Therefore:

$$\text{BR}\left(H_1 \to \bar{b}s + \bar{s}b\right)_{(L)}^{\max} \simeq \left|\left(\mathbf{V}^\dagger \mathbf{R_d^{-1}} \mathbf{V}\right)_{32(L)}\right|^2 \frac{3\kappa_{QCD}\times(\delta_1^2+\eta_1^2)}{\left(3\kappa_{QCD}+\frac{m_\tau^2}{m_b^2}\right)+I_{PS}\frac{126^2}{m_b^2}} \sim 5 \cdot 10^{-4}\,(\delta_1^2 + \eta_1^2)$$
$$(6.52)$$

$$\text{BR}\left(H_2 \to \bar{b}s + \bar{s}b\right)_{(L)}^{\max} \simeq \left|\left(\mathbf{V}^\dagger \mathbf{R_d^{-1}} \mathbf{V}\right)_{32(L)}\right|^2 \frac{3\kappa_{QCD}}{3\kappa_{QCD}+\frac{m_\tau^2}{m_b^2}} \sim 10^{-3}$$
$$(6.53)$$

Fig. 6.1 shows the results of our scans. Blue points are those which satisfy the whole set of constraints while red points are excluded because of the violation of one or more of them. In the upper frames of Fig. 6.1, we represent the branching ratios for H_1 and H_2 versus $\tan\beta$ (for all considerations, H_3 will be equivalent to H_2 given that they are nearly degenerated for the range of masses considered here). As can be seen in these two plots, before applying the low-energy constraints, the branching ratio grows with $\tan\beta$ (red points). However, the final result is very different from this when we impose

---

[4]Notice that, effectively, there is no bound from low-energy FC processes on this MI for such heavy gluinos and squarks.

Figure 6.1: A full MSSM framework with LL insertion with $\delta_L \neq 0$ and $\delta_{A_u} = \delta_R = 0$: The upper frames show the dependence of the estimated branching ratios for $H_{1,2} \to \bar{b}s + \bar{s}b$ on $\tan \beta$. The lower-left frame is for the dependence of B($H_1 \to bs$) on δ_1^2 and the lower-right frame for the δ_1^2 dependence on $\tan \beta$. Blue (dark) points satisfy all the constraints considered, while red (light) points violate one or several of these constraints.

experimental limits from B-mesons (blue points). Whereas for heavy Higgses few points become excluded, in the case of the lightest Higgs the effect is more notable. Indeed, looking at the upper-left frame of Fig. 6.1 we can say that the tendency is completely opposite and the branching ratio decreases for $\tan \beta > 20$.

This behaviour is mainly due to the $B_s^0 \to \mu^+\mu^-$ constraint. This branching ratio is given in Eq. (6.81) with C_S, Eq. (6.83), and C_P, Eq. (6.84), containing the SUSY contributions. The dominant contributions come from the heavy Higgses and we have:

$$C_{S,P} \propto 2 \frac{\tan^2 \beta}{m_{H_j}^2} \left(\mathbf{V}^\dagger \mathbf{R}_d^{-1} \mathbf{V}\right)_{32}^* \left[\left(\mathcal{O}_{1j} - \frac{\mathcal{O}_{2j}}{\tan^2 \beta}\right)^2 + \mathcal{O}_{3j}^2\right] \sim 2 \frac{\tan^2 \beta}{m_{H_j}^2} \left(\mathbf{R}_d^{-1}\right)_{32}^* \quad (6.54)$$

with $j = 2, 3$. This dependence on $\tan^3 \beta$ (the matrix element $\left(\mathbf{R}_d^{-1}\right)_{32}^*$ carries an additional $\tan \beta$) and the heavy Higgs masses explains why this decay provides such a restrictive constraint for relatively small m_{H_2, H_3}^2 and medium-to-large values of $\tan \beta$.

In fact, BR($H_1 \to bs$) is suppressed at medium and large $\tan \beta$ values while BR($H_2 \to bs$) is not. This is due to fact that BR($H_1 \to bs$) is proportional to δ_1 and η_1, which in the MSSM are of order $v^2/M_{H_2}^2$. Then, B-meson constraints are more restrictive for light m_{H_2} which also correspond to the largest BR($H_1 \to bs$). On the other hand BR($H_2 \to bs$) is independent of δ_1 or η_1 and the H_2 mass. The B-meson constraints are not effective here if m_{H_2} is large enough and therefore we can reach large branching ratios for large $\tan \beta$ values. Furthermore, this branching ratio saturates for medium-to-large values of $\tan \beta$ when both the FC decay width and the total decay width have the same $\tan \beta$ dependence.

Moreover, the lower-left frame of Fig. 6.1 shows the branching ratio for H_1 versus δ_1^2. As seen in Eq. (6.52), for $\delta_1^2 \gtrsim 0.02$ the branching ratio is of the order 10^{-5}. However, the
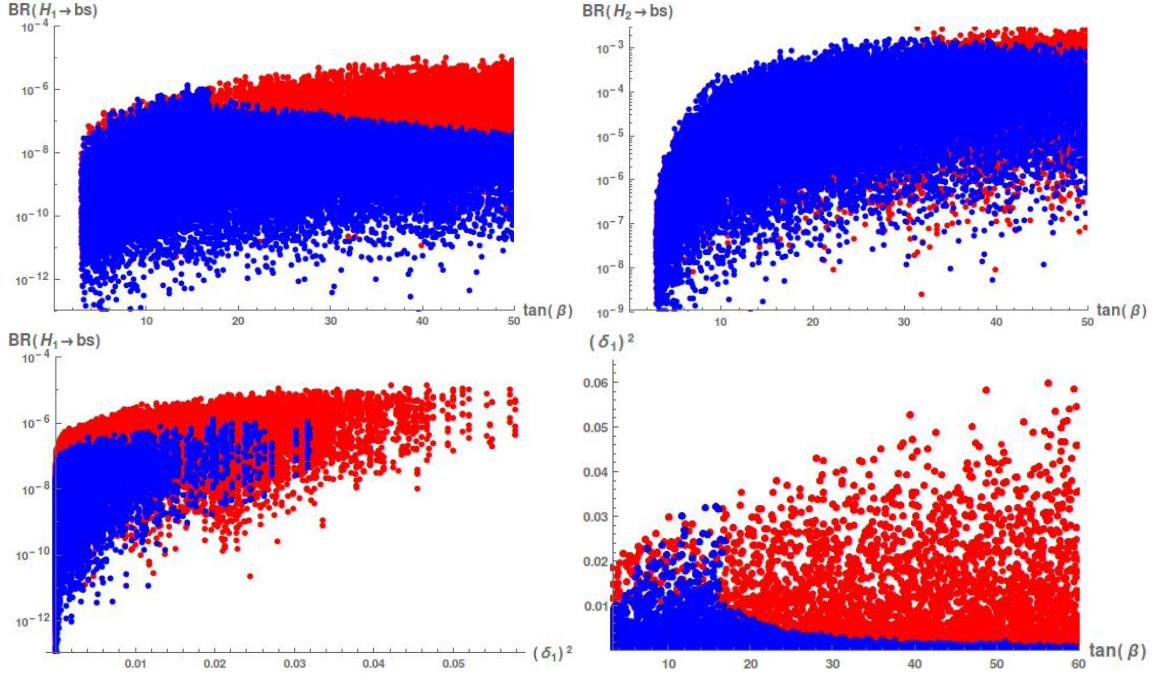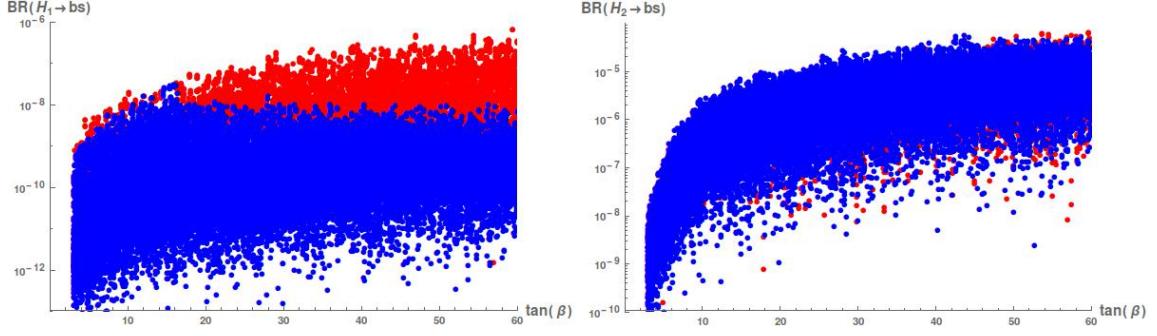
Figure 6.2: A full MSSM framework with RR insertion with $\delta_R \neq 0$ and $\delta_{A_u} = \delta_L = 0$: The left frame shows the dependence of BR($H_1 \to bs$) on $\tan\beta$ and the right frame shows the dependence of BR($H_2 \to bs$) on $\tan\beta$. Again, blue (dark) points satisfy all the constraints considered, while red (light) points violate one or several of these constraints.

implementation of B-meson constraints here reduces this value by more than one order of magnitude.

Finally, in the lower-right frame of Fig. 6.1, we present the δ_1^2 dependence on $\tan\beta$. We observe that, before imposing B-meson constraints, larger values of (δ_1^2) are possible when $\tan\beta$ grows. However, B-meson constraints become very effective for $\tan\beta \gtrsim 17$ as shown by the blue points in this plot. This could be understood by noting that the Higgs contributions to the $\Delta B = 1$ and $\Delta B = 2$ processes are inversely proportional to the heavy Higgs mass squared. Therefore, to suppress these processes for large $\tan\beta$, large Higgs masses are required. Accordingly, we expect smaller $|\delta_1|$ as $\tan\beta$ grows since, as we have seen, $|\delta_1| \propto v^2/m_{H_2}^2$ in the MSSM.

6.4.1.2   Right-handed (R) insertion

Now we consider the case, $\delta_R \neq 0$ and $\delta_L = \delta_{A_u} = 0$, we have from Eqs. (6.34) and (6.50):

$$\delta\epsilon_{32(R)} \simeq \delta_R \left(\frac{\mathbf{V}^*_{22} \, y_s}{\mathbf{V}^*_{33} \, y_b} - \frac{\mathbf{V}^{*\,2}_{23} \, y_b}{\mathbf{V}^*_{22} \, \mathbf{V}^*_{33} \, y_s} \right) \frac{\delta\epsilon_{32(L)}}{\delta_L} \sim 0.013 \times 3 \times 10^{-3} \, \delta_R \sim 5 \cdot 10^{-5} \, \delta_R, \quad (6.55)$$

$$\left(\mathbf{R}_d^{-1} \right)_{32(R)} \simeq \left(\frac{\mathbf{V}^*_{22} \, y_s}{\mathbf{V}^*_{33} \, y_b} - \frac{\mathbf{V}^{*\,2}_{23} \, y_b}{\mathbf{V}^*_{22} \, \mathbf{V}^*_{33} \, y_s} \right) \left(\mathbf{R}_d^{-1} \right)_{32(L)} \sim 4 \cdot 10^{-4} \, \delta_R \,. \quad (6.56)$$

In this case, the value of the off-diagonal element $(\mathbf{R}_d^{-1})_{32}$ is of the order of 10^{-4} and this implies that the contributions $\mathbf{V}^*_{23} \mathbf{V}_{22}$ in Eq. (6.38) and $\left(\mathbf{R}_d^{-1} \right)_{23}$ in Eq. (6.37) or y_{R_i} in Eq. (6.42), can be important. Thus:

$$\left(\mathbf{V}^\dagger \mathbf{R}_d^{-1} \mathbf{V} \right)_{32(R)}^{\max} \simeq \left(\mathbf{R}_d^{-1} \right)_{32(R)} + 2 \cdot 10^{-3} \left(\mathbf{R}_d^{-1} \right)_{23(R)} + 0.04 \frac{(1+\epsilon\tan\beta)\eta\tan\beta}{\mathrm{Det}(\mathbf{R}_d)}$$

$$\sim -4 \cdot 10^{-4}\delta_R - 2 \cdot 10^{-3} \frac{\delta\epsilon_{23(R)} \times 1.5 \times 60}{4} + 0.04 \frac{1.5 \times 4 \cdot 10^{-3} \times 60}{4} \quad (6.57)$$

where we used the same values for the parameters as in Eq. (6.51) and $\delta\epsilon_{23(R)}$ is now enhanced by a factor y_b/y_s:

$$\delta\epsilon_{23(R)} \sim \delta_R \frac{2\alpha_s}{3\pi} \frac{y_b}{y_s} \mu^* M_3^* \tilde{M}_{D_3}^2 \, K\left(\tilde{M}_Q^2, \tilde{M}_D^2, |M_3|^2 \right) \sim -0.1 \, \delta_R \,. \quad (6.58)$$

Therefore, we obtain,

$$\left(\mathbf{V}^\dagger \mathbf{R}_d^{-1} \mathbf{V} \right)_{32(R)}^{\max} \sim 4(\delta_R + 1) \cdot 10^{-3} \quad (6.59)$$
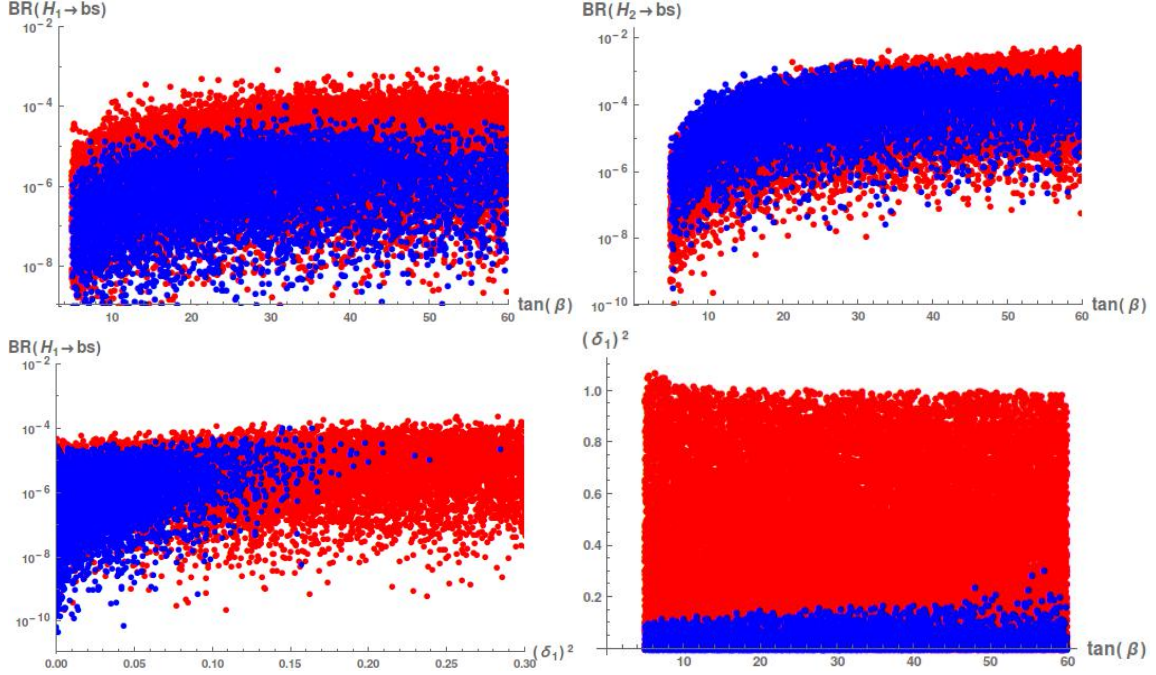
Figure 6.3: A generic supersymmetric SM with L insertion with $\delta_L \neq 0$ and $\delta_{A_u} = \delta_R = 0$: The upper frames show the dependence of the estimated branching ratios for $H_{1,2} \to \bar{b}s + \bar{s}b$ on $\tan\beta$. The lower-left frame is for the dependence of B$(H_1 \to bs)$ on δ_1^2 and the lower-right frame for the δ_1^2 dependence on $\tan\beta$. Blue (dark) points satisfy all the constraints considered, while red (light) points violate one or several of these constraints.

Thus, for $\delta_R = 0.5$, the branching ratios are:

$$\text{BR}\left(H_1 \to \bar{b}s + \bar{s}b\right)^{\max}_{(R)} \simeq \left|\left(\mathbf{V}^\dagger \mathbf{R}_d^{-1} \mathbf{V}\right)_{32(R)}\right|^2 \frac{3\,\kappa_{QCD}(\delta_1^2 + \eta_1^2)}{\left(3\,\kappa_{QCD} + \frac{m_{\tilde{t}}^2}{m_b^2}\right) + I_{PS}\frac{126^2}{m_b^2}} \sim 1.5 \cdot 10^{-5}\left(\delta_1^2 + \eta_1^2\right)$$

(6.60)

$$\text{BR}\left(H_2 \to \bar{b}s + \bar{s}b\right)^{\max}_{(R)} \simeq \left|\left(\mathbf{V}^\dagger \mathbf{R}_d^{-1} \mathbf{V}\right)_{32(R)}\right|^2 \frac{3\,\kappa_{QCD}}{3\,\kappa_{QCD} + \frac{m_{\tilde{t}}^2}{m_b^2}} \sim 2 \cdot 10^{-5}$$

(6.61)

The results of our scans for this case are shown in Fig. 6.2. As before, these results are in agreement with the numerical values if B-meson constraints are not taken into account. Once they are incorporated into the analysis, the lightest Higgs branching ratio is reduced by more than one order of magnitude. Also, taking into account, from Eq. (6.57), that both the MI and MI-independent contributions are of the same order only for large δ_R, the BR is completely independent of δ_R.

6.4.2 Generic supersymmetric SM

After computing these branching ratios in the MSSM framework, we now perform our analysis in a generic supersymmetric model. Therefore, we present here a model-independent analysis, meaning that, in fact, we consider a generic Higgs mixing matrix with possible additional Higgs states. In this case, we have $\mathcal{O}_{11}^2 + \mathcal{O}_{21}^2 + \mathcal{O}_{31}^2 \leq 1$ and the parameters δ_1 and/or η_1 entering $\Gamma(H_1 \to \bar{b}s + \bar{s}b)$ can be sizeable.

The expressions for the decay widths and branching ratios, Eqs. (6.43–6.49), are still valid in the generic supersymmetric scenario. The main difference now is that the parameters δ_1 and η_1 are only constrained by experimental results on Higgs decays and low-energy FCNC processes. Notice, however, that the flavour-changing entries in $\mathbf{R_d^{-1}}$ do not change in the two models.

In Fig. 6.3, we show the FC branching ratios of H_1 and H_2 for $\delta_L \neq 0$ and $\delta_{A_u} = \delta_R = 0$ in the generic supersymmetric SM. These figures can be compared with Fig. 6.1 which shows the corresponding branching ratios in the MSSM framework.

In the MSSM framework, the mixing angles are obtained through a minimization of the scalar potential and both δ_1 and η_1 are of the order of $v^2/m_{H_2}^2$ from the diagonalization of the neutral Higgs mass matrix. In the generic supersymmetric scenario we treat δ_1 and η_1 as free parameters that do not depend a priori on the ratio $v^2/m_{H_2}^2$, but are only constrained by the different experimentally measured Higgs branching ratios and B-meson constraints. This is why $\mathrm{BR}(H_1 \to bs)$ in Fig 6.1 is two orders of magnitude smaller that the largest possible value in Figure 6.3. The different distribution of the points allowed by B-meson constraints is due to the same reason. In the MSSM scenario, Higgs flavour changing processes are mediated by the heavy Higgses and therefore are only important for light m_{H_2} which, as we have seen, correspond also to the largest δ_1 and η_1 and therefore to the largest branching ratios. In the generic supersymmetric SM, it is, in principle, possible to have a large δ_1 with a heavy H_2 and therefore the B-meson constraints are not so efficient.

On the other hand, the FC decays of the heavy Higgses $H_{2,3}$ are independent of the values of δ_1 and η_1 as can be seen in Eq. (6.49). Therefore, the upper-right frames of Figs. 6.1 and 6.3 are very similar and we obtain very similar results for $\mathrm{BR}(H_2 \to bs)$ in the MSSM framework and in the generic supersymmetric SM.

Also, as shown in the lower-right plot in Fig. 6.3, the allowed values of $(\delta_1)^2$ are completely independent of $\tan \beta$ as the B-meson constraints, which depending on $(\tan \beta)^n/m_{H_2}^4$ can always be satisfied by adjusting conveniently the value of m_{H_2}. In this case, the upper limit for $(\delta_1)^2$ is fixed by the $H_1 \to \gamma\gamma$ decay which as shown in [59], requires $\left(\mathcal{O}_{11}^2 + \mathcal{O}_{31}^2\right) \sim 1/\tan^2 \beta$ and $\mathcal{O}_{21}^2 \sim 1 - 1/\tan^2 \beta$. Using the definition of δ_1 and in the limit $\mathcal{O}_{31} \ll 1$, with the above constraints, $(\delta_1)^2 \lesssim 0.17$ for $\tan \beta \gtrsim 10$, as we see numerically in this plot.

In summary, the main difference in the generic supersymmetric SM is that $\mathrm{BR}(H_1 \to bs)$ could reach a value of $\sim 10^{-4}$ consistently with present experimental constraints. This value is still too small to be observed in the large background of a hadron collider, but it could be tested in a leptonic linear collider in the near future.

6.5   Conclusions

In this paper, we have analyzed the FC Higgs decay $H_i \to bs$ for the different Higgs states in both an MSSM scenario and a more general supersymmetric SM framework. The importance of this observable is that effects of heavy particles do not decouple and may provide a first sign of new physics for heavy supersymmetric masses beyond collider reach. Before we carried out our numerical analysis, we derived approximated analytic expressions for the off-diagonal entries of $\left(\mathbf{V}^\dagger \mathbf{R}_d^{-1} \mathbf{V}\right)$ which dictate the size of flavour violation. In an MSSM framework we showed that, even in the presence of large off-diagonal flavour entries in the sfermion mass matrices, for the light Higgs, $\mathrm{BR}(H_1 \to bs) \lesssim 10^{-6}$ consistently with present experimental constraints, while for heavy Higgs states $\mathrm{BR}(H_{2,3} \to bs)$ can still be $\sim 10^{-3}$. In a more general supersymmetric scenario, where we allowed for non-minimal

Higgs mixings, the branching ratio $\mathrm{BR}(H_1 \to bs)$ can reach values $\sim \mathcal{O}(10^{-4})$, while $\mathrm{BR}(H_{2,3} \to bs)$ remain of the order of $\sim 10^{-3}$. We find that the results of the numerical analysis are well in accord with the estimations made using the approximated analytic expression for $\left(\mathbf{V}^\dagger \mathbf{R}_d^{-1} \mathbf{V}\right)$. Although these small branching ratios are clearly out of reach for the LHC due to the very large b-quark background, a full study in a linear collider environment could still be worth pursuing.

APPENDICES

6.A   FC Higgs couplings

In this appendix, we present the explicit expression for $\mathbf{G}_d^0$ associated with the FCNC Higgs couplings in Eq. (6.14),

$$\mathbf{G}_d^0 = \langle \boldsymbol{\Delta}_d^{\Phi_2} + \delta\boldsymbol{\Delta}_d^{\Phi_2} \rangle_0 \tag{6.62}$$

$$
\begin{aligned}
\langle \boldsymbol{\Delta}_d^{\Phi_2} \rangle_0 &= \mathbf{1}\,\frac{2\alpha_3}{3\pi}\,\mu^*\,M_3^*\,I\left(\widetilde{M}_Q^2, \widetilde{M}_D^2, |M_3|^2\right) - \mathbf{1}\,\frac{\alpha_1}{36\pi}\mu^*\,M_1^*\,I\left(\widetilde{M}_Q^2, \widetilde{M}_D^2, |M_1|^2\right) \\
&\quad + \frac{\mathbf{h}_u^\dagger \mathbf{h}_u}{16\pi^2}\,\mu^*\,A_u^*\,I\left(\widetilde{M}_Q^2, \widetilde{M}_U^2, |\mu|^2\right) - \frac{3\alpha_2}{8\pi}\mu^*\,M_2^*\,I\left(\widetilde{M}_Q^2, \widetilde{M}_D^2, |\mu|^2\right) \\
&\quad - \mathbf{1}\,\frac{\alpha_1}{24\pi}\,\mu^*\,M_1^*\,I\left(\widetilde{M}_Q^2, |M_1|^2, |\mu|^2\right) - \mathbf{1}\,\frac{\alpha_1}{12\pi}\,\mu^*\,M_1^*\,I\left(\widetilde{M}_D^2, |M_1|^2, |\mu|^2\right)
\end{aligned} \tag{6.63}
$$

$$
\begin{aligned}
\langle \delta\boldsymbol{\Delta}_d^{\Phi_2} \rangle_0 &= \frac{2\alpha_3}{3\pi}\,\mu^*\,M_3^*\left[\delta\widetilde{\mathbf{M}}_Q^2\,K\left(\widetilde{M}_Q^2, \widetilde{M}_D^2, |M_3|^2\right) + \mathbf{h}_d^{-1}\delta\widetilde{\mathbf{M}}_D^2\mathbf{h}_d\,K\left(\widetilde{M}_D^2, \widetilde{M}_Q^2, |M_3|^2\right)\right] \\
&\quad - \frac{\alpha_1}{36\pi}\mu^*\,M_1^*\left[\delta\widetilde{\mathbf{M}}_Q^2\,K\left(\widetilde{M}_Q^2, \widetilde{M}_D^2, |M_1|^2\right) + \mathbf{h}_d^{-1}\delta\widetilde{\mathbf{M}}_D^2\mathbf{h}_d\,K\left(\widetilde{M}_D^2, \widetilde{M}_Q^2, |M_1|^2\right)\right] \\
&\quad + \frac{1}{16\pi^2}\,\mu^*\,A_u^*\left[\mathbf{h}_u^\dagger\delta\widetilde{\mathbf{M}}_U^2\mathbf{h}_u\,K\left(\widetilde{M}_U^2, \widetilde{M}_Q^2, |\mu|^2\right) + \delta\widetilde{\mathbf{M}}_Q^2\mathbf{h}_u^\dagger\mathbf{h}_u\,K\left(\widetilde{M}_Q^2, \widetilde{M}_U^2, |\mu|^2\right)\right] \\
&\quad + \frac{\delta\mathbf{a}_u^\dagger\mathbf{h}_u}{16\pi^2}\,\mu^*\,I\left(\widetilde{M}_Q^2, \widetilde{M}_U^2, |\mu|^2\right) - \frac{3\alpha_2}{8\pi}\,\mu^*M_2^*\delta\widetilde{\mathbf{M}}_Q^2\,K\left(\widetilde{M}_Q^2, \left|\widetilde{M}_2\right|^2, |\mu|^2\right)
\end{aligned} \tag{6.64}
$$

$$
- \frac{\alpha_1}{24\pi}\,\mu^*\,M_1^*\delta\widetilde{\mathbf{M}}_Q^2\,K\left(\widetilde{M}_Q^2, |M_1|^2, |\mu|^2\right) - \frac{\alpha_1}{12\pi}\,\mu^*\,M_1^*\mathbf{h}_d^{-1}\delta\widetilde{\mathbf{M}}_D^2\mathbf{h}_d\,K\left(\widetilde{M}_D^2, |M_1|^2, |\mu|^2\right)
$$

where the loops functions are given by:

$$I(a, b, c) = \frac{ab\,\ln(a/b) + bc\,\ln(b/c) + ac\,\ln(c/a)}{(a-b)(b-c)(a-c)} \tag{6.65}$$

$$K(a, b, c) = \frac{\mathrm{d}}{\mathrm{d}a}\left[I(a, b, c)\right] = \frac{b\,\ln(a/b) + c\,\ln(c/a)}{(a-b)(b-c)(a-c)} + \frac{(b+c-2a)\,I(a,b,c) + 1}{(a-b)(a-c)} \tag{6.66}$$

From here, the elements ϵ, δ, used in the $\mathbf{G}_d^0$ matrix in Eq. (6.32) are:

$$\epsilon = \frac{2\alpha_s}{3\pi}\,\mu^*\,M_3^*\,I\left(\tilde{M}_Q^2, \tilde{M}_D^2, |M_3|^2\right) + \frac{\rho-1}{3}\left[\frac{2\alpha_s}{3\pi}\,\mu^*\,M_3^*\left(\tilde{M}_{D_3}^2 + \tilde{M}_{Q_3}^2\right)\,K\left(\tilde{M}_Q^2, \tilde{M}_D^2, |M_3|^2\right)\right] \tag{6.67}$$

$$\eta = \frac{|y_t|^2}{16\pi^2}\,\mu^* A_u^*\, I\left(\tilde{M}_Q^2, \tilde{M}_U^2, |\mu|^2\right) - \delta_R\left[\frac{2\alpha_s}{3\pi}\,\mu^* M_3^*\,\frac{V_{23}^*}{V_{33}^*}\tilde{M}_{D_3}^2\,K\left(\tilde{M}_Q^2, \tilde{M}_D^2, |M_3|^2\right)\right] \quad (6.68)$$

$$+ (1-\rho)\left[\frac{2}{3}\frac{|y_t|^2}{16\pi^2}\,\mu^*\left(A_t^*\,I\left(\tilde{M}_Q^2, \tilde{M}_U^2, |\mu|^2\right) + A_u^*\left(\tilde{M}_{U_3}^2 + \tilde{M}_{Q_3}^2\right)K\left(\tilde{M}_Q^2, \tilde{M}_U^2, |\mu|^2\right)\right)\right.$$

$$\left.+\frac{2\alpha_s}{3\pi}\,\mu^* M_3^*\left(\tilde{M}_{D_3}^2 + \tilde{M}_{Q_3}^2\right)K\left(\tilde{M}_Q^2, \tilde{M}_D^2, |M_3|^2\right)\right]$$

6.B B-physics constraints

The main FC processes associated with B-Mesons that we consider in our analysis are ΔM_{B_s} and $\bar{B}_s^0 \to \mu^+\mu^-$, although other constraints like $\mathrm{BR}(B \to X_s\gamma)$ are also included.

In the case of ΔM_{B_s}, we use the expression in [55], given by:

$$\Delta M_{B_s} = 2\left|\langle\bar{B}_s^0|H_{eff}^{\Delta B=2}|B_s^0\rangle_{SM} + \langle\bar{B}_s^0|H_{eff}^{\Delta B=2}|B_s^0\rangle_{SUSY}\right| \quad (6.69)$$

where the SUSY contribution is [55]:

$$\langle\bar{B}_s^0|H_{eff}^{\Delta B=2}|B_s^0\rangle_{SUSY} = 2310\mathrm{ps}^{-1}\left(\frac{\widehat{B}_{B_s}^{1/2}F_{B_s}}{265\,\mathrm{MeV}}\right)^2\left(\frac{\nu_B}{0.55}\right)\times$$

$$\left[0.88\left(C_2^{LR(DP)} + C_2^{LR(2HDM)}\right) - 0.52\left(C_1^{SLL(DP)} + C_1^{SRR(DP)}\right)\right] \quad (6.70)$$

where the Wilson coefficients above $C_2^{LR(DP)}$, $C_2^{LR(2HDM)}$, $C_1^{SLL(DP)}$ and $C_1^{SRR(DP)}$ are associated with double-penguin and box diagrams.

The Wilson coefficients $C_1^{SLL(DP)}$, $C_1^{SRR(DP)}$, $C_2^{LR(DP)}$ and $C_2^{LR(2HDM)}$ related to the SUSY contribution of the B_s-meson mass difference in Eq. (6.70) are,

$$C_1^{SLL(DP)} = -\frac{16\pi^2 m_b^2}{\sqrt{2}G_F M_W^2}\sum_{i=1}^{3}\frac{\mathbf{g}_{H_i\bar{b}s}^L\,\mathbf{g}_{H_i\bar{b}s}^L}{m_{H_i}} \quad (6.71)$$

$$C_1^{SRR(DP)} = -\frac{16\pi^2 m_s^2}{\sqrt{2}G_F M_W^2}\sum_{i=1}^{3}\frac{\mathbf{g}_{H_i\bar{b}s}^R\,\mathbf{g}_{H_i\bar{b}s}^R}{m_{H_i}} \quad (6.72)$$

$$C_2^{LR(DP)} = -\frac{32\pi^2 m_b m_s}{\sqrt{2}G_F M_W^2}\sum_{i=1}^{3}\frac{\mathbf{g}_{H_i\bar{b}s}^L\,\mathbf{g}_{H_i\bar{b}s}^R}{m_{H_i}} \quad (6.73)$$

$$C_2^{LR(2HDM)} = \left.C_2^{LR(2HDM)}\right|_{H^\pm H^\mp} + \left.C_2^{LR(2HDM)}\right|_{W^\pm H^\mp}. \quad (6.74)$$

The couplings of the charged Higgses and Goldstone bosons to fermions, Eq. (3.38) of Ref.[56], are given by:

$$\mathcal{L} \supset -\frac{g}{2M_W}\left[H^-\bar{d}\left(\widehat{\mathbf{M}}_d\,\mathbf{g}_{H^-}^L\,P_L + \mathbf{g}_{H^-}^R\,\widehat{\mathbf{M}}_u\,P_R\right)u + G^-\bar{d}\left(\widehat{\mathbf{M}}_d\,\mathbf{g}_{G^-}^L\,P_L + \mathbf{g}_{G^-}^R\,\widehat{\mathbf{M}}_u\,P_R\right)u\right] + \mathrm{h.c.} \quad (6.75)$$

and in the large $\tan\beta$ limit, we have:

$$\mathbf{g}_{H^-}^L = -\tan\beta\,\mathbf{V}^\dagger\mathbf{R}_d^{-1} + \mathbf{V}^\dagger\mathbf{R}_d^{-1}\mathbf{G}_d^0 \qquad \mathbf{g}_{H^-}^R = -\frac{1}{\tan\beta}\mathbf{V}^\dagger \quad (6.76)$$

$$\mathbf{g}^L_{G^-} = \mathbf{V}^\dagger \qquad\qquad\qquad \mathbf{g}^R_{G^-} = -\mathbf{V}^\dagger \qquad (6.77)$$

Then $C_2^{LR(2HDM)}$ includes two main contributions: one associated with box diagrams for two $H_l^\pm$ and another for $W^\mp H^\pm$ box diagrams. From Eqs. (4.4) and (4.5) in Ref.[69], we have:

$$C_2^{LR(2HDM)}\Big|_{H^\pm H^\mp} = \frac{8m_b m_s m_t^4}{M_W^2} \sum_{k,l=H,G} \mathbf{g}^L_{H_l^-\,33}\, \mathbf{g}^{L\dagger}_{H_l^-\,32}\, \mathbf{g}^R_{H_k^-\,33}\, \mathbf{g}^{R\dagger}_{H_k^-\,32}\, D_0\left(M_{H_l^-}^2, M_{H_k^-}^2, m_t^2, m_t^2\right) \tag{6.78}$$

$$C_2^{LR(2HDM)}\Big|_{W^\pm H^\mp} = -8m_b m_s \sum_{i,j=1}^3 \sum_{k=H,G} \mathbf{g}^L_{H_k^-\,3i}\, \mathbf{g}^{L\dagger}_{H_k^-\,j2}\, \mathbf{V}^\dagger_{3j} \mathbf{V}_{i2}\, D_2\left(M_W^2, M_{H_k^-}^2, m_{q_i}^2, m_{q_j}^2\right) \tag{6.79}$$

where $D_0(a,b,c,d)$ and $D_2(a,b,c,d)$ are the corresponding loop functions which can be found in Ref.[69]

The decay $\bar{B}_s^0 \to \mu^+\mu^-$ is described by the effective Hamiltonian,

$$H_{\text{eff}}^{\Delta B=1} = -2\sqrt{2}G_F V_{tb} V_{ts}^* \left(C_S \mathcal{O}_S + C_P \mathcal{O}_P + C_{10}\mathcal{O}_{10}\right) \tag{6.80}$$

where the relevant operators are $\mathcal{O}_S = \frac{e^2}{16\pi^2} m_b \left(\bar{q}P_R b\right)\left(\bar{\mu}\mu\right)$, $\mathcal{O}_P = \frac{e^2}{16\pi^2} m_b \left(\bar{q}P_R b\right)\left(\bar{\mu}\gamma_5\mu\right)$ and $\mathcal{O}_{10} = \frac{e^2}{16\pi^2} \left(\bar{q}\gamma^\mu P_L b\right)\left(\bar{\mu}\gamma_\mu\gamma_5\mu\right)$.

Neglecting the non-holomorphic vertices on the leptonic sector as well as the contributions proportional to the lighter quark masses $m_{d,s}$, the branching ratio is given by

$$\text{BR}\left(\bar{B}_s^0 \to \mu^+\mu^-\right) = \frac{G_F^2 \alpha_{\text{em}}^2}{16\pi^3} M_{B_s} \tau_{B_s} \left|V_{tb}V_{ts}^*\right|^2 \sqrt{1 - \frac{4m_\mu^2}{M_{B_s}^2}} \left[\left(1 - \frac{4m_\mu^2}{M_{B_s}^2}\right)|F_S^s|^2 + |F_P^s + 2m_\mu F_A^s|^2\right] \tag{6.81}$$

where τ_{B_s} is the total lifetime of the B_s meson and the form factors are:

$$F_{S,P}^s = -\frac{i}{2} M_{B_s}^2 F_{Bs} \frac{m_b}{m_b + m_q} C_{S,P}, \qquad F_A^s = -\frac{i}{2} F_{B_s} C_{10}, \tag{6.82}$$

with the Wilson coefficients,

$$C_S = \frac{2\pi m_\mu}{\alpha_{\text{em}}} \frac{1}{V_{tb}V_{ts}^*} \sum_{i=1}^3 \frac{\mathbf{g}^R_{H_i \bar{s}b}\, g^S_{H_i \bar{\mu}\mu}}{m_{H_i}^2}, \tag{6.83}$$

$$C_P = i\frac{2\pi m_\mu}{\alpha_{\text{em}}} \frac{1}{V_{tb}V_{ts}^*} \sum_{i=1}^3 \frac{\mathbf{g}^R_{H_i \bar{s}b}\, g^P_{H_i \bar{\mu}\mu}}{m_{H_i}^2}, \tag{6.84}$$

$$C_{10} = -4.221 \tag{6.85}$$

where C_{10} is the leading SM contribution, and $g^S_{H_i \bar{\mu}\mu} = \frac{\mathcal{O}_{1i}}{\cos\beta}$ and $g^P_{H_i \bar{\mu}\mu} = -\tan\beta\, \mathcal{O}_{3i}$ are the Higgs couplings to the charged leptons.

Bibliography

[1] G. Aad *et al.* [ATLAS Collaboration], Phys. Lett. B **716**, 1 (2012) [arXiv:1207.7214 [hep-ex]].

[2] S. Chatrchyan *et al.* [CMS Collaboration], Phys. Lett. B **716**, 30 (2012) [arXiv:1207.7235 [hep-ex]].

[3] G. C. Branco, P. M. Ferreira, L. Lavoura, M. N. Rebelo, M. Sher and J. P. Silva, Phys. Rept. **516**, 1 (2012) [arXiv:1106.0034 [hep-ph]].

[4] H. P. Nilles, Phys. Rept. **110**, 1 (1984).

[5] H. E. Haber and G. L. Kane, Phys. Rept. **117**, 75 (1985).

[6] C. Hamzaoui, M. Pospelov and M. Toharia, Phys. Rev. D **59**, 095005 (1999) [hep-ph/9807350].

[7] S. R. Choudhury and N. Gaur, Phys. Lett. B **451**, 86 (1999) [hep-ph/9810307].

[8] K. S. Babu and C. F. Kolda, Phys. Rev. Lett. **84**, 228 (2000) [hep-ph/9909476].

[9] P. H. Chankowski and L. Slawianowska, Phys. Rev. D **63**, 054012 (2001) [hep-ph/0008046].

[10] G. Isidori and A. Retico, JHEP **0111**, 001 (2001) [hep-ph/0110121].

[11] C. Bobeth, T. Ewerth, F. Kruger and J. Urban, Phys. Rev. D **66**, 074021 (2002) [hep-ph/0204225].

[12] A. J. Buras, P. H. Chankowski, J. Rosiek and L. Slawianowska, Phys. Lett. B **546**, 96 (2002) [hep-ph/0207241].

[13] A. J. Buras, P. H. Chankowski, J. Rosiek and L. Slawianowska, Nucl. Phys. B **659**, 3 (2003) [hep-ph/0210145].

[14] P. Paradisi, JHEP **0602**, 050 (2006) [hep-ph/0508054].

[15] A. Arhrib, D. K. Ghosh, O. C. W. Kong and R. D. Vaidya, Phys. Lett. B **647**, 36 (2007) [hep-ph/0605056].

[16] A. J. Buras, M. V. Carlucci, S. Gori and G. Isidori, JHEP **1010**, 009 (2010) [arXiv:1005.5310 [hep-ph]].

[17] A. Crivellin, Phys. Rev. D **83**, 056001 (2011) [arXiv:1012.4840 [hep-ph]].

[18] A. Crivellin, L. Hofer and J. Rosiek, JHEP **1107**, 017 (2011) [arXiv:1103.4272 [hep-ph]].

[19] A. Crivellin and C. Greub, Phys. Rev. D **87**, 015013 (2013) [Phys. Rev. D **87**, 079901 (2013)] [arXiv:1210.7453 [hep-ph]].

[20] A. Goudelis, O. Lebedev and J. h. Park, Phys. Lett. B **707**, 369 (2012) [arXiv:1111.1715 [hep-ph]].

[21] E. Gabrielli and B. Mele, Phys. Rev. D **83**, 073009 (2011) [arXiv:1102.3361 [hep-ph]].

[22] G. Blankenburg, J. Ellis and G. Isidori, Phys. Lett. B **712**, 386 (2012) [arXiv:1202.5704 [hep-ph]].

[23] M. Arana-Catania, E. Arganda and M. J. Herrero, JHEP **1309**, 160 (2013) [arXiv:1304.3371 [hep-ph]].

[24] W. D. Goldberger, B. Grinstein and W. Skiba, Phys. Rev. Lett. **100**, 111802 (2008) [arXiv:0708.1463 [hep-ph]].

[25] J. Fan, W. D. Goldberger, A. Ross and W. Skiba, Phys. Rev. D **79**, 035017 (2009) [arXiv:0803.2040 [hep-ph]].

[26] S. Casagrande, F. Goertz, U. Haisch, M. Neubert and T. Pfoh, JHEP **0810**, 094 (2008) [arXiv:0807.4937 [hep-ph]].

[27] A. Azatov, M. Toharia and L. Zhu, Phys. Rev. D **80**, 035016 (2009) [arXiv:0906.1990 [hep-ph]].

[28] K. Agashe and R. Contino, Phys. Rev. D **80**, 075016 (2009) [arXiv:0906.1542 [hep-ph]].

[29] J. Fuster *et al.* [DELPHI Collaboration], CERN-OPEN-99-393, CERN-DELPHI-99-81.

[30] G. Eilam, Nucl. Phys. Proc. Suppl. **116**, 306 (2003) [hep-ph/0211458].

[31] D. M. Asner *et al.*, arXiv:1310.0763 [hep-ph].

[32] A. Pilaftsis, Phys. Rev. D **58**, 096010 (1998) [hep-ph/9803297].

[33] A. Pilaftsis, Phys. Lett. B **435**, 88 (1998) [hep-ph/9805373].

[34] D. A. Demir, Phys. Rev. D **60**, 095007 (1999) [hep-ph/9905571].

[35] A. Pilaftsis and C. E. M. Wagner, Nucl. Phys. B **553**, 3 (1999) [hep-ph/9902371].

[36] M. Carena, J. R. Ellis, A. Pilaftsis and C. E. M. Wagner, Nucl. Phys. B **586**, 92 (2000) [hep-ph/0003180].

[37] S. Y. Choi, M. Drees and J. S. Lee, Phys. Lett. B **481**, 57 (2000) [hep-ph/0002287].

[38] M. Carena, J. R. Ellis, A. Pilaftsis and C. E. M. Wagner, Nucl. Phys. B **625**, 345 (2002) [hep-ph/0111245].

[39] The ATLAS collaboration [ATLAS Collaboration], ATLAS-CONF-2014-009, ATLAS-CONF-2014-013.

[40] K. Cheung, J. S. Lee, E. Senaha and P. Y. Tseng, JHEP **1406**, 149 (2014) [arXiv:1403.4775 [hep-ph]].

[41] S. Inoue, M. J. Ramsey-Musolf and Y. Zhang, Phys. Rev. D **89**, no. 11, 115023 (2014) [arXiv:1403.4257 [hep-ph]].

[42] T. Banks, Nucl. Phys. B **303**, 172 (1988).

[43] R. Hempfling, Phys. Rev. D **49**, 6168 (1994).

[44] L. J. Hall, R. Rattazzi and U. Sarid, Phys. Rev. D **50**, 7048 (1994) [hep-ph/9306309, hep-ph/9306309].

[45] T. Blazek, S. Raby and S. Pokorski, Phys. Rev. D **52**, 4151 (1995) [hep-ph/9504364].

[46] M. Carena, M. Olechowski, S. Pokorski and C. E. M. Wagner, Nucl. Phys. B **426**, 269 (1994) [hep-ph/9402253].

[47] D. M. Pierce, J. A. Bagger, K. T. Matchev and R. j. Zhang, Nucl. Phys. B **491**, 3 (1997) [hep-ph/9606211].

[48] K. S. Babu and C. F. Kolda, Phys. Lett. B **451**, 77 (1999) [hep-ph/9811308].

[49] F. Borzumati, G. R. Farrar, N. Polonsky and S. D. Thomas, Nucl. Phys. B **555**, 53 (1999) [hep-ph/9902443].

[50] F. Borzumati, G. R. Farrar, N. Polonsky and S. D. Thomas, In *Trieste 1997, Phenomenological aspects of superstring theories* 159-167 [hep-ph/9805314].

[51] H. Eberl, K. Hidaka, S. Kraml, W. Majerotto and Y. Yamada, Phys. Rev. D **62**, 055006 (2000) [hep-ph/9912463].

[52] H. E. Haber, M. J. Herrero, H. E. Logan, S. Penaranda, S. Rigolin and D. Temes, Phys. Rev. D **63**, 055004 (2001) [hep-ph/0007006].

[53] F. Borzumati, C. Greub and Y. Yamada, hep-ph/0305063.

[54] F. Borzumati, C. Greub and Y. Yamada, Phys. Rev. D **69**, 055005 (2004) [hep-ph/0311151].

[55] J. R. Ellis, J. S. Lee and A. Pilaftsis, Phys. Rev. D **76**, 115011 (2007) [arXiv:0708.2079 [hep-ph]].

[56] J. Ellis, R. N. Hodgkinson, J. S. Lee and A. Pilaftsis, JHEP **1002**, 016 (2010) [arXiv:0911.3611 [hep-ph]].

[57] J. S. Lee, A. Pilaftsis, M. Carena, S. Y. Choi, M. Drees, J. R. Ellis and C. E. M. Wagner, Comput. Phys. Commun. **156**, 283 (2004) [hep-ph/0307377].

[58] G. Barenboim, C. Bosch, M. L. L??pez-Iba??ez and O. Vives, JHEP **1311**, 051 (2013) [arXiv:1307.5973 [hep-ph]].

[59] G. Barenboim, C. Bosch, M. L. L??pez-Ib????ez and O. Vives, Phys. Rev. D **90**, no. 1, 015003 (2014) [arXiv:1311.7321 [hep-ph]].

[60] CMS Collaboration [CMS Collaboration], CMS-PAS-HIG-13-021.

[61] G. Aad *et al.* [ATLAS Collaboration], JHEP **1411**, 056 (2014) [arXiv:1409.6064 [hep-ex]].

[62]   [ATLAS Collaboration], (2014),
       http://atlas.web.cern.ch/Atlas/GROUPS/PHYSICS/CombinedSummaryPlots/SUSY/

[63]   [CMS Collaboration], (2014),
       https://twiki.cern.ch/twiki/bin/view/CMSPublic/SUSYSMSSummaryPlots8TeV

[64]   V. Khachatryan *et al.* [CMS and LHCb Collaborations], Nature **522**, 68 (2015)
       [arXiv:1411.4413 [hep-ex]].

[65]   Y. Amhis *et al.* [Heavy Flavor Averaging Group (HFAG) Collaboration],
       arXiv:1412.7515 [hep-ex].

[66]   S. Aoki *et al.*, Eur. Phys. J. C **74**, 2890 (2014) [arXiv:1310.8555 [hep-lat]].

[67]   J. S. Lee, M. Carena, J. Ellis, A. Pilaftsis and C. E. M. Wagner, Comput. Phys.
       Commun. **180**, 312 (2009) [arXiv:0712.2360 [hep-ph]].

[68]   J. S. Lee, M. Carena, J. Ellis, A. Pilaftsis and C. E. M. Wagner, Comput. Phys.
       Commun. **184**, 1220 (2013) [arXiv:1208.2212 [hep-ph]].

[69]   A. J. Buras, P. H. Chankowski, J. Rosiek and L. Slawianowska, Nucl. Phys. B **619**,
       434 (2001) [hep-ph/0107048].

<div style="text-align: right;">

7

</div>

Prospects for constraining the shape of non-Gaussianity with the scale-dependent bias

Jorge Noreña, Licia Verde, Gabriela Barenboim, Cristian Bosch

Abstract

We consider whether the non-Gaussian scale-dependent halo bias can be used not only to constrain the local form of non-Gaussianity but also to distinguish among different shapes. In particular, we ask whether it can constrain the behavior of the primordial three-point function in the squeezed limit where one of the momenta is much smaller than the other two. This is potentially interesting since the observation of a three-point function with a squeezed limit that does not go like the local nor equilateral templates would be a signal of non-trivial dynamics during inflation. To this end we use the quasi-single field inflation model of Chen & Wang [1, 2] as a representative two-parameter model, where one parameter governs the amplitude of non-Gaussianity and the other the shape. We also perform a model-independent analysis by parametrizing the scale-dependent bias as a power-law on large scales, where the power is to be constrained from observations. We find that proposed large-scale structure surveys (with characteristics similar to the dark energy task force stage IV surveys) have the potential to distinguish among the squeezed limit behavior of different bispectrum shapes for a wide range of fiducial model parameters. Thus the halo bias can help discriminate between different models of inflation.

7.1   Introduction

The study of the deviation from Gaussianity of the initial conditions set by inflation is one of the most active fields of research in cosmology today. This is for a good reason since it is a potential observational handle on the interactions of the inflaton. Indeed, a free field is Gaussian and all its correlation functions are fixed by Wick's theorem in terms of its

two-point correlation function

$$\langle \zeta(\vec{k}_1)\zeta(\vec{k}_2)\rangle = (2\pi)^3 \delta(\vec{k}_1 + \vec{k}_2)P_\zeta(k) \,, \tag{7.1}$$

where ζ is the comoving curvature perturbation, and $P_\zeta(k) = 2\pi^2 \Delta_\zeta^2 (k/k_p)^{(n_s-1)}(1/k^3)$. The spectral index n_s and amplitude of the scalar power spectrum Δ_ζ^2 have been measured by the WMAP satellite [3] to be $n_s = 0.968 \pm 0.012$ and $\Delta_\zeta^2 = (2.430 \pm 0.091) \times 10^{-9}$ at the 68% confidence level, and k_p is an arbitrary pivot scale there chosen to be $k_p = 0.002 \, \mathrm{Mpc}^{-1}$. The interactions of the field induce non-trivial higher-order correlation functions which if observed can serve to discriminate between different models of inflation. In the context of cosmology, Non-Gaussianity refers to the study of the generation of these higher-order correlation functions in different models of the early universe, their modification through the non-linear evolution of the later universe, and how observations may be used to measure them. Of these, the three-point function is expected to be the most accessible to observations; it can be written as

$$\langle \zeta(\vec{k}_1)\zeta(\vec{k}_2)\zeta(\vec{k}_3)\rangle = (2\pi)^3 \delta(\vec{k}_1 + \vec{k}_2 + \vec{k}_3)B_\zeta(k_1, k_2, k_3) \,, \tag{7.2}$$

where B_ζ is called the bispectrum. Early work focused on the study of the three-point function given by the following phenomenological prescription

$$\zeta = \zeta_g + \frac{3}{5}f_{\mathrm{NL}}^{\mathrm{Loc}}(\zeta_g^2 - \langle\zeta_g^2\rangle) \,, \tag{7.3}$$

where ζ_g is a Gaussian random field. This generates a bispectrum with the following shape

$$B_\zeta^{\mathrm{loc}}(k_1, k_2, k_3) = \frac{6}{5}f_{\mathrm{NL}}^{\mathrm{Loc}}\big[P_\zeta(k_1)P_\zeta(k_2) + \mathrm{cycl.}\big] \,. \tag{7.4}$$

This type of bispectrum is called local since it stems from a local redefinition of the field. Note that it is divergent in the limit in which one of the momenta is much smaller than the other two, often called the squeezed limit; this divergence goes as $\langle \zeta(\vec{k}_1)\zeta(\vec{k}_2)\zeta(\vec{q})\rangle \overset{q\to 0}{\sim}$ $1/q^3$.

The three-point function generated by the simplest single-field slow-roll models with a standard kinetic term was first computed by [4, 5], who found it to be too small to be accessible to observations in the foreseeable future. A "large" non-Gaussianity can be generated by introducing new ingredients in the model such as additional light fields (see e.g. [6]), a non-trivial kinetic term (see e.g. [7]), or features in the power spectrum (see e.g. [8]). Each of these models generates a characteristic type of non-Gaussianity. Furthermore, within the context of single-field slow-roll inflation, the observation of the three-point function could potentially fix the coefficients of the leading terms in the effective Lagrangian for the perturbations of the inflaton [9, 10].

The best constraints on the primordial three-point function to date come from the WMAP satellite observing the cosmic microwave background radiation (CMB) [3]. A non-trivial three-point function has yet to be observed, but the Planck satellite promises to greatly improve on current bounds [11]. Another promising probe comes from the observation of large scale structure in the universe (LSS). Competitive constraints on the non-Gaussianity have been found [12] using the fact that a non-Gaussianity of the local type, Eq. (7.4), induces a characteristic scale, redshift and mass dependence on the halo bias [13, 14, 15].

In this paper we wish to study the power of LSS surveys in the near future to constrain the shape of non-Gaussianity through the observation of the halo bias. The halo bias is

sensitive to a configuration in which one of the three Fourier modes is much smaller than the other two, the so-called squeezed limit, where the long mode is the scale of observation. The local non-Gaussianity has a divergent squeezed limit and gives a contribution to the large-scale halo bias that goes like $\sim 1/k^2$. In section 7.2 we summarize the information about inflation contained in the squeezed limit of the bispectrum. It has been shown [4, 16, 17, 18] that the bispectrum of single-field inflationary models is suppressed in the squeezed limit by two powers of the small momentum, thus giving a negligible contribution to the halo bias unless there are features in the power spectrum close to the relevant scales. Models with several light fields may generate a bispectrum which has a squeezed limit that behaves like the local non-Gaussianity thus giving potentially interesting effects to the halo bias in future surveys, as studied for example in [19]. In order for the three-point function to have a non-standard behavior in the squeezed limit, some non-trivial dynamics must be present during inflation. One such model is the "quasi single-field" inflation model of [1, 2], which is the one we use as an example of the power of a future survey to constrain the behavior of the three-point function in the squeezed limit. It consists of a light inflaton coupled to an isocurvaton with a mass which is close to the Hubble scale during inflation. In section 7.3 we summarize how the presence of primordial non-Gaussianity affects the halo bias in the peak background split formalism. In section 7.4 we describe the survey setup we consider, with the characteristics of the specific Dark Energy Task Force stage IV survey. In particular, we use a survey similar to that used in [20] and we refer the reader to the survey description given on that reference. In section 7.5 we present our main result, namely the forecast of the constraints that such a survey would be able to impose on the parameters of the quasi-single field inflation model, which can also be thought as a parametrization of the squeezed limit of a three-point function. We also perform the same analysis for a power-law parametrization of the non-Gaussian bias on large scales. Finally, in section 7.6 we draw conclusions and discuss the results.

7.2   Model of non-Gaussianity

As we will review in the following section, the non-Gaussian modification of the halo bias is mainly sensitive to the squeezed limit of the bispectrum in which one of the momenta, here denoted by q, is much smaller than the other two. It is thus of interest to consider what information can be gained about inflation from constraints on the squeezed limit of the three-point function.

Generic single-field models of inflation must satisfy the following consistency relation

$$\langle \zeta(\vec{k}_1)\zeta(\vec{k}_2)\zeta(\vec{q})\rangle \stackrel{q\to 0}{=} -(2\pi)^3\delta(\vec{k}_1 + \vec{k}_2 + \vec{q})P(k_1)P(q)\left[-(n_s - 1) + \mathcal{O}\left(\frac{q^2}{k^2}\right)\right]. \quad (7.5)$$

This relation was first derived in Refs. [4, 16], while Ref. [17] showed that the corrections are suppressed by the square of the small momentum (*i.e.*, the second term in the square brackets). This implies that all single field models of inflation generate a bispectrum which in the squeezed limit goes like $\langle \zeta^3\rangle \sim 1/q$ [1]. This was understood in reference [18] to be a consequence of the fact that, under the assumption of adiabaticity, correlation functions of ζ are endowed with a $SO(4,1)$ symmetry which is non-linearly realized by ζ.

The exact momentum dependence of the bispectra as predicted by different models of inflation is too cumbersome to be used in CMB data analysis. What is often done is

---

[1]In order to prove this, one must assume that the time variation of ζ outside of the horizon is suppressed at least as q^2. This is the case for most models of inflation present in the literature.

to look for a bispectrum shape, often called a *template*, which has a high overlap with the exact bispectrum and use it to analyze the data. Two such templates which are often used are the equilateral one [21] and the orthogonal one [10]. They are similar to shapes generated by different operators in the effective Lagrangian for single field inflation [9, 10]. However, one must be careful when using these templates with the scale-dependent halo bias to put constraints on the models which inspired them. Indeed, the orthogonal template has a squeezed limit going like $\langle \zeta^3 \rangle \sim 1/q^2$, which is in contradiction with the above-mentioned fact that all single field models of inflation must have a squeezed limit going like $\langle \zeta^3 \rangle \sim 1/q$ [(2)]. One can still view studies using the orthogonal template and the halo bias as examples of the usefulness of this method in constraining intermediate shapes. Nevertheless, at the time of writing, no model in the literature generates a bispectrum which has both a large overlap with and a squeezed limit like that of the orthogonal template.

For models with several light fields which can contribute to the generation of primordial perturbations none of the above arguments hold, and the bispectrum can generically be large in the squeezed limit. For example, curvaton models (see e.g. [6]) predict a bispectrum which is very close to having a shape like that of the local template, and which goes like $\langle \zeta^3 \rangle \sim 1/q^3$ in the squeezed limit. This is one of the reasons why observing a large non-Gaussianity of the local type is compelling, as it would rule out all single-field models of inflation. However, there is still more information contained in the behavior of the bispectrum in the squeezed limit. Reference [17] argues that in multi-field models, when all the fields are much lighter than the Hubble scale during inflation and are thus scale invariant, the squeezed limit of the bispectrum is proportional to the power spectrum of the long mode, *i.e.*, $\propto 1/q^3$, with corrections which are again quadratic in the small momentum. Thus, in single-field models of inflation and in models with multiple light fields the bispectrum always goes as $1/q^3$ or $1/q$ in the squeezed limit.

If one wishes to obtain a non-standard behavior in the squeezed limit, the alternative is to consider a multi-field model where at least one of the fields has a mass close to H, which is high enough to invalidate the arguments of the previous paragraph, but low enough so that it can't be trivially integrated out. An interesting realization of this is the model of Ref. [1, 2], termed "quasi-single field inflation". It consists of two fields, one being a light inflaton and the other an isocurvaton with a mass of order H. The inflaton and isocurvaton are coupled through a turning trajectory in field space, which allows for the isocurvaton to have a sizeable contribution to the three-point function of ζ. Reference [1] computes the bispectrum for such a model, and suggest the following template as a good approximate description

$$B_\zeta(k_1, k_2, k_3) = (2\pi)^4 \Delta_\zeta^4 k_p^{2(1-n_s)} \frac{3^{7/2}}{10 N_\nu(\alpha/27)} \frac{f_{\rm NL}}{(k_1 k_2 k_3)^{3/2}(k_1+k_2+k_3)^{3/2}} N_\nu\left(\frac{\alpha k_1 k_2 k_3}{(k_1+k_2+k_3)^3}\right),$$
(7.6)

where N_ν is the Neumann function, α is fixed to be 8, and $\nu \equiv \sqrt{9/4 - m^2/H^2}$, with m being the mass of the heavy isocurvaton. The factors in front fix the normalization of the template to be equal to the local template at the equilateral point $k_1 = k_2 = k_3$. The amplitude $f_{\rm NL}$ is related to ν, the third derivative of the isocurvaton potential, and the angular velocity in the turning trajectory $\dot{\theta}_0$ as $f_{\rm NL} = \alpha(\nu) P_\zeta^{-1/2} (\dot{\theta}_0/H)^3 (-V'''/H)$, where $\alpha(\nu)$ is the function plotted in figure 8 of Ref. [1].

In the squeezed limit, the template of Eq. (7.6) goes like $\langle \zeta^3 \rangle \sim 1/q^{3/2+\nu}$; thus different values of ν give different behaviors in the squeezed limit. For $\nu = 1.5$, the template behaves

---

[2] It is worth noting however that Reference [10] gives in their Appendix a template for the orthogonal shape which does have the correct behavior in the squeezed limit.

like the local one in the squeezed limit; for $\nu = 0.5$ it behaves like the orthogonal *template* in the squeezed limit; other values of ν give intermediate behaviors. One therefore expects future surveys to constrain the value of ν using the halo bias.

The halo bispectrum is actually not sensitive to the exact squeezed limit in which one of the Fourier modes is infinitely much smaller than the other two. This means that even if all single field models must satisfy the consistency relation of equation (7.5) in the exact squeezed limit, there might be single field models with features in the bispectrum close to the actual scales relevant for observations such that they can still produce a large effect in the halo bias. Some work in this direction has been done in Ref. [22]. Another possibility is that the bispectrum breaks scale invariance, again in this case the model must satisfy the consistency relation of equation (7.5) but can still have an effect on the halo bias, see Ref. [23]. Refs. [24, 25] very recently argued that a modified vacuum state can have a feature near to the squeezed limit that induces a scale dependence of the halo bias which is stronger than that generated by the local template.

In this paper we wish to forecast the constraints that a future survey with the characteristics of the Dark Energy Task Force stage IV [26] can put simultaneously on ν and f_{NL} as defined in equation (7.6). In the context of the quasi-single field model, a constraint on ν translates into a constraint on the mass of the heavy isocurvaton. More generally, one can see this as an estimate of the power of future surveys to constrain the behavior of the squeezed limit of the three-point function. In section 7.3 we also introduce a parametrization of the non-gaussian modification to the halo bias on large scales in order to perform this analysis in a model independent way. All of this is potentially interesting since if a bispectrum with a squeezed limit that does not go like $1/q$ or $1/q^3$ is observed, it would signal the presence of heavy fields or other non-trivial dynamics during inflation.

Let us now estimate the values of f_{NL} that are allowed by current observations. Though no dedicated data analysis has been performed for the template of Eq. (7.6), it has a sizable overlap with the local template. To be more quantitative, define the "cosine" between two bispectra as

$$\cos(B_1, B_2) \equiv \frac{B_1 \cdot B_2}{\sqrt{B_1 \cdot B_1 B_2 \cdot B_2}} \qquad \text{where} \quad B_1 \cdot B_2 \equiv \sum_{k_1, k_2, k_3} B_1(k_1, k_2, k_3) B_2(k_1, k_2, k_3) \, . \tag{7.7}$$

One can then use current constraints on the local, equilateral and orthogonal templates [3] to estimate the values of f_{NL} compatible with current data analyses:

$$f_{\mathrm{NL}} \approx f_{\mathrm{NL}}^{\mathrm{Loc}} \cos(B_\zeta, B_{loc}) + \dots \, , \tag{7.8}$$

where the dots indicate other templates which have been analyzed; we don't use them here since the tightest constraints come from those on the local template. Indeed, the cosine between the template under study, Eq. (7.6), and the local template, Eq. (7.4), is always $\gtrsim 0.6$. We plot the estimated 1–σ constraints in figure 7.1. Note that this is only a rough estimate, since the true constraints coming from the CMB data would require a dedicated data analysis, which is beyond the scope of this article. One can also improve on this estimate by using a spherical cosine rather than the flat one defined in Eq. (7.7); we expect the results to be of the same order of magnitude as those plotted in figure 7.1.

7.3 Modeling of the non-Gaussian halo bias

In this section we wish to summarize the computation of the modification of the halo power spectrum in the presence of non-Gaussian initial conditions. Let us begin by introducing some notation.
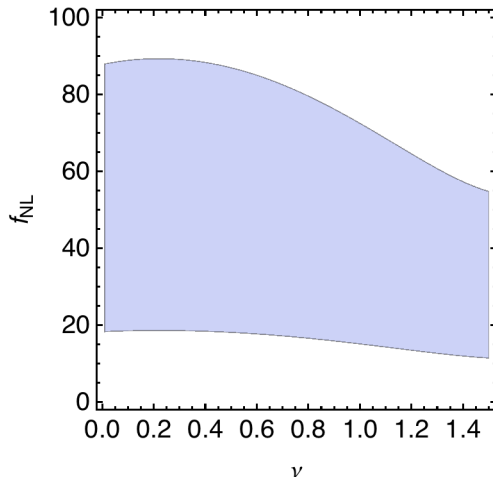
Figure 7.1: Estimated WMAP 7 constraints on f_{NL} at 1–σ coming from the overlap between the quasi-single field inflation template of Eq. (7.6) and the local template of Eq. (7.4) as defined in Eq. (7.7).

The comoving gauge curvature perturbation ζ, in terms of which the initial conditions set by inflation are often expressed, is related to the linear dark matter density contrast δ at redshift z through the transfer function T and the linear growth factor D normalized to one at redshift zero

$$\delta(k) = k^2 T(k) D(z) \zeta(k) \,, \tag{7.9}$$

where we have written this equation in Fourier space. These factors contain the evolution of the gravitational potentials once the perturbation enters the horizon[3]. The transfer function as written here can be readily computed using publicly available numerical codes like CAMB [27].

In the high-peak formalism, one considers a halo to form when a region of space has an average density contrast larger than some threshold δ_c. Let us define this average as

$$\delta_R = \int \frac{\mathrm{d}^3 k}{(2\pi)^3} W(kR) \delta(k) \,, \tag{7.10}$$

where W is a window function that averages out modes with a wavelength larger than the region under consideration. We will take this filter to be a top-hat in real space, which in Fourier space takes the form

$$W(kR) = \frac{3}{(kR)^3} (\sin kR - kR \cos kR) \,. \tag{7.11}$$

The critical density contrast threshold δ_c is often estimated by computing the time at which a perfectly spherical halo completely collapses and extrapolating the linear density to that point. In an Einstein-de Sitter space one obtains $\delta_c = 1.686$, while in ΛCDM this estimate receives a small correction and is slightly redshift dependent. The scale R over which one averages is related to the mass of the halo formed by $M = 4\pi/3\Omega_m \rho_c R^3$, where

---

[3]Note that a different definition of the transfer function is often used, such that it is normalized to one on large scales. We do not normalize to one, but rather use equation (7.9) as the definition, which is the one that appears directly in the output file of CAMB at redshift zero (though one must be careful with the factors of h).

ρ_c is the critical density of the universe $\rho_c = 3H_0^2/8\pi G$. Equations (7.9) and (7.10) suggest the following definition

$$\mathcal{M}_M(k) \equiv k^2 T(k) W(kR) \,, \tag{7.12}$$

where R is expressed in terms of M as above. Thus for example the variance of the filtered density contrast can be computed as

$$\sigma_M^2 = \int \frac{\mathrm{d}^3 k}{(2\pi)^3} \mathcal{M}_M^2(k) P_\zeta(k) \,. \tag{7.13}$$

In the presence of non-Gaussian initial conditions, the (Eulerian) halo power spectrum $P(k)$ is modified

$$P(k) = (b_E^{(g)} + \Delta b)^2 P_\delta(k) \,, \tag{7.14}$$

where g denotes the Gaussian case. It was realized in Refs. [13, 14, 12, 15] that this correction to the power spectrum can have a characteristic scale dependence that makes it relatively easy to observe. One can estimate this correction with an arbitrary bispectrum shape using the peak background split formalism as done originally in Ref. [14]

$$\Delta b(k, M) = \frac{1}{\mathcal{M}_M(k)} \left(\frac{(b_E^{(g)} - 1)\delta_c}{D(z)} \mathcal{F}(k, M) + \frac{\mathrm{d}\mathcal{F}(k, M)}{\mathrm{d} \ln \sigma_M} \right) \,, \tag{7.15}$$

where the second term in the parenthesis was computed in Refs. [28, 29], and is due mainly to the modulation of the variance with mass due to the non-Gaussianity. The "form factor" $\mathcal{F}$ for an arbitrary bispectrum is defined as

$$\mathcal{F}(k, M) = \frac{1}{8\pi^2 \sigma_M^2 P_\zeta(k)} \int \mathrm{d}k_1 \, k_1^2 \mathcal{M}_M(k_1) \int_{-1}^1 \mathrm{d}\mu \, \mathcal{M}_M\big(\sqrt{k^2 + k_1^2 + 2k_1 k\mu}\big) B_\zeta\big(k, k_1, \sqrt{k^2 + k_1^2 + 2k_1 k\mu}\big) \,. \tag{7.16}$$

In reference [28] equations (7.15) and (7.16) were found to agree well with simulations [30] including a local, orthogonal and equilateral templates for the bispectrum of the initial conditions. This agreement has been seen to be good up to a scale of $k \sim 0.1 \, h \, \mathrm{Mpc}^{-1}$ [31].

In the integral of equation (7.16), the scale k corresponds to the scale of observation which for the survey we will study varies between $k \sim 0.003 \, h \, \mathrm{Mpc}^{-1}$ and[4] $k \sim 0.1 \, h \, \mathrm{Mpc}^{-1}$. On the other hand, for a halo mass of order $M = 10^{12} \, M_\odot h^{-1}$, the filter $W(k_1 R)$ suppresses the integral at scales $k_1 \gtrsim 3 \, h \, \mathrm{Mpc}^{-1}$, while the transfer function and the factor of k_1^2 in the integral suppress the integral at scales $k_1 \lesssim 0.1 \, h \, \mathrm{Mpc}^{-1}$. The measure of the integral will thus peak at $k_1 \sim \mathcal{O}(1) \, \mathrm{Mpc}^{-1}$. Therefore the integral will receive a sizable contribution only from the squeezed configuration of the momenta appearing as the arguments of the bispectrum in which k is at least an order of magnitude smaller than k_1. We will use equations (7.15) and (7.16) to compute the non-Gaussian modification to the halo bias induced by a template of the form given by equation (7.6).

At very large scales the non-Gaussian modification to the halo bias probes very squeezed configurations. In such a regime $\Delta b(k, M)$ often behaves as a power law in k as can be seen from equations (7.15) and (7.16). Indeed one expects that for a bispectrum going as $\langle \zeta^3 \rangle \overset{q \to 0}{\sim} 1/q^a$, the bias behaves as $\Delta b(k, M) \sim 1/k^{a-1}$. In order to perform a model-independent (though perhaps rough) analysis of the power of future surveys to constrain

---

[4]In previous analyses that did not consider the correction to the halo bias given by the second term in the right hand side of Eq. (7.16), the maximum k considered was $0.03h/\mathrm{Mpc}$. This more conservative cutoff ensured that the adopted bias description was correct (on these scales the correction is negligible) but reduced the total signal-to-noise.

the behavior of the halo bias at large scales, we use the following parametrization (as suggested by [25])

$$\Delta b(k, M) = f_{\mathrm{NL}}^p \frac{A(M)}{k^\beta} \, , \tag{7.17}$$

where $A(M)$ is a mass-dependent normalization defined such that the bias is the same as that in the presence of a local non-Gaussianity at a scale of $k = 0.03 \, h \, \mathrm{Mpc}^{-1}$, and β is a parameter to be constrained. Note that f_{NL} of equation (7.6) and f_{NL}^p are normalized differently, so that in order to compare the results obtained when using the template of Eq. (7.6) and those obtained using the parametrization (7.17) one should multiply f_{NL}^p roughly by a factor of 8.

7.4   Setup

We wish to estimate the capability of a future survey satisfying the requirements of the Dark Energy Taskforce stage IV [26], to constrain the shape of the bispectrum. For this we assume a survey similar to the one studied in reference [20]. We present the characteristics we assume for such a survey in table 7.1.

Sky coverage	2×10^4 square degrees
Minimum redshift	0.5
Maximum redshift	2.1
Typical galaxy halo mass	$10^{12} \, M_\odot h^{-1}$

Table 7.1: Description of the Dark Energy Task Force stage IV survey used.

We also use the results of Ref. [20] for the average number of galaxies available to the survey, the average mass of the galaxies observed, and the Gaussian bias; let us summarize them here.

For the Gaussian bias we use the results reported in figure 4 of Ref. [20], who in turn use the results of Ref. [32]. There the bias is estimated using the halo model, a semi-analytic model for galaxy formation, and assuming a spectroscopic selection based on $H\alpha$ emission with a threshold given for a survey similar to Euclid.

The modification of the halo power spectrum due to non-Gaussianity will depend on the halo mass. Here we take the typical masses of the haloes of the galaxies observed to be $10^{12} \, M_\odot h^{-1}$ as in [20], see their figure 3. We compute the non-Gaussian modification to the halo bias evaluated at this fixed mass. We don't expect the errors induced by fixing the mass in equation (7.16) to be of qualitative importance for our results.

The number of galaxies at a given redshift can be computed from the halo mass function $n(z, M)$ (the number of haloes in a differential mass interval at a given redshift), and the first moment of the halo occupation distribution $\langle N_g | M \rangle$ (very roughly the probability that there be N_g galaxies in a halo of mass M)

$$n_g(z) = \int_{M_g}^\infty n(M, z) \langle N_g | M \rangle \, \mathrm{d}M \, , \tag{7.18}$$

where M_g is the minimum halo mass for a galaxy observed by the survey for which we again follow Ref. [20] and take $M_g = 10^{11} \, M_\odot h^{-1}$, see their section 4.4. Since the average number of galaxies is important only in computing the shot noise, which we have verified has a small effect, we neglect the non-Gaussian correction to the mass function and use

the Sheth and Tormen mass function [33]. As for the first moment of the halo occupation distribution, we follow Ref. [20] and use the following expression [34, 35]

$$\langle N_g | M \rangle = N_{g,0} \left(\frac{M}{M_0} \right)^{\theta} , \qquad (7.19)$$

and the parameters θ, M_0 and $N_{g,0}$ depend on the type of galaxy considered. We assume here typical galaxies to be blue, for which $N_{g,0} = 0.7$ and $\theta = 0$ if $M \leq M_0$ and $\theta = 0.8$ otherwise and take $M_0 = 4 \times 10^{12} \, M_{\odot} h^{-1}$ as in section 4.1 of Ref. [20]. Let us stress that the average number of galaxies affects only the shot noise which we verify to be small and our results will not be very sensitive to the assumptions made in computing it.

7.5 Forecast

We work under the approximation that the Likelihood for the (Eulerian) halo power spectrum is a Gaussian centered around a "fiducial" model for which the values of the parameters of interest $f_{\rm NL}$ and ν are fixed at $\bar{f}_{\rm NL}$ and $\bar{\nu}$

$$\ln \mathcal{L} = -\frac{1}{2} \frac{(\Delta P)^2}{\sigma_P^2} , \qquad (7.20)$$

where $\Delta P \equiv P - P|_{\bar{f}_{\rm NL}, \bar{\nu}}$ is the deviation from the fiducial model. The standard procedure is to assume the behavior of the halo power spectrum to be nearly linear on the parameters of interest (here called generically θ_i), so that the Likelihood function is a Gaussian also in terms of those parameters. One can then estimate the variance and covariance of a future survey by computing the Fisher information matrix on the parameters

$$F_{ij} = \frac{\partial^2 |\ln \mathcal{L}|}{\partial \theta_i \partial \theta_j} . \qquad (7.21)$$

This is a good approximation when one is interested in a region in parameter space around the fiducial model which is small with respect to the typical variation of the power spectrum with the parameters, *i.e.*, when the resulting estimated uncertainties are small. However, in the model we are studying the variation of the power spectrum with respect to ν is highly non-linear and this approximation need not hold. We will instead compute the $\Delta \chi^2$ of each point in parameter space

$$\Delta \chi^2 = \sum_{z,k} \left(\frac{\Delta P}{\sigma_P} \right)^2 = \sum_{z,k} \left(\frac{P}{\sigma_P} \right)^2 \frac{\Delta P^2}{P^2} , \qquad (7.22)$$

where we sum over the different redshift shells and Fourier modes available to the survey. This quantity is in general costly to compute when dealing with a high-dimensional parameter space. However, we will be interested only in varying $f_{\rm NL}$ and ν since our main focus is the measurement of the non-Gaussianity and its behavior in the squeezed limit. This implies that we keep other cosmological parameters fixed at the WMAP 7 best fit values [3], and the actual uncertainties on $f_{\rm NL}$ and ν are expected to be somewhat larger than our estimates. Reference [36] estimated this increase in the errors to be mild in the case of a local non-Gaussianity (around $10\% \sim 30\%$ depending on the survey if the number of relativistic neutrino species is kept fixed). This can be understood as being due to the fact that no other cosmological parameter induces a scale dependence and a redshift dependence on the halo bias as the one induced by a local non-Gaussianity. The

same argument holds for the range of ν we will study, and we thus expect the increase in the estimated uncertainty on f_{NL} and ν due to the uncertainty on other cosmological parameters to be small.

For an infinitesimal shell in Fourier space with a width Δk and effective volume V_{eff} the relative error can be estimated by counting the number of Fourier modes

$$\left(\frac{\sigma_P}{P}\right)^2 = \frac{2}{4\pi k^2 \Delta k V_{eff}/(2\pi)^3} \; . \tag{7.23}$$

The effective volume is the volume corrected by taking into account the shot noise

$$V_{eff} = V(z)\left(1 - \frac{1}{n_g(z)P(k)}\right)^2 , \tag{7.24}$$

where n_g is the average number of galaxies, V is the volume of each redshift shell, and we've explicitly stated the dependence on redshift and Fourier mode. Equation (7.22) can now be written explicitly

$$\Delta\chi^2 = \sum_i \frac{V(z_i)}{(2\pi)^2} \int_{k_{min}}^{k_{max}} \mathrm{d}k \, k^2 \left(1 - \frac{1}{n_g(z_i)P(k)}\right)^2 \left(\frac{\Delta P(k, z_i)}{P(k, z_i)}\right)^2 , \tag{7.25}$$

where the sum is over redshift shells, we take $k_{max} \simeq 0.1 \, h/\mathrm{Mpc}$ since it is the scale up to which we trust the calculation of the non-Gaussian modification to the bias [31], and the minimum k is computed as $k_{min} = 2\pi/V(z_i)^{1/3}$. We divide the redshift range in shells with a width $\Delta z = 0.1$. The halo power spectrum and average number of galaxies are given respectively in equations (7.14) and (7.18). The deviation of the halo power spectrum from the fiducial model was computed by taking the difference between the halo power spectra of the given model and the fiducial one computed using equation (7.15) to model the effect of non-Gaussianity.

In figure 7.2 we show the $\Delta\chi^2 \leq 2.3$ regions corresponding to 68.3% *joint* confidence levels for different values of the fiducial parameters $\bar{\nu}$ and $\bar{f}_{\mathrm{NL}}$. For $\bar{\nu} = 0.5$, which would correspond to a squeezed limit going like $\langle\zeta^3\rangle \overset{q\to 0}{\sim} 1/q^2$, the constraints on ν will be broad, and even the detection of non-Gaussianity would be challenging, requiring very large values of f_{NL} in mild tension with current CMB constraints. As $\bar{\nu}$ increases, the effect on the bias becomes stronger and the survey becomes more sensitive to both f_{NL} and ν. For $\bar{\nu} = 1.5$, corresponding to a shape that behaves like the local template in the squeezed limit, the survey becomes sensitive to $f_{\mathrm{NL}} = \mathcal{O}(10)$, and is able to put constrains on $\bar{\nu}$. Recall that we plot the 68% 2-parameter joint confidence regions, a similar confidence interval for a 1-parameter only model –i.e., if ν were to be kept fixed– would correspond to $\Delta\chi^2 \leq 1$; thus to compare ours with other analyses where ν is kept fixed, one can "slice" the contours at the preferred ν value, but should interpret the resulting error as similar to a 90% confidence region. Note that for large values of $\bar{\nu}$ and $\bar{f}_{\mathrm{NL}}$ the regions resemble ellipses, signaling the fact that the errors are small relative to the variation of ν and the Fisher approximation holds. For smaller values of $\bar{\nu}$ and $\bar{f}_{\mathrm{NL}}$ this is not the case and the confidence regions adopt more complex shapes.

In figure 7.3, we present the same analysis performed for the model-independent parametrization of equation (7.17). Here we restrict ourselves only to large scales where this parametrization can be relevant, and thus integrate up to $k_{max} = 0.03 \, h \, \mathrm{Mpc}^{-1}$. The amplitude f_{NL} of the template of Eq. (7.6) and f_{NL}^p defined in Eq. (7.17) are normalized differently, and one should multiply f_{NL}^p by a factor ~ 8 in order to compare the results. Thus, the values of f_{NL}^p in figure 7.3 are taken to be small for ease of comparison with
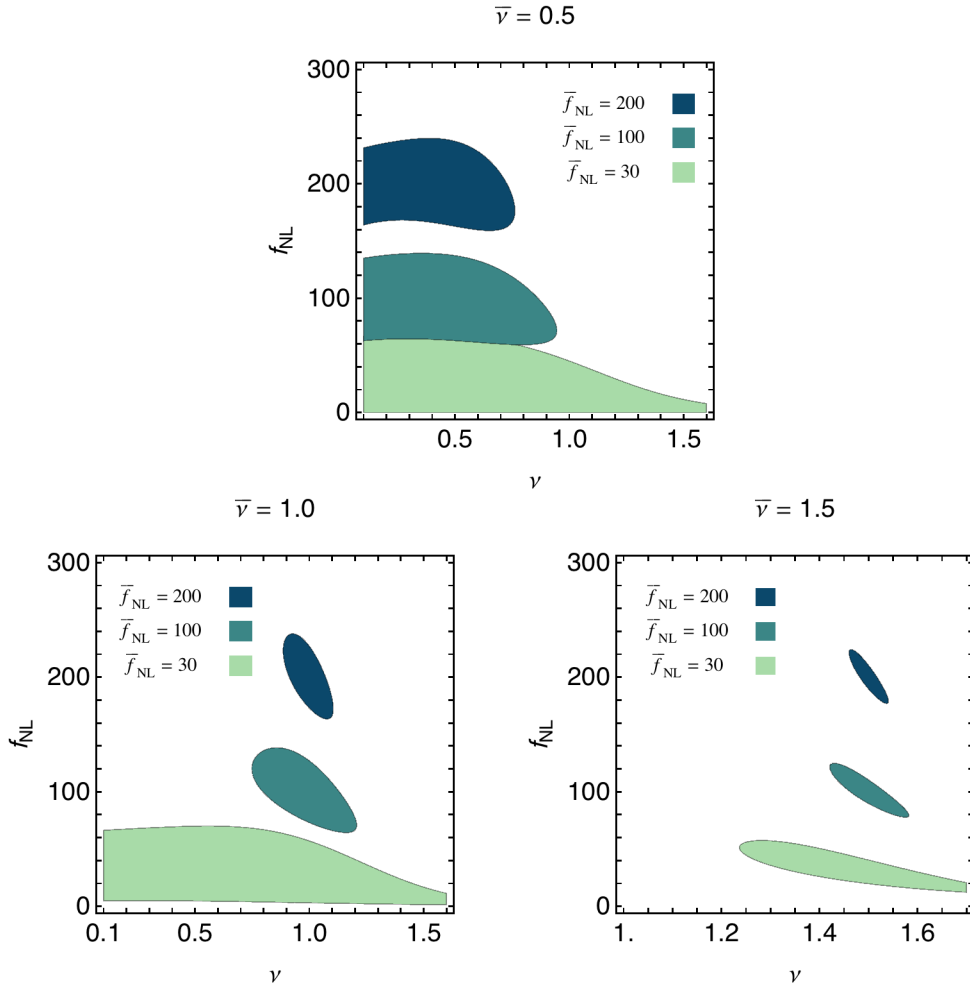
Figure 7.2: Regions in the f_{NL}, ν parameter space defined in Eq. (7.6) satisfying $\Delta\chi^2 \leq 2.3$, corresponding to the 68.3% confidence level. In the squeezed limit this model behaves as $\langle\zeta^3\rangle_{q\to 0} = 1/q^{\nu+3/2}$. We show such regions for several fiducial models, showing that the uncertainties decrease as the fiducial value of f_{NL} becomes larger and the fiducial value of ν approaches 1.5, which corresponds to a bispectrum shape that behaves like the local template in the squeezed limit.

figure 7.2. We present the results for $\beta = 1, 2,$ and 3 corresponding respectively to the behavior of the orthogonal *template*, the local template, and the models studied in Refs. [24, 25]. Again the confidence regions tend to ellipses for larger values of the amplitude f_{NL}^p and power β, and the results are consistent with those obtained for the quasi-single field inflation model in figure 7.2.

7.6 Summary and discussion

We studied the possibility that a future galaxy survey with the characteristics of the Dark Energy Task Force stage IV might be able to constrain the shape of the primordial non-Gaussianity through observations of the halo bias. A non-vanishing primordial three-point function induces a modification of the halo bias that is sensitive mainly to the squeezed

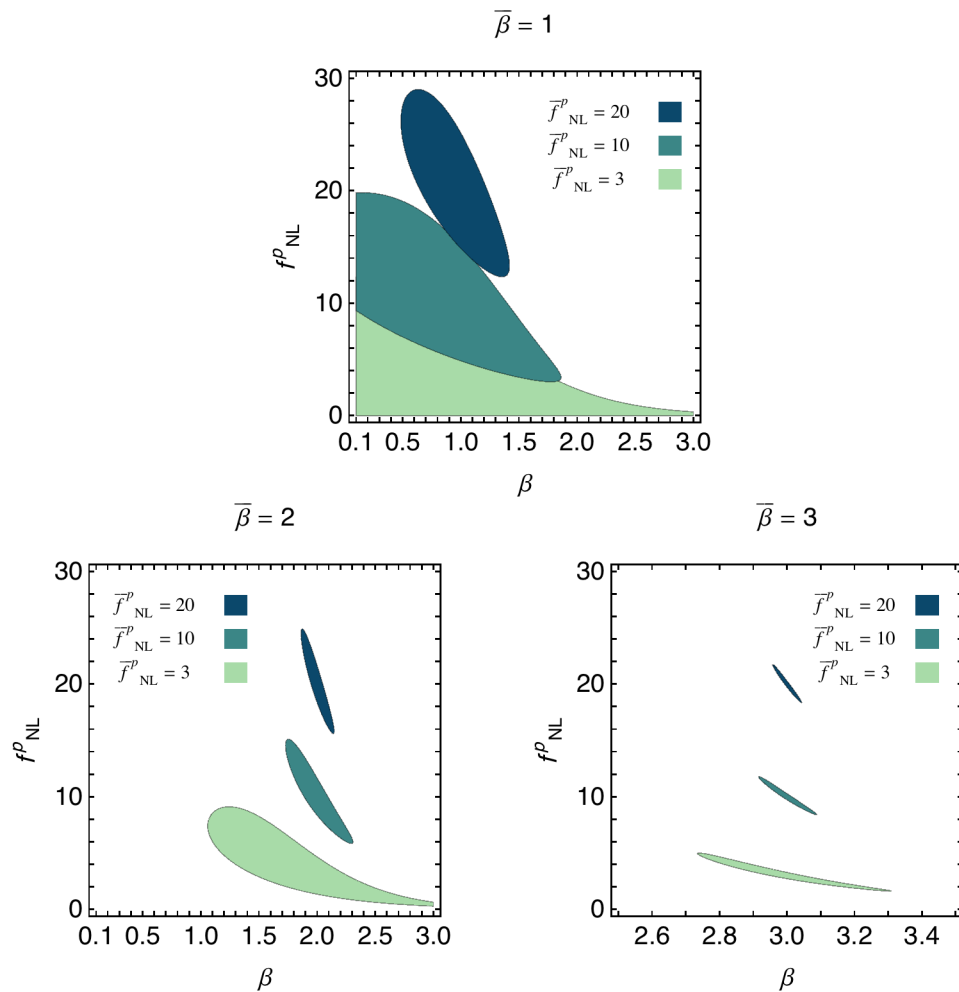Figure 7.3: Forecasts for the parametrization $\Delta b = f_{\mathrm{NL}}^p A/k^\beta$. Green regions correspond to points in the f_{NL}^p, β parameter space satisfying $\Delta\chi^2 \leq 2.3$, corresponding to the 68.3% confidence level. Note that f_{NL}^p is defined such that the non-Gaussian modification to the halo bias, eq. (7.15), is the same as in the presence of a local non-Gaussianity at a scale $k = 0.03\,h\,\mathrm{Mpc}^{-1}$, thus $f_{\mathrm{NL}}(\nu = 1.5) \sim 8 f_{\mathrm{NL}}^p(\beta = 2)$.

limit in which one of the three momenta is smaller than the other two. Single field models produce a bispectrum with a squeezed limit going like $\langle \zeta^3 \rangle \sim 1/q$, where q is the small momentum, while models of inflation with multiple light fields can produce a large non-Gaussianity of the local type, *i.e.*, going like $\langle \zeta^3 \rangle \sim 1/q^3$ in the squeezed limit. Thus, the observation of a squeezed limit with a behavior which is different to these two possibilities might signal the presence of some non-trivial dynamics during inflation. Such can happen for example in the "quasi-single field" inflation model, which consists of a light inflaton and a massive isocurvaton coupled through a turning trajectory. It can produce a shape going as

$$\langle \zeta(\vec{k}_1)\zeta(\vec{k}_2)\zeta(\vec{q}) \rangle \overset{q\to 0}{\sim} 1/q^{3/2+\nu} , \qquad (7.26)$$

where $\nu \equiv \sqrt{9/4 - m^2/H^2}$.

We estimate the ability of a survey such as that described in section 7.4 to constrain the squeezed limit of the primordial three-point function. For this purpose we perform

forcasts on the uncertainties on a measurement of the amplitude and shape of the non-Gaussianity generated by the quasi-single field inflation model (see figure 7.2) and of a phenomenological model-independent parametrization of the non-Gaussian halo bias at large scales $\Delta b = f_{\mathrm{NL}}^p A/k^\beta$ (see figure 7.3).

Since the variation of the halo power spectrum with the power ν or β is large for small values of the amplitue f_{NL} or f_{NL}^p, the Likelihood function in terms of these parameters is not expected to be a Gaussian. We cannot then use the Fisher information matrix approach, and instead compute $\Delta\chi^2$ at each point in parameter space. We report our findings in figures 7.2 and 7.3. We find that the forecasted uncertainties depend quite strongly on the fiducial model. If the fiducial model is taken to be similar to a local non-Gaussianity ($\bar\nu = 1.5$ or $\bar\beta = 2$), the survey will be able to put tight constraints on the parameters of the model, even for $\bar f_{\mathrm{NL}} = \mathcal{O}(10)$. As $\bar\nu$ or $\bar\beta$ decreases the forecasted uncertainties become larger, requiring larger values of $\bar f_{\mathrm{NL}}$ or $\bar f_{\mathrm{NL}}^p$ for non-Gaussianity to be observable. This is to be expected since a milder divergence in the squeezed limit translates into a milder scale dependence in the non-Gaussian modification to the halo bias.

Though the most stringent limits on the primordial non-Gaussianity to date come from CMB observations, the CMB has a limited capacity in constraining the shape of the three-point function. Indeed, it is not sensitive to the physically interesting squeezed limit, and would not distinguish between two shapes which have a large cosine but with different squeezed limits. In this sense halo bias observations are complementary to CMB observations and might open a new window to the physics of inflation. It would still be of interest however to find the constraints on the amplitude of the quasi-single field inflation template coming from CMB data.

Another potentially interesting probe of the squeezed limit is the possibility of observing the μ distortion of the CMB spectrum recently proposed in Ref. [37]. A primordial three-point function induces a correlation between the μ distortion and the temperature which is sensitive to the very squeezed limit. It would be interesting to study the power of such a probe to constrain f_{NL} and ν.

Finally, let us comment on ways in which one can increase the signal to noise ratio in our analysis. If the analysis is repeated for a photometric survey like LSST, which can observe galaxies with fainter magnitudes and thus higher redshift, one expects the gain in volume to reduce the errors by a factor ~ 2. Refs. [38, 39, 40] argue that with the use of several differently biased tracers and an optimal weighting it is possible to reduce the errors on a local f_{NL} by at least an order of magnitude. We expect a similar reduction to take place in our case, greatly improving the sensitivity of the survey. Another way to reduce the uncertainties is that proposed by Ref. [41] who argue in favor of cross-correlating pixels in order to extract more information from the survey; they find that for a local non-Gaussianity the reduction of the uncertainties is again of an order of magnitude. If the uncertainty on f_{NL} can be brought to be of $\mathcal{O}(1)$, general relativistic effects on the halo bias become relevant and might then be observable (e.g., [42] and refs therein).

While this paper was being completed, we became aware of a similar analysis being carried out by another group, see Ref. [43]. We have carried out a rough comparison of our results and find them to be consistent. We are grateful to the authors for coordinating with us the publication on the ArXiv website.

Bibliography

[1] X. Chen and Y. Wang, JCAP **1004** (2010) 027 doi:10.1088/1475-7516/2010/04/027 [arXiv:0911.3380 [hep-th]].

[2] X. Chen and Y. Wang, Phys. Rev. D **81** (2010) 063511 doi:10.1103/PhysRevD.81.063511 [arXiv:0909.0496 [astro-ph.CO]].

[3] Komatsu *et al.*, Astrophys. J. Suppl. **192** (2010) 18 doi:10.1088/0067-0049/192/2/18 [arXiv:1001.4538 [astro-ph.CO]].

[4] J. M. Maldacena, JHEP **0305** (2003) 013 doi:10.1088/1126-6708/2003/05/013 [astro-ph/0210603].

[5] V. Acquaviva, N. Bartolo, S. Matarrese and A. Riotto, Nucl. Phys. B **667** (2003) 119 doi:10.1016/S0550-3213(03)00550-9 [astro-ph/0209156].

[6] N. Bartolo, S. Matarrese and A. Riotto, Phys. Rev. D **69** (2004) 043503 doi:10.1103/PhysRevD.69.043503 [hep-ph/0309033].

[7] P. Creminelli, JCAP **0310** (2003) 003 doi:10.1088/1475-7516/2003/10/003 [astro-ph/0306122].

[8] R. Flauger and E. Pajer, JCAP **1101** (2011) 017 doi:10.1088/1475-7516/2011/01/017 [arXiv:1002.0833 [hep-th]].

[9] C. Cheung, P. Creminelli, A. L. Fitzpatrick, J. Kaplan and L. Senatore, JHEP **0803** (2008) 014 doi:10.1088/1126-6708/2008/03/014 [arXiv:0709.0293 [hep-th]].

[10] L. Senatore, K. M. Smith and M. Zaldarriaga, JCAP **1001** (2010) 028 doi:10.1088/1475-7516/2010/01/028 [arXiv:0905.3746 [astro-ph.CO]].

[11] J. Tauber *et al.* [Planck Collaboration], astro-ph/0604069.

[12] A. Slosar, C. Hirata, U. Seljak, S. Ho and N. Padmanabhan, JCAP **0808** (2008) 031 doi:10.1088/1475-7516/2008/08/031 [arXiv:0805.3580 [astro-ph]].

[13] N. Dalal, O. Dore, D. Huterer and A. Shirokov, Phys. Rev. D **77** (2008) 123514 doi:10.1103/PhysRevD.77.123514 [arXiv:0710.4560 [astro-ph]].

[14] S. Matarrese and L. Verde, Astrophys. J. **677** (2008) L77 doi:10.1086/587840 [arXiv:0801.4826 [astro-ph]].

[15] N. Afshordi and A. J. Tolley, Phys. Rev. D **78** (2008) 123507 doi:10.1103/PhysRevD.78.123507 [arXiv:0806.1046 [astro-ph]].

[16] P. Creminelli and M. Zaldarriaga, JCAP **0410** (2004) 006 doi:10.1088/1475-7516/2004/10/006 [astro-ph/0407059].

[17] P. Creminelli, G. D'Amico, M. Musso and J. Norena, JCAP **1111** (2011) 038 doi:10.1088/1475-7516/2011/11/038 [arXiv:1106.1462 [astro-ph.CO]].

[18] P. Creminelli, J. Norena and M. Simonovic, JCAP **1207** (2012) 052 doi:10.1088/1475-7516/2012/07/052 [arXiv:1203.4595 [hep-th]].

[19] C. Carbone, L. Verde and S. Matarrese, Astrophys. J. **684** (2008) L1 doi:10.1086/592020 [arXiv:0806.1950 [astro-ph]].

[20] Fedeli *et al.*, Mon. Not. Roy. Astron. Soc. **414** (2011) 1545 doi:10.1111/j.1365-2966.2011.18490.x [arXiv:1012.2305 [astro-ph.CO]].

[21] D. Babich, P. Creminelli and M. Zaldarriaga, JCAP **0408** (2004) 009 doi:10.1088/1475-7516/2004/08/009 [astro-ph/0405356].

[22] Z. Huang, L. Verde and F. Vernizzi, JCAP **1204** (2012) 005 doi:10.1088/1475-7516/2012/04/005 [arXiv:1201.5955 [astro-ph.CO]].

[23] E. Sefusatti, M. Liguori, A. P. S. Yadav, M. G. Jackson and E. Pajer, JCAP **0912** (2009) 022 doi:10.1088/1475-7516/2009/12/022 [arXiv:0906.0232 [astro-ph.CO]].

[24] J. Ganc and E. Komatsu, Phys. Rev. D **86** (2012) 023518 doi:10.1103/PhysRevD.86.023518 [arXiv:1204.4241 [astro-ph.CO]].

[25] I. Agullo and S. Shandera, JCAP **1209** (2012) 007 doi:10.1088/1475-7516/2012/09/007 [arXiv:1204.4409 [astro-ph.CO]].

[26] A. Albrecht *et al.*, astro-ph/0609591.

[27] A. Lewis, A. Challinor and A. Lasenby, Astrophys. J. **538** (2000) 473 doi:10.1086/309179 [astro-ph/9911177].

[28] Desjacques *et al.*, Phys. Rev. D **84** (2011) 061301 doi:10.1103/PhysRevD.84.061301 [arXiv:1105.3476 [astro-ph.CO]]

[29] Desjacques *et al.*, Phys. Rev. D **84** (2011) 063512 doi:10.1103/PhysRevD.84.063512 [arXiv:1105.3628 [astro-ph.CO]]

[30] Wagner *et al.*, JCAP **1010** (2010) 002 doi:10.1088/1475-7516/2010/10/022 [arXiv:1006.5793 [astro-ph.CO]]

[31] C. Wagner, L. Verde, JCAP **1203** (2012) 002 doi:10.1088/1475-7516/2012/03/002 [arXiv:1102.3229 [astro-ph.CO]]

[32] A. Orsi, C. Baugh, C. Lacey, A. Cimatti, Y. Wang, G. Zamorani, Mon. Not. Roy. Astron. Soc. **405** (2010) 1006 doi:10.1111/j.1365-2966.2010.16585.x [arXiv:0911.0669 [astro-ph.CO]]

[33] R. K. Sheth and G. Tormen, Mon. Not. Roy. Astron. Soc. **329** (2002) 61 doi:10.1046/j.1365-8711.2002.04950.x [astro-ph/0105113].

[34] A. Cooray and R. K. Sheth, Phys. Rept. **372** (2002) 1 doi:10.1016/S0370-1573(02)00276-4 [astro-ph/0206508].

[35] A. R. Cooray, Mon. Not. Roy. Astron. Soc. **348** (2004) 250 doi:10.1111/j.1365-2966.2004.07358.x [astro-ph/0311515].

[36] C. Carbone, O. Mena, L. Verde, JCAP **1007** (2010) 020 doi:10.1088/1475-7516/2010/07/020 [arXiv:1003.0456 [astro-ph.CO]]

[37] E. Pajer and M. Zaldarriaga, Phys. Rev. Lett. **109** (2012) 021302 doi:10.1103/PhysRevLett.109.021302 [arXiv:1201.5375 [astro-ph.CO]].

[38] U. Seljak, Phys. Rev. Lett. **102** (2009) 021302 doi:10.1103/PhysRevLett.102.021302 [arXiv:0807.1770 [astro-ph]].

[39] A. Slosar, JCAP **0903** (2009) 004 doi:10.1088/1475-7516/2009/03/004 [arXiv:0808.0044 [astro-ph]].

[40] N. Hamaus, U. Seljak, V. Desjacques Phis. Rev. D **84** (2011) 083509 doi:10.1103/PhysRevD.84.083509 [arXiv:1104.2321 [astro-ph.CO]]

[41] C. Cunha, D. Huterer, O. Dore Phys. Rev. D **82** (2010) 023004 doi:10.1103/PhysRevD.82.023004 [arXiv:1003.2416 [astro-ph.CO]]

[42] L. Verde, S. Matarrese, ApJLett **706** (2009) L91 doi:10.1088/0004-637X/706/1/L91 [arXiv:0909.3224 [astro-ph.CO]]

[43] E. Sefusatti, J. R. Fergusson, X. Chen and E. P. S. Shellard, JCAP **1208** (2012) 033 doi:10.1088/1475-7516/2012/08/033 [arXiv:1204.6318 [astro-ph.CO]].

8 ∎

Composite states of two right-handed neutrinos

Gabriela Barenboim, Cristian Bosch

Abstract

In this work, we develop a model for Higgs-like composites based on two generations of right-handed neutrinos that condense. We analyze the spontaneous symmetry breaking of the theory with two explicit breakings, setting the different scales of the model and obtaining massive bosons as a result. Finally, we calculate the gravitational wave imprint left by the phase transition associated with the symmetry breaking of a generic potential dictated by the symmetries of the composites.

8.1   Introduction

The observation of neutrino oscillations suggests that there must be physics beyond the Standard Model of particle physics due to the inclusion of right-handed neutrinos that are sterile with respect to the Standard Model gauge interactions. These additional states mix with the usual neutrinos of the Standard Model through Yukawa interactions with the left-handed leptons. If these new sterile neutrinos become massive, then masses for the Standard Model (SM) neutrinos are also generated by the mixing between the sterile and active neutrinos. It is important to notice that the right-handed mass scale is not protected by any symmetry and therefore can take any value. On general grounds, one can assume it will take the highest possible value.

Despite not being active players of the SM dynamics, as mentioned before, right-handed (RH) neutrino existence is well motivated by the evidence of nonzero neutrino masses provided by the oscillation experiments and by the yet unconfirmed but still intriguing evidence of reactor and accelerator experiments for additional light sterile neutrino states. Without any direct experimental evidence, there could be a wide range (from sub-eV to 10^{15} GeV) for the scale of masses for the right-handed neutrinos.

While Majorana mass terms for the sterile neutrinos could be directly added to the theory, we wish to explore a dynamical origin of these masses through sterile neutrino condensates. Inspired by the Bardeen-Hill-Lindner (BHL) [1][2] model of composite Higgs fields, first described by [3], the role of the top quark condensates will be played by a condensate of the sterile neutrinos. The sterile neutrinos have no SM gauge interactions except for the gravitational interactions which are flavor neutral. We will assume that gravity or some other flavor neutral dynamics is responsible for driving the formation of the sterile neutrino condensates. The minimal model of sterile neutrino condensates will require at least two flavors of sterile neutrinos to explain the observed neutrinos oscillations.

With two flavors of sterile neutrinos and flavor neutral dynamics, the neutrino condensates will transform as a symmetric tensor representation of the U(2) sterile neutrino flavor symmetry. The dynamical breaking of this flavor symmetry is triggered by the formation of the sterile neutrino condensates and a number of composite scalars that will have their own low-scale interactions. A possible realization of the dynamics involved in the condensation can be reviewed in [4] where the gravitational interactions of the RH sterile neutrinos is the mechanism inducing the condensation. This gravitational attraction (see [5], where the condensation source is a topological formulation of gravitational anomaly), or different and undetermined short-range interactions (e.g., as a torsion in the reheating era, right after inflation, as presented in [6]), is independent of the sterile neutrino flavor thus forming composite scalars that are not constrained by the need for neutralizing their flavor charge implying a larger number of scalar bound states. While there could be a larger number of sterile neutrinos, we will focus on the minimal set needed to explain the observed neutrino oscillations that consists of the two flavors mentioned above. The two-flavor model will generate masses for only two of the three SM neutrinos so one of the neutrino mass eigenstates will have zero mass. One may wonder if this condensation mechanism applies to other particles. As explained in [4], sterile neutrinos are the only neutral fermions in a SM scenario (plus the sterile neutrino extension). Thus, any other fermion of the theory would have desintegration channels that would ensure the short survival of their condensates.

In the BHL model, the Higgs field is formed as a top quark bound state at a high scale, Λ. At a much lower scale, the electroweak symmetry is dynamically broken generating particle masses and a physical Higgs boson. We will explore the nature of flavor symmetry breaking in the corresponding version of the sterile neutrino condensate model.

The reader may wonder what is the interest, if there is any, of an effective theory that will have to deal with the appearance of new Nambu-Goldstone bosons and pseudo-Goldstone bosons once its symmetries are broken, and where to fit their masses in a particle catalogue that is not growing experimentally. However, this is not as troublesome as it may seem, and we can explore the convenience of these condensates for the treatment of some theoretical puzzles still unsolved.

One of them would be cosmological inflation. Keeping in mind models based on the same idea we are dealing with here [7], we will propose a series of bosons after symmetry breaking that could be interesting for this purpose.

Another possibility would be to explore the prospect of solving the electroweak vacuum instability present in the running of the Higgs quartic coupling [8]. Unfortunately, as we will see, our particular realization of RH neutrino condensation will prove not enough to fix this situation. RH neutrino composite scalars are a promising line of work for solving this problem nonetheless.

Additionally, we will address the experimental signature of the phase transition we are

proposing, its imprint in the gravitational wave spectrum. In February 2016, Advanced Laser Interferometer Gravitational Observatory (LIGO) [9] confirmed experimentally the existence of gravitational waves. As the scientical outbreak of the year, it would be quite interesting to determine the signature that our phase transition would leave in the gravitational spectrum. LIGO's discovery has already motivated the searches of new physics, as shown in [10]. A neutrino condensate would, thus, be recognizable if a gravitational wave signal matches the theoretical prediction of the phase transition corresponding to a spontaneous symmetry breaking.

This paper is organized as follows: Section 8.2 is dedicated to introduce the scalar fields, the change into vectorial notation, and the calculation of the spontaneous symmetry breaking (SSB) of the scalar theory. Section 8.3 introduces an explicit breaking in a lower energy scale, and in Sec. 8.4 we persent the last breaking, due to the Yukawa interaction of the scalar, being the lowest energy scale of the theory. In Sec. 8.5, the print left as gravitational waves by a potential featuring the same symmetries as the one presented in this analysis is studied. After that, the conclusions are presented in Sec. 8.6.

8.2 Symmetric tensor formalism and Spontaneous Symmetry Breaking

At the energy scale Λ or due to the finite temperature of the universe, the sterile neutrinos can be expected to condense due to the attractive interaction of gravity or some other short-range dynamics. At low energy, the neutrino biliniars effectively become dynamical composite scalars transforming as a symmetric tensor representation of the U(2) flavor symmetry of the sterile neutrinos.

The simplest version of this dynamics invokes an attractive four-fermion interaction between the sterile neutrinos. Following BHL, we can solve for the dynamics of the composite field representing the fermion bilinear operators, $\varphi_{ij} = \langle \nu_i \nu_j \rangle$, where the latin indices represent sterile neutrino flavor. In analogy to the BHL calculation, we can compute the effective potential for the scalar field φ_{ij}, generated by integrating out the sterile neutrinos at one loop. We obtain

$$V\left(\varphi\right) = \frac{1}{2}\lambda\varphi_{ij}^{\dagger}\varphi_{jk}\varphi_{kl}^{\dagger}\varphi_{li} - \frac{1}{2}M^2\varphi_{ij}^{\dagger}\varphi_{ji} \tag{8.1}$$

By tuning the parameters of the four-fermion theory, the scalar bilinear fields become dynamical with the usual kinetic terms. In [4], a calculation of the gravity triggered condensation is computed using a particular large N limit.

For the sake of clarity we will change this notation to a more compact one, which will also prove to be more convenient. Since we have only three scalars, φ_{11}, φ_{12} and φ_{22}, we will change the tensor of scalars into a complex vector formalism $\vec{\varphi} = (\varphi_1, \varphi_2, \varphi_3)$, defined as

$$\varphi_{ij} = (\vec{\sigma}\vec{\varphi}i\sigma_2)_{ij}\,;\ \varphi_{ij}^{\dagger} = (-i\sigma_2\vec{\sigma}\vec{\varphi}^*)_{ij} \tag{8.2}$$

which leaves the previous potential as follows:

$$V = \frac{1}{2}\lambda\,\mathrm{Tr}\left[(-i\sigma_2)\,(\vec{\sigma}\vec{\varphi}^*)\,(\vec{\sigma}\vec{\varphi})\,i\sigma_2\,(-i\sigma_2)\,(\vec{\sigma}\vec{\varphi}^*)\,(\vec{\sigma}\vec{\varphi})\,i\sigma_2\right] - \frac{1}{2}M^2\mathrm{Tr}\left[(-i\sigma_2)\,(\vec{\sigma}\vec{\varphi}^*)\,(\vec{\sigma}\vec{\varphi})\,i\sigma_2\right] =$$
$$= \frac{\lambda}{2}\mathrm{Tr}\left[(\vec{\sigma}\vec{\varphi}^*)\,(\vec{\sigma}\vec{\varphi})\,(\vec{\sigma}\vec{\varphi}^*)\,(\vec{\sigma}\vec{\varphi})\right] - \frac{M^2}{2}\mathrm{Tr}\left[(\vec{\sigma}\vec{\varphi}^*)\,(\vec{\sigma}\vec{\varphi})\right] =$$
$$= \lambda\left[2\,(\vec{\varphi}^*\vec{\varphi})^2 - (\vec{\varphi}^*\vec{\varphi}^*)\,(\vec{\varphi}\vec{\varphi})\right] - M^2\,(\vec{\varphi}^*\vec{\varphi})$$

(8.3)

Now, using that the field has an intuitive geometrical interpretation, we can use rotational symmetry to redefine the vector field, beginning with a redefinition of the global phase that would leave φ_2 real, a rotation that would make φ_2 vanish, and a second global phase shift that would give a real first component, i.e. $\varphi_1 = S$, the second component would remain $\varphi_2 = 0$ and the third component $\varphi_3 = R + iI$ would be a complex field. Replacing that in the previous equation, we have

$$V = \lambda\left[2\left(R^2 + I^2 + S^2\right)^2 - \left(R^2 + S^2 - I^2\right)^2 - 4R^2I^2\right] - M^2\left(R^2 + I^2 + S^2\right) \qquad (8.4)$$

Minimizing it, we arrive at the following gap equations:

$$A : 2R\left[2\lambda\left(R^2 + I^2 + S^2\right) - M^2\right] = 0$$
$$B : 2I\left[2\lambda\left(R^2 + I^2 + 3S^2\right) - M^2\right] = 0 \qquad (8.5)$$
$$C : 2S\left[2\lambda\left(R^2 + 3I^2 + S^2\right) - M^2\right] = 0$$

Their three solutions and vacuum energies are given by:

$$AB : R,\, I \neq 0 \Rightarrow S = 0,\, R^2 + I^2 = \frac{M^2}{2\lambda},\, E = -\frac{M^4}{4\lambda}$$
$$AC : R,\, S \neq 0 \Rightarrow I = 0,\, R^2 + S^2 = \frac{M^2}{2\lambda},\, E = -\frac{M^4}{4\lambda} \qquad (8.6)$$
$$BC : S,\, I \neq 0 \Rightarrow I^2 = S^2,\, R = 0,\, 4I^2 = 4S^2 = \frac{M^2}{2\lambda},\, E = -\frac{M^2}{8\lambda}$$

Thus, we can see that AB and AC are possible ground states whilst BC, with a higher energy, is not.

The AB and AC solutions each preserve a U(1) symmetry, associated to lepton number conservation. Thus, the breaking is $U(2) \to U(1)$ and there should be three Goldstone bosons and three heavy states associated with it. In both cases we can use the residual U(1) symmetry to align the real φ field to be the three direction with all other components vanishing. Hence, AB and AC are really the same solution for the spontaneous symmetry breaking.

We can compute the mass spectrum by expanding around the vacuum with $R = v$, $v^2 = M^2/2\lambda$ and $I,\, S = 0$.

In summary we are left with three massive states, the real longitudinal field, and the imaginary transverse fields, with masses given by $m^2 = 2M^2$, and three massless Goldstone modes, which will remain this way in the absence of any additional symmetry breaking. In [5], this relationship between masses is shown to be compatible with a standard seesaw mechanism.

8.3 Explicit symmetry breaking terms

The explicit breaking of the lepton number can be achieved by adding the following term to the effective potential presented in Eq. 8.3:

$$\Delta V_1 = -\mu^2 \left(\vec{\varphi}^*\right)^2 - \mu^2 \left(\vec{\varphi}\right)^2 + 2\mu^2 \left(\vec{\varphi}^* \vec{\varphi}\right) \tag{8.7}$$

This term does not shift $\langle \varphi \rangle$, but the Goldstone field associated with the imaginary longitudinal field becomes a massive pseudo-Goldstone boson. The other two fields, associated with the real transverse part, remain massless.

The Yukawa interactions can provide the explicit breaking needed to make the remaining two Goldstone bosons massive. This one-loop effective Yukawa interaction can be written as

$$\Delta V_2 \propto \left[\varphi_{ij}^* \varphi_{kl} \left(Y^\dagger Y\right)_{ik} \left(Y^\dagger Y\right)_{ji}\right] = \left[\vec{\sigma}\vec{\varphi}^\dagger \left(Y^\dagger Y\right) \vec{\sigma}\vec{\varphi} \left(i\sigma_2\right) \left(Y^\dagger Y\right)^T \left(-i\sigma_2\right)\right] \tag{8.8}$$

Since the factor involving the Yukawa coupling is Hermitian, we can write it in the general form,

$$\left(Y^\dagger Y\right) = \vec{\alpha}\vec{\sigma} + \beta; \ (\vec{\alpha}, \ \beta) \ \ \text{real} \tag{8.9}$$

Inserting this into the above expression, we get

$$\Delta V_2 \propto \cdot \text{Tr} \left[\left(\vec{\sigma}\vec{\varphi}^\dagger\right) \left(\vec{\sigma} \cdot \vec{\alpha} + \beta\right) \left(\vec{\sigma}\vec{\varphi}\right) \left(-\vec{\sigma} \cdot \vec{\alpha} + \beta\right)\right]$$
$$= 2 \left[-2 \left(\vec{\alpha}\vec{\varphi}^\dagger\right) \left(\vec{\alpha}\vec{\varphi}\right) + \left(\vec{\alpha}^2 + \beta^2\right) \left(\vec{\varphi}^\dagger\vec{\varphi}\right) + 2i\beta\vec{\alpha} \left(\vec{\varphi} \times \vec{\varphi}^\dagger\right)\right] \tag{8.10}$$

8.4 Scalar Potential

Now we want to find the last breaking of the model, which will define the smallest scale associated with it and give mass to the remaining Goldstone bosons. The source of this breaking will be the effective Yukawa term, as we stated in the previous section. For that purpose, we write the symmetric tensor file as a complex three vector field $\vec{\varphi}$.

We presented the explicit symmetry breaking in the last section. In Eq. 8.7, we introduced a term μ^2, which breaks the lepton number but still preserves rotational symmetry. After that, we added a second term to the potential in Eq. 8.8, with the parameter $\vec{\alpha}$ representing the symmetry breaking due to Yukawa interactions. Thus, the full potential will be of the form

$$V = \lambda \left[2 \left(\vec{\varphi}\vec{\varphi}\right)^2 - \left(\vec{\varphi}^*\right)^2 \left(\vec{\varphi}\right)^2\right] - M^2 \left(\vec{\varphi}^*\vec{\varphi}\right) - \mu^2 \left(\vec{\varphi}^*\right)^2 - \mu^2 \left(\vec{\varphi}\right)^2$$
$$+ 2\mu^2 \left(\vec{\varphi}^*\vec{\varphi}\right) - \left(\vec{\alpha}\vec{\varphi}^*\right) \left(\vec{\alpha}\vec{\varphi}\right) + \vec{\alpha}^2 \left(\vec{\varphi}^*\vec{\varphi}\right) \tag{8.11}$$

This potential has a minimum where its vacuum expectation value (VEV) $\langle \vec{\varphi} \rangle$ is in the real part of $\vec{\varphi}$, pointing in the direction of $\vec{\alpha}$ (defined by the Yukawa interactions),

$$\vec{\varphi} = \vec{\varphi}^\dagger = \langle \vec{\varphi} \rangle \vec{\alpha} \tag{8.12}$$

$$V = \lambda \left[2 \langle \vec{\varphi} \rangle^4 - \langle \vec{\varphi} \rangle^4 \right] - M^2 \langle \vec{\varphi} \rangle^2 = \lambda \left(\langle \vec{\varphi} \rangle^2 \right)^2 - M^2 \langle \vec{\varphi} \rangle^2 \tag{8.13}$$

At its minimum: $\langle \vec{\varphi} \rangle^2 = M^2/2\lambda$. Now expanding to second order in φ fields, the transverse fields part of the potential will look like

$$
\begin{aligned}
V =& \lambda \left[4 \langle \vec{\varphi} \rangle^2 \left(\vec{\varphi}_T^\dagger \vec{\varphi}_T \right) - \langle \vec{\varphi} \rangle^2 \left(\vec{\varphi}_T^\dagger \right)^2 - \langle \vec{\varphi} \rangle^2 (\vec{\varphi}_T)^2 \right] - M^2 \left(\vec{\varphi}_T^\dagger \vec{\varphi}_T \right) + \\
&+ \vec{\alpha}^2 \left(\vec{\varphi}_T^\dagger \vec{\varphi}_T \right) - \mu^2 \left(\vec{\varphi}_T^\dagger \right)^2 - \mu^2 (\vec{\varphi}_T)^2 + 2\mu^2 \left(\vec{\varphi}_T^\dagger \vec{\varphi}_T \right)^2 = \\
=& -\lambda \langle \vec{\varphi} \rangle^2 \left(\vec{\varphi}_T^\dagger - \vec{\varphi}_T \right)^2 + \vec{\alpha}^2 \left(\vec{\varphi}_T^\dagger \vec{\varphi}_T \right) - \mu^2 \left(\vec{\varphi}_T^\dagger - \vec{\varphi}_T \right)^2 = \\
=& \vec{\alpha}^2 (\mathrm{Re}\,\vec{\varphi}_T)^2 + \left(\vec{\alpha}^2 + 4\lambda \langle \vec{\varphi} \rangle^2 + 4\mu^2 \right) (\mathrm{Im}\,\vec{\varphi}_T)^2
\end{aligned}
\tag{8.14}
$$

While the masses of the pseudo-Goldstone bosons arise as follows, for the real transverse field, the mass will be $m_{RT}^2 = \vec{\alpha}^2$, and for the imaginary transverse field, it will have a value of $m_{IT}^2 = \vec{\alpha}^2 + 4\lambda \langle \vec{\varphi} \rangle^2 + 4\mu^2 = \vec{\alpha}^2 + 2M^2 + 4\mu^2$

Focusing now in the longitudinal fields part of the potential,

$$
\begin{aligned}
V =& \lambda \left(\varphi_L^\dagger \varphi_L \right)^2 - M^2 \left(\varphi_L^\dagger \varphi_L \right) - \mu^2 \left(\left(\varphi_L^\dagger \right)^2 + (\varphi_L)^2 - 2\left(\varphi_L^\dagger \varphi_L \right) \right) = \\
=& \lambda \left(\langle \vec{\varphi} \rangle^2 + 2 \langle \vec{\varphi} \rangle \varphi_{RL} + \varphi_{RL}^2 + \varphi_{IL}^2 \right)^2 - M^2 \left(\langle \vec{\varphi} \rangle^2 + 2 \langle \vec{\varphi} \rangle \varphi_{RL} + \right. \\
&\left. + \varphi_{RL}^2 + \varphi_{IL}^2 \right) + 4\mu^2 \varphi_{IL}^2 = \\
=& \left(6\lambda \langle \vec{\varphi} \rangle^2 - M^2 \right) \varphi_{RL}^2 + \left(2\lambda \langle \vec{\varphi} \rangle^2 - M^2 \right) \varphi_{IL}^2 + 4\mu^2 \varphi_{IL}^2
\end{aligned}
\tag{8.15}
$$

for which the following masses are obtained:

$$
\begin{aligned}
m_{RL}^2 =& 4\lambda \langle \vec{\varphi} \rangle^2 = 2M^2 \\
m_{IL}^2 =& 4\mu^2
\end{aligned}
\tag{8.16}
$$

We must note that there are three states associated with the high mass scale M, one state μ associated with the lepton number symmetry breaking, and two states α associated with the symmetry breaking induced by the Yukawa interactions.

All in all, the original symmetry is U(2) and breaks to U(1) if we include both symmetry breaking effects. The U(1) is a preserved rotational symmetry in the space transverse to the $\vec{\alpha}$ direction.

8.5   Calculating the gravitational wave spectrum from the phase transition

A SSB as the one proposed in Sec. 8.2 is a natural source of gravitational waves [11, 16].

For the computation of these effects, we choose to put the potential in isovector notation and consider the couplings after renormalization (see Appendix). The potential then becomes

$$V = m^2 (\vec{\varphi}^* \vec{\varphi}) + \frac{\lambda_1}{2} (\vec{\varphi}^* \vec{\varphi})^2 - \frac{\lambda_2}{4} (\vec{\varphi}^* \vec{\varphi}^*)(\vec{\varphi} \vec{\varphi}) \tag{8.17}$$
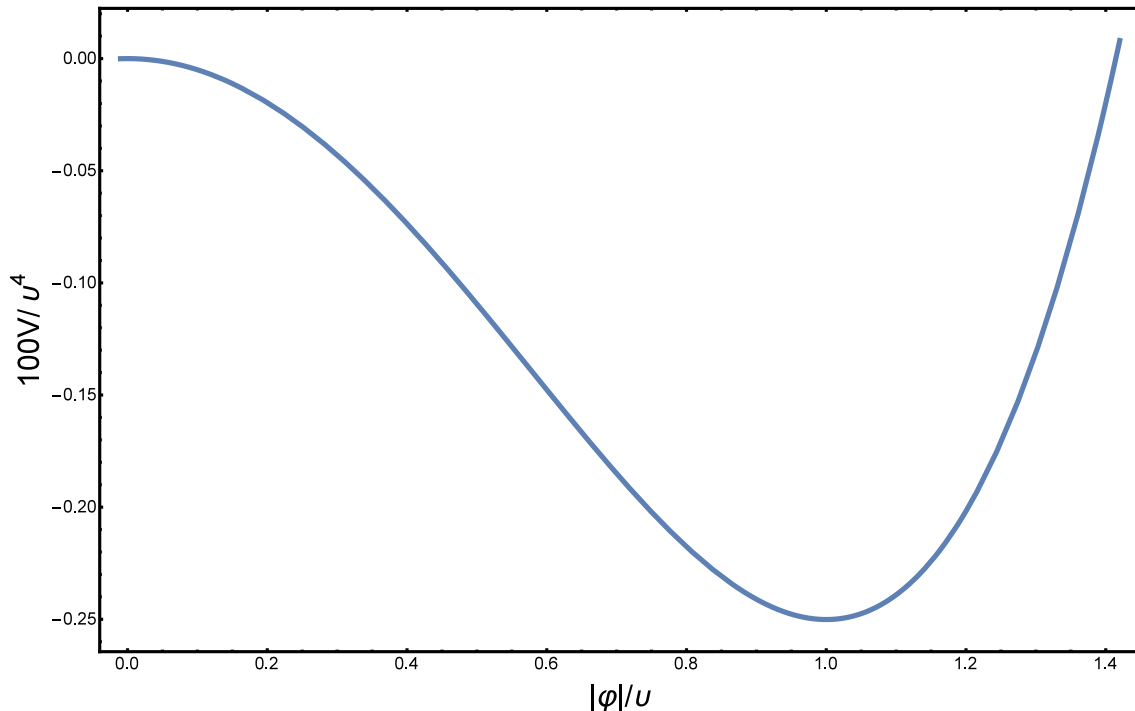
Figure 8.1: Potential at zero temperature.

In this potential, the mass term is a parameter of the evolved theory (follow Appendix) and, since in Eq. 8.3 we have the negative of M^2 extracted (with a positive sign the squared mass would be negative as expected in a SSB), we will have that sign absorbed as $m^2 \propto -M^2$. It must be clear that this is a potential compatible with all the symmetries of the initial sterile neutrino condensate potential we have developed through this article, with a particular choice of the parameter set to be used as a toy model. It is not meant to be the ultimate potential describing the sterile neutrino composite Higgs dynamics.

For our estimations we chose this squared mass related to the VEV [Eq. 8.6] as $\left|m^2\right| \simeq 10^{-2}v$. The couplings are selected in a way that the running is stable at every energy scale (Fig. 8.5 in the Appendix) with values $\lambda_1 = 0.23$ and $\lambda_2 = 0.94$. This is just one amongst the many choices available for solving this problem, with no other singular interest. We have selected these particular values for illustration purposes exclusively.

The SSB scale would naturally be much lower than the condensation scale, which makes it a second order phase transition. However, the difference between scales can be slightly reduced by fine-tuning the value of m^2. For that reason, we will explore different values for v, and therefore, different values of m^2, at the end of this section. Although the standard line is to associate first order phase transitions with significant gravitational wave production [17], the potential developed by the RH neutrino condensate can source an interesting signal for an appropriate choice of parameters, as can be seen in Figs. 8.1 and 8.2.

Since the fields have two components, one of them complex, a path has been chosen for the analysis, defining them according to the parameter t as $\vec{\varphi} = \left(t/\sqrt{2}, 0, t/2 + it/2\right)$

As we can see in Fig. 8.1, the true vacuum of this potential at zero temperature is not located at $\langle\varphi\rangle = 0$, in agreement to the vacuum of the potential this is inspired in, presented in Sec. 8.2. At higher temperatures, the vacuum of the theory will be located at the origin, as shown in Fig. 8.2. This temperature dependence is introduced in the
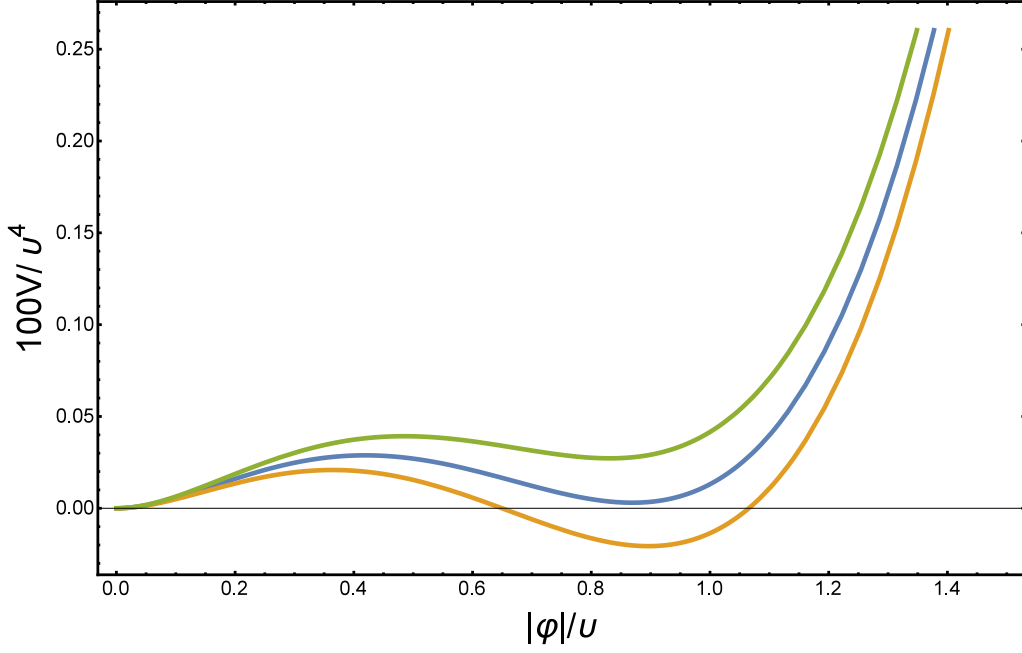
Figure 8.2: Evolution of the potential according to temperature, using $V + \Delta V$ as in Eqs. 8.17 and 8.18 for $T = 0.31\upsilon$ (orange curve), $T = 0.32\upsilon$ (blue curve) and $T = 0.33\upsilon$ (green curve).

standard way, by adding the following term:

$$\Delta V_T = \frac{3T^2}{2\pi^2} \left[\int_0^\infty dq q^2 \log \left(1 - \exp \left(-\sqrt{q^2 + \vec{\varphi}^* \vec{\varphi} \left(\frac{g(\mu)}{T} \right)^2} \right) \right) + \int_0^\infty dq q^2 \log \left(1 - \exp\left(-q\right) \right) \right] \tag{8.18}$$

with two integrals accounting for the three massive bosons and the three massless ones [17][18]. The VEV will be defined as $\upsilon = 1$ through the whole calculation, leaving the factor accounting for its real value in the determination of the gravitational wave frequencies.

The thin wall approximation [17] has two markers of optimality. The first one is the gap between the true vacuum (υ_{T_C}) at the critical temperature $(T \simeq 0.32\upsilon$ for us) and the energy at the origin,

$$\epsilon = V_{T_C}(0) - V_{T_C}(\upsilon_{T_C}) \simeq 0.0698 \tag{8.19}$$

This value has to be $0 < \epsilon \ll 1$, which fits our model. The second reference for gravitational waves generation comes from the three-dimensional action, defined by

$$S_3 = 4\pi \int_0^R dr \, r^2 V_T(\upsilon_{T_C}) + 4\pi R^2 \int_0^{\upsilon_{T_C}} d\varphi \sqrt{2 V_T(\varphi)} \tag{8.20}$$

Where R is the bubble radius. We choose $T_* = 0.29\upsilon$ as the temperature that makes an extreme action (with respect to the bubble radius) of $S_3/T_* \simeq S_3/T_C \simeq 105$, which as explained in [17], maximizes the probability of tunneling from the vacuum at $\langle \varphi \rangle = 0$ to the true vacuum once the temperature has decreased.

After selecting an appropriate temperature for the transition to leave an interesting gravitational wave signal, we proceed to extracting the relevant parameters, which are α and β, defined as

$$\alpha = \frac{\rho_{vac}}{\rho_{rad}^*} = \frac{\epsilon}{g_* \pi^2 T_*^4 / 30} = 0.97$$

$$\frac{\beta}{H_*} = \left[T \frac{d}{dT} \left(\frac{S_3}{T} \right) \right]_{T \to T_*} = -1600$$

(8.21)

where $g_* = 100$ is the number of relativistic degrees of freedom. These two parameters are everything needed to calculate the frequency spectrum of the phase transition. First, we define the peak frequencies of bubble walls collisions (col), sound waves in the plasma (sw) and magnetohydrodynamic turbulences after the collisions (mhd) as derived in [19],

$$f_{col} = 16.5 \cdot 10^{-6} \left(\frac{0.62}{1.8 - 0.1v + v^2} \right) \left| \frac{\beta}{H_*} \right| \left(\frac{T_* (v \cdot \text{in GeV})}{100} \right) \left(\frac{g_*}{100} \right)^{\frac{1}{6}} \text{ Hz}$$

$$f_{sw} = 1.9 \cdot 10^{-5} \left(\frac{1}{v} \right) \left| \frac{\beta}{H_*} \right| \left(\frac{T_* (v \cdot \text{in GeV})}{100} \right) \left(\frac{g_*}{100} \right)^{\frac{1}{6}} \text{ Hz}$$

(8.22)

$$f_{mhd} = 1.42 f_{sw}$$

And then, the gravitational waves background gets the following contributions:

$$\Omega_{GW} \sim \Omega_{col} + \Omega_{sw} + \Omega_{mhd}$$

(8.23)

defined by ([19])

$$h^2 \Omega_{col} = 1.67 \cdot 10^{-5} \left(\frac{H_*}{\beta} \right)^2 \left(\frac{\kappa_{col} \alpha}{1 + \alpha} \right)^2 \left(\frac{100}{g_*} \right)^{\frac{1}{3}} \frac{0.11 v^3}{0.42 + v^2} \frac{3.8 \left(f/f_{col} \right)^{2.8}}{1 + 2.8 \left(f/f_{col} \right)^{3.8}}$$

$$h^2 \Omega_{sw} = 2.65 \cdot 10^{-6} \left| \frac{H_*}{\beta} \right| \left(\frac{\kappa_{sw} \alpha}{1 + \alpha} \right)^2 \left(\frac{100}{g_*} \right)^{\frac{1}{3}} v \frac{f}{f_{sw}} \left(\frac{7}{4 + 3 \left(f/f_{sw} \right)^2} \right)^{\frac{7}{2}}$$

(8.24)

$$h^2 \Omega_{mhd} = 3.35 \cdot 10^{-4} \left| \frac{H_*}{\beta} \right| \left(\frac{\kappa_{sw} \alpha}{1 + \alpha} \right)^{\frac{3}{2}} \left(\frac{100}{g_*} \right)^{\frac{1}{3}} v \frac{\left(f/f_{mhd} \right)^3}{\left(1 + f/f_{mhd} \right)^{\frac{11}{3}} \left(1 + 8\pi f/h_* \right)}$$

In this expressions, v is the bubble wall velocity (we have chosen v = 1) and the different κ are the latent heat fractions (we decided to set all of them to $\kappa = 0.5$). In Fig. 8.3, the gravitational signal obtained with these equations is represented for different values of v.
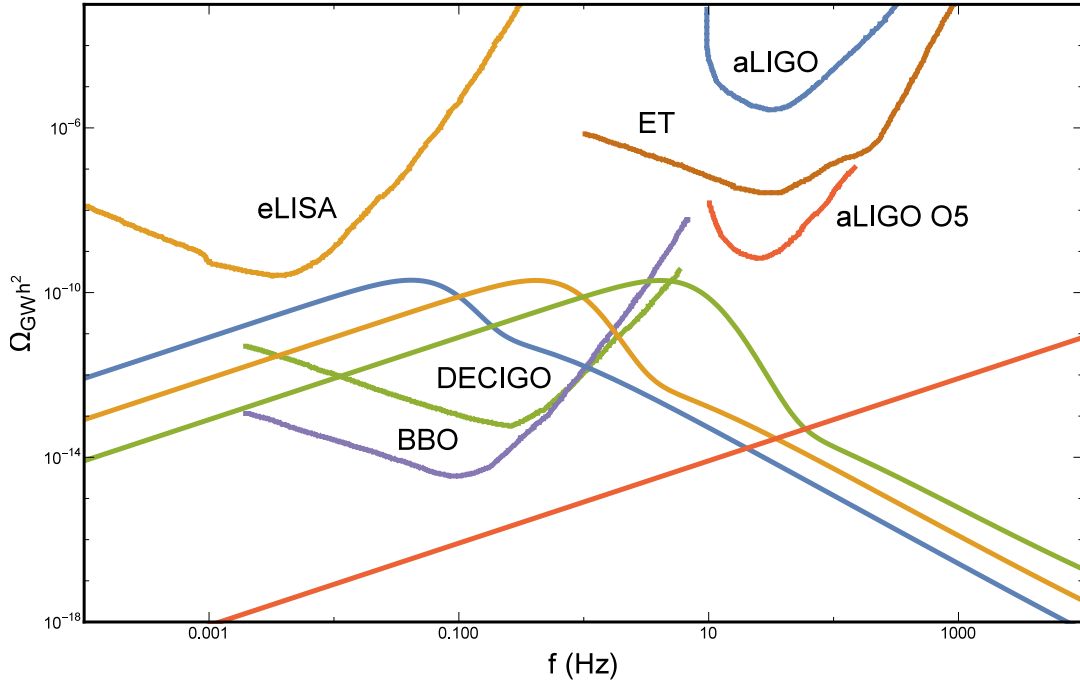
Figure 8.3: Gravitational wave signal for different mass and v energy scales (1 TeV: blue curve; 10 TeV: orange curve; 100 TeV: green curve; $10^{-9}M_P$: red curve) compared to detectors reading spectra.

8.6   Conclusions

Considering at least two generations of right-handed neutrinos has proven quite interesting for addressing several physical problems. First of all, we have determined, after successive breakings (spontaneous and explicit), that they leave composite scalars at three different mass scales that could be experimentally found and used as proof of the condensate formation and reveal information about it. Besides, these scalars could be of use for theories that require additional singlet degrees of freedom at high scales.

Inflation, already considered by [7], would have a new set of particles being plausible inflaton candidates, a scenario probably worth considering. The composite scalar fields have a potential that may be interesting for an inflationary model as well.

The aid of these condensates for the stabilization of the Electroweak Vacuum has been an unfortunate failure, apparently due to having renormalization group equations equations with a weaker self-coupling than that presented in [8], thus not being enough for this purpose.

Besides, since we do not know yet whether the only scalar particle found in nature so far, the Higgs boson, is fundamental (see [20]), this work presents a way to get a spectrum of scalar particles associated to different energy scales.

However, the implications of these neutrino condensates do not only end there. The gravitational waves signal hypothetically generated by the SSB of the their potential, estimated using toy model parameters, has been determined, obtaining a theoretical prediction that, if correct, would be measurable in the forthcoming years, when the experimental search of gravitational waves will presumably be a strong research field. Our results (Fig. 8.3) show that a value from one to several tens up to few hundred TeV for Λ (see Sec.

8.5) would be observable by DECIGO and BBO. Nonetheless, we would expect the bosons coming from the broken symmetries to show up in accelerator experiments too, putting bounds on the different energy scales present in the theory. A neutrino condensate located at a very high energy scale (Fig. 8.3, in red) would not be observable by any current or planned detector.

APPENDIX

8.A Renormalization of the theory

Majorana fermions:

Let us stablish first how we jump from the usual Dirac notation to the one that best suits our study,

$$\gamma^\mu p_\mu \gamma^0 = p^0 - \gamma_5 \vec{\sigma}\vec{p} \tag{8.25}$$

The RH neutrino renormalized propagator will be (considering the contributions from the composite structure of the scalars) of the form

$$\left\langle \psi_R(x)\,\psi_R^\dagger(x) \right\rangle_{\alpha\beta} = \frac{i}{(2\pi)^4} \int d^4p\, e^{-ip^\mu(x-y)_\mu} \frac{(p_0 + \vec{\sigma}\vec{p})_{\alpha\beta}}{p^2} \tag{8.26}$$

which, if we apply the same transformation we are using to change the notation into the isovector formalism, is

$$(-i\sigma_2)_{\alpha\gamma} \left\langle \psi_R^*(x)\,\psi_R^T(x) \right\rangle_{\gamma\delta} (i\sigma_2)_{\delta\beta} = \frac{i}{(2\pi)^4} \int d^4p\, e^{-ip^\mu(x-y)_\mu} \frac{(p_0 - \vec{\sigma}\vec{p})_{\alpha\beta}}{p^2} \tag{8.27}$$

We define the Majorana mass operators as

$$\mathcal{O}_\psi(x) = (i\sigma_2)_{\alpha\beta}\,\psi_{R\alpha}(x)\,\psi_{R\beta}(x)\,;\; \mathcal{O}_\psi^\dagger(x) = (-i\sigma_2)_{\alpha\beta}\,\psi_{R\alpha}^*(x)\,\psi_{R\beta}^*(x) \tag{8.28}$$

which we will include in the fermion bubble function of neutrinos, in order to calculate this loop contribution,

$$-i\int d^4y\, e^{ik^\mu y_\mu} \left\langle O_\psi(x)\, O_\psi^\dagger(y) \right\rangle =$$

$$= -i\int d^4y\, e^{ik^\mu y_\mu} \left\langle (i\sigma_2)_{\alpha\gamma}\,\psi_{R\alpha}(x)\,\psi_{R\beta}(x)\,,\, (-i\sigma_2)_{\gamma\delta}\,\psi_{R\gamma}^*(y)\,\psi_{R\delta}^*(y) \right\rangle =$$

$$= -i\int d^4y\, e^{ik^\mu y_\mu}\,(-2)\left\langle \psi_{R\beta}(x)\,\psi_{R\gamma}^*(y) \right\rangle (-i\sigma_2)_{\gamma\delta}\left\langle \psi_{R\delta}^*(y)\,\psi_{R\alpha}(x) \right\rangle (\sigma_2)_{\alpha\beta} =$$

$$
\begin{aligned}
&= (-2)\frac{i}{(2\pi)^4}\int d^4p \frac{(p_0+\vec{\sigma}\vec{p})_{\beta\gamma}}{p^2}\frac{\left((p+k)_0-\vec{\sigma}\left(\vec{p}+\vec{k}\right)\right)_{\gamma\beta}}{(p+k)^2} = \\
&= -2\frac{i}{(2\pi)^4}\int d^4p\frac{\mathrm{Tr}\left[(p_0+\vec{\sigma}\vec{p})\left((p+k)_0-\vec{\sigma}\left(\vec{p}+\vec{k}\right)\right)\right]}{p^2\,(p+k)^2} = \\
&= -2\frac{i}{(2\pi)^4}\int d^4p\frac{2p_\mu\,(p+k)^\mu}{p^2\,(p+k)^2} = \\
&= -4\frac{i}{(2\pi)^4}\int d^4p\frac{1}{p^2} + 2k^2\frac{i}{(2\pi)^4}\int d^4p\frac{1}{p^2\,(p+k)^2}
\end{aligned}
\tag{8.29}
$$

These mass operators will appear in the condensation mechanism, a BHL analysis equivalent to that peformed to the top quark in the literature,

$$
\begin{aligned}
\mathcal{L} = G\mathcal{O}_\psi\left(x\right)\mathcal{O}_\psi^\dagger\left(x\right) &= -\tfrac{g^2}{G}\varphi^*\left(x\right)\varphi\left(x\right) - g\left[\varphi^*\mathcal{O}_\psi + \varphi\mathcal{O}_\psi^\dagger\right]\left(x\right) \\
&\to Z_\varphi\partial\varphi^*\partial\varphi - \Delta m^2\varphi^*\varphi - \tfrac{1}{2}\lambda\left(\varphi^*\varphi\right)^2
\end{aligned}
\tag{8.30}
$$

$$
Z_\varphi\left(\mu^2\right) = 2g^2\frac{1}{(4\pi)^2}\mathrm{Ln}\frac{\Lambda^2}{\mu^2}
\tag{8.31}
$$

$$
\Delta m^2\left(\mu^2\right) = \frac{g^2}{G} - 4g^2\frac{1}{(4\pi)^2}\Lambda^2
\tag{8.32}
$$

where we can see the renormalized mass and kinetic term below the scale Λ, which is a dummy variable that we will set as the scale where the RH neutrinos have effectively condensed.

We can renormalize the four scalar coupling constant in the following way:

$$
\begin{aligned}
\lambda\left(\mu^2\right) =&\frac{1}{2}g^4\left(-i\int d^4x\right)\left(-i\int d^4y\right)\left(-i\int d^4z\right)\left\langle\mathcal{O}_\psi\left(0\right)\mathcal{O}_\psi^\dagger\left(x\right)\mathcal{O}_\psi\left(y\right)\mathcal{O}_\psi^\dagger\left(z\right)\right\rangle = \\
=&-\frac{1}{2}g^4\frac{i}{(2\pi)^4}\int d^4p\,2\,(2)^3\frac{\mathrm{Tr}\left[(p_0+\vec{\sigma}\vec{p})(p_0-\vec{\sigma}\vec{p})(p_0+\vec{\sigma}\vec{p})(p_0-\vec{\sigma}\vec{p})\right]}{\left(p^2\right)^4} = \\
=&-16g^4\frac{i}{(2\pi)^4}\int d^4p\frac{1}{\left(p^2\right)^2} = 16g^4\frac{1}{(4\pi)^2}\mathrm{Ln}\left(\frac{\Lambda^2}{\mu^2}\right)
\end{aligned}
\tag{8.33}
$$

which will leave the following effective couplings at the scale μ (BHL approximation):

$$
g^2 \to \frac{g^2}{Z_\varphi} = \frac{1}{2}\frac{(4\pi)^2}{\mathrm{Ln}\left(\Lambda^2/\mu^2\right)}
\tag{8.34}
$$

$$
\lambda \to \frac{\lambda}{Z_\varphi^2} = 4\frac{(4\pi)^2}{\mathrm{Ln}\left(\Lambda^2/\mu^2\right)}
\tag{8.35}
$$

Two flavour theory

In this section we will study the dynamical effects of our effective theory of condensed scalars. Interpreting the symmetric tensor condensate field as an isovector field, the extension of the mass operators will be

$$
\mathcal{O}_\psi^{ij}\left(x\right) = \left(i\sigma_2\right)_{\alpha\beta}\psi_{R\alpha}^i\left(x\right)\psi_{R\beta}^j\left(x\right); \; \mathcal{O}_\psi^{\dagger ij}\left(x\right) = \left(-i\sigma_2\right)_{\alpha\beta}\psi_{R\alpha}^{*i}\left(x\right)\psi_{R\beta}^{*j}\left(x\right)
\tag{8.36}
$$

Leaving the following interaction Lagrangian:

$$\mathcal{L}_I = G\mathcal{O}_\psi^{ij}(x)\,\mathcal{O}_\psi^{\dagger ij}(x) = -\frac{g^2}{G}\varphi^{*ij}\varphi^{ij}(x) - g\left[\varphi^{*ij}\mathcal{O}_\psi^{ij} + \varphi^{ij}\mathcal{O}_\psi^{\dagger ij}\right](x) \tag{8.37}$$

Setting the same renormalization constants we have already presented,

$$\to Z_\varphi \partial\varphi^{*ij}\partial\varphi^{ij} - \Delta m^2\varphi^{*ij}\varphi^{ij} - \frac{\lambda}{2}\left(\varphi^{*ij}\varphi^{jk}\varphi^{*kl}\varphi^{li}\right) \tag{8.38}$$

Using now the isovector Notation,

$$\varphi^{ij} \to \frac{1}{\sqrt{2}}(\vec{\tau}\vec{\varphi}i\tau_2)^{ij} \tag{8.39}$$

$$\Rightarrow Z_\varphi \partial\varphi^{*ij}\partial\varphi{ij} - \Delta m^2\varphi^{*ij}\varphi^{ij} - \frac{\lambda}{2}\left(\varphi^{*ij}\varphi^{jk}\varphi^{*kl}\varphi^{li}\right) =$$
$$= \frac{Z_\psi}{2}\mathrm{Tr}\left[\partial\left((\vec{\tau}\vec{\varphi}^*)\,\partial(\vec{\tau}\vec{\varphi})\right)\right] - \frac{\Delta m^2}{2}\mathrm{Tr}\left[(\vec{\tau}\vec{\varphi}^*)(\vec{\tau}\vec{\varphi})\right] - \frac{\lambda}{8}\mathrm{Tr}\left[(\vec{\tau}\vec{\varphi}^*)(\vec{\tau}\vec{\varphi})(\vec{\tau}\vec{\varphi}^*)(\vec{\tau}\vec{\varphi})\right] = \tag{8.40}$$
$$= Z_\psi\left(\partial\vec{\varphi}^*\partial\vec{\varphi}\right) - \Delta m^2\left(\vec{\varphi}^*\vec{\varphi}\right) - \frac{\lambda}{4}\left(2\left(\vec{\varphi}^*\vec{\varphi}\right)^2 - \left(\vec{\varphi}^*\right)^2\left(\vec{\varphi}\right)^2\right)$$

where Z_φ, Δm^2 and λ are the same as before,

$$Z_\varphi\left(\mu^2\right) = 2g^2\frac{1}{(4\pi)^2}\mathrm{Ln}\left(\frac{\Lambda^2}{\mu^2}\right) \tag{8.41}$$

$$\Delta m^2\left(\mu^2\right) = \frac{g^2}{G} - 4g^2\frac{\Lambda^2}{(4\pi)^2} \tag{8.42}$$

$$\lambda\left(\mu^2\right) = \frac{16g^4}{(4\pi)^2}\mathrm{Ln}\left(\frac{\Lambda^2}{\mu^2}\right) \tag{8.43}$$

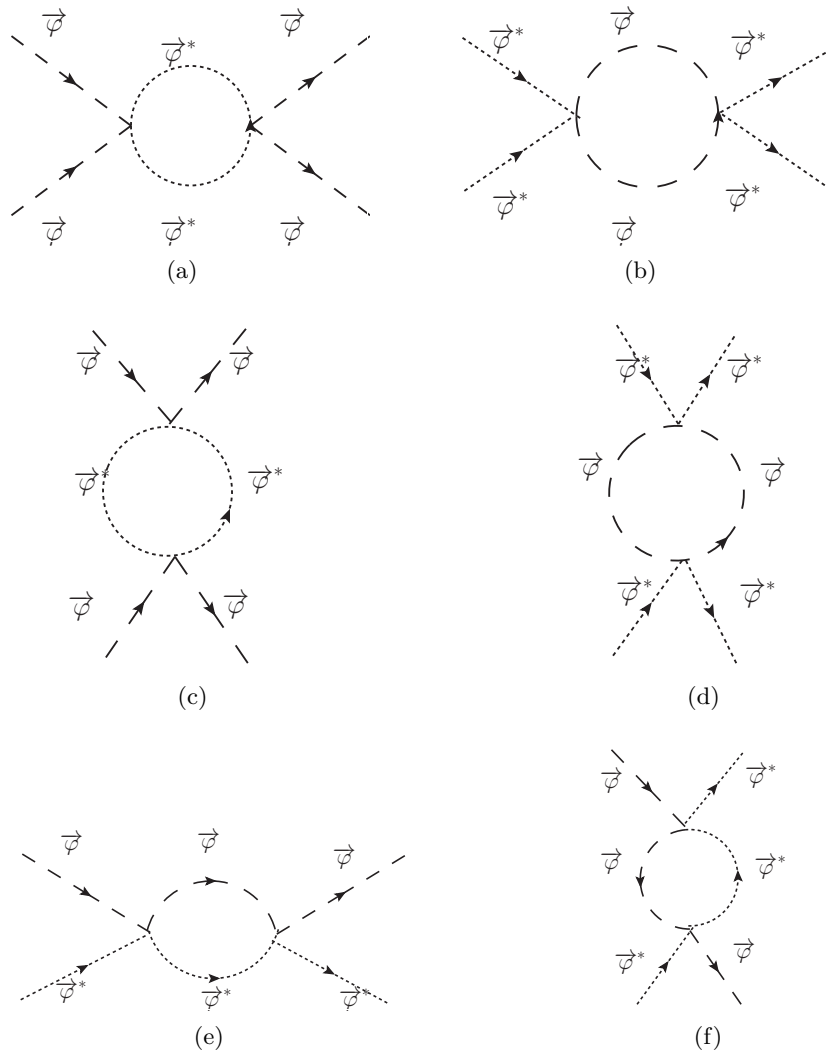The computation of the bosonic loops gives (isovector normalization), see Fig. 8.4

$$\mathcal{L} = \partial\vec{\varphi}^*\partial\vec{\varphi} - m^2\vec{\varphi}^*\vec{\varphi} - \frac{\lambda_1}{2}\left(\vec{\varphi}^*\vec{\varphi}\right)^2 + \frac{\lambda_2}{4}\left(\vec{\varphi}^*\right)^2\left(\vec{\varphi}\right)^2 \tag{8.44}$$

$$\Delta\left(\lambda_1\right) = \left[3\lambda_1^2 + 2\lambda_1\lambda_2 + \lambda_1^2\right]\frac{i}{(2\pi)^4}\int d^4p\frac{1}{(p^2)^2} =$$
$$= -\left[4\lambda_1^2 + 2\lambda_1\lambda_2\right]\frac{1}{(4\pi)^2}\mathrm{Ln}\left(\frac{\Lambda^2}{\mu^2}\right) \tag{8.45}$$

$$\Delta\left(\lambda_2\right) = \left[\frac{3}{2}\lambda_2^2 + 2\lambda_1\lambda_2\right]\frac{i}{(2\pi)^4}\int d^4p\frac{1}{(p^2)^2} =$$
$$= -\left[\frac{3}{2}\lambda_2^2 + 2\lambda_1\lambda_2\right]\frac{1}{(4\pi)^2}\mathrm{Ln}\left(\frac{\Lambda^2}{\mu^2}\right) \tag{8.46}$$

$$\Delta\left(\lambda_1\right) = -\lambda_1\left(4\lambda_1 + 2\lambda_2\right)\frac{1}{(4\pi)^2}\mathrm{Ln}\left(\frac{\Lambda^2}{\mu^2}\right) \tag{8.47}$$

$$\Delta\left(\lambda_2\right) = -\lambda_2\left(\frac{3}{2}\lambda_2 + 2\lambda_1\right)\frac{1}{(4\pi)^2}\mathrm{Ln}\left(\frac{\Lambda^2}{\mu^2}\right) \tag{8.48}$$

Figure 8.4: Loops involved in the renormalization of λ_1 and λ_2.

Now adding the fermion loop contribution (conventional definition with bosonic kinetic term normalized to 1), see Fig. 8.4

$$\Delta\left(\lambda_1\right) = \left[-\lambda_1\left(4\lambda_1 + 2\lambda_2\right) - 4g^2\lambda_1 + 16g^4\right]\frac{1}{\left(4\pi\right)^2}\mathrm{Ln}\left(\frac{\Lambda^2}{\mu^2}\right) \tag{8.49}$$

$$\Delta\left(\lambda_2\right) = \left[-\lambda_2\left(\frac{3}{2}\lambda_2 + 2\lambda_1\right) - 4g^2\lambda_2 - 16g^4\right]\frac{1}{\left(4\pi\right)^2}\mathrm{Ln}\left(\frac{\Lambda^2}{\mu^2}\right) \tag{8.50}$$

The right-handed fermion mass matrix is

$$\left(MM^\dagger\right)_{ij} = 2g\varphi_{ik}2g\varphi_{kj}^* = 2g^2\left[\left(\vec{\tau}\vec{\varphi}\right)\left(\vec{\tau}\vec{\varphi}^*\right)\right]_{ij} \tag{8.51}$$

And the fermion wavefunction renormalization,

$$
\frac{(p_0 + \vec{\sigma}\vec{p})}{p^2} \frac{\tau^a i \tau_2}{\sqrt{2}} \frac{i}{(2\pi)^4} \int d^4k \frac{1}{k^2} \frac{\left((p+k)_0 - \vec{\sigma}\left(\vec{p}+\vec{k}\right)\right)}{p^2} 2g \frac{(-i\tau_2)\tau^a}{\sqrt{2}} \frac{(p_0 + \vec{\sigma}\vec{p})}{p^2} =
$$

$$
= 6g^2 \frac{(p_0 + \vec{\sigma}\vec{p})}{p^2} \frac{i}{(2\pi)^4} \int d^4k \left((p+k)_0 - \vec{\sigma}\left(\vec{p}+\vec{k}\right)\right) \frac{(p_0 + \vec{\sigma}\vec{p})}{p^2}
$$

$$
\cdot \int d\alpha \Gamma(2) \left[-\alpha(1-\alpha)p^2 - (k+\alpha p)^2\right]^{-2} =
$$

$$
= -\frac{6g^2}{(4\pi)^2} \frac{(p_0 + \vec{\sigma}\vec{p})}{p^2} \int d\alpha (1-\alpha)(p_0 - \vec{\sigma}\vec{p}) \frac{p_0 + \vec{\sigma}\vec{p}}{p^2} \Gamma\left(2 - \frac{d}{2}\right) \left[-\alpha(1-\alpha)p^2\right]^{\frac{d}{2}-2} =
$$

$$
= -\frac{3g^2}{(4\pi)^2} \frac{(p_0 + \vec{\sigma}\vec{p})}{p^2} \int d\alpha \mathrm{Ln}\left(\frac{\Lambda^2}{-\alpha(1-\alpha)p^2}\right)
$$

$$(8.52)$$

$$
Z_\psi = 1 + \frac{3g^2}{(4\pi)^2} \mathrm{Ln}\left(\frac{\Lambda^2}{\mu^2}\right); \ Z_\varphi = 1 + \frac{2g^2}{(4\pi)^2} \mathrm{Ln}\left(\frac{\Lambda^2}{\mu^2}\right) \tag{8.53}
$$

The Yukawa renormalization is

$$
g \to \frac{g}{Z_\psi \sqrt{Z_\varphi}} = g - \frac{3g^3}{(4\pi)^2} \mathrm{Ln}\left(\frac{\Lambda^2}{\mu^2}\right) - \frac{g^2}{(4\pi)^2} \mathrm{Ln}\left(\frac{\Lambda^2}{\mu^2}\right) = g - \frac{4g^3}{(4\pi)^2} \mathrm{Ln}\left(\frac{\Lambda^2}{\mu^2}\right) \tag{8.54}
$$

The perturbative summary is thus made from the following equations:

$$
\left(MM^\dagger\right)_{ij} = 2g\varphi_{ik} 2g\varphi_{kj}^* = 2g^2 \left[(\vec{\tau}\vec{\varphi})(\vec{\tau}\vec{\varphi}^*)\right]_{ij} \tag{8.55}
$$

$$
\Delta\left(g^2\right) = -\frac{8g^4}{(4\pi)^2} \mathrm{Ln}\left(\frac{\Lambda^2}{\mu^2}\right) \tag{8.56}
$$

$$
\Delta\left(\lambda_1\right) = \left[-\lambda_1\left(4\lambda_1 + 2\lambda_2\right) - 4g^2\lambda_1 + 16g^4\right] \frac{1}{(4\pi)^2} \mathrm{Ln}\left(\frac{\Lambda^2}{\mu^2}\right) \tag{8.57}
$$

$$
\Delta\left(\lambda_2\right) = \left[-\lambda_2\left(\frac{3}{2}\lambda_2 + 2\lambda_1\right) - 4g^2\lambda_1 - 16g^4\right] \frac{1}{(4\pi)^2} \mathrm{Ln}\left(\frac{\Lambda^2}{\mu^2}\right) \tag{8.58}
$$

And the one-loop perturbative beta-functions will be (running in Fig. 8.5)

$$
\beta_{g^2} = 16\pi^2 \left(\mu^2 \partial\mu^2 g^2\right) = 8g^4 \tag{8.59}
$$

$$
\beta_{\lambda_1} = 16\pi^2 \left(\mu^2 \partial\mu^2 \lambda_1\right) = \left[\lambda_1\left(4\lambda_1 + 2\lambda_2\right) + 4g^2\lambda_1 - 16g^4\right] \tag{8.60}
$$

$$
\beta_{\lambda_2} = 16\pi^2 \left(\mu^2 \partial\mu^2 \lambda_2\right) = \left[\lambda_2\left(\frac{3}{2}\lambda_2 + 2\lambda_1\right) + 4g^2\lambda_1 + 16g^4\right] \tag{8.61}
$$

which have the potential for Coleman-Weinberg instability if $(2\lambda_1 + \lambda_2) < 0$ in IR.
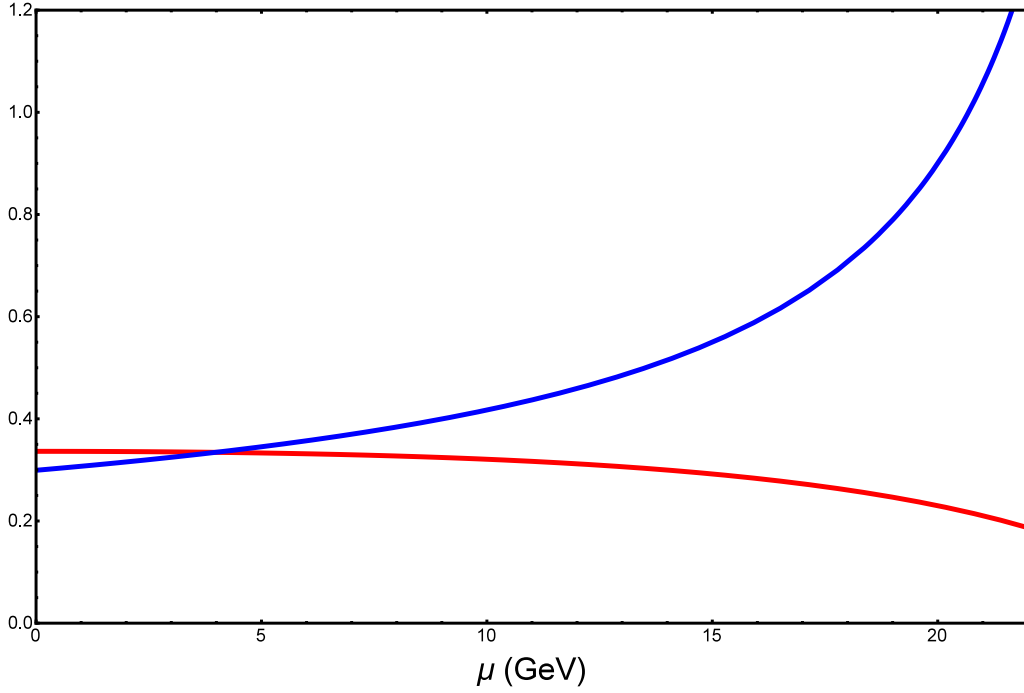
Figure 8.5: Running of the couplings λ_1 (red curve) and λ_2 (blue curve) with boundaries selected for Sec. 8.5.

After applying the BHL boundary conditions of the effective couplings at scale μ (bubble approximation with Landau poles at $\mu = \Lambda$), the BHL results follow:

$$g^2 \to \frac{1}{2} \frac{(4\pi)^2}{\operatorname{Ln}(\Lambda^2/\mu^2)}; \ \ \beta_{g^2} = 16\pi^2 \left(\mu^2 \partial \mu^2 g^2\right) = \frac{1}{2} \left(\frac{(4\pi)^2}{\operatorname{Ln}(\Lambda^2/\mu^2)}\right)^2 \tag{8.62}$$

$$\lambda_1 \to 4 \frac{(4\pi)^2}{\operatorname{Ln}(\Lambda^2/\mu^2)}; \ \ \beta_{\lambda_1} = 16\pi^2 \left(\mu^2 \partial \mu^2 \lambda_1\right) = 4 \left(\frac{(4\pi)^2}{\operatorname{Ln}(\Lambda^2/\mu^2)}\right)^2 \tag{8.63}$$

$$\lambda_2 \to -4 \frac{(4\pi)^2}{\operatorname{Ln}(\Lambda^2/\mu^2)}; \ \ \beta_{\lambda_2} = 16\pi^2 \left(\mu^2 \partial \mu^2 \lambda_2\right) = -4 \left(\frac{(4\pi)^2}{\operatorname{Ln}(\Lambda^2/\mu^2)}\right)^2 \tag{8.64}$$

Note that you would match the actual amplitudes at scale μ, not the beta functions, $[\lambda_i + \Delta(\lambda_i)]_{effective\ theory} = [\lambda_i]_{BHL}$ at scale μ.

Bibliography

[1] W. A. Bardeen, C. T. Hill and M. Lindner, Phys. Rev. D **41** (1990) 1647. doi:10.1103/PhysRevD.41.1647

[2] H. Terazawa, Phys. Rev. D **22**, 2921 (1980) Erratum: [Phys. Rev. D **41**, 3541 (1990)]. doi:10.1103/PhysRevD.41.3541, 10.1103/PhysRevD.22.2921

[3] H. Terazawa, K. Akama and Y. Chikashige, Phys. Rev. D **15**, 480 (1977). doi:10.1103/PhysRevD.15.480

[4] G. Barenboim, Phys. Rev. D **82** (2010) 093014 doi:10.1103/PhysRevD.82.093014 [arXiv:1009.2504 [hep-ph]].

[5] G. Dvali and L. Funcke, Phys. Rev. D **93**, no. 11, 113002 (2016) doi:10.1103/PhysRevD.93.113002 [arXiv:1602.03191 [hep-ph]].

[6] J. M. Weller, Phys. Rev. D **88**, 083511 (2013) doi:10.1103/PhysRevD.88.083511 [arXiv:1307.2423 [gr-qc]].

[7] G. Barenboim, JHEP **0903** (2009) 102 doi:10.1088/1126-6708/2009/03/102 [arXiv:0811.2998 [hep-ph]].

[8] J. Elias-Miro, J. R. Espinosa, G. F. Giudice, H. M. Lee and A. Strumia, JHEP **1206** (2012) 031 doi:10.1007/JHEP06(2012)031 [arXiv:1203.0237 [hep-ph]].

[9] B. P. Abbott, *et al.*, Phys. Rev. Lett. **116** (2016) 061102 doi:http://dx.doi.org/10.1103/PhysRevLett.116.061102

[10] P. S. B. Dev and A. Mazumdar, Phys. Rev. D **93**, no. 10, 104001 (2016) doi:10.1103/PhysRevD.93.104001 [arXiv:1602.04203 [hep-ph]].

[11] R. Jinno, K. Nakayama and M. Takimoto, Phys. Rev. D **93**, no. 4, 045024 (2016) doi:10.1103/PhysRevD.93.045024 [arXiv:1510.02697 [hep-ph]].

[12] R. Jinno and M. Takimoto, arXiv:1604.05035 [hep-ph].

[13] A. Kosowsky and M. S. Turner, Phys. Rev. D **47** (1993) 4372 doi:10.1103/PhysRevD.47.4372 [astro-ph/9211004].

[14] M. Kamionkowski, A. Kosowsky and M. S. Turner, Phys. Rev. D **49** (1994) 2837 doi:10.1103/PhysRevD.49.2837 [astro-ph/9310044].

[15] C. Grojean and G. Servant, Phys. Rev. D **75** (2007) 043507 doi:10.1103/PhysRevD.75.043507 [hep-ph/0607107].

[16] J. T. Giblin, Jr., L. R. Price, X. Siemens and B. Vlcek, JCAP **1211** (2012) 006 doi:10.1088/1475-7516/2012/11/006 [arXiv:1111.4014 [astro-ph.CO]].

[17] J. Jaeckel, V. V. Khoze and M. Spannowsky, arXiv:1602.03901 [hep-ph].

[18] L. Dolan and R. Jackiw, Phys. Rev. D **9** (1974) 3320. doi:10.1103/PhysRevD.9.3320

[19] R. Jinno and M. Takimoto, arXiv:1605.01403 [astro-ph.CO].

[20] A. Strumia, arXiv:1605.09401 [hep-ph].

Aknowledgements

This has been a long path, and long paths let you meet and sometimes share some part of the walk with many people. Let us hope no one gets into oblivion.

First of all, I would like to thank the institutions that made this possible, beginning with the Spanish Ministry of Education, funding my PhD grant, and the University of Valencia, hosting me as a PhD student. Since the research is not developed isolatedly, I have to thank all the members of the Theoretical Physics department for taking me as one of their own, with special regards to Prof. Jordi Vidal, head of the department, and Prof. Francisco José Botella, former head of IFIC.

My deepest gratitude goes for Gabriela, not only a director but a true mentor through many years. Her help and guidance are invaluable and can not possibly be appreciated by words.

I want to aknowledge those who shared research with me, Dr. Óscar Vives for his unbreakable optimism and my partner Marisa, who completed the team that achieved the goals that form a big part of this thesis. Besides them, I consider myself lucky for meeting and working with Prof. William A. Bardeen, as kind as he is wise. The time with him was priceless. I also thank Fermilab for allowing me such an opportunity.

I want to express my profound gratitude towards my family, who have always supported me throughout my career and to Mariana, with whom I expect to reach many milestones after this one.

For our those friends I have met who are walking a similar path, I wish you the best of lucks, and for those who have joined mine whilst it detoured from duty, thank you for easing the walk.